ERDC TR-12-4

Engineer Research and Development Center

US Army Corps of Engineers®
Engineer Research and Development Center

Fragility Analysis of a Concrete Gravity Dam Embedded in Rock and Its System Response Curve Computed by the Analytical Program GDLAD_Foundation

Robert M. Ebeling, Moira T. Fong, Johannes L. Wibowo, and Amos Chase, Sr.

June 2012

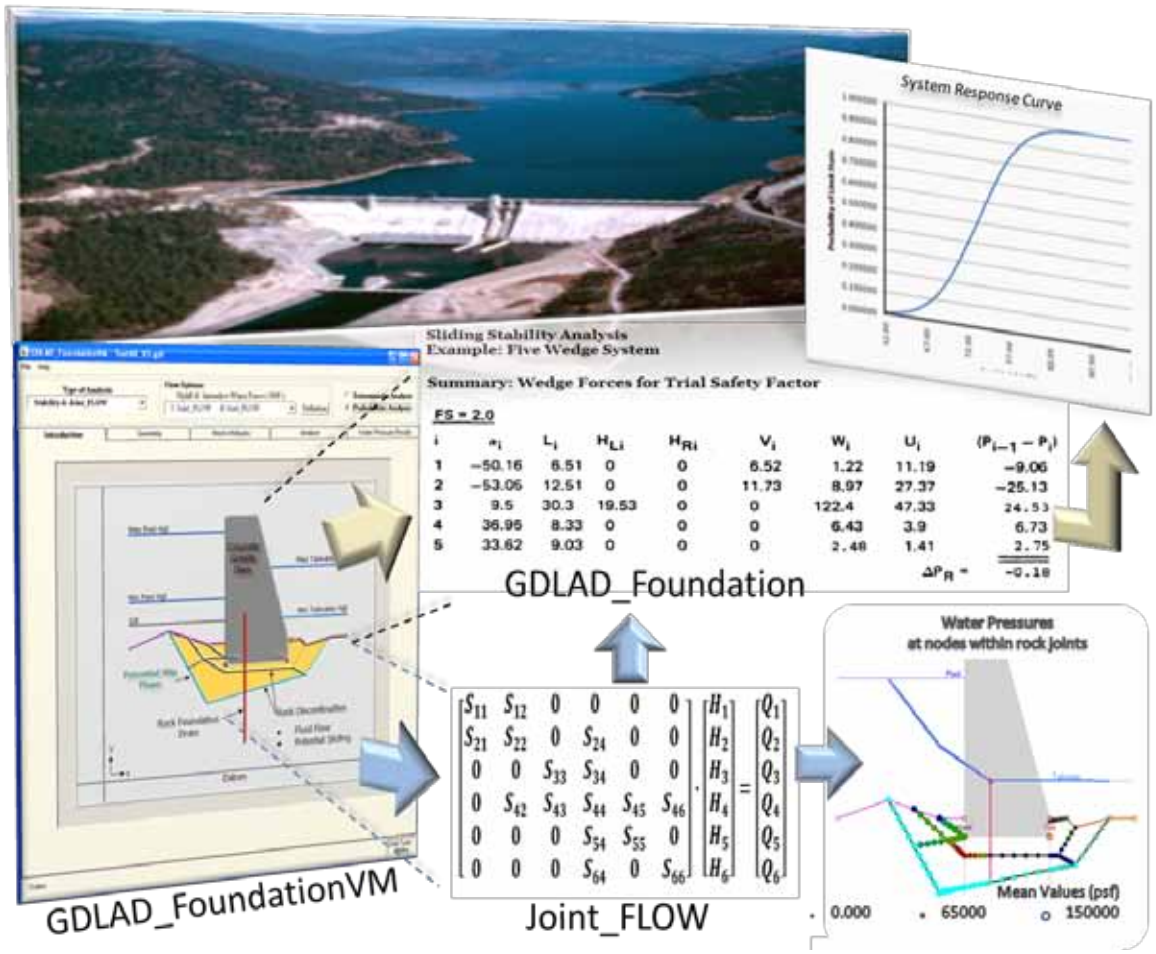

CEERD-IE 5 February 2013

Errata Sheet

No. 1

Fragility Analysis of a Concrete Gravity Dam Embedded in Rock and Its System Response Curve Computed by the Analytical Program GDLAD_Foundation

by

Robert M. Ebeling, Moira T. Fong, Johannes L. Wibowo, and Amos Chase Sr.

ERDC Technical Report ERDC TR-12-4

June 2012

This errata sheet discusses a geometrical constraint that should be imposed by the user, when conducting a sliding stability calculation, on the slope of the potential sliding plane of the wedges forming the resisting wedge. The resisting wedge is downstream of the toe of the gravity dam. The geometrical constraint is needed because of the assumptions made in the ETL 1110-2-256 formulation for the governing wedge equation given in Equation 6.6 of this report.

The equation in question is the governing equation for the horizontal interslice forces (P_{i-1}-P_i, see ETL 1110-2-256), which is introduced in Chapter 6 as Equation 6.6, shown here:

$$(P_{i-1} - P_i) = \frac{[(W_i+V_i)\cos\alpha_i - U_i + (H_{Li}-H_{Ri})\sin\alpha_i]\frac{\tan\phi_i}{FS_i} - (H_{Li}-H_{Ri})\cos\alpha_i + (W_i+V_i)\sin\alpha_i + \frac{c_i}{FS_i}L_i}{(\cos\alpha_i - \sin\alpha_i\frac{\tan\phi_i}{FS_i})} \qquad \text{(bis 6.6)}$$

On page 225 in Duncan and Wright (2005), the authors discuss this problem. They show an error occurs in the calculation when the resultant force *(R)* which acts at an angle, ϕ(*mobilized*), from the normal to the slip plane, due to normal stress force vector and the mobilized shear strength force vector, is equivalent to the angle of the interslice forces (0° for GDLAD_Foundation). The weight of the wedge has no component of force resisting it, therefore causing the interslice force difference expressed in Equation 6.6 to approach infinity because the denominator of Equation 6.6 becomes 0.0.

The denominator of Equation 6.6 can be defined as:

$$m_\alpha = \cos\alpha - \sin\alpha\frac{\tan\phi}{FS} \qquad (1)$$

where α is the angle of the slip plane for the toe slice region (Figure 1), ϕ is the angle of internal friction, and FS is the factor of safety. Given a friction angle and a factor of safety, it is possible to determine a mobilized friction angle.

$$\tan(\phi(mobilized)) = \frac{\tan\phi}{FS} \quad (2)$$

Rearranging,

$$\phi(mobilized) = \tan^{-1}(\frac{\tan\phi}{FS}) \quad (3)$$

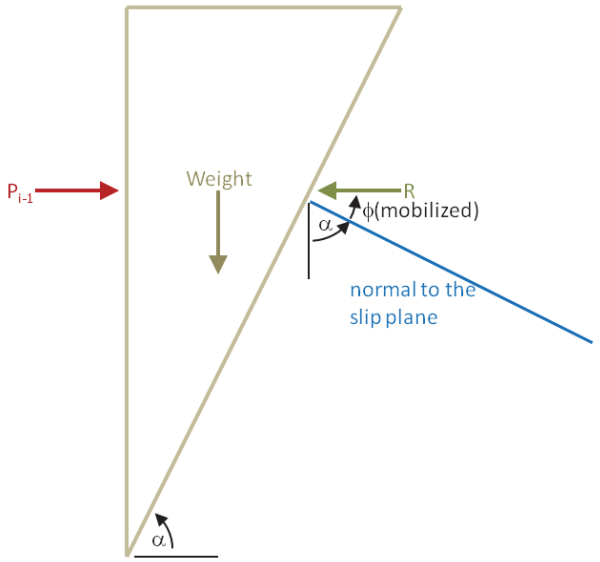

Figure 1 The resisting wedge geometry, showing the condition where the mobilized force *(R)* is in line with the interslice force *(P_{i-1})*.

As shown in Figure 1, the problem arises when the angle of incidence for the resisting force is horizontal. This occurs when:

$$\alpha + \phi(mobilized) \cong 90° \quad (4)$$

Because Equation 6.6 becomes asymptotic when the denominator approaches 0.0, Whitman and Bailey (1967) observed that, when the Simplified Bishop procedure is used and the value m_α (from Equation 1) becomes less than 0.2, alternative solutions should be explored.

For automatic searches, Duncan and Wright (2005) suggest requiring the user to constrain the inclination of the slip surface by avoiding steep slip surfaces where unreasonable solutions might exist due to negative stresses at the toe of the slope. This is a viable option when using GDLAD_Foundation, in which this problem is encountered.

The GDLAD_Foundation wedgeforces.out output file containing the results of the forces acting on the driving, structural, and resisting wedges should be monitored for high-magnitude imbalance forces contained within any of the wedges comprising the resisting wedge.

Duncan and Wright (2005) also notice that the critical slip surface exits at the toe with angles similar to those expected based on passive earth theory (see Table 1). They conclude that a critical slip surface usually could be found with no problems, if the search was started with a reasonable starting angle (45° or less, depending on the shear strength properties of the soil).

Table 1. Slip surface inclination for minimum passive earth pressures with horizontal interslice force inclination.

Slip Surface Inclination (α)	ϕ(*mobilized*)
10	40.0
15	37.5
20	35.0
25	32.5
30	30.0
35	27.5
40	25.0
45	22.5
50	20.0

A limited set of parametric tests were performed with GDLAD_Foundation to determine a range of values for α, given a factor of safety of 1.0, where $\phi = \phi(mobilized)$. It was determined that, to have values that do not asymptotically approach infinity for the horizontal interslice force P_{i-1} (equal to the value for $(P_{i-1}-P_i)$ by Equation 6.6 since P_i will be zero for the last wedge) which occurs at ± 5° from the horizontal, the value of α should be set so that:

$$\alpha + \phi \leq 85° \tag{5}$$

Rearranging,

$$\alpha \leq 85° - \phi \tag{6}$$

Equation 6 is a more liberal constraint on the limiting slope (α) than a constraint based on the Table 1 values. When using either Table 1 or Equation 6 guidance to establish the limiting slip plane angle to be used for the resisting wedge, monitor the imbalance force (Equation 6.6) value reported in the GDLAD_Foundation wedgeforces.out output file for high-magnitude imbalance forces contained in any of the wedges comprising the resisting wedge.

With respect to the GDLAD_Foundation software, the following observations apply:

1) When applying Equation 6.6 to the deterministic sliding stability analysis of a user-defined wedge system, an iterative procedure is used to determine the value for the factor of safety against sliding. This iterative procedure is performed many times in a probabilistic analysis.
2) When computing factors of safety for high pools during the construction of a system response curve in a probabilistic analysis, the stability calculations tend towards FS =1 in the computations.

3) The critical cases were observed to occur for low trial FS values used in the sliding stability calculation, especially values of FS close to or below 1. This is the area where ϕ*(mobilized)* is close to or less than ϕ.

The constraints suggested in this errata apply only in the GDLAD_Foundation software when an analysis must be performed to determine the factor of safety against sliding or a system response curve. This occurs when the type of analysis is Stability & Joint_FLOW or Stability & Simplified Seepage.

References:

[Duncan and Wright, 2005]

Duncan, J. M., and S. G. Wright. 2005. *Soil strength and slope stability*. New York: John Wiley & Sons.

[Whitman and Bailey, 1966]

Whitman, R. V., and W. A. Bailey. 1966. Use of computers for slope stability analyses. In *Journal of the Soil Mechanics and Foundations Division.* Berkeley, CA: ASCE.

CEERD-IE 5 February 2013

Errata Sheet

No. 2

Fragility Analysis of a Concrete Gravity Dam Embedded in Rock and Its System Response Curve Computed by the Analytical Program GDLAD_Foundation

by

Robert M. Ebeling, Moira T. Fong, Johannes L. Wibowo, and Amos Chase Sr.

ERDC Technical Report ERDC TR-12-4

June 2012

This errata sheet has been assembled using the discussion and findings of Errata Sheet No. 1. Section 1 of this sheet provides the coordinates necessary to generate a shallower inclination (~ 32 °) of the slip surface of the resisting wedge.

1) Page 55, Table 2.5, is updated for Point Id's listed in Table 1.

The location of the downstream points and associated regions were modified to reflect the change in the angle of inclination of the potential sliding plane. Specifically, Point Id's 12 and 13 of Table 1 list the revised ground surface points.

Table 1. Update to Table 2.5 description of points and locations.

Point Id	Point Description	X-coordinate	Y-coordinate
6	Right upper corner of Region 1	140.0	943.45
12	Downstream ground surface point of Region 1	132.0	943.45
13	Downstream ground surface point of Region 1	115.0	943.45
23	Downstream rock foundation corner point delineating Regions 1 and 2	136.22	927.14
25	Right lower corner of Region 2	135.97	910.69

2) Page 214, Figure 7.10, is replaced with the one below, which shows a maximum pool elevation of 1058 ft, a minimum pool elevation of 1028 ft, and a constant tailwater of 978.7 ft, resulting in 31 variable pools.

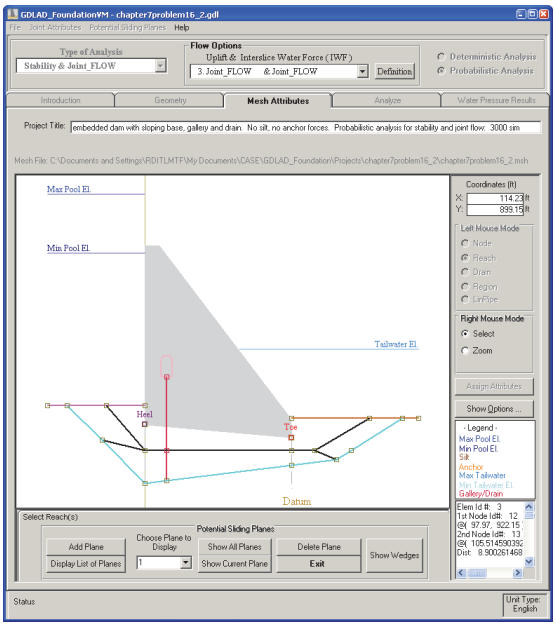

Figure 7.10. Concrete gravity dam embedded in rock with rock foundation drain.

3) Page 215, Figure 7.11, is replaced with:

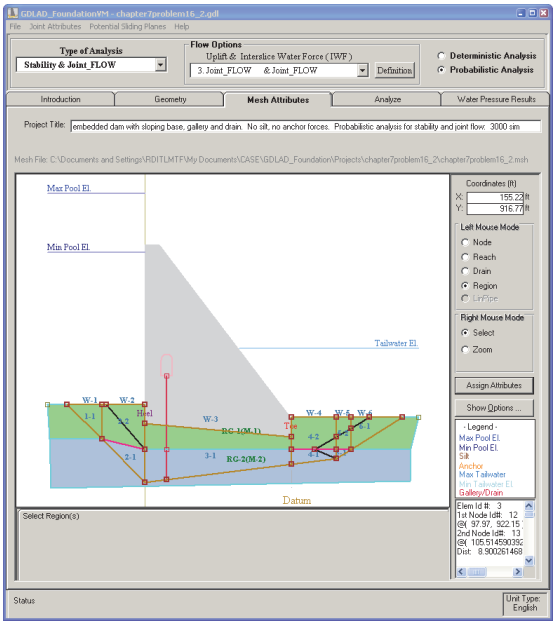

Figure 7.11. Concrete gravity dam with six wedges and two material regions.

4) Page 217, Figure 7.14, is replaced with:

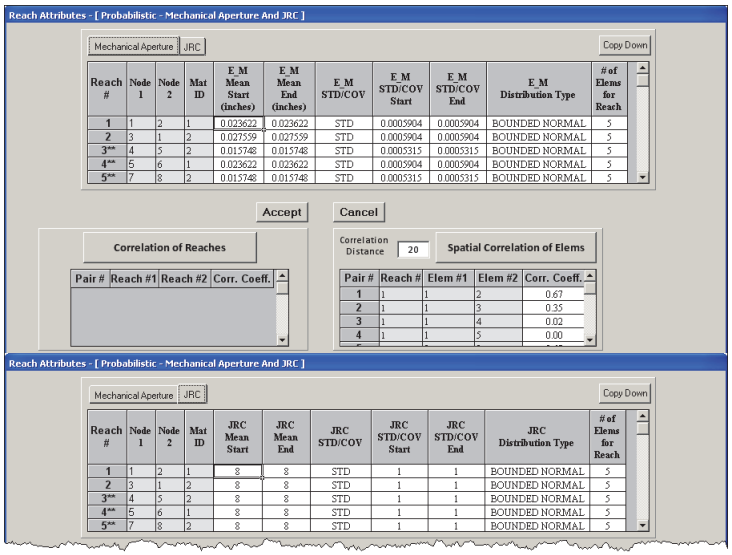

Figure 7.14. Reach attributes defining values for the Mechanical Aperture and JRC.

5) Page 218, Figure 7.15, is replaced with:

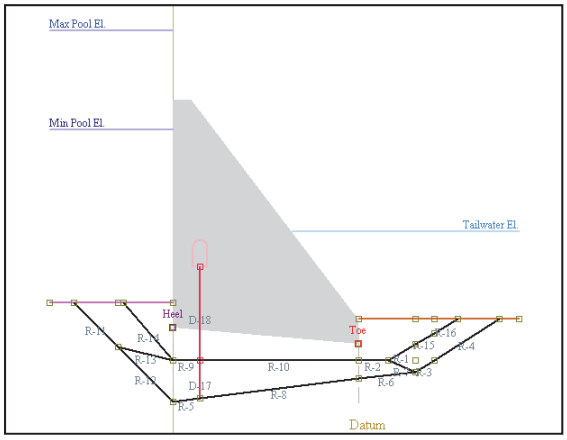

Figure 7.15. Reach numbers defining both rock joint reaches and rock drain reaches.

6) Page 219, Figure 7.16, is replaced with:

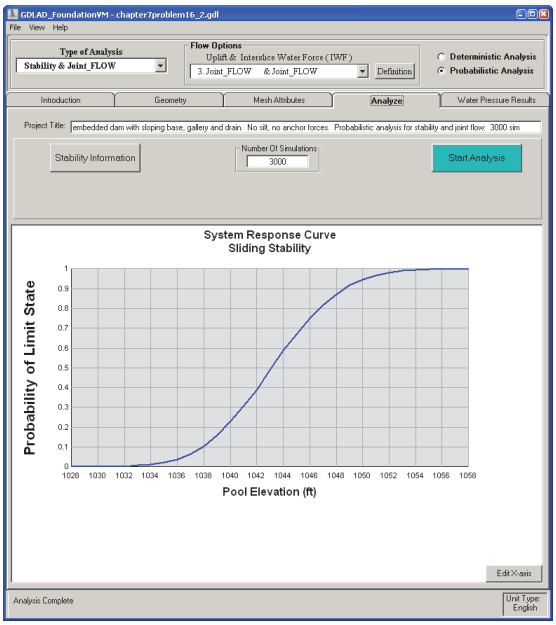

Figure 7.16. System response curve for a Stability and Joint_Flow analysis.

7) Page 220, Figure 7.17, is replaced with:

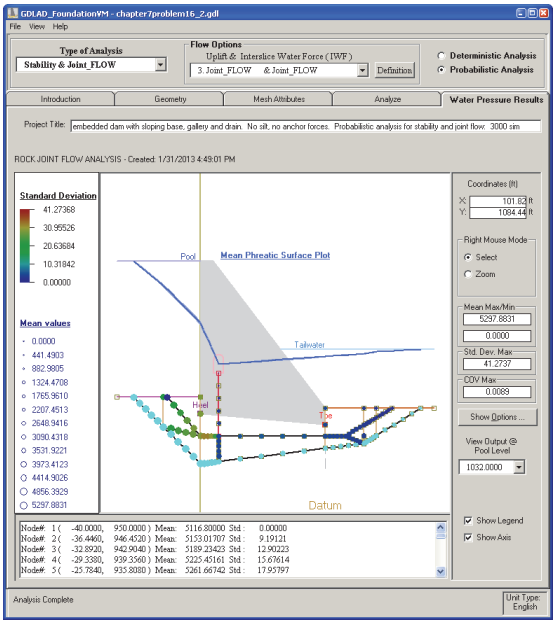

Figure 7.17. Mean phreatic surface at selected nodal points.

CEERD-IE 5 February 2013

Errata Sheet

No. 3

Fragility Analysis of a Concrete Gravity Dam Embedded in Rock and Its System Response Curve Computed by the Analytical Program GDLAD_Foundation

by

Robert M. Ebeling, Moira T. Fong, Johannes L. Wibowo, and Amos Chase Sr.

ERDC Technical Report ERDC TR-12-4

June 2012

1) Page 15, Figure 1.7, is replaced with:

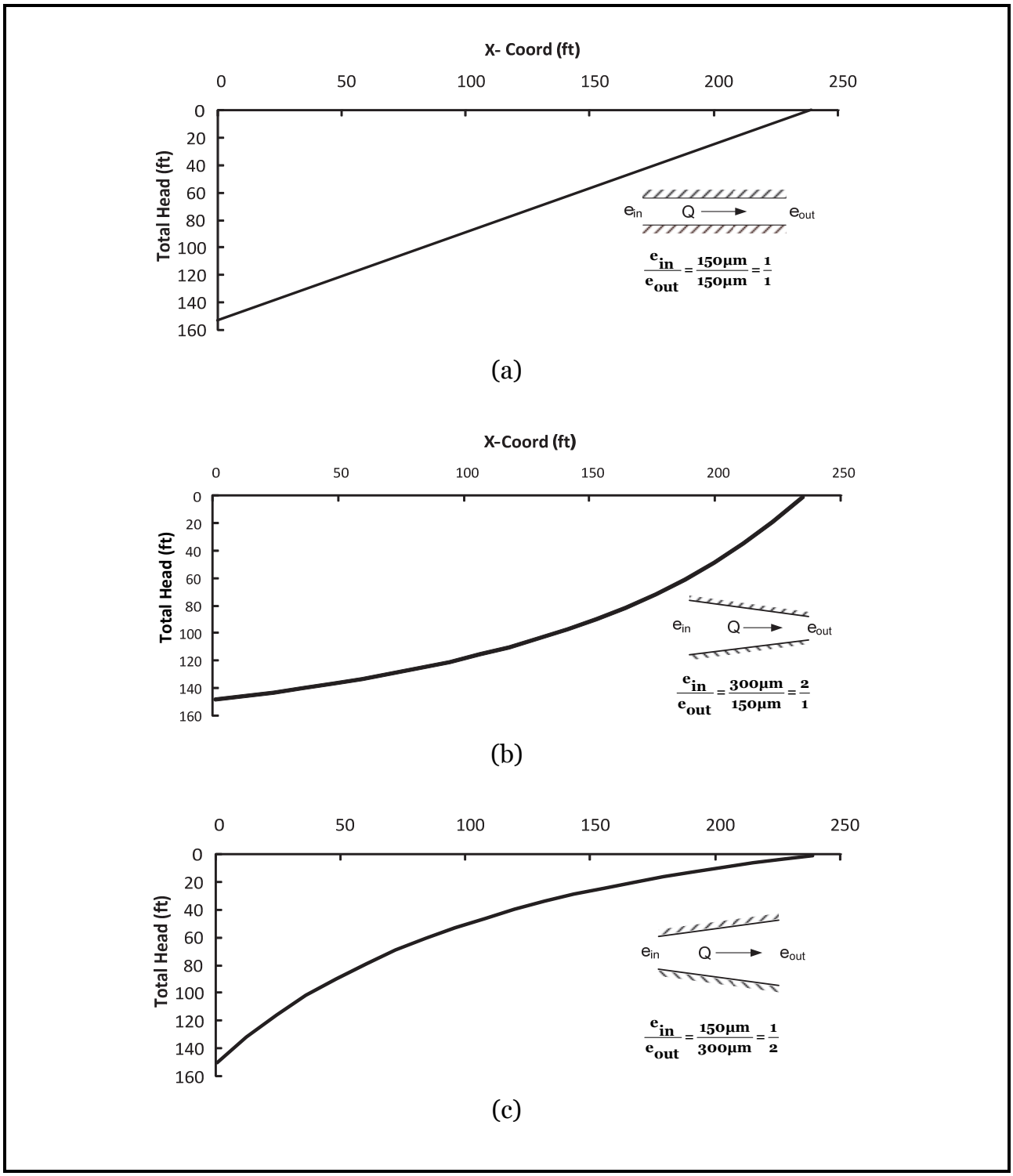

Figure 1.7. Variation in uplift pressure (head) along (a) uniform, (b) tapered heel to toe, and (c) tapered toe to heel. *e* is the conducting joint aperture.

ERDC TR-12-4
June 2012

Fragility Analysis of a Concrete Gravity Dam Embedded in Rock and Its System Response Curve Computed by the Analytical Program GDLAD_Foundation

Robert M. Ebeling, Moira T. Fong, and Amos Chase, Sr.

Information Technology Laboratory
U.S. Army Engineer Research and Development Center
3909 Halls Ferry Road
Vicksburg, MS 39180-6199

Johannes L. Wibowo

Geotechnical and Structures Laboratory
U.S. Army Engineer Research and Development Center
3909 Halls Ferry Road
Vicksburg, MS 39180-6199

Final report

Prepared for USACE Risk Management Center – Eastern Office
William S. Morehead Federal Building – 11th Floor
1000 Liberty Avenue
Pittsburgh, PA 15222-4186

Abstract: This research report describes the engineering formulation and corresponding software developed for expressing the computed stability results for an idealized two-dimensional cross-section of a non-overflow concrete gravity dam embedded in rock in terms of a fragility curve for a potential sliding mode of failure. Within the Corps, the term system response curve is being used to describe what is commonly referred to in the technical literature as the fragility curve; used for the hydrologic fragility assessment of concrete gravity dams embedded in rock. This report uses this Corps terminology. Uncertainty in strength, rock joint parameters that impact the flow of water within the rock joints, silt induced earth pressure and (post-tensioned) anchor force(s) are accounted for in a multivariate probabilistic stability analysis resulting in the computation of a system response curve. The PC software package GDLAD_Foundation (Gravity Dam Layout And Design) is used in this R&D effort to perform the computations and construct the system response curve.

A sliding stability assessment of a non-overflow gravity dam embedded in rock requires the assignment of uplift water pressure forces acting on the driving, structural and resisting wedges. Incorporated within the GDLAD_Foundation software package is the program Joint_FLOW that is used to assess laminar fluid flow within rock joints, fissure and/or faults contained within the rock foundation. Results from the analysis of steady state laminar seepage within the joints provides for the calculation of uplift water pressures along the joints. Resultant uplift forces are then computed from the distribution of water pressures along these rock joints.

The resulting engineering methodology and corresponding software is applicable to a two dimensional model of a non-overflow (concrete) gravity dam founded within rock. GDLAD_Foundation is also capable of performing a deterministic steady state seepage analysis of laminar flow within rock joints or a seepage analysis followed by a sliding stability evaluation.

Contents

Figures and Tables viii

Preface xvi

Unit Conversion Factors xviii

1 Uplift and Sliding Stability System Response Curve for a 2-D Non-Overflow Gravity Dam Section Embedded in Rock 1

1.1 Introduction 1

1.1.1 Deterministic and probabilistic analysis capabilities 2

1.1.2 The system response curve 2

1.2 Analytical methods in uplift prediction 4

1.2.1 Open and closed drainage gallery systems 7

1.2.2 Interrelationships between uplift pressure, pressure head, and total head 8

1.3 Joint aperture and uplift pressure distribution 9

1.4 Laminar and turbulent flow in joints 16

1.4.1 The cubic law 19

1.4.2 Fluid flow conditions 21

1.4.3 The effect of surface roughness on the mechanical aperture 22

1.5 Report contents 23

2 Stability and Seepage Analysis of a Non-Overflow Dam (2-D) Cross-Section Embedded in Rock 25

2.1 Introduction 25

2.2 2-D drain model idealization 27

2.3 Drain model iteration method 29

2.4 Loading conditions on the structural wedge for pools above crest of dam 30

2.5 Uplift and interslice water pressure resultant forces for flow options 1, 2, and 3 31

2.6 Problem 1: Stability analysis with seepage computed along rock joints using Joint_FLOW and no interslice water pressure resultant forces. (Flow Option 1) 32

2.7 Problem 2: Stability analysis with seepage computed along rock joints using Joint_FLOW and near hydrostatic interslice water pressure resultant forces. (Flow Option 2) 38

2.8 Problem 3: Stability analysis with seepage and interslice water pressure resultant forces computed along rock joints using Joint_FLOW. (Flow Option 3) 40

2.9 Discussion of results for stability and Joint_FLOW analysis 42

3 The Visual Modeler – GDLAD_ FoundationVM 46

3.1 The Introduction tab 46

3.1.1 Defining the type of analysis 47

3.1.1.1 Stability and Joint_FLOW 49

3.1.1.2 Stability and Simplified Seepage 49

3.1.1.3 Joint_FLOW only 50

3.1.2 The Menu Bar *51*
3.1.2.1 File Item *51*
3.1.2.2 Help Item *52*
3.1.3 The Status Bar *52*
3.2 The Geometry tab 52
3.2.1 The Project Title *53*
3.2.2 The Cursor and Mouse buttons *53*
3.2.3 The Left Mouse Mode *54*
3.2.3.1 Adding or modifying points *54*
3.2.3.2 Creating a point on a line *55*
3.2.3.3 Adding and deleting lines *56*
3.2.3.4 Split intersecting lines *57*
3.2.3.5 Creating and modifying regions *57*
3.2.4 The Right Mouse Mode *58*
3.2.4.1 The Select Mode *58*
3.2.4.2 The Zoom Mode *58*
3.2.5 Generate Mesh *59*
3.2.6 Show Options *59*
3.2.7 Legend and geometry information *60*
3.2.8 The Menu Bar *60*
3.2.8.1 File menu item *60*
3.2.8.2 Reservoir menu item *61*
3.2.8.3 Silt menu item *62*
3.2.8.4 Anchor menu item *64*
3.2.8.5 Gallery menu item *66*
3.2.8.6 Assign Heel and Toe menu item *68*
3.2.8.7 Help menu item *69*
3.3 The Mesh Attributes tab 70
3.3.1 The Project Title *70*
3.3.2 The Menu Bar *71*
3.3.2.1 File menu item *71*
3.3.2.2 Joint Attributes menu item *72*
3.3.2.3 Potential Sliding Planes menu item *73*
3.3.2.4 Help menu item *76*
3.3.3 Type of analysis menu *76*
3.3.3.1 Stability and Joint_FLOW type of analysis *76*
3.3.3.2 Stability and Simplified Seepage Type of Analysis *88*
3.3.3.3 Joint_FLOW only type of analysis *94*
3.3.4 Show Options *99*
3.3.5 Legend and Geometry information *100*
3.4 The Analyze tab 100
3.4.1 The Type of Analysis *101*
3.4.2 The project title *101*
3.4.3 Number of Simulations *102*
3.4.4 Stability Information *102*
3.4.5 Start Analysis *103*
3.4.6 The Menu Bar *104*
3.4.6.1 File Menu Item *105*

3.4.6.2 View menu item *106*
3.4.6.3 Help menu item *108*
3.5 View Pressure Results tab 109
3.5.1 The project title *110*
3.5.2 The Right Mouse Mode *110*
3.5.2.1 The Select Mode *111*
3.5.2.2 The Zoom Mode *111*
3.5.3 Show Options *111*
3.5.4 Select pool elevation, legend and axis *112*
3.5.5 The Menu Bar *112*
3.5.5.1 File menu item *112*
3.5.5.2 View menu item *112*
3.5.5.3 Help menu item *113*
3.6 Probabilistic supplementary material 114
3.6.1 Reach Mode (Stability and Joint_FLOW and Joint_FLOW Only) *115*
3.6.2 Region Mode (Stability and Joint_FLOW and Stability and Simplified Seepage with flow option 4 and 5) *116*
3.6.3 Region with Reach Mode (Stability and Simplified Seepage with flow option 6) *118*

4 Fluid Flow Along Rock Joints 123
4.1 Introduction 123
4.2 Fluid flow along a single reach rock joint with three different tapered rock joints 123
4.2.1 Problem 1: Fluid flow along a uniform rock joint; a single horizontal reach joint at the dam-to-foundation interface *129*
4.2.2 Problem 2: Fluid flow along a tapered downstream rock joint; a single reach, horizontal joint at the dam-to-foundation interface tapered in the direction of flow *132*
4.2.3 Problem 3: Fluid flow along a tapered upstream rock joints; a single reach, horizontal joint at the dam-to-foundation interface tapered in the direction opposite to flow *135*
4.2.4 Comparison of results for a single reach with three different tapered rock joints *139*
4.3 Fluid flow along multi-reach rock joints contained within the rock foundation 141
4.3.1 Problem 4: A single potential sliding plane *143*
4.3.2 Problem 5: Multiple potential sliding planes *143*
4.3.3 Problem 6: Network of inter-connected rock joints with multiple potential sliding planes *146*
4.3.4 Discussion of results for multiple-reach rock joints with multiple potential sliding planes *147*
4.4 Summary and conclusions 153

5 Head Loss in Rock Joints Using the Linear Method (Computed by LinPipe) 156
5.1 Problem 10: Multiple-reaches of rock joints modeled as a pipe network and using the Linear Method to compute the distribution of total heads 158
5.2 Comparison of total head results for flow along rock joints with and without the LinPipe methodology 163

6 Stability with Simplified Seepage Analysis 166
6.1 Introduction to Limit Equilibrium Procedure and Procedure of Slices 166

6.2 Uplift and interslice water pressure resultant forces for Flow Options 4, 5, and 6 172
6.2.1 Introduction to Flow Option 4 ..... *174*
6.2.2 Introduction to Flow Option 5 ..... *177*
6.2.3 Introduction to Flow Option 6 ..... *180*
6.3 Problem 11: Sliding stability with no vertical interslice water pressure resultant forces for the ETL 1110-2-256 Gravity Dam example (Flow Option 4) 182
6.3.1 Discussion of drain efficiency with Flow Option 4 ..... *184*
6.3.1.1 Closed drainage gallery system *186*
6.3.1.2 Open drainage gallery system *187*
6.3.2 Discussion of drain efficiency E value with Flow Option 4 ..... *188*
6.4 Problem 12: Sliding stability with simplified seepage Along the structural wedge (Flow Option 5) 189
6.4.1 Discussion of drain efficiency with Flow Option 5 ..... *191*
6.4.1.1 Closed drainage gallery system *191*
6.4.1.2 Open drainage gallery system *193*
6.4.2 Discussion of drain efficiency E value with Flow Option 5 ..... *193*
6.5 Problem 13: Sliding stability using the line of seepage method with uniform permeability and no interslice water pressure resultant forces (Flow Option 6) 195
6.5.1 Discussion of drain efficiency with Flow Option 6 ..... *196*
6.5.1.1 Closed drainage gallery system *197*
6.5.1.2 Open drainage gallery system *199*
6.5.2 Discussion of drain efficiency E value with Flow Option 6 ..... *201*
6.6 Discussion of results for stability with simplified seepage analysis 201

7 Probabilistic Analysis 203
7.1 Introduction 203
7.1.1 Multivariate probabilistic analysis of uncertain variables *203*
7.1.2 System response curves for rock-founded gravity dams with a sloping base *206*
7.2 Problem 14: Validation of stability analysis 207
7.3 Problem 15: Validation of system response curve 211
7.4 Problem 16: Analysis and system response curve 213

8 Summary, Conclusions, and Recommendations 222
8.1 Summary 222
8.2 Conclusions 223
8.3 Recommendations 224

References 228

Appendix A: Stability Analysis of the ETL 1110-2-256 Non-Overflow Dam Embedded in Rock Example 232

Appendix B: Mathematical Equations Representing Steady State Flow along Rock Joints (Joint_FLOW) 235

Appendix C: Head Loss in Rock Joint Flow Using Linear Method (LinPipe) 241

Appendix D: Description of the GDLAD_ Foundation ASCII Input Data File (GDLAD_Foundation.in) 254

Appendix E: Description of the Joint_FLOW with optional LinPipe ASCII Input Data File (Jointflow.in) 265

Appendix F: Line of Seepage Formulation 269

Report Documentation Page

Figures and Tables

Figures

Figure 1.1. System response curve for sliding limit state. 3
Figure 1.2. Uplift distribution with foundation drains for an "open drainage gallery system" 6
Figure 1.3. Hypothetical gravity dam cross-section with a horizontal rock joint along the dam-to rock foundation interface 8
Figure 1.4. Natural rock joint with mechanical aperture *E* and equivalent parallel plates with conducting aperture *e* 10
Figure 1.5. Distribution of uplift pressure in (a) joint of uniform aperture, (b) two-joint network, and (c) tapered joint 13
Figure 1.6. Nonlinear response of uplift pressure (as head) to rising reservoir headwater at six positions along a continuous joint of uniform aperture 14
Figure 1.7. Variation in uplift pressure (head) along (a) uniform, (b) tapered heel to toe, and (c) tapered toe to heel. *e* is the conducting joint aperture. 15
Figure 1.8. Variation in uplift pressure with changes in joint hydraulic conductivity (changes in joint aperture) with rising reservoir levels at a point in a dam foundation 16
Figure 1.9. Range of validity of Darcy's law 19
Figure 2.1. Gravity dam embedded in a rock foundation with rock foundation drain with interconnect rock joints. 26
Figure 2.2. Gravity dam embedded in a rock foundation with wedge and region information. 26
Figure 2.3. Concrete monolith with foundation drains. 28
Figure 2.4. Rock drain configuration (a) actual rock foundation drain (b) ideal 2-dimensional slotted drain per foot run of dam. 29
Figure 2.5. Current drain model. 30
Figure 2.6. Loading of structural wedge model of the embedded concrete gravity dam with rock foundation drain (a) pool and tailwater below crest (b) pool and tailwater above the crest of the dam. 31
Figure 2.7. Gravity dam embedded in a rock foundation with rock foundation drain. 34
Figure 2.8. Rock foundation drain attributes. 35
Figure 2.9. Mechanical aperture and JRC values for each rock joint. 35
Figure 2.10. Embedded concrete gravity dam with two material regions and a six wedge system. 36
Figure 2.11. Table of properties of materials and the mapping of regions. 36
Figure 2.12. Resultant factor of safety with residual imbalance of a six wedge system with Flow Option 1. 37
Figure 2.13. Resultant water pressures for Flow Option 1. 38
Figure 2.14. Resultant factor of safety with residual imbalance of a six wedge system with Flow Option 2. 40
Figure 2.15. Water pressures at nodal points for Flow Option 2. 41
Figure 2.16. Resultant factor of safety with residual imbalance of a six wedge system with Flow Option 3. 43

Figure 2.17. Water pressures at nodal points for flow option 3. 44
Figure 3.1. Depiction of a concrete gravity dam embedded in rock. 47
Figure 3.2. Selection of Stability & Joint_FLOW type of analysis with flow options 1, 2, and 3. 49
Figure 3.3. Definitions of calculations of uplift and interslice water forces for flow option 1. 49
Figure 3.4. Selection of Stability & Simplified Seepage type of analysis with flow options 4, 5, and 6. 50
Figure 3.5. Definitions of calculations of uplift and interslice water forces for flow option 4. 50
Figure 3.6. Selection Joint_FLOW only. 51
Figure 3.7. Creating and updating project, geometry and mesh files. 51
Figure 3.8. Initializing units for a new project. 51
Figure 3.9. Guidance to GDLAD_Foundation. 52
Figure 3.10. The Status Bar. 52
Figure 3.11. Depiction of a concrete gravity dam embedded in rock. 53
Figure 3.12. Image of embedded concrete gravity dam. 54
Figure 3.13. Adding or modifying points. 55
Figure 3.14. Adding or modifying lines. 56
Figure 3.15. Adding and modifying regions. 58
Figure 3.16. Right side menu functions of the Geometry tab. 59
Figure 3.17. Creating and updating project, geometry and mesh files. 61
Figure 3.18. Reservoir input information. (a) Reservoir menu item, (b) Pool elevations, (c) Tailwater elevations, and (d) Reservoir and tailwater levels. 62
Figure 3.19. Silt parameters. 63
Figure 3.20. The *Anchor* menu item provides graphical presentation of Anchor positions relative to the concrete gravity dam and additional information relating to these post-tensioned anchors. 65
Figure 3.21.The Drainage and Gallery system. 67
Figure 3.22. Assigning the location of Heel and Toe. 69
Figure 3.23. Guidance to GDLAD_Foundation. 70
Figure 3.24. Generated mesh of a Stability & Joint_FLOW analysis. 71
Figure 3.25. Guidance to GDLAD_Foundation. 72
Figure 3.26. Aperture type menu item. 72
Figure 3.27. Drain type menu item. 72
Figure 3.28. LinPipe Menu Item. 73
Figure 3.29. A Potential Sliding Plane. 74
Figure 3.30. Display Wedge information. 75
Figure 3.31. List of Sliding Planes. 75
Figure 3.32. Guidance to GDLAD_Foundation. 76
Figure 3.33. Stability & Joint_FLOW type of analysis. 77
Figure 3.34. Joint Attributes for a Stability and Joint_FLOW type of analysis. 77
Figure 3.35. Joint Attributes (a) Aperture Type, (b) Drain Type and (c) LinPipe. 78
Figure 3.36. Potential Sliding Planes menu item for Stability and Joint_FLOW type of analysis. 79

Figure 3.37. Conducting Aperture with one element per reach. 80
Figure 3.38. Drain with one element per reach. 82
Figure 3.39. Material properties and regions. 83
Figure 3.40. An image of rock joints in *Reach Mode* 84
Figure 3.41. LinPipe assignments (a) Image of network of rock joints (b) LinPipe attributes table. 85
Figure 3.42. Negative flow into a junction (red) and positive flow out of the junction (blue) are drawn to signify direction of flow at a junction after row 3 of the Junction/Inflow Table has been selected. 86
Figure 3.43. A positive (clockwise) flow pattern after row 2 of the Closed Loop Table has been selected. 87
Figure 3.44. A negative (counter-clockwise) flow pattern after row 1 of the Open Loop Table has been selected. 88
Figure 3.45. Stability & Simplified Seepage type of analysis. 89
Figure 3.46. Joint Attributes for a Stability and Simplified Seepage type of analysis. 90
Figure 3.47. Potential Sliding Planes menu item. 91
Figure 3.48. Material Properties and Regions. 92
Figure 3.49. Attribute tables for (a) Material Properties and (b) Rock Joint attributes. 93
Figure 3.50. Selection Joint_FLOW only. 94
Figure 3.51. Aperture type in the Joint Attributes menu item. 95
Figure 3.52. Aperture Type of a Rock joint. 95
Figure 3.53. Drain Type. 96
Figure 3.54. LinPipe. 96
Figure 3.55. Potential Sliding Planes menu item. 97
Figure 3.56. Hydraulic conductivity values with one element per reach. 98
Figure 3.57. Show Options. 100
Figure 3.58. Generated mesh of a Stability & Joint_FLOW analysis. 101
Figure 3.59. Stability output selection. 103
Figure 3.60. Run time information. 104
Figure 3.61. System response curve. 105
Figure 3.62. File menu item. 105
Figure 3.63. GDLAD_Foundation Input and Output file selection. 106
Figure 3.64. GDLAD_Foundation input file. 106
Figure 3.65. GDLAD_Foundation system response curve. 107
Figure 3.66. GDLAD_Foundation wedge forces. 107
Figure 3.67. Joint_FLOW Input and Output. 107
Figure 3.68. Joint_FLOW input. 108
Figure 3.69. Joint_FLOW output. 108
Figure 3.70. Guidance for GDLAD_Foundation. 108
Figure 3.71. Probabilistic analysis with water pressures at nodal points. 109
Figure 3.72. Mean Phreatic Surface at selected nodal points. 110
Figure 3.73. Right selection panel of water pressure results tab. 112

Figure 3.74. File menu item. 112
Figure 3.75. GDLAD_Foundation Input and Output file selection. 113
Figure 3.76. Selection of water pressure files. 113
Figure 3.77. Guidance for GDLAD_Foundation. 114
Figure 3.78. Reach Attributes for a Probabilistic Analysis (a) Table for K-Direct values (b) Std/Cov and Distribution type selection (c) correlation coefficient between elements. 114
Figure 3.79. Region Attributes for a Probabilistic Analysis for flow options 4 and 5. (a) Material attributes table (b) Std/Cov and Distribution type selection 117
Figure 3.80. Region Attributes for a Probabilistic Analysis for flow option 6 (a) Material attributes table (b) Std/Cov and Distribution type selection. 119
Figure 3.81. Reach Attributes for a Probabilistic Analysis of (a) Table for K-Direct values (b) Std/Cov and Distribution type selection (c) correlation coefficient between elements. 120
Figure 4.1. Variation of head along a tapered joint. 127
Figure 4.2. Geometry of dam used in three example problems. 129
Figure 4.3. Geometry of dam with a single horizontal rock joint of twenty elements with uniform conductive aperture. 130
Figure 4.4. Water pressures at specific locations along a single horizontal rock joint of 20 elements with uniform conductive aperture. 130
Figure 4.5. Variation in total head and uplift pressure along a uniform, horizontal rock joint. 131
Figure 4.6. Geometry of dam with a single horizontal rock joint of twenty elements with tapered downstream conductive aperture; $e_{in} = z \cdot e_{out}$. 133
Figure 4.7. Water pressures at specific locations along a single horizontal rock joint of 20 elements with tapered downstream conductive aperture. 133
Figure 4.8. Variation in total head and uplift pressure along a tapered downstream, horizontal rock joint; $e_{in} = z \cdot e_{out}$. 134
Figure 4.9. Geometry of dam with a single horizontal rock joint of twenty elements with tapered upstream conductive aperture; $z \cdot e_{in} = e_{out}$. 136
Figure 4.10. Water pressures at specific locations along a single horizontal rock joint of 20 elements with tapered upstream conductive aperture. 137
Figure 4.11. Variation in total head and uplift pressure along a tapered upstream horizontal rock joint; $z \cdot e_{in} = e_{out}$. 137
Figure 4.12. Variations in head and uplift pressures along a single reach, horizontal rock joint. 140
Figure 4.13. Multi-reach network of permeable joints within a rock foundation with one rock foundation drain. 142
Figure 4.14. Zero-level single-reach network of permeable joints within a rock foundation with one rock foundation drain (Case 1). 144
Figure 4.15. Zero-level single-reach network of permeable joints within a rock foundation with no rock foundation drain (Case 7). 144
Figure 4.16. Zero-level multi-reach network of permeable joints within a rock foundation with one rock foundation drain (Case 2). 145
Figure 4.17. One-level multi-reach network with two upstream sources of permeable joints within a rock foundation with one rock foundation drain (Case 3). 146
Figure 4.18. One-level multi-reach network with multi-upstream sources of permeable joints within a rock foundation with one rock foundation drain (Case 4). 147

Figure 4.19. Multi-level multi-reach network with two-upstream sources of permeable joints within a rock foundation with one rock foundation drain (Case 5). 148
Figure 4.20. Multi-level multi-reach network with multi-upstream sources of permeable joints within a rock foundation with one rock foundation drain (Case 6). 149
Figure 4.21. Variations in head along a potential sliding plane for various rock joint networks. 150
Figure 4.22. Variations in uplift pressures along a potential sliding plane with various rock joint networks. 151
Figure 4.23. Refined mesh of Figure 4.19 for multi-level multi-reach network with two-upstream sources of permeable joints within a rock foundation with one rock foundation drain (Case 5). 152
Figure 4.24. Variation in head along a potential sliding plane of Case 5 and its refined mesh. 152
Figure 4.25. Variations in uplift pressures along a potential sliding plane for Case 5 and its refined mesh. 153
Figure 5.1. Schematic diagram describing relation 5.1. 157
Figure 5.2. A hypothetical dam with segments of rock joints and a drain segment defining two potential inner loops. 157
Figure 5.3. A hypothetical embedded dam with segments of rock joints and a rock foundation drain. 159
Figure 5.4. Reach attributes showing five elements per rock joint reach. 160
Figure 5.5. Drain Attributes showing one element per rock drain reach. 160
Figure 5.6. LinPipe Attributes. 161
Figure 5.7. Flow directions (a) at a junction (b) closed loop (c) open loop 162
Figure 5.8. Water pressure results. 164
Figure 5.9. Variation in head along a potential sliding plane for a rock joint network 165
Figure 5.10. Variation in water pressures along a potential sliding plane for a rock joint network 165
Figure 6.1. The ETL 1110-2-256 hypothetical gravity dam embedded in a rock foundation with no rock foundation drain. 167
Figure 6.2. A Five wedge system for the ETL 1110-2-256 hypothetical gravity dam embedded in a rock foundation with no rock foundation drain. 169
Figure 6.3. Distribution of pressures and resulting forces acting on a generalized wedge in the ETL 1110-2-256 formulation. 170
Figure 6.4. Free body diagram of the i^{th} wedge according to the ETL 1110-2-256 formulation. 171
Figure 6.5. Free body diagram - Sliding stability analysis for a general wedge system 173
Figure 6.6. ETL 1110-2-256 hypothetical gravity dam embedded in a rock foundation with no rock foundation drain 174
Figure 6.7. A Five wedge system for the ETL 1110-2-256 hypothetical gravity dam embedded in a rock foundation with no rock foundation drain 175
Figure 6.8. ETL 1110-2-256 hypothetical gravity dam embedded in a rock foundation with no rock foundation drain 177
Figure 6.9. A Five wedge system for the ETL 1110-2-256 hypothetical gravity dam embedded in a rock foundation with no rock foundation drain 178

Figure 6.10. Five wedge system for the ETL 1110-2-256 hypothetical gravity dam embedded in a rock foundation with no rock foundation drain 181
Figure 6.11. Geometry of dam with a five wedge system. 183
Figure 6.12. Table of properties of materials and the mapping of regions. 184
Figure 6.13. Resultant factor of safety with residual imbalance of a five wedge system with Flow Option 4. 185
Figure 6.14. Drain efficiency of a closed drainage gallery system with Flow Option 4 (a) Wedge and uplift pressure diagram (water pressures not to scale) (b) Variation on total head along potential slip plane. 186
Figure 6.15. Drain efficiency of an open drainage gallery system with Flow Option 4 (a) Wedge and uplift pressure diagram (water pressures not to scale) (b) Variation on total head along potential slip plane. 188
Figure 6.16. Resultant factor of safety with residual imbalance of a five wedge system with Flow Option 5. 190
Figure 6.17. Drain efficiency of a closed drainage gallery system with Flow Option 5. (a) Wedge and uplift pressure diagram (water pressures not to scale) (b) Variation on total head along embedded part of the concrete gravity dam (c) Variation on total head along the slip plane. 192
Figure 6.18. Drain efficiency of an open drainage gallery system with Flow Option 5. (a) Wedge and uplift pressure diagram (water pressures not to scale) (b) Variation on total head along embedded part of the concrete gravity dam (c) Variation on total head along the slip plane. 194
Figure 6.19. Resultant factor of safety with residual imbalance of a five wedge system with Flow Option 6. 197
Figure 6.20. Drain efficiency of a closed drainage gallery system with Flow Option 6. (a) Wedge and uplift pressure diagram (water pressures not to scale) (b) Variation on total head along potential slip plane. 198
Figure 6.21. Drain efficiency of an open drainage gallery system with Flow Option 6. (a) Wedge and uplift pressure diagram (water pressures not to scale) (b) Variation on total head along potential slip plane. 200
Figure 7.1. System response curve for sliding limit state. 206
Figure 7.2. Geometry of concrete gravity dam 208
Figure 7.3. Three wedge system at base of dam. 210
Figure 7.4. Material attributes. 210
Figure 7.5. Resultant factor of safety with residual imbalance of a three wedge system with Flow Option 4. 211
Figure 7.6. Geometry of concrete gravity dam with variable pools. 212
Figure 7.7. Material attributes of probabilistic parameters. 213
Figure 7.8. System response curve with Flow Option 4 and 3000 simulations. 214
Figure 7.9. System response curves of GDLAD_Foundation and GDLAD_Sloping_Base. 214
Figure 7.10. Concrete gravity dam embedded in rock with rock foundation drain. 215
Figure 7.11. Concrete gravity dam with six wedges and two material regions. 216
Figure 7.12. Material Attributes of probabilistic parameters. 217
Figure 7.13. Attributes of drain model. 217
Figure 7.14. Reach attributes defining values for the Mechanical Aperture and JRC. 218

Figure 7.15. Reach numbers defining both rock joint reaches and rock drain reaches. 219
Figure 7.16. System response curve for a Stability and Joint_FLOW analysis. 220
Figure 7.17. Mean phreatic surface at selected nodal points. 221
Figure 8.1. Spillway layout and design 225
Figure A.1. Free body diagram of forces acting on each wedge. 232
Figure A.2. Table of wedge forces for trial safety factors. 234
Figure B.1. Five rock joints. 235
Figure B.2. Head boundary conditions. 237
Figure B.3. Generated rock joint element: (a) external sources, and (b) total head boundary conditions. 238
Figure C.1. Schematic diagram describing relationship expressed in bis 5.1. 250
Figure C.2. Schematic diagram example to illustrate the development of stiffness matrices. 252
Figure F.1 Original and Transformed sections for one-dimensional flow within two rock joint reaches in a single series. 270
Figure F.2. Non-overflow gravity dam embedded within a rock foundation: (a) Potential slip plane within rock regions with different hydraulic conductivities (K) (rock joint lengths not to scale), (b) Constant slope in total head with distance along the transformed length of the potential slip plane, and (c) Variation of slope in total head with distance along the three rock regions of the potential slip plane. 276

Tables

Table 1.1. Classifications of mechanical aperture of Ebeling et al. (1997) after Lee and Farmer (1993) and Barton (1973). 11
Table 2.1. Categorization and mapping of unit weights and effective shear strength parameter values to the three rock regions. 26
Table 2.2. Joint lengths and orientation along the base of each wedge/sub-wedge within a region. 27
Table 2.3. Rock joint apertures and the number of elements. 27
Table 2.4. Classification of uplift and interslice water forces as flow options. 32
Table 2.5. Description of Points and Locations 33
Table 2.6. Uplift resultant water pressure force U_i for flow options 1, 2, and 3. 44
Table 2.7. Computed factors of safety for flow options 1, 2, and 3. 45
Table 2.8. Difference between resultant water pressure forces acting on either side of the vertical face of wedges for flow options 1, 2, and 3. 45
Table 3.1. Classification of uplift and interslice water forces as flow options. 48
Table 4.1. Uniform aperture. 132
Table 4.2. Tapered downstream aperture; $e_{in} = z \cdot e_{out}$. 135
Table 4.3. Tapered upstream aperture; $z \cdot e_{in} = e_{out}$. 138
Table 4.4. Resultant uplift force and bending moments of variable apertures. 140
Table 5.1. Number of elements comprising each of the three major wedges. 157
Table 5.2. Values of the Hazen-Williams Coefficient, C_{HW}, and the Manning Roughness Coefficient, n, for common pipe materials. 158

Table 6.1. Categorization and mapping of unit weights and effective shear strength parameter values to the three rock regions. 167
Table 6.2. Joint Lengths and Orientation along the base of each wedge/sub-wedge. 167
Table 6.3. Classification of uplift and interslice water forces as flow options. 173
Table 6.4. Uplift resultant water pressure force U_i for Flow Options 4, 5, and 6. 201
Table 6.5. Computed factors of safety for Flow Options 4, 5 and 6. 202
Table 7.1. Model parameters with inherent uncertainty and default statistical values for non-site specific uplift pressures. 204
Table 7.2. Model parameters with inherent uncertainty and default statistical values for site specific uplift pressures. 205
Table 7.3. Model parameters with inherent uncertainty and statistical values for rock joint attributes. 205
Table 7.4. Description of nodes and locations. 209
Table 8.1. Description of wetted surface region no.'s. 225
Table C.1. Summary of friction factor equations for Darcy-Weisbach equation 244
Table C.2. Values of the Hazen-Williams Coefficient, C_{HW}, and the Manning's n, for common pipe materials 249
Table D.1. Table of units. 256
Table E.1 Table of units. 267
Table F.1. Summary of Original and Transformed section rock joint reach lengths and hydraulic gradients. 274

Preface

This research report describes the engineering formulation and corresponding software developed for expressing the computed stability results for an idealized two-dimensional cross-section of a non-overflow concrete gravity dam embedded in rock in terms of a fragility curve for a potential sliding mode of failure. Within the Corps, the term *system response curve* is being used to describe what is commonly referred to in the technical literature as the fragility curve; used for the hydrologic fragility assessment of concrete gravity dams embedded in rock. This report uses this Corps terminology. Uncertainty in strength, rock joint parameters that impact the flow of water within the rock joints, silt induced earth pressure and (post-tensioned) anchor force(s) are accounted for in a multivariate probabilistic stability analysis resulting in the computation of a system response curve. The PC software package GDLAD_Foundation (Gravity Dam Layout And Design) is used in this research and development (R&D) effort to perform the computations and construct the system response curve. Funding over the three years of R&D came from two sources: The first two years of partial funding to initiate research and software development was provided by Headquarters, U.S. Army Corps of Engineers (HQUSACE), as part of the Water Resources Infrastructure R&D Program. The research was performed under a Work Unit entitled “Simplified Probabilistic Models for Concrete Gravity Dams” for which Dr. Robert M. Ebeling, Computational Science and Engineering Division (CSED), Information Technology Laboratory (ITL), was the Principal Investigator. In addition, partial funding for the first two years and full funding during the third and final year of R&D was provided by the Risk Management Center. Dr. Maureen K. Corcoran, Geotechnical and Structures Laboratory, (GSL), was the Water Resources Infrastructure (WRI) Program Manager and Dr. Michael Sharp (GSL) was the WRI Technical Director for the first two years that WRI provided partial funding. Andy Harkness, Richard A. Allwes and David A. Margo have been the points of contact at the Pittsburgh, PA, Risk Management Center throughout this research effort.

The resulting engineering methodology and corresponding software is applicable to a two-dimensional model of a non-overflow (concrete) gravity dam founded within rock. GDLAD_Foundation is also capable of performing a deterministic steady state seepage analysis of laminar flow

within rock joints or a seepage analysis followed by a sliding stability evaluation.

This R&D study was conducted by Dr. Robert M. Ebeling, Moira T. Fong, ITL, Dr. Johannes L. Wibowo, GSL, and by Amos Chase, Sr., contractor. Dr. Ebeling was author of the scope of work for this research for this research. Initial programming of *Joint_FLOW*, based on the formulation developed by Dr. Ebeling, was made by Ronald E. Wahl, GSL, and Dr. Ebeling. This Joint_FLOW programming effort was then extended by Dr. Wibowo and concluded by Fong. The Drain Model Iteration Method discussed in Section 2.3 was proposed by Wahl. Initial programming of LinPipe was made by Dr. Wibowo and was concluded by Fong. The Appendix C summary of LinPipe was consolidated by Fong from earlier writings and notes made by Dr. Wibowo, who also provided final input to this Appendix. The final integration of the programs Joint_FLOW, LinPipe, GDLAD_Foundation stability, GDLAD_Foundation GUI and Visual Modeler was made by Fong, Chase and Dr. Ebeling. The report was prepared by Dr. Ebeling and Ms. Fong under the supervision of Dr. Robert M. Wallace, Chief, EISD, ITL and Dr. Reed L. Mosher, Director, ITL.

COL Kevin J. Wilson was Commander and Executive Director. Dr. Jeffery P. Holland was Director of ERDC.

Unit Conversion Factors

Multiply	By	To Obtain
cubic feet	0.02831685	cubic meters
cubic inches	1.6387064 E-05	cubic meters
degrees (angle)	0.01745329	radians
degrees Fahrenheit	(F-32)/1.8	degrees Celsius
feet	0.3048	meters
foot-pounds force	1.355818	joules
inches	0.0254	meters
inch-pounds (force)	0.1129848	newton meters
microns	1.0 E-06	meters
pounds (force)	4.448222	newtons
pounds (force) per foot	14.59390	newtons per meter
pounds (force) per inch	175.1268	newtons per meter
pounds (force) per square foot	47.88026	pascals
pounds (force) per square inch	6.894757	kilopascals
pounds (mass)	0.45359237	kilograms
pounds (mass) per cubic foot	16.01846	kilograms per cubic meter
pounds (mass) per cubic inch	2.757990 E+04	kilograms per cubic meter
pounds (mass) per square foot	4.882428	kilograms per square meter
square feet	0.09290304	square meters
square inches	6.4516 E-04	square meters

1 Uplift and Sliding Stability System Response Curve for a 2-D Non-Overflow Gravity Dam Section Embedded in Rock

1.1 Introduction

Uplift is a major force affecting the stability of concrete gravity dams founded on rock. Uplift forces decrease the resistance of the dam to sliding. A sliding stability assessment of a non-overflow gravity dam embedded in rock requires the assignment of uplift water pressure forces acting on the driving, the structural and the resisting wedges. This report summarizes an engineering methodology and corresponding PC-based software environment, (Gravity Dam Layout and Design) GDLAD_Foundation that is used in the evaluation of the sliding stability analysis of a non-overflow gravity dam two-dimensional (2-D) section embedded in rock for a hydraulic hazard. This software package is referred to as GDLAD_Foundation. The PC-based software GDLAD_Foundation offers a comprehensive environment for the following:

1. A Visual Modeler that facilitates problem definition, development of data input, execution of the engineering software and visualization of computed results;
2. FORmula TRANslation (FORTRAN) engineering software to compute the stability, via the wedge method of analysis, of the embedded gravity non-overflow (2-D) cross-section;
3. The computation of uplift caused by flow along rock joints contained within the rock foundation. Incorporated within the GDLAD_Foundation software is the FORTRAN program Joint_FLOW that is used to assess fluid flow along rock joints, fissure and/or faults contained within the rock foundation.

From the user specified definition of rock joint reaches within the foundation, the stability of the user selected potential failure plane(s) is made. There are three sets of “wedges” in this methodology, the driving, structural and resisting wedges. These wedges are evaluated in the equilibrium analysis and include consideration of the distribution of water pressures (derived, e.g., from the flow of water contained within the joints by

Joint_FLOW) in the computation of the uplift force acting on the base of each of the wedges.

1.1.1 Deterministic and probabilistic analysis capabilities

Deterministic and probabilistic methods of analysis are available by GDLAD_Foundation for the hydraulic hazard. Deterministic analyses currently result in the computation of a factor of safety (*FS*) against sliding. With the specification of a range in pool and tailwater elevations, probabilistic analyses result in the computation of a system response curve for the sliding limit state due to statistically defined uncertainties in rock joint strength parameters and parameters that are used to define rock joint permeability. Statistical uncertainties in silt load and anchor forces, if present, may also be included in the analysis.

1.1.2 The system response curve

In safety or risk assessment of dams, limit states or probability of failure serve as yardsticks of system performance. The system response curve is used to predict the probably of dam failure, given the hydraulic hazard. Consider the example of a dam in which the sliding limit state, i.e., $FS_{slide} \leq 1.0$, is the limit state resulting in failure of the dam. Introducing the names for the variables used in this report into Equation 5.1 of Tekie and Ellingwood (2002), the probability of failure, $P_{failure}$, is given by the expression

$$\boldsymbol{P}_{\boldsymbol{failure}} = \sum_{\boldsymbol{H}_{\boldsymbol{Pool}}} \boldsymbol{P}(\boldsymbol{FS}_{\boldsymbol{slide}} \leq 1.0 | \boldsymbol{Pool} = \boldsymbol{H}_{\boldsymbol{Pool}}) \boldsymbol{P}(\boldsymbol{Pool} = \boldsymbol{H}_{\boldsymbol{Pool}}) \tag{1.1}$$

in which *Pool* is a vector of random variables describing the intensity of demand (e.g. pool elevation, etc.) and other factors; $P(Pool = H_{Pool})$ is the hazard, considering channel inflows and storm runoff from the watershed behind the dam, and is expressed in terms of annual probability; and $P(FS_{slide} \leq 1.0 \mid Pool = H_{Pool})$ is the conditional probability of structural failure, given that $Pool = H_{Pool}$, is obtained for the Figure 1.1 system response curve developed using the engineering procedure and corresponding PC-based software discussed in this report. Expressing the limit state probability as in Eq. 1.1 allows the overall risk to be deconstructed into its significant contributors.

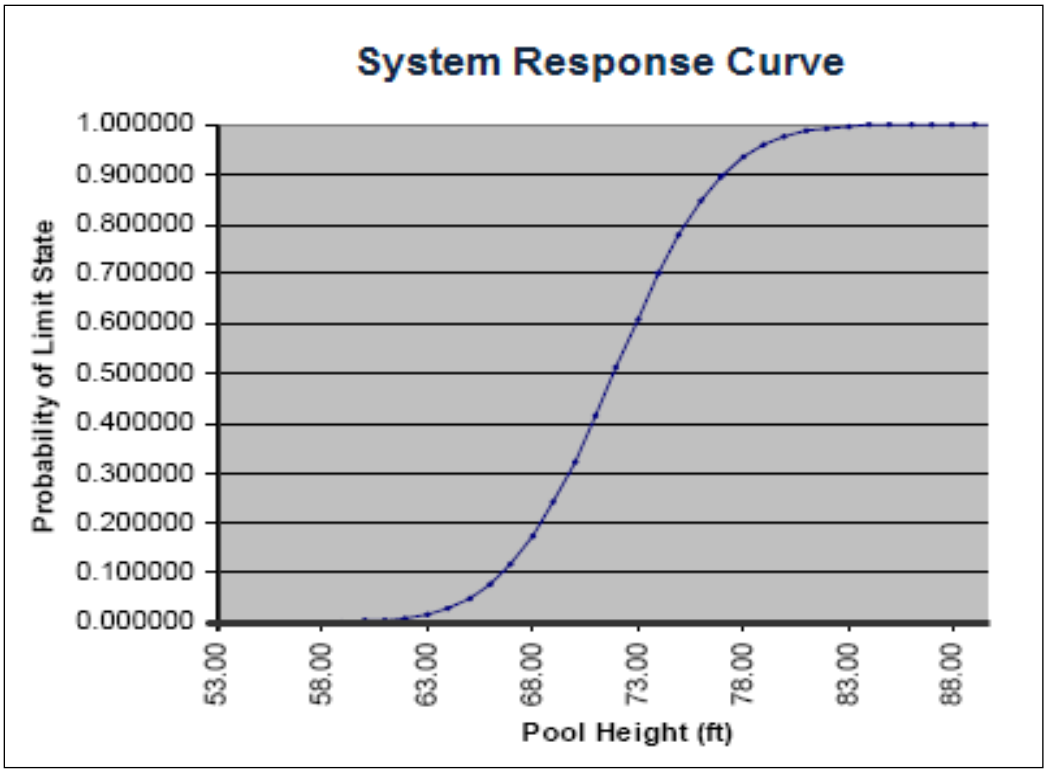

Figure 1.1. System response curve for sliding limit state.

Tekie and Ellingwood (2002, Chapter 6) observe that a fully coupled probabilistic safety assessment combines the probabilistic/statistical definitions of hazard (i.e., demand) and system response curve (i.e., capacity) and leads to a point or interval estimate of failure state probability for the limit state associated with dam failure, depending on how the epistemic uncertainties are incorporated in the analysis. The hazard is described by the complementary cumulative distribution function (CCDF) and the system response curve is defined by the cumulative distribution function (CDF) of the system response curve. Tekie and Ellingwood observe that the probability of failure can be expressed as the convolution of the hazard function and the system response curve in their Equation 6.1, an integral form of Equation 1.1 above. Additionally, modeling (epistemic) uncertainties propagated through the analysis of the hazard and fragility will give rise to a distribution for the probability of failure, $P_{failure}$, as depicted in Figure 6.1 in Tekie and Ellingwood (2002). So if the mean hazard and mean system response curve are used, they observe that the convolution integral (their Equation 6.1) yields a point estimate for the limit state probability. Citing previous research published by Ellingwood, they conclude that this point estimate does not necessarily yield the mean of $P_{failure}$, as the uncertainties are not propagated in the same way but this estimate is usually close to the mean of $P_{failure}$.

Within the Corps, the term system response curve is now being introduced to describe what has been referred to commonly in the technical literature as the fragility curve; the term is used for the hydrologic fragility assessment of rock-founded concrete gravity dams. This report uses this new Corps terminology. Tekie and Ellingwood (2002), along with others, discuss the development of fragility curves used in a hydrologic fragility assessment and the computation of the probability of failure of a rock-founded gravity dam.

1.2 Analytical methods in uplift prediction

There are several problems associated with analysis of uplift and its effects on dam stability. Problems arise when trying to determine the magnitude and distribution of uplift pressures and resultant uplift forces in foundations that are heterogeneous and that have discrete rock discontinuities[1] (e.g., joints, faults, and bedding planes). Another problem is extrapolating foundation uplift pressures to pools above the pool of record. Stability problems arise if drains are not maintained, because the ability of drains to dissipate uplift pressures diminishes with time. Similarly, discontinuities may close and become less permeable with time as rising pool levels compress the foundation, resulting in higher uplift pressures. Nonuniform stresses imposed by the dam may deform discontinuities differentially, resulting in tapered joints with varying apertures and variable distribution of uplift pressures.

Conventional equilibrium methods of analysis of the stability of gravity dams involve assumptions regarding the loading and resisting forces that act on a dam. Analyses of loading and resisting forces consider the magnitude and distribution of uplift pressures and effective compressive stresses, respectively, acting normal to the base of the dam (Pace and Ebeling 1998). Uplift pressure is water pressure, defined at any point along the rock joints that contain the fluid flow within the foundation as the unit weight of water (γ_w) times the depth below the piezometric surface. Water pressure reduces the effective stress on potential failure planes, such as the base of a gravity dam situated on rock, and thereby lowers the resistance to shear failure along a plane. The relationship is shown mathematically in the familiar expression:

[1] Throughout this report, for brevity, the term joint or jointed is substituted for the more general term discontinuity or discontinuous. In many cases, joints are the proper and intended reference. It should be understood, however, that other discontinuities, including bedding planes, shears, etc., are equally pertinent.

$$\tau = c + \sigma - u \cdot \tan\varphi \quad (1.2)$$

where

τ = the shear strength, or shear stress required to cause sliding along a plane
c = cohesion of the rock/rock or concrete/rock interface
σ = the total normal stress component of load on the plane
u = the pore (uplift) pressure produced by the head of groundwater
φ = the angle of internal friction along the potential failure plane

The term (σ - u) is the effective stress on the plane resulting from the reduction in normal stress by the pore, or uplift, pressure. In rock foundations, uplift pressures commonly develop in discrete discontinuities (e.g., rock joins) within the rock mass.

Following Stone and Webster Engineering Corporation (1992), uplift pressures can be reported as equivalent piezometric head in feet of water (gauge pressure in psi, times 2.31 ft of water per psi, plus the elevation of the gauge). Reporting uplift pressures as piezometric head allows comparison directly with reservoir (headwater) and tailwater elevations. Uplift pressures are controlled by the flow regime within the rock foundation. The flow regime is a function of site-specific geology, especially the distribution and geometry of the discontinuities through which groundwater flows. Both the geological interpretation of foundation conditions and the analytical procedures used to calculate flow within the foundation introduce uncertainty into the prediction of uplift pressures.

Grenoble et al. (1995) studied the influence of deformation of discontinuities on uplift pressures in concrete gravity dams [also in Stone and Webster Engineering Corporation (1992), for the Electric Power Research Institute (EPRI)]. They state that stability calculations often assume that the rock mass behaves like a porous medium and that foundation uplift pressure is distributed linearly from the upstream face of the dam (or from the position of the drains) to the toe (Figure 1.2)[1]. In considerations of flow and developed uplift pressures, the foundation rock mass cannot be treated as a porous medium unless the joint spacing is so small that the

[1] Non-site-specific uplift pressure distribution used in the design and analysis of Corps dams is given in EM 1110-2-2200, EM 1110-2-2100, and discussed in Ebeling et al. (2000).

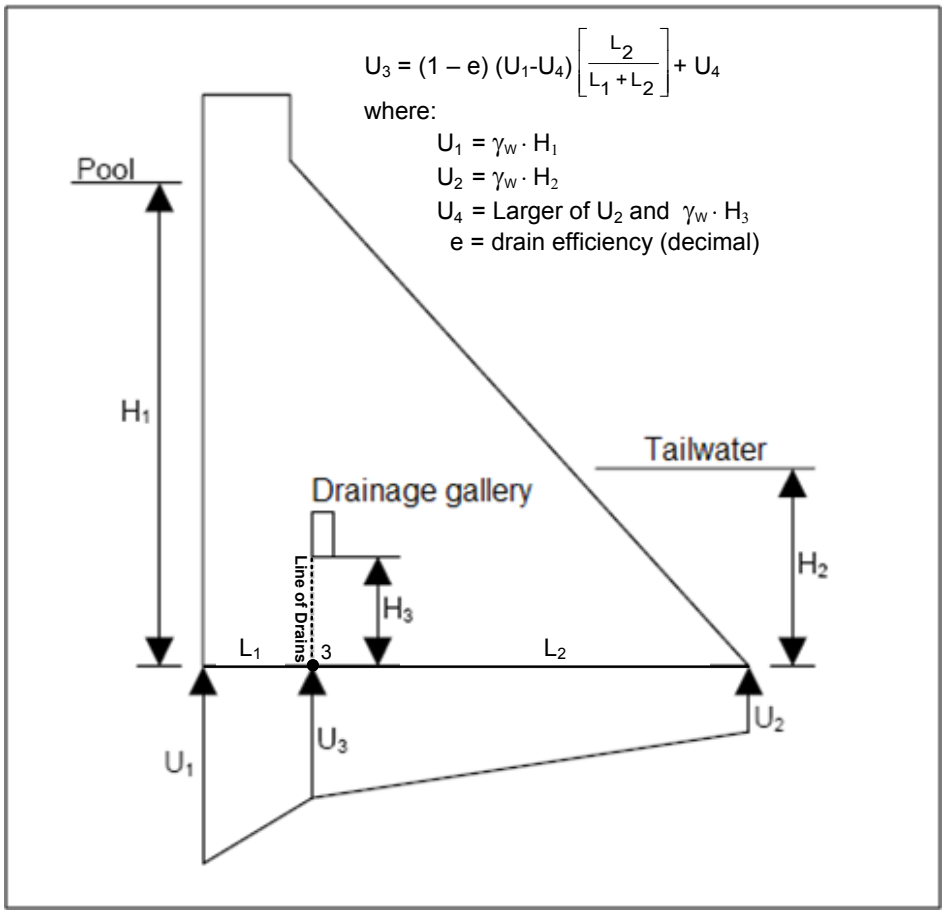

Figure 1.2. Uplift distribution with foundation drains for an "open drainage gallery system" (after EM 1110-2-2100).

rock is effectively a continuum. In jointed rock masses, the distribution of uplift pressure is controlled by the geometry and hydraulic conductivity of the intersecting joints that make up the flow paths beneath the dam.

The preferred method for determining uplift pressures beneath dams is the use of accurate piezometric instrumentation data. When instrumentation data are not available or when the reservoir levels to be analyzed exceed those for which the piezometric measurements were made, other procedures must be used to establish the distribution of flow and the corresponding uplift pressures. One method used widely by engineers to establish uplift pressures along a section within a rock foundation is to compute uplift pressures from flow within rock joints. Ebeling and Pace (1996a) investigated the fundamentals of flow through jointed rock and how the dimensions of rock joints, especially joint aperture, influence computed uplift pressures.

1.2.1 Open and closed drainage gallery systems

The authors of this report categorize a drainage gallery system as either open or closed when applying (Figure 1.2) non-site specific uplift pressure distribution relationships. Observe via the (Figure 1.2) insert equation for U_4 that an "open drainage gallery system" is inferred. This is because at the intersection of the line of drains with the potential horizontal slip plane, designated by the authors of this report as point 3 in this figure, the pressure head used in the uplift pressure distribution calculation (for U_4) is the larger of (1) a tailwater pressure head of H_2 or (2) a pressure head corresponding to the vertical distance from point 3 to the elevation of gallery floor (a vertical distance equal to H_3). In an open drainage gallery system, foundation drainage water collected from a shallow channel over the drain openings in the gallery floor is being drained out through an "open drainage gallery system" that extends from this shallow gallery floor channel out to the downstream face of the dam under gravity flow. If not "blocked" by say a one-way valve, this gallery drainage feature will also allow high tailwater to induce the tailwater to flow back up this same drainage feature and into the gallery. This case is idealized in the Figure A2a depiction given in Appendix A of Ebeling et al. (2000). The authors of this report observe that the uplift water pressure equation for U_4 of Figure 1.2 is valid for a horizontal failure plane of an open drainage gallery system. An inclined failure plane requires a higher fidelity figure for the uplift pressure distribution calculation.

A "closed drainage gallery system" is a second type: In this case, foundation drainage water collected from a shallow channel over the drain openings in the gallery floor is collected in a sump that is in-turn, pumped out of the gallery. A closed drainage gallery system requires that the outlet feature downstream of the dam is of sufficient height that tailwater cannot back-up into this outlet and then on into the gallery. The authors of this report observe that the uplift water pressure equation insert for U_4 given in Figure 1.2 would need to be altered for a closed drainage gallery system. For a horizontal potential slip plane and a closed drainage gallery system, the value assigned to U_4 would be set equal to H_2 times the unit weight of water (γ_w). An inclined failure plane requires a higher fidelity figure for the uplift pressure distribution calculation.

1.2.2 Interrelationships between uplift pressure, pressure head, and total head

In the simplified case of flow along the horizontal dam-to-foundation interface, as depicted in Figure 1.3, there is a convenient interrelationship between uplift pressure and total head.

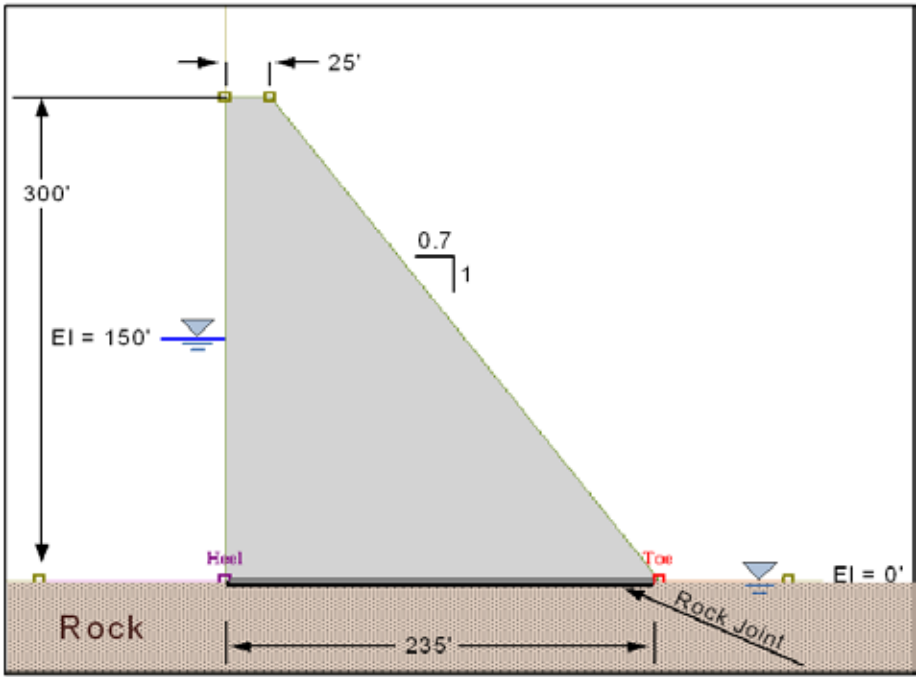

Figure 1.3. Hypothetical gravity dam cross-section with a horizontal rock joint along the dam-to rock foundation interface (no drain).

According to the Bernoulli equation for ideal flows, i.e. steady, frictionless, incompressible flows, the total head, H, at any point can be determined by taking the sum of the pressure head, h_p, the velocity head, h_v, and the elevation head, h_z

$$H = h_p + h_v + h_z \tag{1.3}$$

where the pressure head is defined as the ratio of the water pressure to the unit weight of water ($h_p = u/\gamma_w$), the velocity head is the ratio of velocity squared to twice the gravitational constant ($h_v = V^2/2g$), and the elevation head is the elevation with respect to the datum ($h_z = z$). The total head can therefore be represented as

$$H = \frac{u}{\gamma_w} + \frac{v^2}{2g} + z = \text{constant} \tag{1.4}$$

The authors of this report are finding that the Joint_FLOW analyses are showing that lamina flow occurs at very low velocities within the rock joints. The velocity head, in this case is negligible, with the total head given by

$$H = h_p + h_z \tag{1.5}$$

In our applications to Figure 1.3 type of problems involving a horizontal rock joint, we apply the simplified hydrostatic Bernoulli's equation, Equation 1.5, in order to determine the pressure head, $h_p = H - h_z$. Consequently, the water pressure at a specified point within a rock joint is

$$u = \gamma_w (H - h_z) \tag{1.6}$$

In this report, water pressure, u, at a point within a rock joint is sometimes referred to as uplift pressure.

Consider the special case of a single horizontal rock joint located below the base of the (Figure 1.3) concrete monolith. Assume the datum at EL 0, the case shown is for a 150 ft pool and 0.0 ft tailwater. The Figure 1.3 hypothetical dam is 300 ft high and 235 ft wide. Again, assuming lamina flow occurs at very low velocities within the rock joints, the velocity head is approximately zero. Since the single rock joint is located at an elevation (el) of 0.0 ft, the elevation head, h_z, will be zero. Consequently, the total head, H, is equal to the pressure head, h_p. Thus Equation 1.5 simplifies to

$$H = h_p \tag{1.7}$$

and the water pressure, u, is given by

$$u = \gamma_w \cdot h_p \tag{1.8}$$

1.3 Joint aperture and uplift pressure distribution

Flow through a joint is a function of the aperture (size of the opening) and joint roughness. (This is also true for flow through a pipe.) Joint aperture, discussed further in Chapter 4 of this report, can be measured in the field with techniques such as borehole camera surveys. Aperture determines the effective porosity and hydraulic conductivity of a jointed rock mass and ultimately affects the distribution of uplift pressure beneath a dam. Field measurements of rock joints provide what is known as a mechanical aper-

ture (Barton et al. 1985). A mechanical aperture has a degree of asperity, or roughness, manifested by irregularities or undulations on its surface. Joint roughness affects the flow of water through the joint. Mathematical simulation of flow through the joint requires that the mechanical joint aperture be reduced to a pair of smooth parallel plates, or a conducting aperture, for computations of laminar flow and hydraulic conductivity. The mechanical aperture is designated *E* and the equivalent, or conducting, aperture is designated *e*. The conducting aperture is the distance between two smooth, parallel plates that would allow the same flow as a mechanical (joint) aperture with rough walls. Conducting aperture e is always smaller than mechanical aperture *E* except in the case of smooth-walled joints when *E* is equal to *e*. Figure 1.4 illustrates the concept. Mechanical aperture is measured directly from a rock sample or, in the field, on exposed joints. Conducting aperture is estimated from permeability or pressure tests.

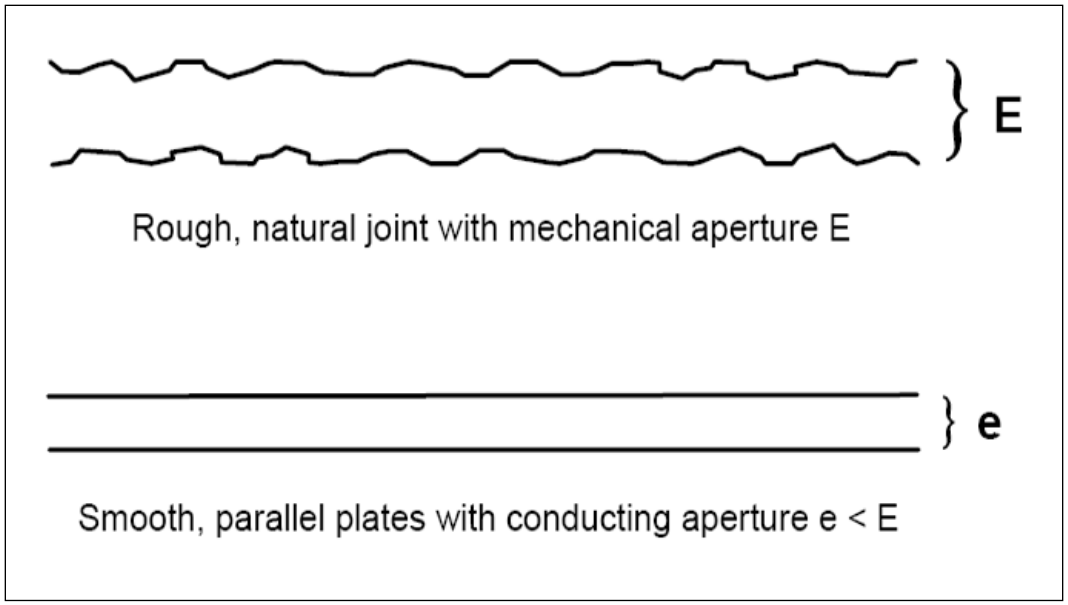

Figure 1.4. Natural rock joint with mechanical aperture *E* and equivalent parallel plates with conducting aperture *e* (not to scale).

The terms “open” and “tight” joints or discontinuities will be used often in this report. Snow (1968) defined open fractures as those having apertures of 35 μm (0.35 mm) or greater. His apertures were apparently equivalent, smooth-walled, *conducting* apertures computed from borehole pressure tests. Bieniawski (1979), for his Rock Mass Rating System for tunnel design, considered joints open at *mechanical* apertures of 2,500 μm (2.5 mm) or greater. International Society for Rock Mechanics (ISRM) (1978), proposing discontinuity descriptors for rock mass classification, defined open joints as

those with *mechanical* apertures of 500 μm (0.5 mm) or greater. Ebeling et al. 1997 adopted a mechanical aperture of 250 μm (0.25 mm) as the lower limit of open joints from work reported in Lee and Farmer (1993), who used data from Barton (1973).

EM 1110-1-2908 applied a similar classification scheme to discontinuities in his discussion of rock mass characterization for rock foundations. Table 1.1 shows the aperture classification used by Lee and Farmer (1993), by Ebeling et al. (1997) and by Nicholson (1983). The relative importance of mechanical and conducting apertures to flow modeling and prediction is discussed by Murphy et al. (2002). Following work by Ebeling and others, a tight joint in this report is assumed to be one with a mechanical aperture less than about 250 μm (0.25 mm).

Table 1.1. Classifications of mechanical aperture of Ebeling et al. (1997) after Lee and Farmer (1993) and Barton (1973).

Mechanical Aperture, mm (μm)[1]	Class
<0.1 (< 100)	Very tight
0.10 – 0.25 (100 - 250)	Tight
0.25 – 0.50 (250 - 500)	Partly open
0.50 – 2.50 (500 - 2,500)	Open
2.50 – 10.0 (2,500 – 10,000)	Moderately wide
>10.0 (> 10,000)	Wide

[1] Mechanical aperture classification of Nicholson (after EM 1110-1-2908):

Very tight: separations of less than 0.1 mm (< 100μm).

Tight: separations between 0.1 and 0.5 mm (100 and 500μm)

Moderately open: separations between 0.5 and 2.5 mm (500 and 2,500μm)

Open: separations between 2.5 and 10 mm (2,500 and 10,000μm)

Very wide: separations between 10 and 25 mm (10,000 and 25,000μm)

Grenoble et al. (1995) simulated foundation loading using finite element analysis and measured uplift pressures on 17 dams over a period of a year. Their studies showed that rising reservoir levels differentially deformed discontinuities in the foundation and caused the hydraulic conductivity in rock joints to increase at the heel and to decrease at the toe, a condition simulated by a tapered joint. If the hydraulic conductivity does not change, the uplift pressure beneath the dam is linearly proportional to the headwater pressure (reservoir level). However, if joint hydraulic conductivity changes because of induced joint deformations (i.e., the taper of the joint changes with rising reservoir levels), the relationship between uplift pres-

sure and headwater pressure is nonlinear. The next several paragraphs discuss the relationship of uplift pressure with reservoir loading. Note that one relationship is the variation in uplift pressure with distance along the dam base, and the other is the variation in uplift pressure *at a point* within the foundation as headwater pressure changes.

Change in aperture in the direction of flow causes uplift pressure to follow a curved rather than a linear distribution. Figure 1.5a shows the linear pressure distribution within a joint of constant aperture from the heel to the toe of a dam. Figure 1.5b shows the pressure distribution in a joint network represented by a large-aperture pipe and a small-aperture pipe. Most of the pressure loss occurs in the smaller pipe because of high frictional losses. The result is, in effect, a nonlinear pressure distribution between the heel and toe. Figure 1.5c shows the analogy extended to nonlinear pressure distribution for a tapered joint, for which the aperture changes (steps down) continuously from the heel to the toe.

Changes in loading of the dam foundation, for example by rising reservoir levels, can decrease joint aperture near the toe and increase joint aperture near the heel. Pressure against the upstream face of the dam tilts the dam. Deformation of joints affects the hydraulic conductivity and the uplift pressures that develop in the dam foundation. Ebeling and Pace (1996b) and Pace and Ebeling (1998) investigated the effect of foundation loading (increasing pool elevation) on uplift pressures using finite element modeling. In their model, they varied the pool elevation, which resulted in changes in stresses on foundation joints during reservoir loading (and unloading when the pool was lowered). Figure 1.6 shows the nonlinear change in uplift pressure (as head) with rising reservoir (headwater) elevation, measured at six locations along the joint. The nonlinear variation in uplift head with headwater elevation along the joint reflects the changes in aperture with loading and unloading along the joint. The nonlinear response of uplift pressure to reservoir height was obtained in what are considered tight joints, i.e., joints with mechanical apertures less than about 250 μm (0.25 mm). Stone and Webster Engineering Corporation (1992) reported that of 17 dams and locks investigated for uplift stability evaluation, two dams and one lock wall showed a nonlinear response (in gauge readings) of uplift pressure to reservoir elevation changes, eight showed linear responses, and six had insufficient data for a determination.

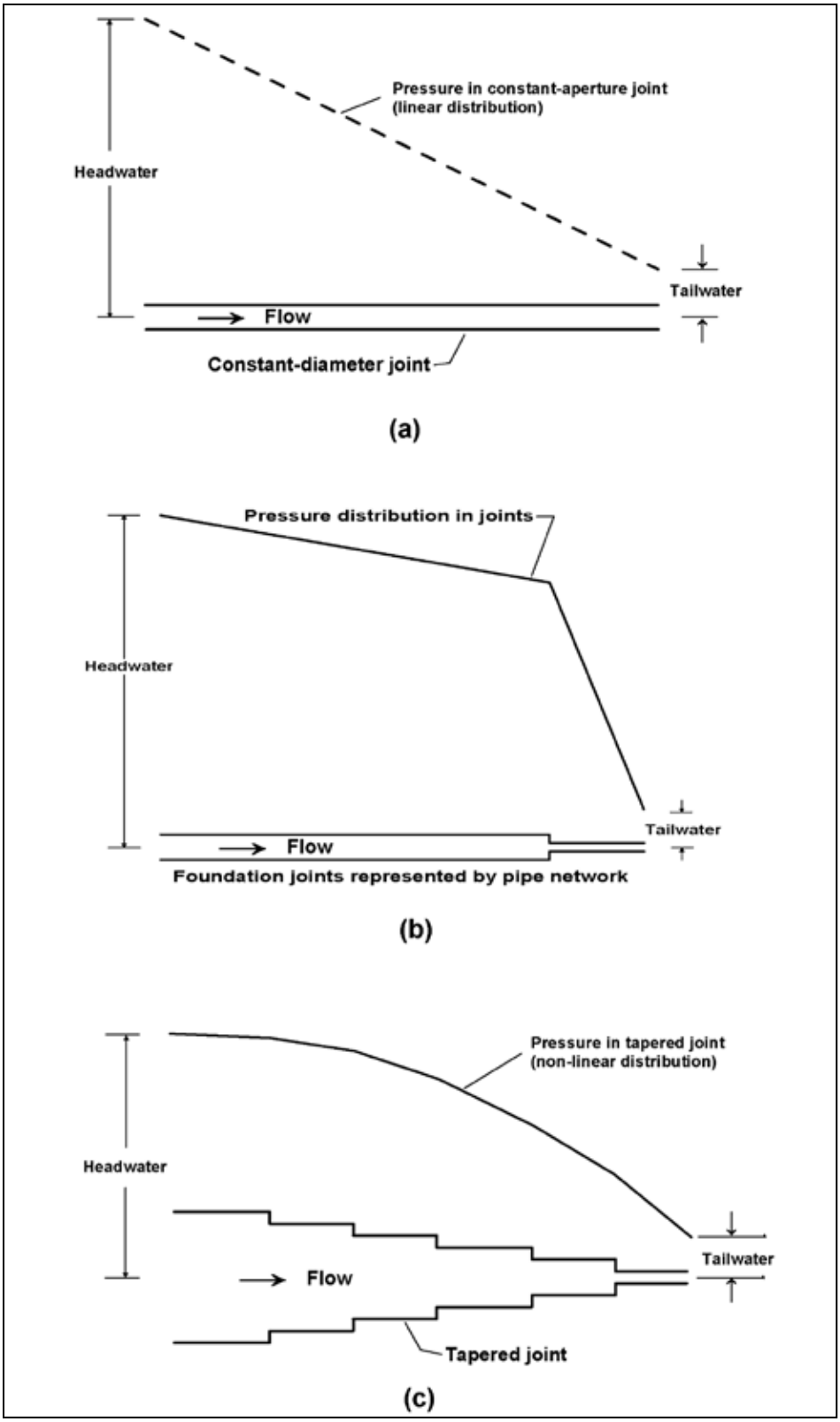

Figure 1.5. Distribution of uplift pressure in (a) joint of uniform aperture, (b) two-joint network, and (c) tapered joint (after Grenoble et al. 1995).

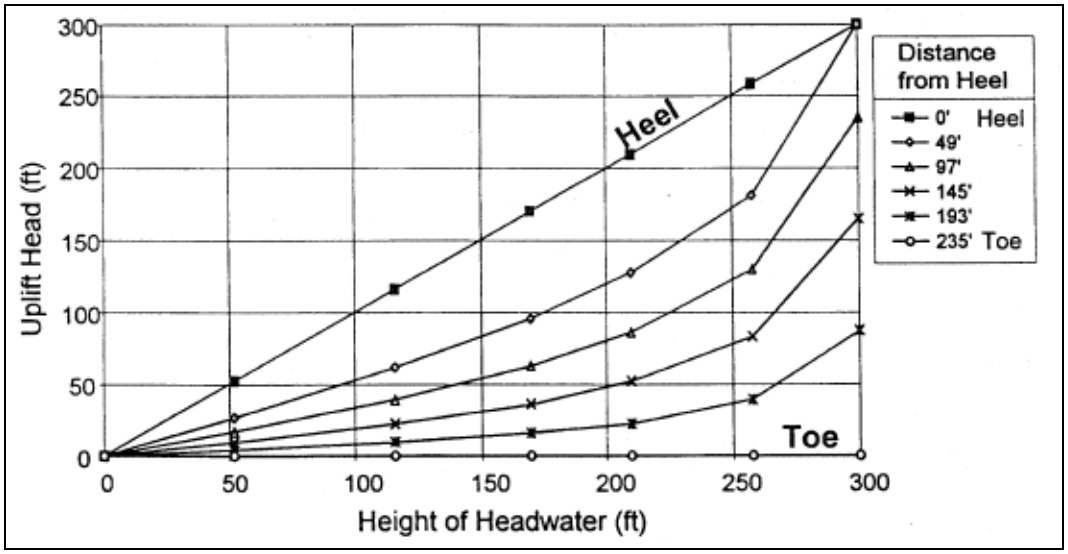

Figure 1.6. Nonlinear response of uplift pressure (as head) to rising reservoir headwater at six positions along a continuous joint of uniform aperture (Ebeling and Pace 1996b).

Murphy et al. (2002) expanded the discussion of the influence of joint aperture by looking at the effect of tapered joints on the distribution of uplift pressure across the base of the dam. The direction of the taper influenced the distribution of uplift pressure. A joint of uniform aperture across the base of the dam produced a linear pressure response (Figure 1.7a). A taper with a larger aperture at the heel than at the toe produced an uplift pressure distribution that is greater than the conventional linear assumption (i.e., the pressure increased more rapidly along the length of the dam, Figure 1.7b). A taper with a smaller aperture at the heel than at the toe of a dam produced an uplift pressure distribution that is less than the conventional linear assumption (i.e., the pressure increased more slowly along the length of the dam, Figure 1.7c).

Figure 1.7 shows the distribution of total head along the horizontal rock joint. Assuming a datum along the centerline and using the Bernoulli equation for ideal flow with an assumption that the velocity is small, the total head equals the pressure head. Consequently, the uplift pressure in Figure 1.7 is equal to the head value times the unit weight of water, γ_w.

Grenoble et al. (1995) illustrated the nonlinearity effect of changing joint taper at a point in the dam foundation as headwater elevations increased (Figure 1.8). If joint taper and hydraulic conductivity do not change, the uplift pressure at a point changes linearly with rising headwaters. If joint taper increases with rising headwater (joint hydraulic conductivity decreases toward the toe), uplift pressure at the point increases nonlinearly.

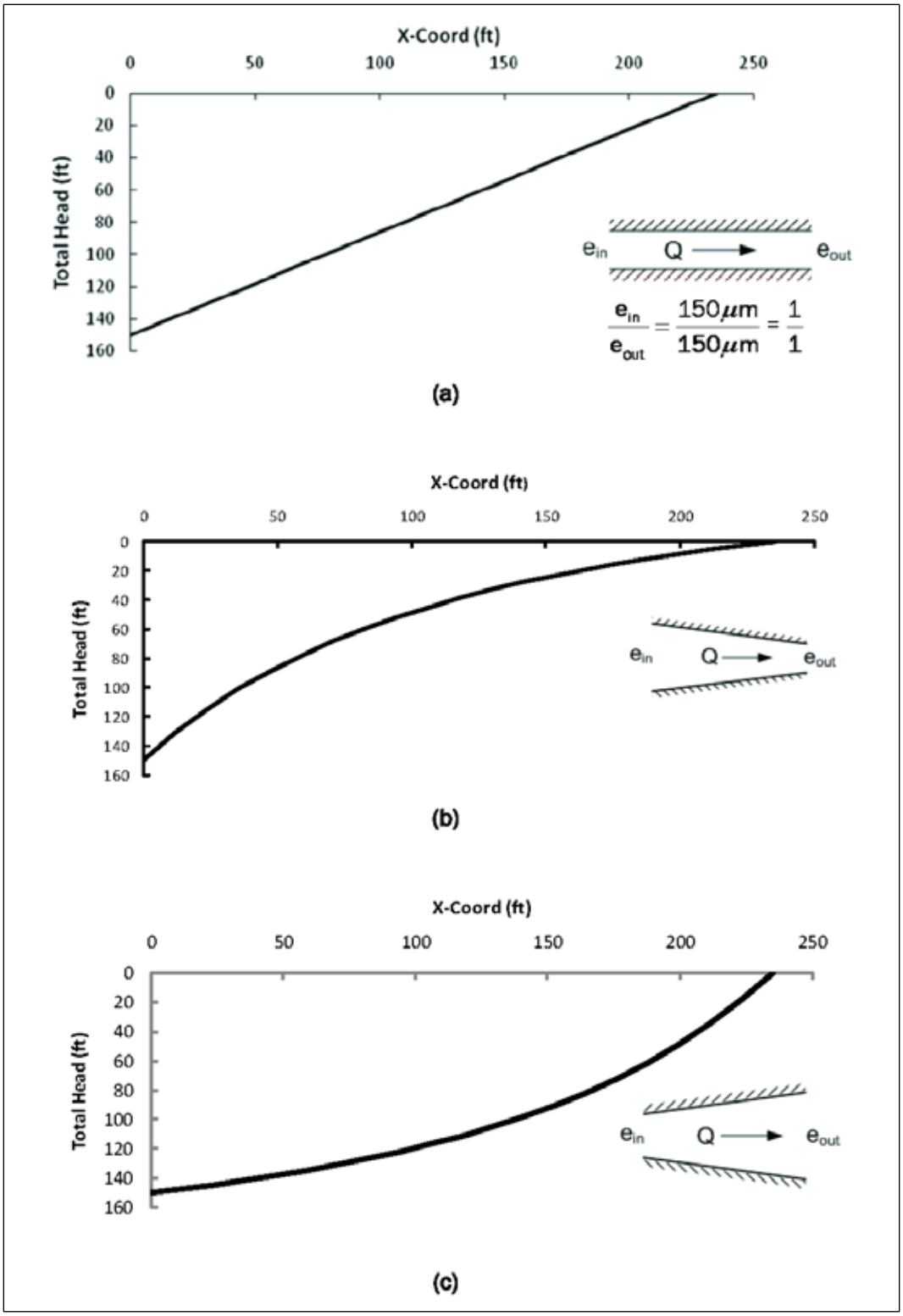

Figure 1.7. Variation in uplift pressure (head) along (a) uniform, (b) tapered heel to toe, and (c) tapered toe to heel. *e* is the conducting joint aperture.

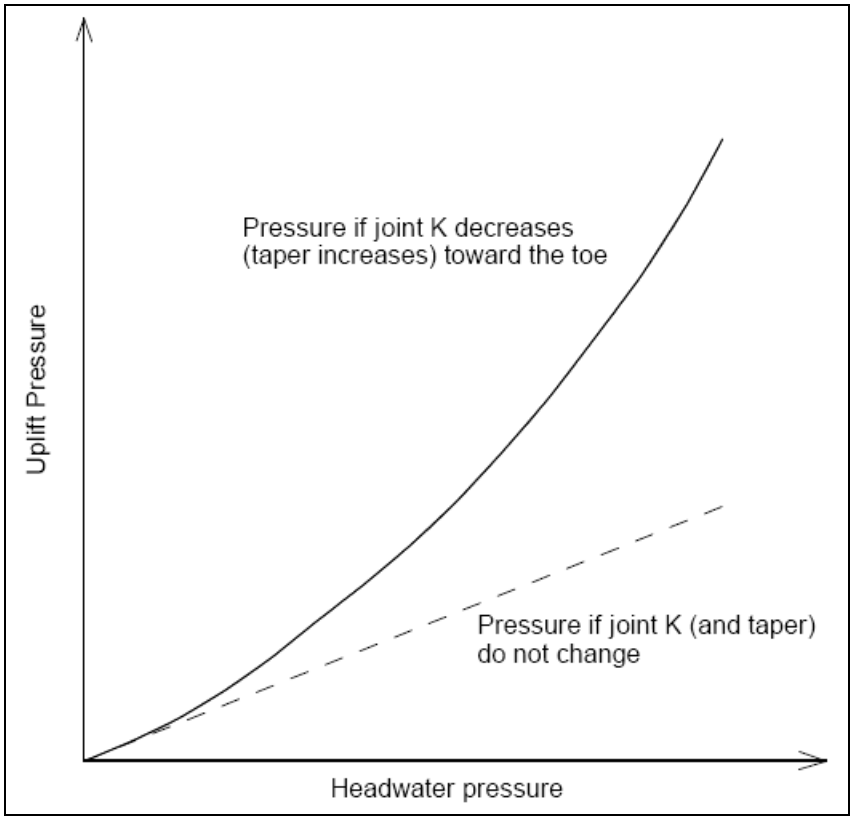

Figure 1.8. Variation in uplift pressure with changes in joint hydraulic conductivity (changes in joint aperture) with rising reservoir levels at a point in a dam foundation (after Grenoble et al. 1995).

Murphy et al. (2002) discuss other geological aspects of discontinuities in controlling the distribution of uplift pressure in a dam foundation, including joint aperture, joint length, and joint interconnectivity. Risk assessment of a dam must account for uncertainties in all factors that impact the computation of uplift pressures. To compute realistic deterministic or probabilistic estimates of uplift pressures within a rock foundation, investigative methods must be formulated to permit the development of a realistic fluid flow model for a rock foundation with discontinuities. Stone and Webster Engineering Corporation (1992) provide an excellent evaluation of the effects of geologic conditions on uplift pressure distributions for several existing large concrete gravity dams.

1.4 Laminar and turbulent flow in joints

Estimates of the hydraulic conductivity of jointed rock masses using Darcy's law are valid only for laminar flow. It is important to understand the relationship between the size of joint openings (aperture), joint roughness, and laminar flow. Todd (1980) discussed the range of validity

of Darcy's law for flow in porous media. By analogy with flow in a tube, the Reynolds number (R_e) was employed to define the limit of flows described by Darcy's law. Experiments showed that Darcy's law is valid for porous media, i.e., that flow is laminar, for a Reynolds number up to about 10.

Ebeling et al. 1997 discussed the importance of determining whether flow within a rock joint is laminar or turbulent. The cubic law assumes a linear relationship between Darcian velocity (or specific discharge) and the hydraulic gradient; and thus, is valid only for laminar flow conditions. The Reynolds number is a dimensionless number expressing the ratio of inertial to viscous forces in flow. Specifically,

$$R_e = \frac{v \bullet D_h}{v_w} \tag{1.9}$$

where

R_e = Reynolds number
v = mean specific discharge (Darcian velocity)
D_h = equivalent hydraulic diameter
= 2 times the conducting aperture, e, (Ebeling et al. 1997), and
= 4 times the average flow passage area divided by the perimeter (Iwai 1976)
v_w = kinematic viscosity of water = $(g \cdot \mu_w/\gamma_w)$, where μ_w is the dynamic viscosity, γ_w, the unit weight of water, and g, the acceleration by gravity (Zeigler 1976, p 9).

Zeigler (1976)[1] provided the following relationships for laminar, transitional (nonlinear laminar), and turbulent flow, respectively, in rock fissures:

$$v_w = K_{RJ} \cdot i \quad \text{(laminar flow)} \tag{1.10}$$

$$v_w{}^{m1} = K'_j \cdot i \quad \text{(hydraulically smooth regime - turbulent flow) [nonlinear laminar flow]} \tag{1.11}$$

$$v_w{}^{m2} = K'_j \cdot i \quad \text{(rough regime - turbulent flow)} \tag{1.12}$$

[1] Zeigler (1976) provides a rigorous and thorough review and evaluation of the theory of flow in fractured rock and of practices for determining rock mass hydraulic properties. He also presents derivations of most of the equations of flow used in this report.

where K'_j is the turbulent fissure hydraulic conductivity, K_{RJ} is the hydraulic conductivity of a single rock joint, and i is the hydraulic gradient. Equations 1.10 through 1.12 were derived in work by Sharp (1970) and Louis (1969). The exponent m is generally between 1 and 2 (Zeigler 1976), with $m1 < m2$. Equation 1.11 illustrates that the change in v_w is not linear with respect to the hydraulic conductivity in the transitional range.

The higher the Reynolds number, the more likely that turbulence will occur. The equivalent hydraulic diameter, D_h, for confined flow in a rock joint is defined as four times the average flow passage area divided by the perimeter, and is equal to two times the conducting aperture e [Ebeling et al. (1997), citing Iwai (1976)]. From Equation 1.9 with $D_h = 2e$,

$$R_e = \frac{v \cdot (2e)}{u_w} \tag{1.13}$$

which is the expression for the Reynolds number for flow between smooth parallel plates.

The critical R_e is the Reynolds number at which nonlinear laminar flow starts to occur. Flow in cylindrical pipes is laminar for $R_e < 2{,}100$ and turbulent for $R_e >> 2{,}100$. For values of R_e between 2,100 and 4,000, the flow is transitional between laminar and turbulent. For open flow in parallel walls, the critical R_e is 1,000. For flow in an open channel, the critical R_e is 500.

A geometric dependence on R_e delineating laminar and turbulent flow also exists for flow in rock joints. Iwai (1976) showed from studies of flow in rock joints that turbulent flow was evident when the Reynolds number exceeded a value of 100. The critical Reynolds number decreases with increasing aperture roughness. Figure 1.9 shows one example from the technical literature of a curve relating flow condition to specific discharge and Reynolds number. The curve shows that nonlinear laminar flow can occur for Reynolds numbers between 5 and 100. Nonlinear laminar flow is a transitional state between laminar and turbulent flow. Laminar and Darcian flow are typical when the Reynolds number is less than about 5. As Freeze and Cherry state, specific discharge (Darcian velocity, $K\,i$) and Reynolds numbers are high in wide rock joints.

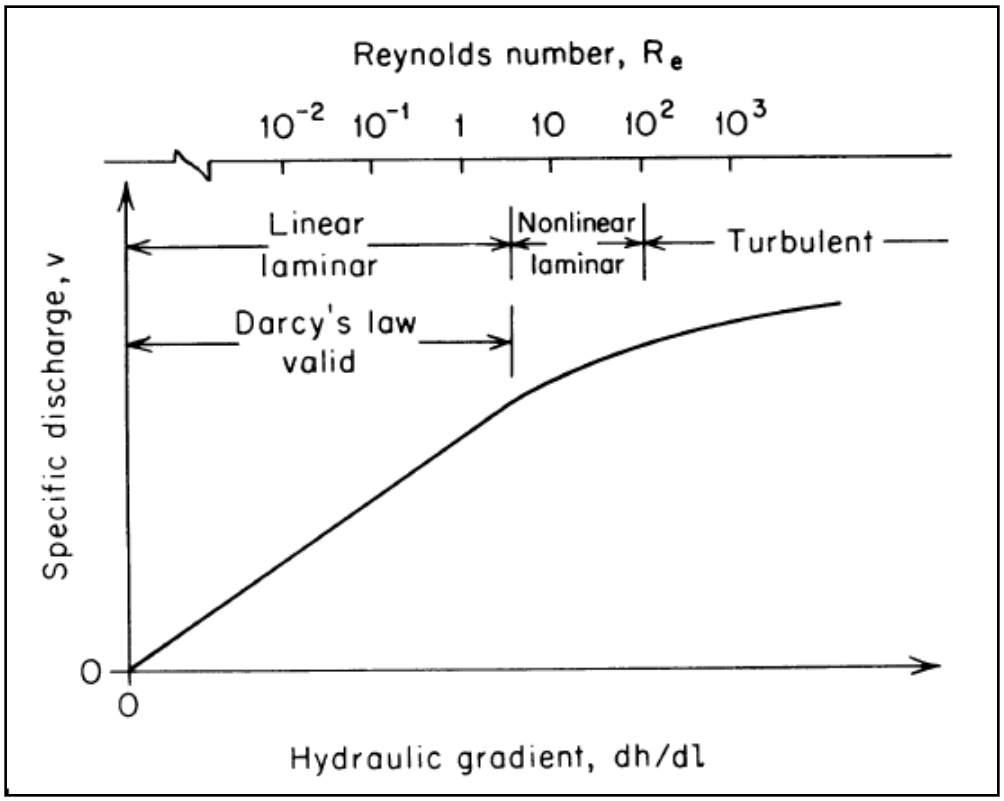

Figure 1.9. Range of validity of Darcy's law (after Freeze and Cherry 1979).

1.4.1 The cubic law

The cubic law is derived by assuming that the flow of water in a rock joint occurs between two smooth parallel plates with a separation distance denoted as the conducting aperture, *e*, in this report. The flow rate per unit width of joint, *Q*, is given by

$$Q = \frac{\gamma_w e^2}{12\mu_w} \cdot \left(\frac{\partial h}{\partial l}\right) \cdot e \tag{1.14}$$

where γ_w is the unit weight of water (lb/ft^3), *e* is the conducting aperture (ft), μ_w is the dynamic viscosity (lb-s/ft^2), and the term within the parenthesis (the ratio of the change in total head to length of joint), is the hydraulic gradient (ft/ft). Equation 1.14 is known as the cubic law. By analogy, the relationship of hydraulic conductivity to flow rate in an open joint was established with Darcy's law; therefore, the equation for a single joint can be rewritten (Ebeling and Pace, 1996b)

$$Q = K_{RJ} \cdot (i) \cdot A_{flow} \tag{1.15}$$

where A_{flow} is

$$A_{flow} = e \tag{1.16}$$

the area of flow at any point along the single joint is equal to the conductive aperture, e times unit width into the cross-section for this two-dimensional joint flow model. The joint hydraulic conductivity K_{RJ} can be expressed as (Ebeling and Pace, 1996b)

$$K_{RJ} = \left(\frac{\gamma_w}{12 \cdot \mu_w} \right) \cdot e^2 \tag{1.17}$$

Many researchers over the years have investigated the validity of the cubic law to predict flow within a rock joint with varying conclusions. Iwai (1976) found that the cubic law is valid at low stress levels for natural, rough, uneven discontinuities when the discontinuity is open. From Iwai's research, flow in rock fractures was found to obey the cubic law if the aperture was larger than 6.562 x 10^{-5} ft (20 μm) and the Reynolds number was no greater than about 100. Witherspoon et al. (1980) concluded that the cubic law was valid for apertures down to 1.312 x 10^{-5} ft (4 μm), normal stresses up to 4.177 x 10^5 psf (20 MPa), and fractures that were open or closed. Also, the results were not dependent on the rock type. Tsang and Witherspoon (1981) studied the hydromechanical behavior of a single horizontal rough-walled fracture. They concluded that the cubic law held if the effects of roughness were accounted for by replacing the fracture aperture with a statistical average. Gale (1982a) found that the cubic law broke down for rough deformable fractures subjected to stresses between 2.089 x 10^5 psf and 3.133 x 10^5 psf (10 and 15 MPa). Gale found that this maximum value of stress could be lower for natural fractures. Gale (1982b) found that the cubic law did not apply to rough, deformable, induced, or natural fractures when the residual apertures were computed on the basis of flow rates measured at stresses exceeding 6.266 x 10^5 psf (30 MPa).

One fact that is very evident from the above-mentioned research is that it is very difficult to produce a completely closed fracture (the stress levels must be very high, approximately 4.177 x 10^6 psf to 6.266 x 10^6 psf (200 to 300 MPa) (Kranz et al. 1979). Several key factors that were considered by the various researchers were the levels of stress involved, the roughness of the rock apertures, and whether the fractures were open (no contact between adjacent walls) or closed (some contact between adjacent walls). For this report, the maximum normal stress applied to the foundation is

approximately 6.266 x 10^4 psf (3 MPa). Therefore, the cubic law is assumed to apply to our rock joints.

1.4.2 Fluid flow conditions

The condition of flow within the rock joint is of interest. That is, is the flow turbulent or laminar? The cubic law assumes a linear relationship between the flow velocity and the pressure gradient and thus is valid only for laminar flow conditions. The condition of flow may be predicted by examining the Reynolds number and the roughness of the joint. As stated earlier, Iwai (1976) found from his research that laminar flow existed when the Reynolds number was no greater than 100. The Reynolds number at which turbulent flow initiates, decreases with increasing aperture roughness. Wilson (1970) reported in his research that turbulent flow conditions occurred only when abnormally large fractures were subjected to abnormally large gradients. Louis (1969) performed extensive research of both laminar and turbulent flow conditions on smooth and rough joints. From his work, he established five regions of flow governed by varying flow laws. The regions of flow are delineated by a surface roughness index and the Reynolds number. The surface roughness index, S, is computed as

$$S = \frac{R_r}{D_h} \tag{1.18}$$

where

R_r = height of the surface asperities
D_h = equivalent hydraulic diameter, equal to (2 times a).
a = average conducting aperture

The average conducting aperture, a, in this case is equivalent to the conducting aperture, e, (Ebeling et al. 1997), and the Reynolds number, R_e, for flow between parallel plates is equal to

$$R_e = \frac{v(2a)}{\upsilon_w} \tag{bis 1.13}$$

where

v = mean flow velocity
= kinematic viscosity of water
e is replaced by a in Equation 1.13

The Reynolds number defines the relationship of the inertial forces to the viscous forces in the flow region. The lower the Reynolds number, the more important the contribution of the viscous forces is to the flow. The higher the Reynolds number, the more important the inertial forces are to the flow and the more likely turbulence is to occur. In one example analysis of a rock joint that is classified as a "tight joint", i.e., the initial joint aperture ($\leq 250\ \mu m$), the Reynolds number was computed to be approximately 10 for the velocities computed in the Ebeling et al. (1997) Chapter 5 problem of a hypothetical 300-ft high gravity dam with a horizontal joint along the 235-ft long dam-to-rock foundation interface (with no drain); therefore, laminar flow is assumed to prevail in this problem.

1.4.3 The effect of surface roughness on the mechanical aperture

The mechanical aperture, E, is the actual aperture of the rock joint. This value can be a challenge to obtain in some situations due to the effects of surface roughness and contact areas. An alternative method for establishing values for aperture can be obtained through hydraulic testing, resulting in values of conducting aperture, e, which represents the true mechanical aperture, E. The theoretical conducting aperture derived according to the smooth parallel plate flow model is often considerably smaller than the true mechanical aperture. Flow channel tortuosity and roughness are probably responsible for the differences (Barton 1982). Barton (1982) proposed a relationship given by Equation 1.19 that relates the conducting aperture to the mechanical aperture

$$e = \frac{JRC^{2.5}}{\left(\frac{E}{e}\right)^2} \quad (\mu m) \tag{1.19}$$

where

E = mechanical aperture (μm)
e = conducting aperture (μm)
JRC = joint roughness coefficient

Equation 1.19 was formulated in SI units and is valid only if E is greater than or equal to e within a range of l μm (3.281 x 104 ft) to 1,000 μm (3.251 x 10-3 ft). This relationship was used in this study and accounts for the effects of surface roughness and tortuosity.

1.5 Report contents

Chapter 2 discusses the drain model used in Joint_FLOW, the results from combined steady-state seepage and stability analyses for three problems using Flow Options 1 through 3, as well as the loading condition in the special case of a pool specified above the crest of a non-overflow gravity dam.

Chapter 3 will present an overview of the Visual Modeler Graphical User Interface (GUI) for GDLAD_Foundation. The GDLAD_Foundation Visual Modeler accepts user input, executes the FORTRAN engineering formulations, and displays the resultant analyses for evaluation.

Chapter 4 discusses the result from two sets of Joint_FLOW analyses; (1) fluid flow along a single reach rock joint with three different types of tapered rock joint; and (2) fluid flow along multi-reach rock joints contained within the rock foundation.

Chapter 5 will present the assessment of water pressures computed within a network of rock joints using LinPipe.

Chapter 6 will present the assessment of the stability of a non-overflow gravity dam cross-section model of gravity dams within the categories of either no flow along foundation rock joints and in the category of steady state laminar flow within the joints of the rock foundation. In this latter category, two procedures will be used to assess uplift resultant pressures acting on the driving, structural and resisting wedges, a steady state seepage analysis of laminar flow within the network of rock joints and a simplified seepage analysis of a rock joint assemblage. Flow Options 4 through 6 are discussed in this chapter.

Chapter 7 discusses the construction of a System Response Curve for a two-dimensional gravity dam model of non-overflow concrete dam embedded in rock.

Chapter 8 presents a summary of the engineering methodology and PC-base software environment with conclusions and recommendations. One recommendation is to extend this software to analyze a spillway section embedded in rock and containing a network of rock joints. Water pressures will be computed within the jointed rock using Joint_FLOW. The proposed

formulation will also compute the water pressures acting on the various regions of the “wetted” spillway surface as water passes over the spillway.

Appendix A summarizes the results from a stability analysis made of the ETL 110-2-256 non-overflow dam.

Appendix B presents the formulation for the analysis of laminar fluid flow within a network of rock joints using Joint_FLOW.

Appendix C presents the formulation for the analysis of laminar fluid flow within a network of rock joints using LinPipe.

Appendix D summarizes the GDLAD_Foundation ASCII input data file.

Appendix E summarizes the Joint_FLOW and the optional LinPipe ASCII input data file.

Appendix F discusses the Line of Seepage methodology used to compute uplift water pressure acting within a single flow path consisting of a series of rock joints for Flow Option 6. Chapter 6 discusses this simplified steady state seepage analysis. The authors of this report observe that in this flow option, different rock joints may be assigned with different values of hydraulic conductivity.

2 Stability and Seepage Analysis of a Non-Overflow Dam (2-D) Cross-Section Embedded in Rock

2.1 Introduction

This chapter focuses on the assessment of the stability and seepage of a non-overflow gravity dam cross-section model that is embedded in rock foundation with a rock foundation drain. Three separate analyses will be conducted using different joint flow assumptions in the analyses. All three analyses will use the same gravity dam cross-section. Water pressures and resultant uplift water pressure forces discussed in this chapter are produced from the Joint_FLOW program as described in Section 4.3 of Chapter 4, whereas the assessment of stability is determined by the GDLAD_Foundation program, which is discussed in Section 6.1 of Chapter 6. Three flow options, designated as flow options 1, 2, and 3, are methods of analysis which account for a network of interconnected rock joints. For flow option 3, the user defined flow network of rock joints solved by Joint_FLOW is expanded by considering flow along the vertical interslice plane between wedge interfaces. Flow option 1 does not consider flow along the vertical interslice plane; flow option 2 calculates near hydrostatic water pressures along the vertical interslice planes; and flow option 3 accounts for flow along the vertical rock joints with interslice water pressure forces calculated from Joint_FLOW.

The hypothetical non-overflow gravity dam cross-section of Figure 2.1 shows the interconnected rock joints with the potential slip plane in light blue and the vertical interslice planes as dashed lines in purple. The rock foundation consist of two rock types with the unit weights and Mohr-Coulomb effective shear strength parameter values listed in Table 2.1 for each of the two regions used to designate each type of rock as found shaded in light blue and green for regions 1 and 2, respectively, in Figure 2.2. A user selected potential slip plane coincident with a continuous series of connected rock joints (from upstream to downstream of the dam) is displayed (in light blue) in Figure 2.1 with the corresponding joint lengths and orientations defined in Table 2.2. Table 2.3 specifies the Mechanical Aperture and JRC values together with the number of

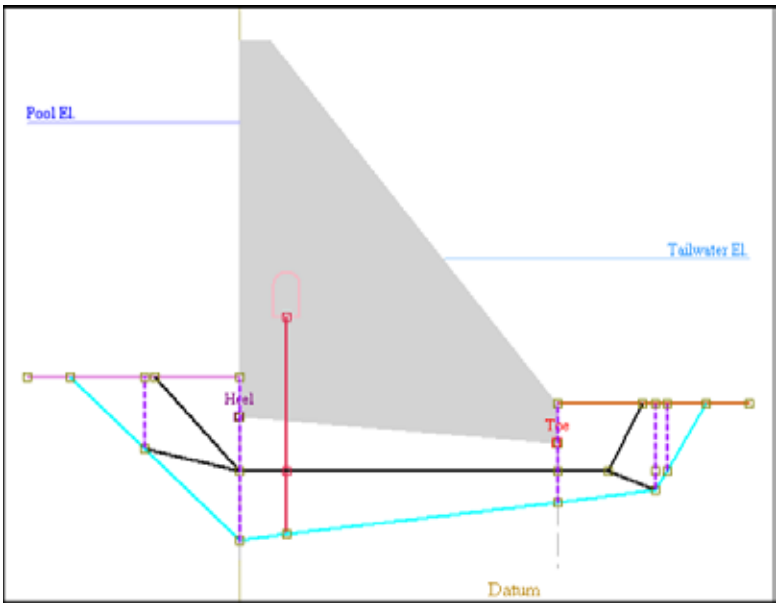

Figure 2.1. Gravity dam embedded in a rock foundation with rock foundation drain with interconnect rock joints.

Table 2.1. Categorization and mapping of unit weights and effective shear strength parameter values to the three rock regions.

Region	γ (pcf)	C' (psf)	ϕ' (deg)
Region 1	117	100	30
Region 2	122	120	20

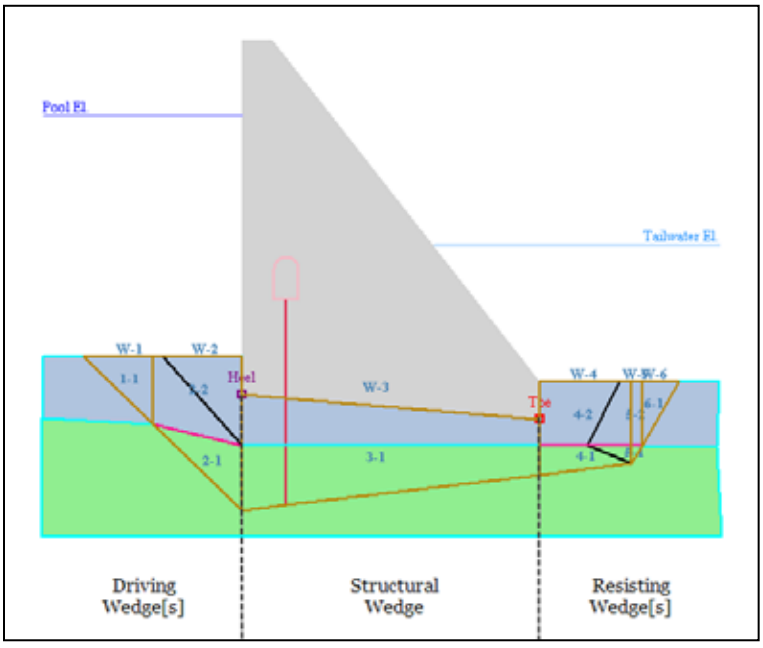

Figure 2.2. Gravity dam embedded in a rock foundation with wedge and region information.

Table 2.2. Joint lengths and orientation along the base of each wedge/sub-wedge within a region.

Wedge Base	L (ft)	α (deg)	Region
1	25.11	-44.95	1
2	31.46	-45.04	2
3	75.47	7.07	2
4	23.25	7.07	2
5	5.21	60.54	2
6	19.25	60.54	1

Table 2.3. Rock joint apertures and the number of elements.

Reach	E (microns)	JRC	Number of Elements per Reach
1 through 14	600	8	5

elements comprising each joint.[1] A Joint_FLOW seepage analysis will be conducted that calculates the water pressures at all nodes and the uplift water pressure forces normal to each wedge base. These uplift forces are then provided as input to the GDLAD_Foundation program to conduct a stability analysis for this user selected potential slip plane. The GDLAD_Foundation Visual Modeler distinguishes among three types of major wedges as labeled in Figure 2.2; the Driving Wedge(s), the Structural Wedge; and the Resisting Wedge(s). The Driving Wedge(s) consists of 2 wedges, the Structural Wedge has 1 wedge and the Resisting Wedge(s) has 2 wedges. From Figure 2.2, with Tables 2.2 and 2.3, this six wedge system is defined by the mechanical apertures, joint lengths along the base of each wedge/sub-wedge and the angle between the inclined potential slip surface and the horizontal. There are two sub-wedges contained within the driving wedge, a single structural wedge, and three sub-wedges contained within the resisting wedge.

2.2 2-D drain model idealization

The simplified two-dimensional Drain model developed for this initial version of GDLAD_FoundationVM package is best described by starting with the Figure 2.3 three-dimensional geometry for the drainage gallery and the drains. This figure is a side view of the concrete monolith embedded in

[1] Uniform Mechanical Aperture and JRC values are used throughout all rock joint reaches.

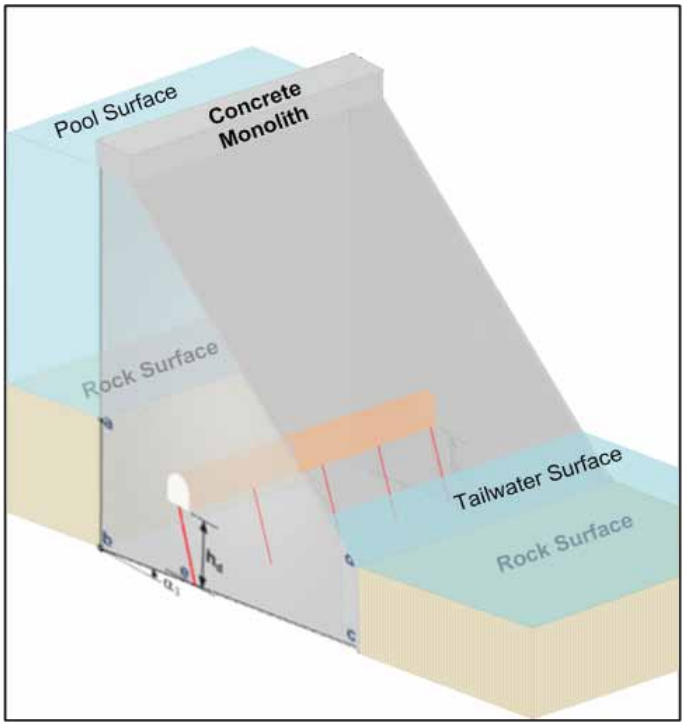

Figure 2.3. Concrete monolith with foundation drains.

rock with a rock foundation drain. The drain is 5 in. across in diameter with drain spacings that are 20 ft apart along the gallery floor. The gallery drainage system is likely to be a three dimensional geometric feature (e.g., Figure 6.18 in Murphy et al. 2002) as it pertains to heads and water flow within the rock joint(s). Since GDLAD_Foundation and Joint_FLOW are a two-dimensional formulation and analysis package, a simplified, two-dimensional drain model is developed using a "slotted drain" idealization.

Figure 2.4a illustrates the actual gallery with two rock foundation drains (actual). Figure 2.4b shows the idealization of the slotted drain per unit (length) run of the dam used in this initial version of Joint_FLOW contained within the GDLAD_FoundationVM.

An important detail is to determine the conducting aperture of the slotted drain. The approximate conducting aperture of the slotted drain is calculated from the knowledge of the drain diameter and the separation between drains, i.e., the ratio of the area of the drain (each considered as a circle) and the separation of the drains. The following equation for the slotted drain conducting aperture, $E_{Slotted\ Drain}$ is given as

$$E_{Slotted\ Drain} = \frac{\left(\frac{\pi}{4}\right) D_{Drain}^{\ 2}}{S_{Drain}} \tag{2.1}$$

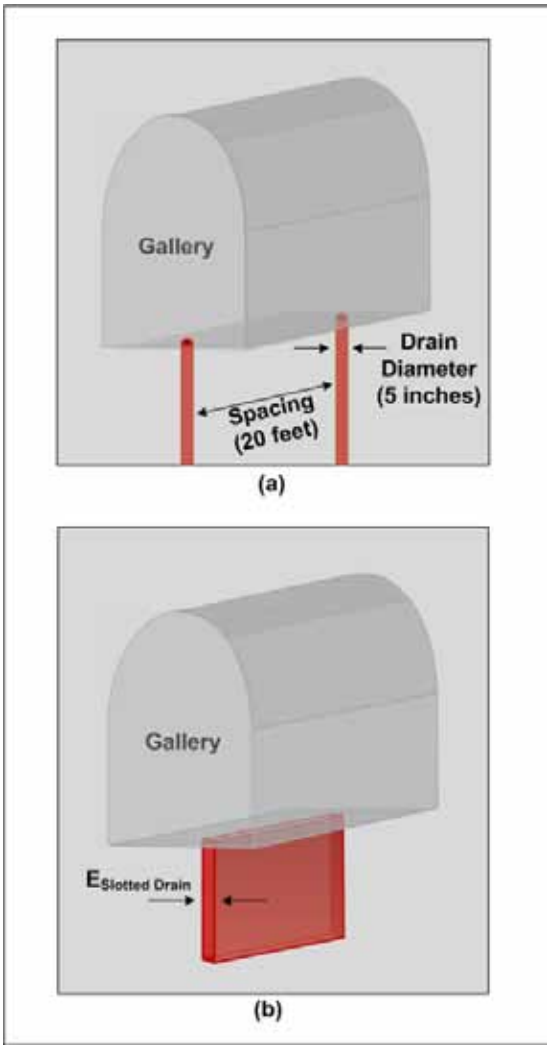

Figure 2.4. Rock drain configuration (a) actual rock foundation drain (b) ideal 2-dimensional slotted drain per foot run of dam.

where $E_{Slotted\ Drain}$ is the approximate conducting aperture of the slotted drain, D_{Drain} is the diameter of drain in inches (converted into feet) and S_{Drain} is the spacing between the drains with user input in feet.

2.3 Drain model iteration method

For the initial calculation of flow, there is the assumption of no flow at the drain and a sink source for the flow boundary condition at the top of drain node is set equal to zero (Q=0) in the Joint_FLOW finite element analysis of two-dimensional steady-state seepage. Figure 2.5 illustrates the following procedure for implementing the drain model iteration method.

1. Left hand side of Figure 2.5:
   If the computed Total Head (H) at the drain is greater than the elevation head (H_e) for the top of drain node, the total head boundary condition is set to the elevation head and the flow boundary condition is removed. A second calculation is performed with these new set of boundary conditions and the flow coming out of the drain Q is computed.
2. Right hand side of Figure 2.5:
   If the computed Total Head at the (top of) drain node is less than or equal to the elevation head, the initial assumption was correct and the resulting flow solution is used.

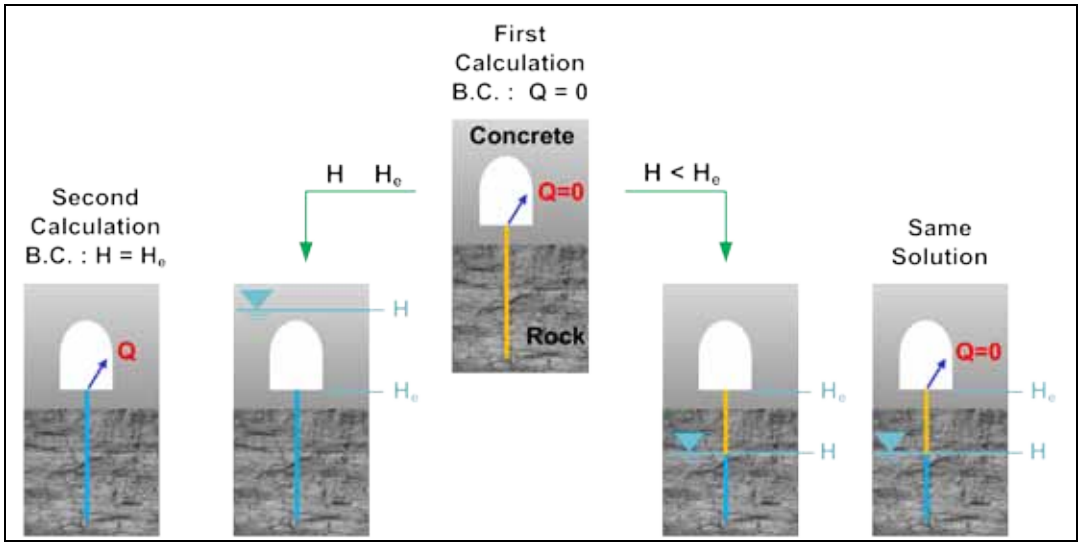

Figure 2.5. Current drain model.

2.4 Loading conditions on the structural wedge for pools above crest of dam

Loading conditions are considered as a linear variation in hydrostatic water pressures with depth acting on the structural wedge model of the non-overflow gravity dam cross-section. Figure 2.6a shows the loading conditions for pool and tailwater levels below the crest of dam. The extreme case is considered when both pool and tailwater levels are above the crest of the embedded concrete gravity dam. This is a complex overflow problem. Figure 2.6b shows the simplified assumptions being used in the GLDAD_FoundationVM when the pool overtops the crest and tailwater is above the crest of dam. The resultant horizontal water pressure forces are listed in both figures as H_L and H_R for left and right forces acting on the embedded concrete gravity dam (i.e., the structural wedge). When pool and tailwater is above the dam crest, as in Figure 2.6b, the weight of

the overtopping water, designated as W_{Flood}, is defined as the dashed polygon from the tailwater level to the top of the dam in this simplified idealization of a complex overflow problem.

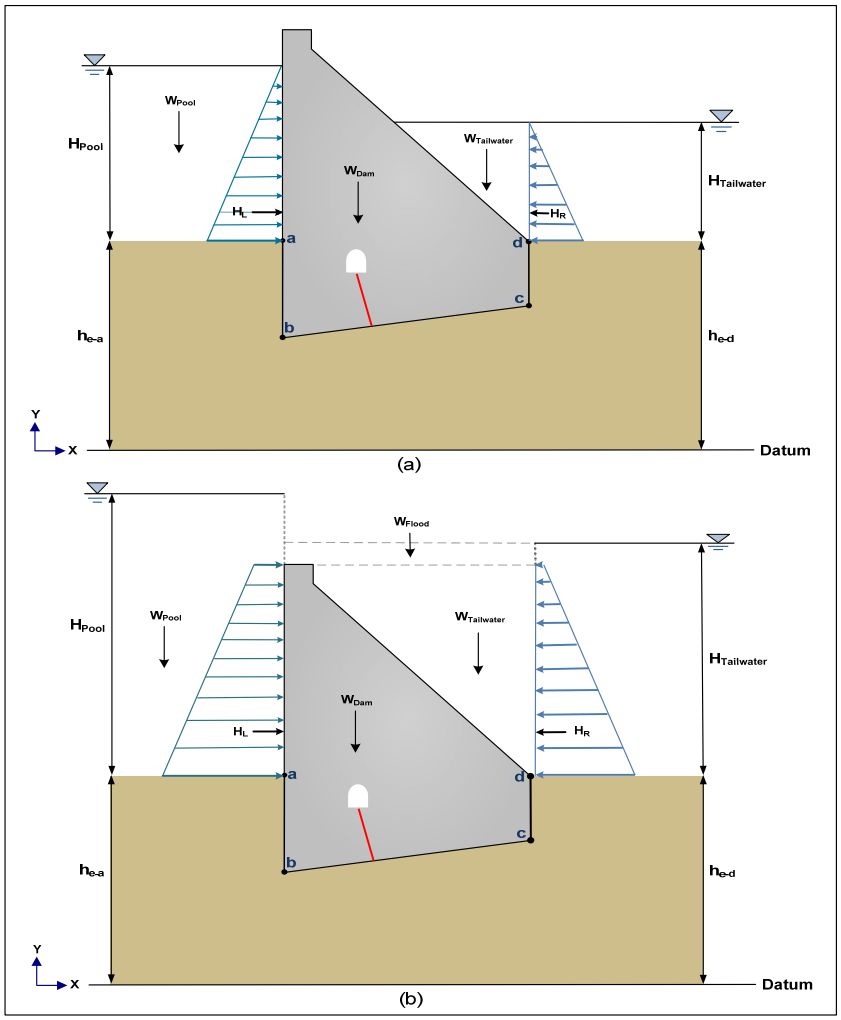

Figure 2.6. Loading of structural wedge model of the embedded concrete gravity dam with rock foundation drain (a) pool and tailwater below crest (b) pool and tailwater above the crest of the dam.

2.5 Uplift and interslice water pressure resultant forces for flow options 1, 2, and 3

The assessment of the uplift pressures at the slip plane and interslice forces at the vertical interfaces resulting from laminar flow within individual rock joints or networks of rock joints is examined further for certain conditions and categorized as flow options 1, 2, and 3. Table 2.4 lists the methods used for the calculations of uplift water pressures and interslice water forces for these flow options, which were introduced in Section 2.1.

Table 2.4. Classification of uplift and interslice water forces as flow options.

Flow Options	Wedge Features	Uplift and Interslice Water Force (IWF)	Driving Wedge	Structural Wedge	Resisting Wedge
1	Wedge Base	Joint_FLOW	Flow Along Slip Plane	Flow Along Slip Plane	Flow Along Slip Plane
	Vertical Interslice	No IWF	No Water Pressures	No Water Pressures	No Water Pressures
2	Wedge Base	Joint_FLOW	Flow Along Slip Plane	Flow Along Slip Plane	Flow Along Slip Plane
	Vertical Interslice	IWF	Near Hydrostatic	Near Hydrostatic	Near Hydrostatic
3	Wedge Base	Joint_FLOW	Flow Along Slip Plane	Flow Along Slip Plane	Flow Along Slip Plane
	Vertical Interslice	Joint_FLOW	Flow Along Interslice	Flow Along Interslice	Flow Along Interslice

2.6 Problem 1: Stability analysis with seepage computed along rock joints using Joint_FLOW and no interslice water pressure resultant forces. (Flow Option 1)

A deterministic analysis of typical static loading conditions for multiple wedge systems of the gravity dam cross-section with a rock foundation drain is presented in Figure 2.7. Recall that Table 2.1 lists the values of unit weights and Mohr-Coulomb effective shear strength parameters for the two rock foundation regions; that Table 2.2 summarizes the lengths and orientations of the base of each of the six wedges/sub-wedges; and that Table 2.3 gives the aperture values for the rock joints. This analysis was conducted to demonstrate the application of the general wedge equation to the sliding analysis of multiple wedge systems given the uplift water pressure results derived from Joint_FLOW. The case considered is for a pool at elevation (el) 1012 ft and tailwater at el 978.7 ft. Top of rock is at el 950 ft on the upstream side and at el 943.447 ft on the downstream side of the dam. This hypothetical embedded concrete gravity dam is 82 ft high and approximately 75.186 ft wide. It is embedded 10 ft into rock at its heel and embedded 10 ft into rock at its toe. The gallery opening is defined by a rectangle that is 6 feet wide and 8 feet high with a dome or half circle added on top. Table 2.5 provides a listing of the functions and approximate coordinates of all nodes in the geometry.

Table 2.5. Description of Points and Locations

Point Id	Point Description	X-coordinate	Y-coordinate
1	Upstream ground surface point at dam vertically above heel	0	950
2	Downstream ground surface point at dam vertically above toe	74.9	943.45
3	Left upper corner of region 1	-50	950
4	Point at upstream side of crest	0	1032
5	Point at downstream side of crest	7.6	1032
6	Right upper corner of region 1	120	943.45
7	Mid-point at base of gallery (i.e., top of drain)	11	964.67
8	Toe	74.9	933.45
9	Heel	0	940
10	Upstream ground surface point of region 1	-40	950
11	Upstream ground surface point of region 1	-20	950
12	Downstream ground surface point of region 1	110	943.45
13	Downstream ground surface point of region 1	95	943.45
14	Upstream rock foundation point Delineating regions 1 and 2	0	926.71
15	Upstream rock foundation point Vertically beneath heel	0	910
16	Upstream rock foundation point Delineating regions 1 and 2	-22.23	932.26
17	Downstream rock foundation point Delineating regions 1 and 2	86.94	926.71
18	Downstream rock foundation point Delineating regions 1 and 2	74.9	926.71
19	Downstream rock foundation point	97.97	922.15
20	Downstream rock joint point Vertically beneath toe	74.9	919.29
21	The line of drains that intersect a rock foundation point within the structural wedge	11	911.36
22	Upstream rock foundation corner point Delineating regions 1 and 2	-50.14	933.76
23	Downstream rock foundation corner point Delineating regions 1 and 2	119.46	926.65
24	Left lower corner of Region 2	-50.14	903.30
25	Right lower corner of Region 2	120.48	903.30

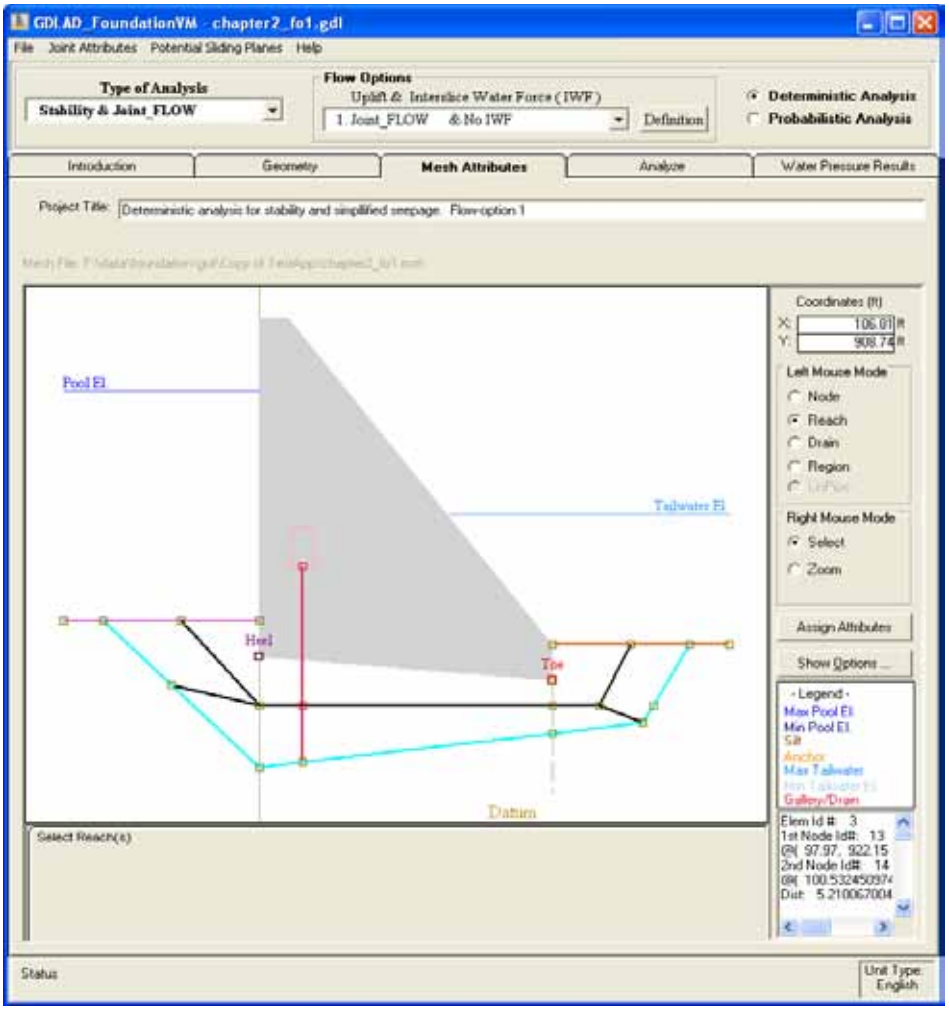

Figure 2.7. Gravity dam embedded in a rock foundation with rock foundation drain.

Rock foundation drain diameter and the spacing between drains are displayed in Figure 2.8 while uniform mechanical apertures of 600 microns and JRC of 8.0 are the values given for each rock joint element. Figure 2.9a lists the values of mechanical aperture with the number of elements for each rock joint and Figure 2.9b lists the uniform JRC values.

The six wedge system developed to analyze the stability of this system can be seen in the Figure 2.10 as the brown lines defining both wedges and sub wedges. The first number in each triangular or rectangular geometric feature designates the wedge number, while the second number is a count of the geometric features comprising the particular sub-wedge. Two material regions were formed in the Geometry tab (shown shaded in blue and green in Figure 2.10) and two material properties were defined and mapped to the two regions in the Mesh Attributes tab (as defined in Chapter 3) and illustrated in Figure 2.11.

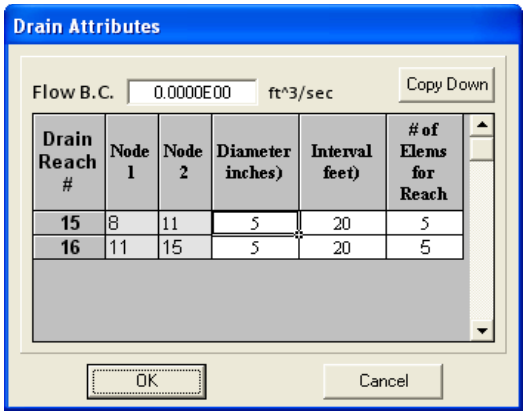

Figure 2.8. Rock foundation drain attributes.

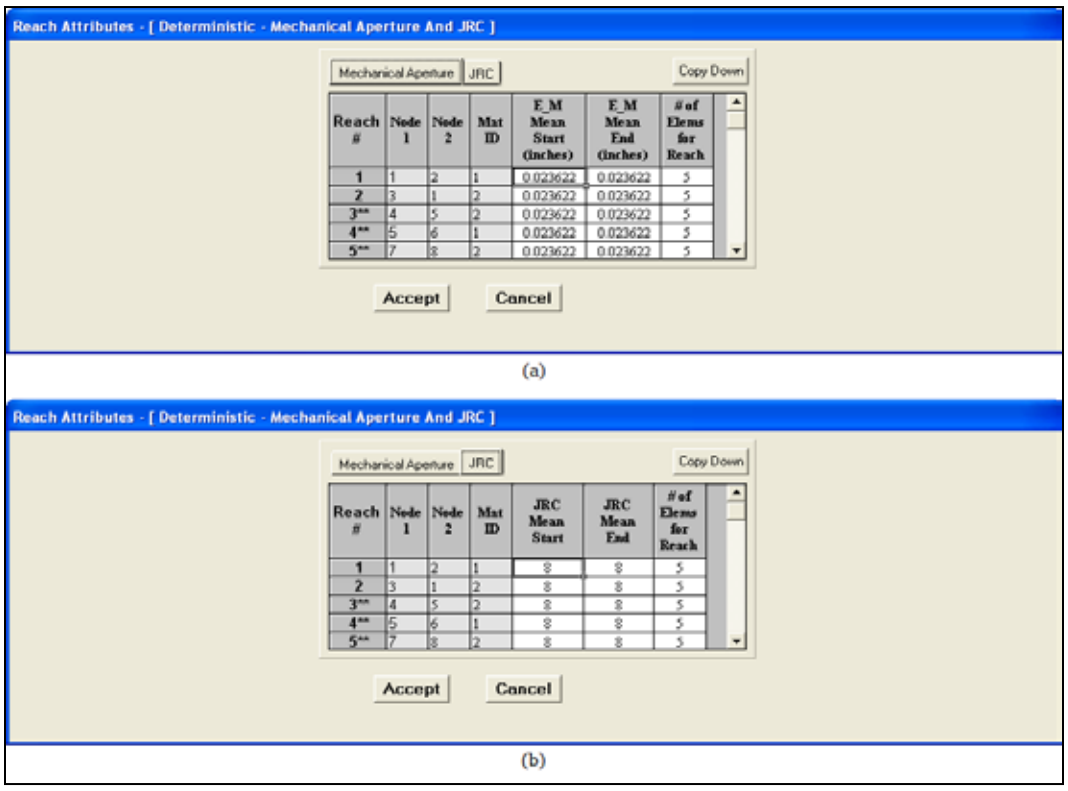

Figure 2.9. Mechanical aperture and JRC values for each rock joint.

The resulting computed factor of safety (*FS*) against sliding for this multiple wedge system was found to be 2.584 with a residual imbalance Force of -0.086 kips after 11 iterations (see Figure 2.12). Values within the table of Figure 2.12, include the interslice force imbalance of $P_{i-1} - P_i$ for wedge *i*, which is the governing wedge equation and given as Equation 6.6 of Chapter 6; the (total) force acting normal to wedge *i* of the potential slip plane, N_i; and T_i, the shear force required for equilibrium at the base of wedge *i*, along the potential slip plane. The equations for calculating both N_i and T_i are given:

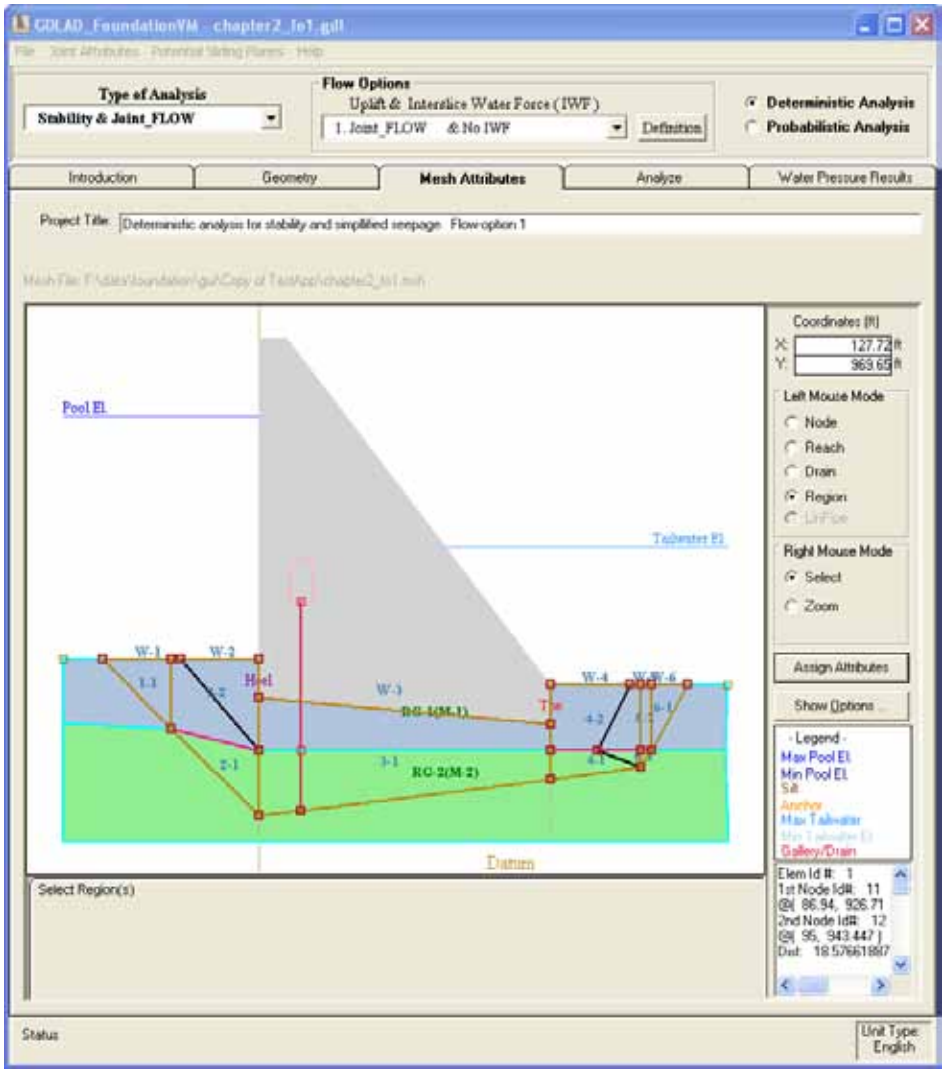

Figure 2.10. Embedded concrete gravity dam with two material regions and a six wedge system.

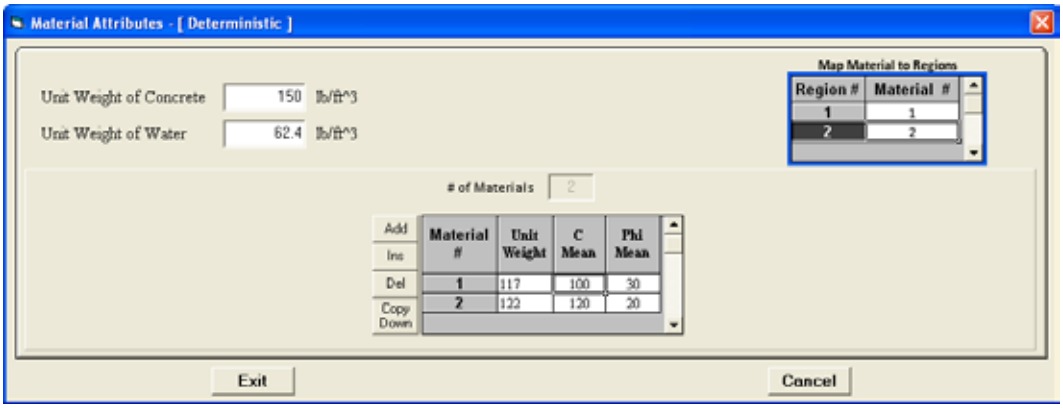

Figure 2.11. Table of properties of materials and the mapping of regions.

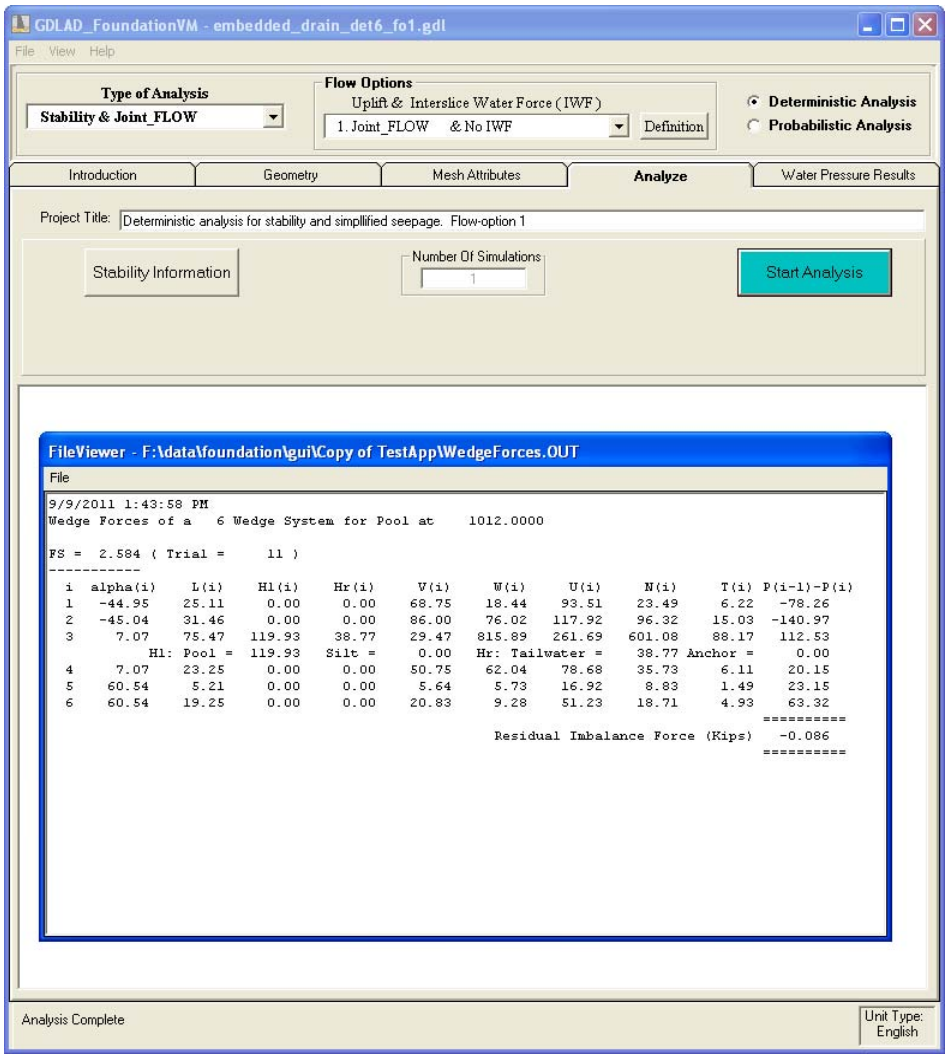

Figure 2.12. Resultant factor of safety with residual imbalance of a six wedge system with Flow Option 1.

$$N_i = (W_i + V_i)\cos\alpha_i - U_i + (H_{Li} - H_{Ri})\sin\alpha_i + (P_{i-1} - P_i)\sin\alpha_i \qquad (2.2)$$

$$T_i = (H_{Li} - H_{Ri})\cos\alpha_i - (W_i + V_i)\sin\alpha_i + (P_{i-1} - P_i)\cos\alpha_i \qquad (2.3)$$

where W is the total weight of wedge i; V is the overburden weight acting down on the wedge i; H_L and H_R are the applied horizontal forces acting from left and right side of wedge i; P is the horizontal interslice forces acting on wedge i; and a is the angle at the base of wedge i from the horizontal. Figure 6.3 gives a good representation of these resulting forces acting on a generalized wedge.

The resultant water pressure force U_i, in units of kips, acting normal to the base of each wedge i, with i = 1 to 6, is listed in Figure 2.12. Joint_FLOW

water pressure results computed at all nodes contained within the rock joint flow network are displayed in Figure 2.13. Each U_i force is computed as the resultant of the set of Figure 2.13 water pressure nodal points that are situated along each of the six wedge bases. Recall that for flow option 1, there are no interslice water pressure forces being considered between wedges/sub-wedges.

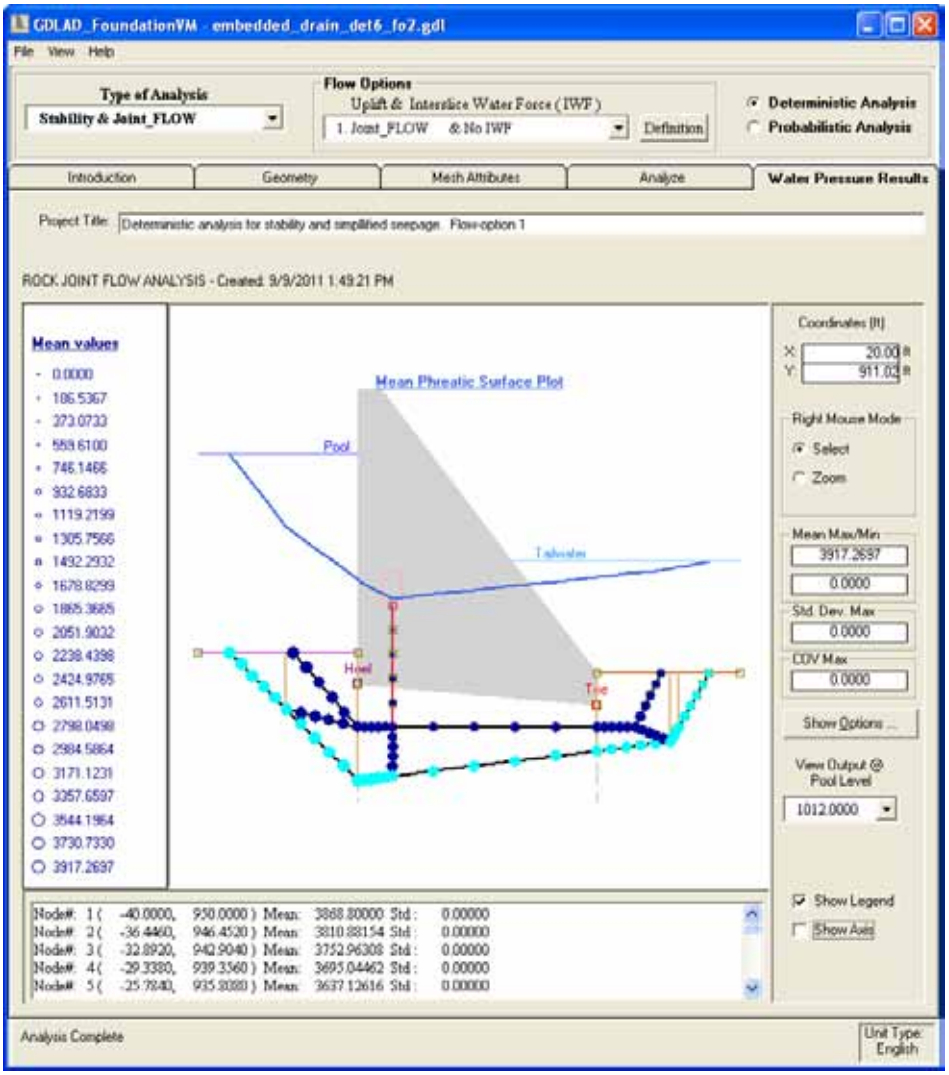

Figure 2.13. Resultant water pressures for Flow Option 1.

2.7 Problem 2: Stability analysis with seepage computed along rock joints using Joint_FLOW and near hydrostatic interslice water pressure resultant forces. (Flow Option 2)

A deterministic analysis of typical static loading conditions for multiple wedge systems of the Gravity Dam cross-section with rock foundation drain has been presented in Figure 2.7. Recall that Table 2.1 lists the values of unit

weights and Mohr-Coulomb effective shear strength parameters for the two rock foundation Regions and that Table 2.2 summarizes the lengths and orientations of the base of each of the six wedges/sub-wedges and Table 2.3 provides the Mechanical Aperture and JRC values for all rock joints. This analysis was conducted to demonstrate the application of the general wedge equation to the sliding analysis of multiple wedge systems given the resultant uplift water pressures derived from Joint_FLOW. The case of the hypothetical embedded concrete gravity dam considered is identical to the one in Section 2.6 for a Pool at el 1012 ft and tailwater at el 978.7 ft. Top of rock is at el 950 ft on the upstream side and at el 943.447 ft on the downstream side of dam. This hypothetical embedded concrete gravity dam is 82 ft high and approximately 75.186 ft wide. It is embedded 10 ft into rock at its heel and embedded 10 ft into rock at its toe. Rock foundation drain diameter and the spacing between drains are displayed in Figure 2.8 while uniform Mechanical Apertures of 600 microns and JRC of 8.0 are the values given for each rock joint element. Figure 2.9a lists the values of Mechanical Aperture with the number of elements for each rock joint and Figure 2.9b lists the uniform JRC values. The six wedge system developed to analyze the stability of this system can be seen in the Figure 2.10 as the brown lines defining both wedges and sub wedges. The first number in each triangular or rectangular geometric feature designates the wedge number, while the second number is a count of the geometric features comprising the particular sub-wedge. Two material regions were formed within the Geometry tab and two material properties were defined and mapped to the two regions in the Mesh Attributes tab (as defined in Chapter 3) and illustrated in Figure 2.11.

The resulting computed factor of safety (*FS*) against sliding for this multiple wedge system was found to be 2.584 with a residual imbalance Force of -0.086 kips after 11 iterations (see Figure 2.14). Recall that for flow option 2, the interslice water pressure forces are being calculated from hydrostatic water pressures at the rock surface combined with water pressure results computed from Joint_FLOW at the joint-to-vertical wedge interface points. Water pressure results at all nodes of the network of rock joints are also displayed in Figure 2.15.

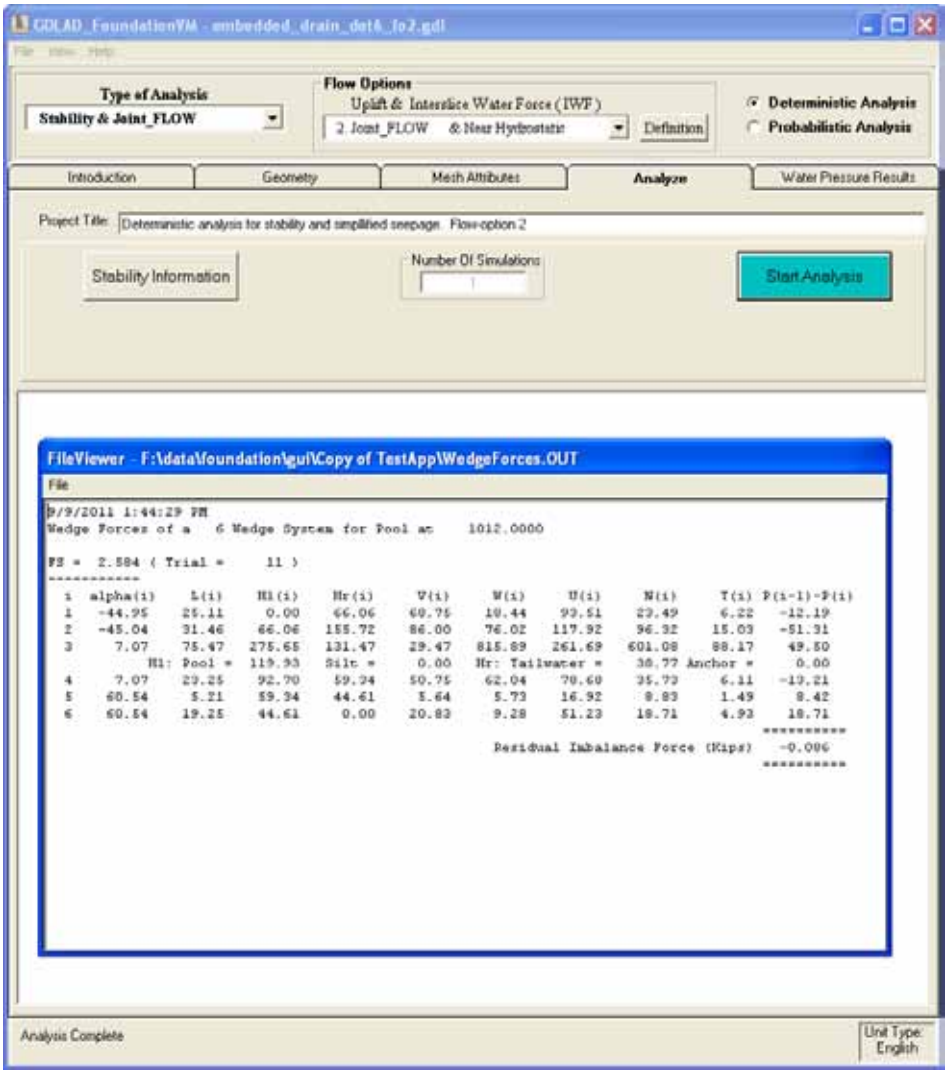

Figure 2.14. Resultant factor of safety with residual imbalance of a six wedge system with Flow Option 2.

2.8 Problem 3: Stability analysis with seepage and interslice water pressure resultant forces computed along rock joints using Joint_FLOW. (Flow Option 3)

A deterministic analysis of typical static loading conditions for multiple wedge systems of the Gravity Dam cross-section with rock foundation drain has been presented in Figure 2.7. Recall that Table 2.1 lists the values of unit weights and Mohr-Coulomb effective shear strength parameters for the two rock foundation Regions and that Table 2.2 summarizes the lengths and orientations of the base of each of the six wedges/sub-wedges and Table 2.3 provides the Mechanical Aperture and JRC values for all rock joints. This analysis was conducted to demonstrate the application of the general wedge equation to the sliding analysis of multiple wedge systems given the

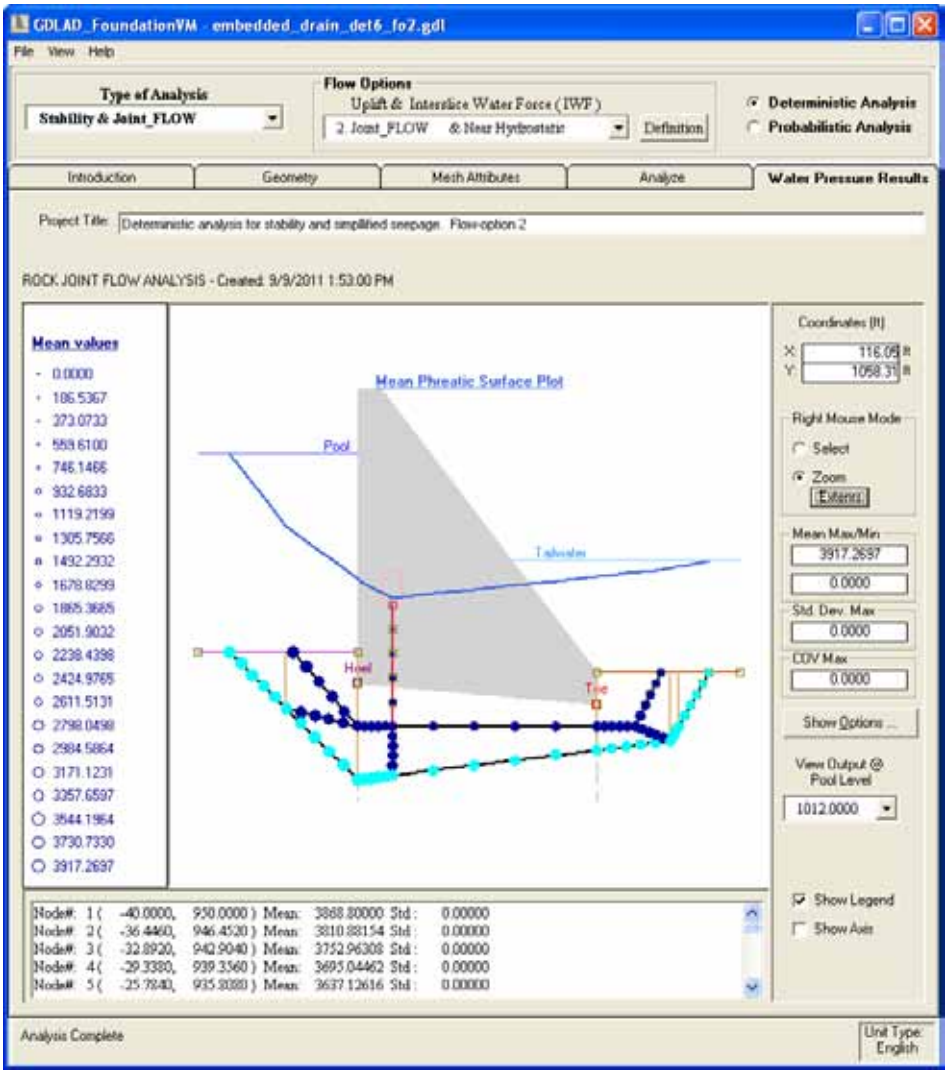

Figure 2.15. Water pressures at nodal points for Flow Option 2.

resultant uplift water pressures derived from Joint_FLOW. The case of the hypothetical embedded concrete gravity dam considered is identical to the one in Section 2.6 for a Pool at el 1012 ft and tailwater at el 978.7 ft. Top of rock is at el 950 ft on the upstream side and at el 943.447 ft on the downstream side of dam. This hypothetical embedded concrete gravity dam is 82 ft high and approximately 75.186 ft wide. It is embedded 10 ft into rock at its heel and embedded 10 ft into rock at its toe. Rock foundation drain diameter and the spacing between drains are displayed in Figure 2.8 while uniform Mechanical Apertures of 600 microns and JRC of 8.0 are the values given for each rock joint element. Figure 2.9a lists the values of Mechanical Aperture with the number of elements for each rock joint and Figure 2.9b lists the uniform JRC values. The six wedge system developed to analyze the stability of this system can be seen in the Figure 2.10 as the

brown lines defining both wedges and sub wedges. The first number in each triangular or rectangular geometric feature designates the wedge number, while the second number is a count of the geometric features comprising the particular sub-wedge. Two material regions were formed within the Geometry tab and two material properties were defined and mapped to the two regions in the Mesh Attributes tab (as defined in Chapter 3) and illustrated in Figure 2.11.

The resulting computed factor of safety (*FS*) against sliding for this multiple wedge system was found to be 2.568 with a residual imbalance Force of -0.044 kips after 11 iterations (see Figure 2.16). Recall that for flow option 3, the user defined flow network of rock joints solved by Joint_FLOW is expanded by considering flow along the vertical interslice plane between wedge interfaces. The interslice water pressure forces are being calculated from the water pressure results computed by Joint_FLOW at the wedge interfaces. Water pressure results at all nodes of the network of rock joints are also displayed in Figure 2.17.

2.9 Discussion of results for stability and Joint_FLOW analysis

Table 2.6 summarizes the uplift resultant water pressure forces acting normal to the base of each of the six wedges/sub-wedges for Flow Options 1, 2, and 3. Recall that wedge number 3 is the structural wedge containing the gravity dam embedded in jointed rock. The greatest uplift occurs normal to the base of the structural wedge when using Flow Option 3 and the smaller occurs when Flow Option 1 and 2 are specified. Both Flow Option 1 and 2 have the same values for uplift resultant force *U* due to the fact that the nodes and elements modeling the rock joint network are the same in each of the two Joint_FLOW stead-state seepage analyses.

Table 2.7 summarizes the computed Factors of Safety for the Figure 2.7 potential slip plane below the hypothetical gravity dam embedded in a rock foundation using Flow Options 1, 2, and 3. Flow Option 3 results in a lower computed value for Factor of Safety (*FS*) against sliding of 2.568 and Flow Option1 and 2 result in a larger computed value of 2.584. In this limited rock joint network problem, the authors of this report observe that there is not a large difference among the computed results. The differences among the three results are due to both the uplift pressures applied to the entire potential sliding plane (i.e., not just to the structural wedge) and the interslice water pressure forces assumptions made.

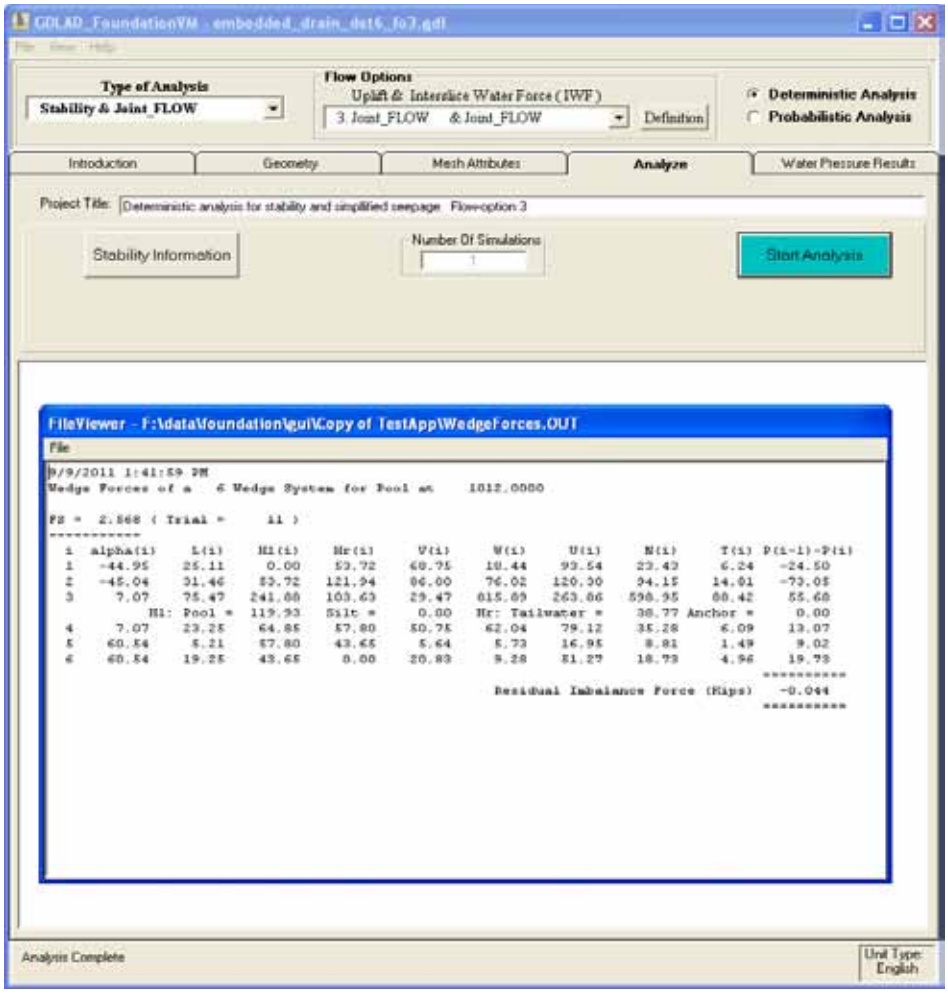

Figure 2.16. Resultant factor of safety with residual imbalance of a six wedge system with Flow Option 3.

Table 2.8 summarizes the computed Governing equation for each of the six wedges of the Figure 2.10 hypothetical gravity dam embedded in a rock foundation using Flow Options 1, 2, and 3. Flow Option 1 shows results giving the highest interslice water pressure imbalance forces and Flow Option 2 shows results giving the lowest interslice water pressure imbalance forces. Please note that a negative value of the difference ($P_{i-1} - P_i$) indicates that the applied forces acting on the i^{th} wedge exceed the forces resisting sliding along the base of the wedge and a positive value of the difference ($P_{i-1} - P_i$) indicates that the applied forces acting on the i^{th} wedge are less that the forces resisting sliding along the base of the wedge (ETL 1110-2-256). According to this, Wedges 1 and 2 are "driving" sliding wedges and Wedges 3 through 6 are "resisting" sliding for both flow options 1 and 3. Flow option 2 has a negative imbalance force in wedge 4. This indicates the interslice pressure force (P_{i-1}) from wedge 3 is larger than the interslice force from wedge 4 (P_i).

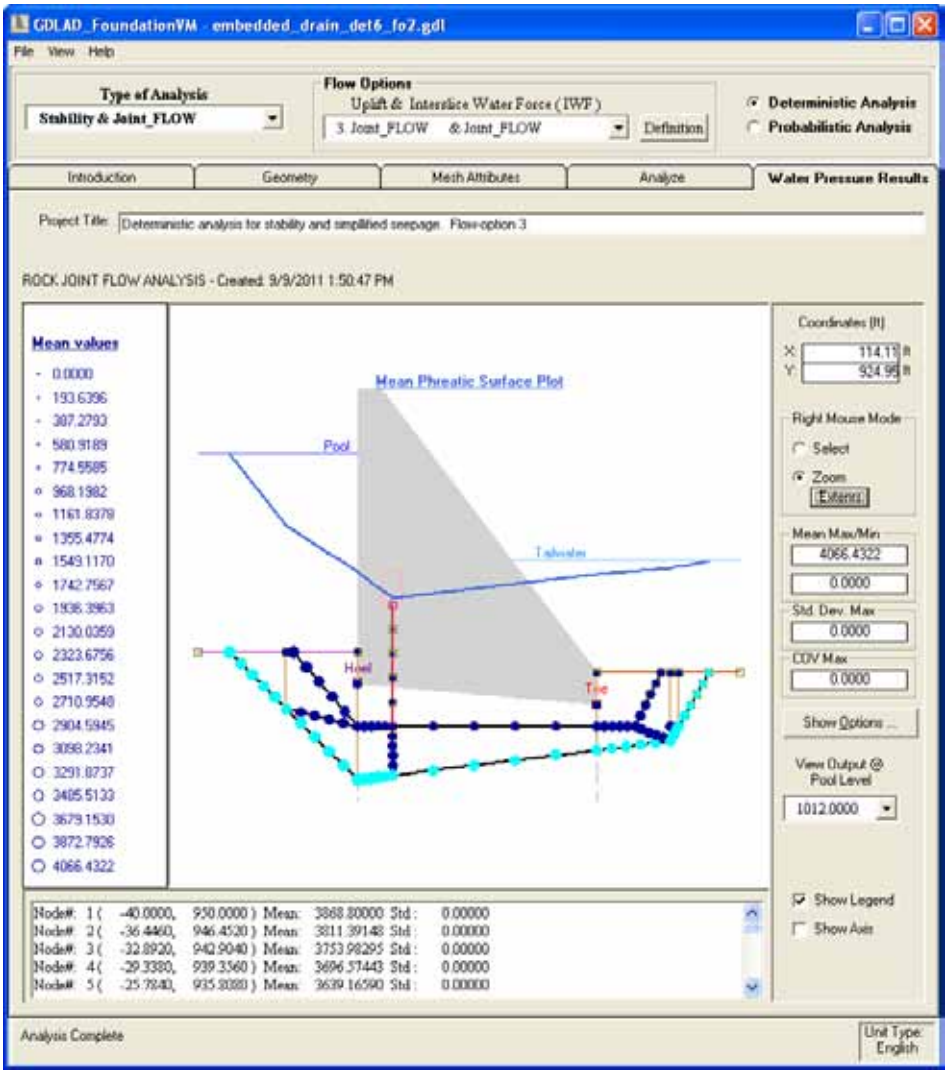

Figure 2.17. Water pressures at nodal points for flow option 3.

Table 2.6. Uplift resultant water pressure force U_i for flow options 1, 2, and 3.

Wedge ID	Uplift Resultant Water Pressure Force (U_i)		
	Flow Option 1	Flow Option 2	Flow Option 3
1	93.51	93.51	95.54
2	117.92	117.92	120.30
3	261.69	261.69	263.86
4	78.68	78.68	79.12
5	16.92	16.92	16.95
6	51.23	51.23	51.27

Table 2.7. Computed factors of safety for flow options 1, 2, and 3.

Factor of Safety	Flow Option 1	Flow Option 2	Flow Option 3
FS	2.584	2.584	2.568

Table 2.8. Difference between resultant water pressure forces acting on either side of the vertical face of wedges for flow options 1, 2, and 3.

Wedge ID	P(i-1) – P(i)		
	Flow Option 1	Flow Option 2	Flow Option 3
1	-78.26	-12.19	-24.50
2	-140.97	-51.31	-73.05
3	112.53	49.50	55.68
4	20.15	-13.21	13.07
5	23.15	8.42	9.02
6	63.32	18.71	19.73

The authors of this report consider the Figure 2.1 example used in this chapter to be a "limited" rock joint network problem with uniform aperture and uniform JRC (thus, uniform rock joint hydraulic conductivity). The authors' caution against applying/extending the observations made to other problems involving geometric variation in aperture and JRC values along rock joints as wells as to "moderate" to "extensive" rock joint networks. As will be shown using example problems provided in subsequent chapters, varying aperture and JRC values along rock joints as wells as moderate to extensive joint networking impacts the magnitude and distribution of uplift pressures, the magnitude of uplift pressures resultant forces acting normal to the base of wedges, and will thus impact the computed factor of safety (*FS*) against sliding for potential slip plane (and its wedges/sub-wedges) being investigated.

3 The Visual Modeler – GDLAD_ FoundationVM

This chapter provides guidance on the details and execution of the graphical environment GDLAD_FoundationVM, which we shall refer to as the Visual Modeler (VM). The VM offers a pre- and post-processing environment by accepting input from the user; the evaluation of the data and execution of either or both of the two FORTRAN engineering software (1) GDLAD_Foundation, for computing the stability of a non-overflow gravity dam embedded in rock, and (2) Joint_FLOW, for computing uplift pressures caused by flow along the rock joints contained within the rock foundation; and the displaying of results in the form of a system response curve and tabular form of data pertaining to water pressures at the sub-surface nodes and resultant uplift water pressure forces at the potential sliding plane for a two-dimensional cross section of a concrete gravity dam embedded in rock.

The VM comprises of a tab for introduction and initialization; two tabs for user input and grid development; and two tabs for user viewing of output and evaluation. Note that the terms grid and mesh are used synonymously throughout the report. The following sections describes the various tabs and there functionality.

3.1 The Introduction tab

The Introduction tab allows the user to create a new project; edit and save changes to a project or individually modify and save changes to the geometry as well as the generated mesh. Figure 3.1 portrays a concrete gravity dam embedded in rock with the ability to accept variable pool and tailwater; applicable silt and anchor forces; a gallery and rock foundation drain as well as a user defined potential slip plane within a subsurface mesh or rock discontinuities. The image of the embedded concrete gravity dam within Figure 3.1 will always be present when the Introduction tab is selected.

Located immediately above the various tabs (i.e. Introduction, Geometry, Mesh Attributes, Analyze, and Water Pressure Results) of Figure 3.1 are a group of options that define the type of analysis that will be conducted.

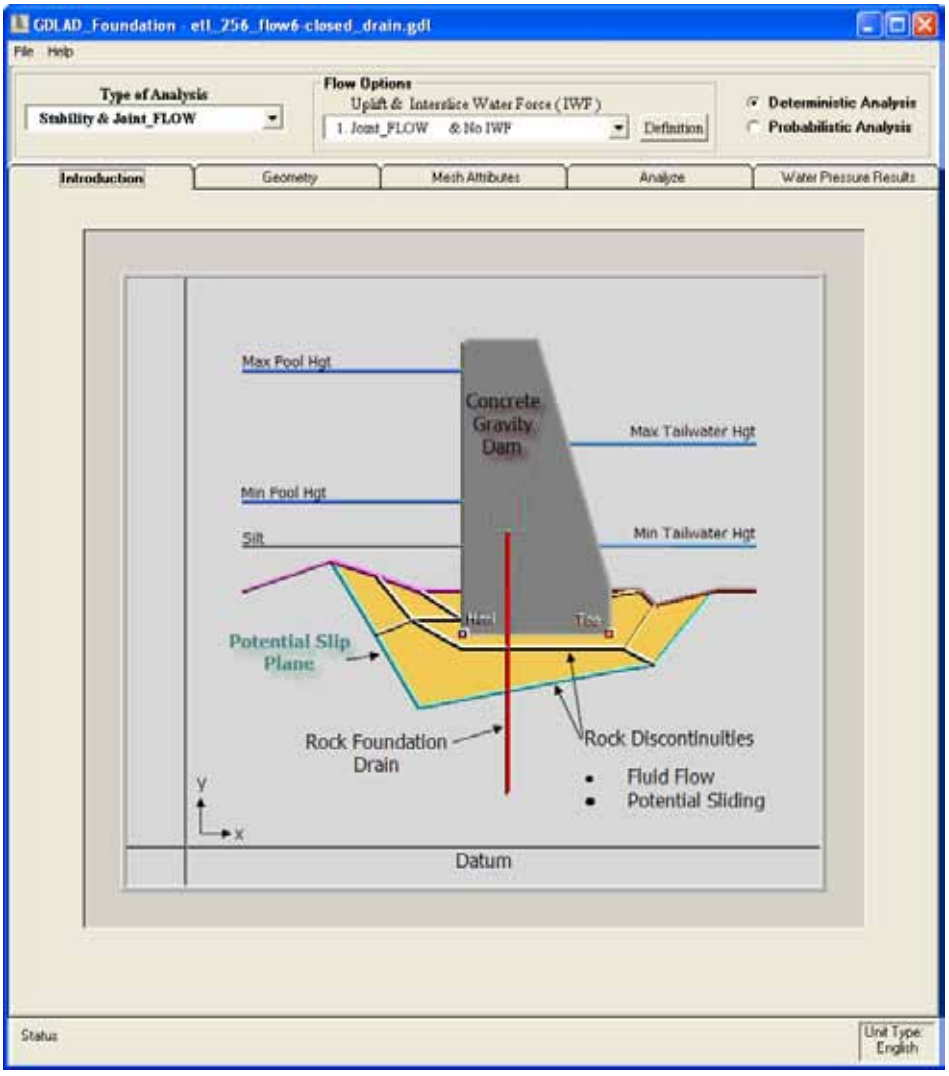

Figure 3.1. Depiction of a concrete gravity dam embedded in rock.

The first group of options is the *Type of Analysis* drop-down menu; the second is the *Flow Options* drop-down menu with the *Definition* button, and lastly, the two radio buttons for selection of either a Deterministic Analysis or a Probabilistic Analysis.

3.1.1 Defining the type of analysis

The three groups of options defined previously in section 3.1 are listed as follows:

1. The drop-down menu located at the furthest left of Figure 3.1 is labeled *Type of Analysis*. Selection of this menu allows the user to specify the type of analysis to perform for their particular study.

2. The drop-down menu at the center of Figure 3.1 is labeled *Flow Option*. It specifies the Uplift and Interslice Water Pressure Resultant Force calculations specific to the flow option selected. These Flow Options are only designed for a Stability and Joint_FLOW (flow options 1, 2, and 3) as well as a Stability and Simplified Seepage (flow options 4, 5, and 6) type of analyses. The Definitions tab that is part of the Flow Options selection menu classifies each specific flow option and is presented in Table 3.1 below. Flow options 1, 2, and 3 are further described in Table 2.2 of Chapter 2 and flow options 4, 5, and 6 are described in Table 6.4 of Chapter 6.
3. The two radio buttons on the far right establish whether the analysis is deterministic or probabilistic.

Table 3.1. Classification of uplift and interslice water forces as flow options.

Flow Options	Wedge Features	Uplift and Interslice Water Force (IWF)	Driving Wedge	Structural Wedge	Resisting Wedge
1	**Wedge Base**	Joint_FLOW	Flow Along Slip Plane	Flow Along Slip Plane	Flow Along Slip Plane
	Vertical Interslice	No IWF	No Water Pressures	No Water Pressures	No Water Pressures
2	**Wedge Base**	Joint_FLOW	Flow Along Slip Plane	Flow Along Slip Plane	Flow Along Slip Plane
	Vertical Interslice	Near Hydrostatic	Near Hydrostatic	Near Hydrostatic	Near Hydrostatic
3	**Wedge Base**	Joint_FLOW	Flow Along Slip Plane	Flow Along Slip Plane	Flow Along Slip Plane
	Vertical Interslice	Joint_FLOW	Flow Along Interslice	Flow Along Interslice	Flow Along Interslice
4	**Wedge Base**	ETL-1110-256	Hydrostatic	Flow Along Slip Plane	Hydrostatic
	Vertical Interslice	No IWF	No Water Pressures	No Water Pressures	No Water Pressures
5	**Wedge Base**	Line of Seepage	Hydrostatic	Flow Along Slip Plane	Hydrostatic
	Vertical Interslice	Structural Wedge Only	No Water Pressures	Flow Along Interslice	No Water Pressures
6	**Wedge Base**	Line of Seepage	Flow Along Slip Plane	Flow Along Slip Plane	Flow Along Slip Plane
	Vertical Interslice	No IWF	No Water Pressures	No Water Pressures	No Water Pressures

3.1.1.1 Stability and Joint_FLOW

The first option listed in the *Type of Analysis* drop-down menu is the *Stability & Joint_FLOW* type of analysis and pertains to the first three types of flow options (namely 1, 2, and 3) and are listed in the *Flow Options* drop down menu and highlighted in blue in Figure 3.2. This option is relevant to the Uplift and Interslice Water Pressure Resultant Force calculations which are explained in greater detail in Section 2.4 of Chapter 2.

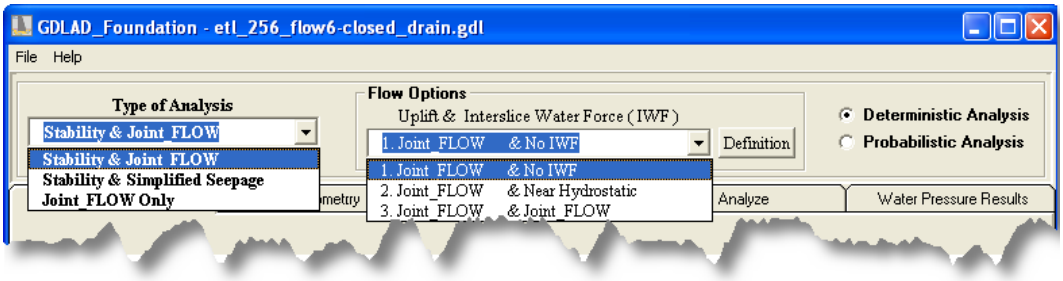

Figure 3.2. Selection of Stability & Joint_FLOW type of analysis with flow options 1, 2, and 3.

The *Definition* toggle button situated to the right of the *Flow Options* drop-down menu of Figure 3.3 gives a brief definition in table form of the selected flow option 1 which is highlighted in blue.

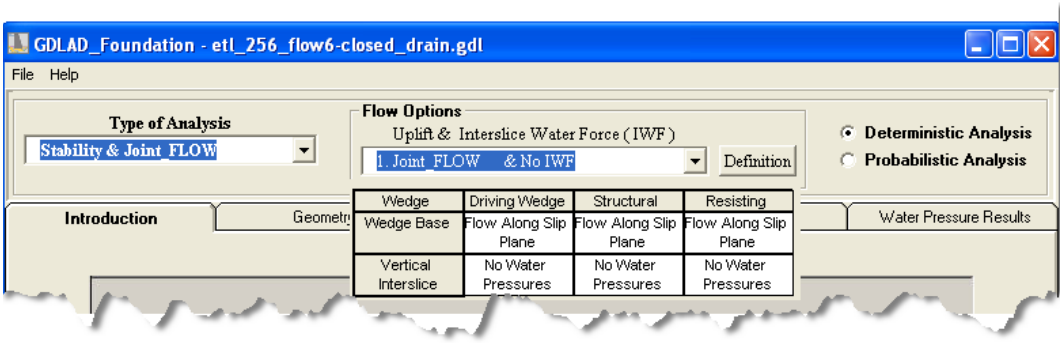

Figure 3.3. Definitions of calculations of uplift and interslice water forces for flow option 1.

For a *Stability & Joint_FLOW* type of analysis, the definitions of each of the first three flow options are further described in Table 2.2 of Chapter 2 which lists the methods used for the calculations for flow options 1, 2, and 3.

3.1.1.2 Stability and Simplified Seepage

The second option listed in the *Type of Analysis* drop-down menu is the *Stability & Simplified Seepage* and pertains to the second three types of

flow options (namely 4, 5, and 6). These are listed in the *Flow Options* drop-down menu and highlighted in blue in Figure 3.4. This option is relevant to the Uplift and Interslice Water Pressure Resultant Force calculations which are explained in greater detail in Section 6.2 of Chapter 6.

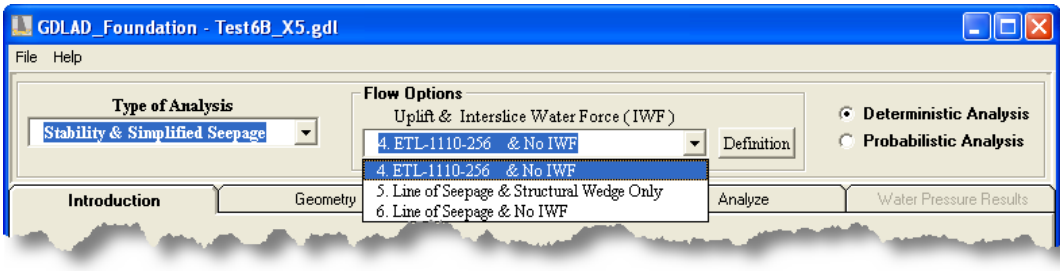

Figure 3.4. Selection of Stability & Simplified Seepage type of analysis with flow options 4, 5, and 6.

The *Definition* toggle button situated next to the *Flow Options* drop down menu of Figure 3.5 gives a brief definition in table form of the selected flow option 4 which is highlighted in blue.

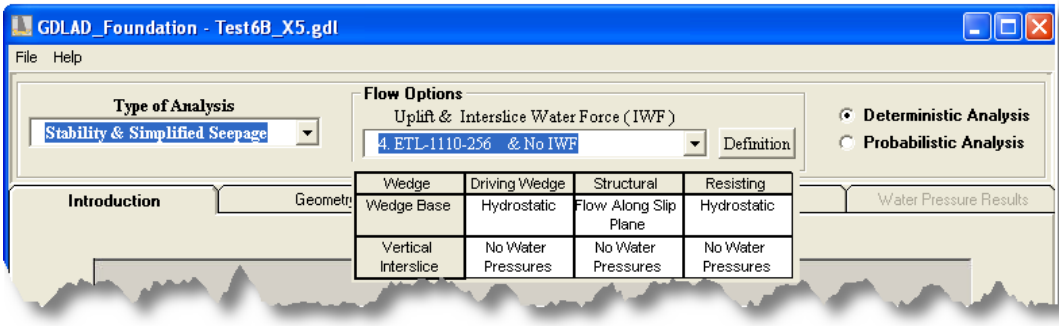

Figure 3.5. Definitions of calculations of uplift and interslice water forces for flow option 4.

For a *Stability & Simplified Seepage* type of analysis, the definitions of each of the second three flow options are further described in Table 6.4 of Chapter 6 which lists the methods used for the calculations for flow options 4, 5, and 6.

3.1.1.3 Joint_FLOW only

The third option listed in the *Type of Analysis* drop-down menu is for a *Joint_FLOW Only* type of analysis. Figure 3.6 shows this selection where nodal point water pressures and resultant water pressure forces will be calculated by the software Joint_FLOW.

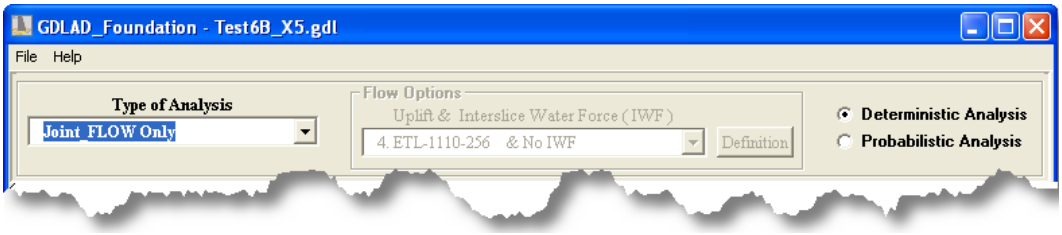

Figure 3.6. Selection Joint_FLOW only.

3.1.2 The Menu Bar

The Menu Bar is located below the window title of Figure 3.7. It consists of two items, *File* and *Help*.

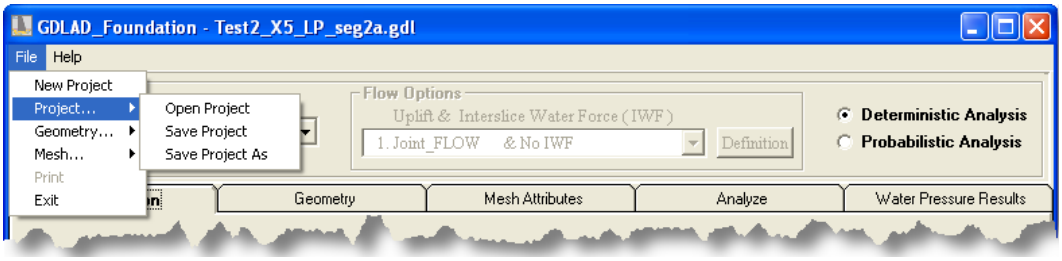

Figure 3.7. Creating and updating project, geometry and mesh files.

3.1.2.1 File Item

At the top left corner of Figure 3.7, the *File* item of the menu bar is highlighted in blue. When selected a list of options are displayed for selection. This is where projects, geometry, and generated mesh files can be created, retrieved or saved. If the *Exit* option is selected, GDLAD_Foundation will terminate.

In the case of a *New Project*, Figure 3.8 is presented for the user to select the type of units this project will work with. Presently, the options for units are English and Metric. Once the units have been selected, they cannot be altered for the remainder of the project.

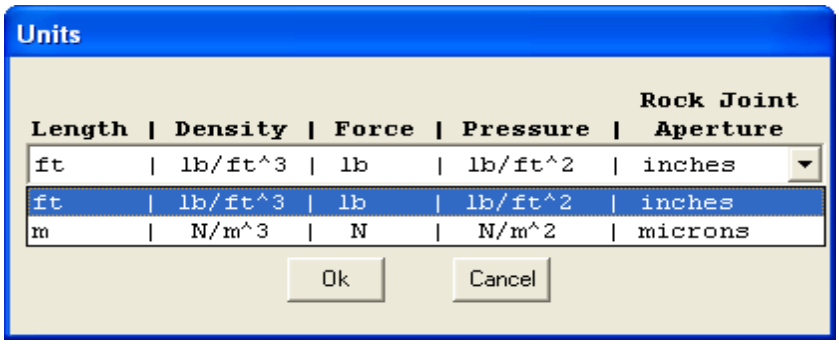

Figure 3.8. Initializing units for a new project.

3.1.2.2 Help Item

The second item at the top left corner of Figure 3.9 is the *Help* item of the menu bar and is highlighted in blue. When selected, two options are displayed:

1. *GDLAD_Foundation* provides guidance to the VM
2. *About GDLAD_Foundation* provides a splash screen with current up-to-date information about the VM

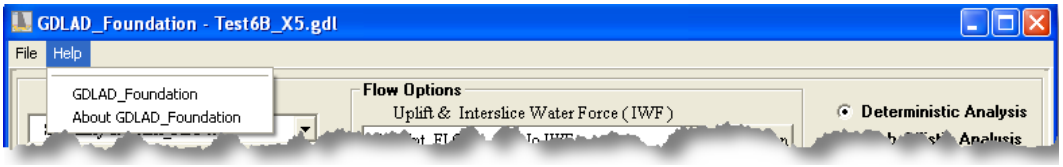

Figure 3.9. Guidance to GDLAD_Foundation.

3.1.3 The Status Bar

At the base of Figure 3.1, and shown in Figure 3.10, the status bar houses two items:

1. *Status* gives an explanation of the current condition of the VM and of any executing software
2. *Unit Type* states the units the current project is working with. The metric unit system is used in this instance.

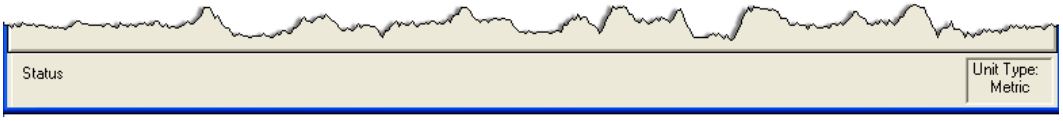

Figure 3.10. The Status Bar.

3.2 The Geometry tab

The Geometry tab allows the user to create a new project or edit and save changes to the geometry of the project. Figure 3.11 portrays a concrete gravity dam embedded in rock with a pool and tailwater; a gallery and rock foundation drain; and the assignment of the location of the heel and the toe.

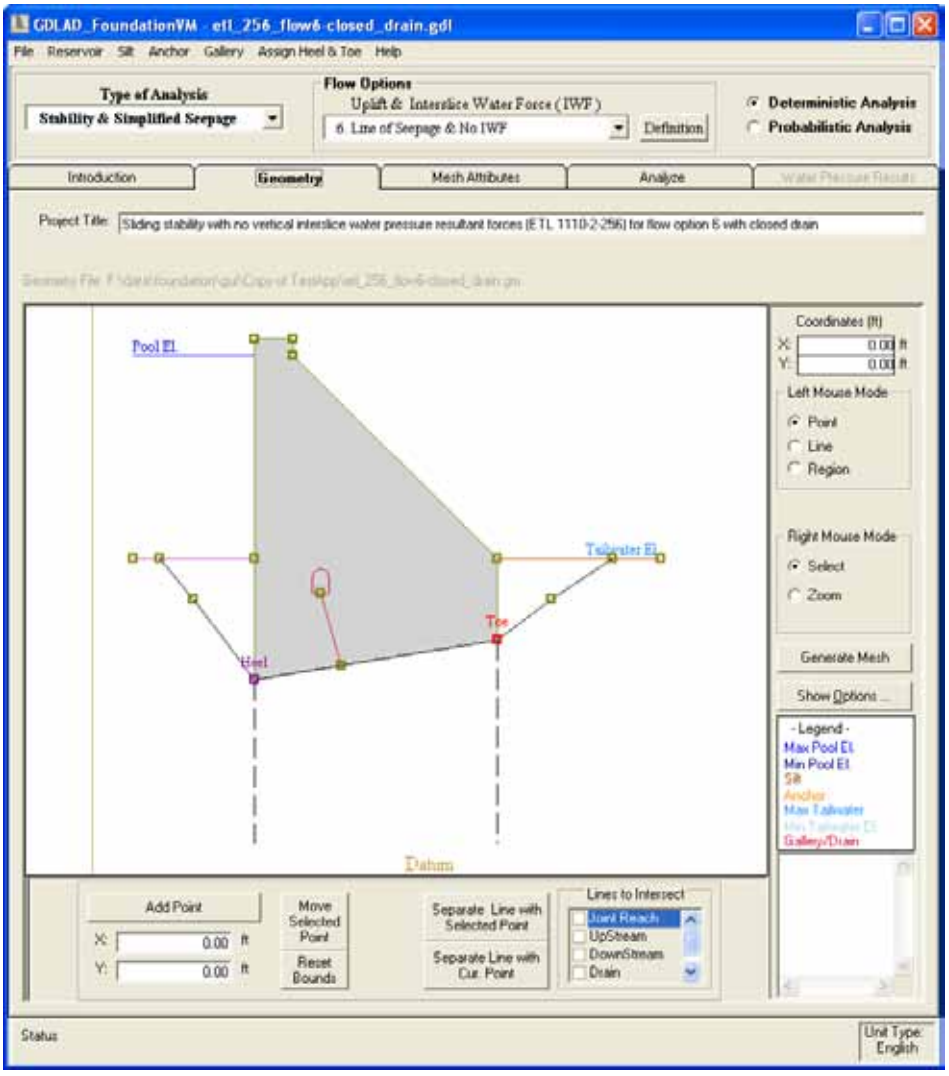

Figure 3.11. Depiction of a concrete gravity dam embedded in rock.

3.2.1 The Project Title

The *Project Title* is located above the image of Figure 3.11 and is a very important feature that allows one to convey information about the project. A total of 512 characters can be used to describe the project. This project title is visible and can be accessed by all the tabs except when the Introduction tab is selected.

3.2.2 The Cursor and Mouse buttons

As the cursor moves across the image window of Figure 3.12, the *X:*, *Y:* coordinates at the upper right hand corner change. The coordinates are in units of feet for this example.

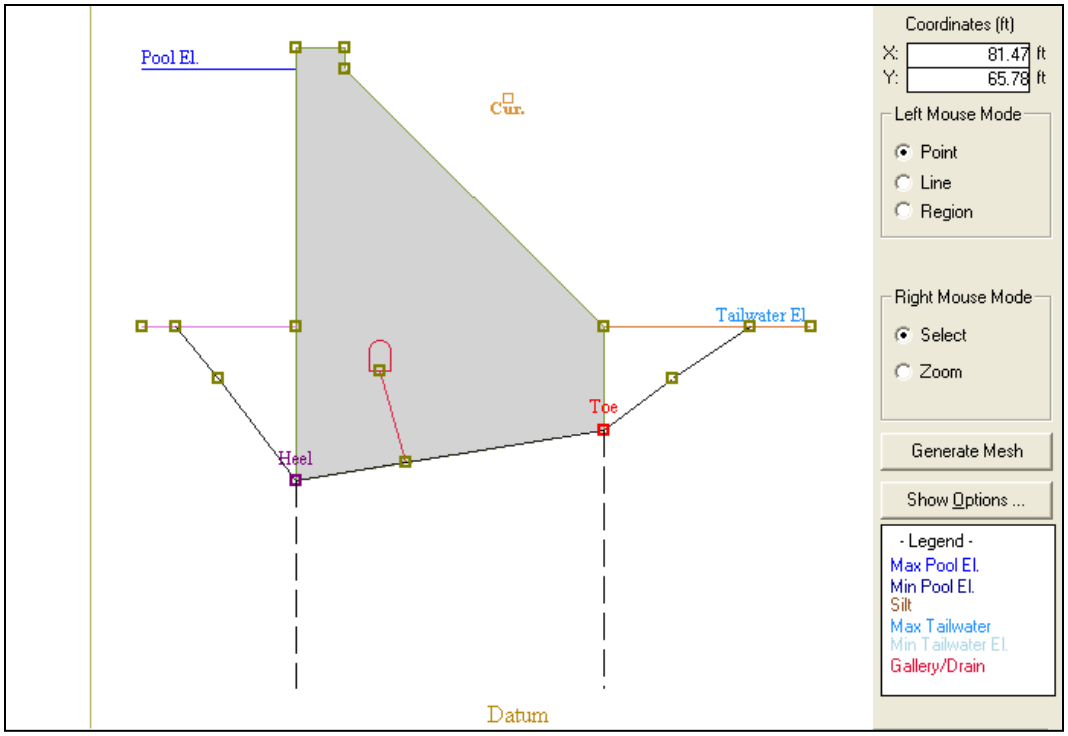

Figure 3.12. Image of embedded concrete gravity dam.

When the left mouse button is used in the image window, a small brown square with the text *Cur.* labeled directly below will appear. This can be used to add a point within the image area. The left mouse button when moved outside the image area is used for selecting radio buttons, check boxes, push down buttons, or pull down menus, basically any function that is available in the VM.

The right mouse button is mainly used when working within the image window and is used for selecting nodes or lines.

3.2.3 The Left Mouse Mode

The *Left Mouse Mode* group of radio buttons located below the *X:*, *Y:* coordinates on the right hand side of Figure 3.12 is used for the creation of points, lines, or regions that specify material properties.

3.2.3.1 Adding or modifying points

The *Point* radio button of the *Left Mouse Mode* (*Point Mode*) has to be selected before any points can be created or deleted. There are two ways to create points. By entering the coordinates directly in the *X:* and *Y:* input boxes located at the bottom left of Figure 3.13 or by a left mouse click at a

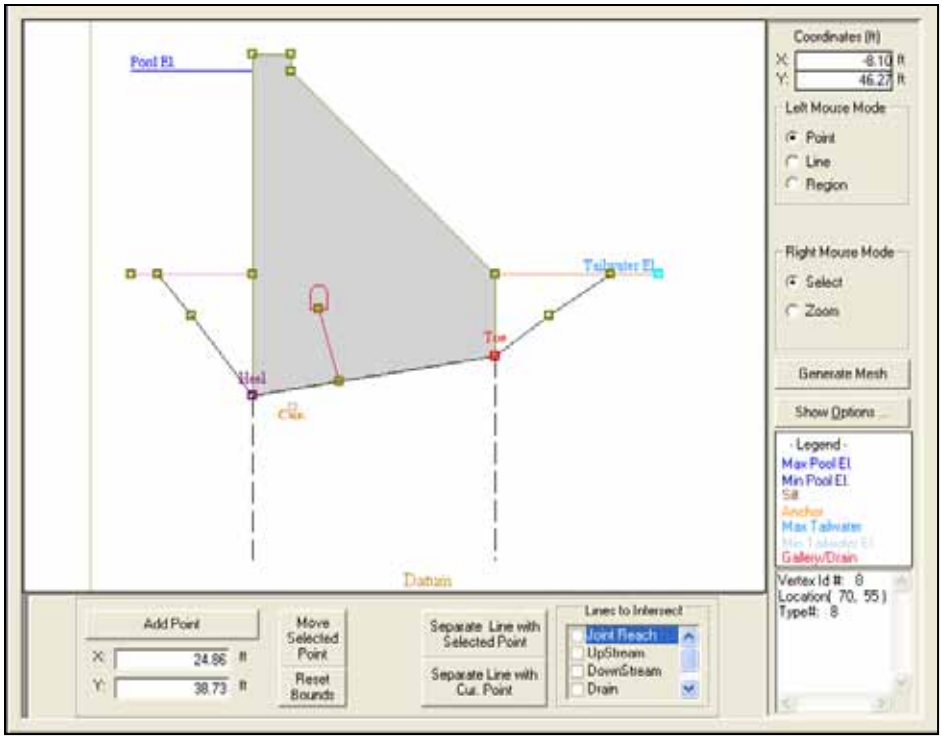

Figure 3.13. Adding or modifying points.

location that displays the brown square (Section 3.2.2) and then selecting the *Add Point* button. If a coordinate is entered that is beyond the current extent of the window, the *Reset Bounds* button will resize the window to accommodate the entire image within the window.

There is also the option of moving a point. Select a point by drawing a box around the point with the right mouse button. Next, left mouse click by placing the cursor at a new location and finally, select the *Move Selected Point* button. This sequence of events will move a point from one location to another. To delete a point, select the point by holding the right mouse button and drawing a window around it. The point will be highlighted in light blue, then hit the *Delete* key at the keyboard. The line that was connected to this point will also be deleted.

3.2.3.2 Creating a point on a line

There are two options where a line can be separated and two lines with the addition of a point will replace the original line. The first option is to add a point with the left mouse and the second is to select an existing point with the right mouse. Refer to Section 3.2.2 for both options. It is relatively simple to create a point on a line.

For the first option and in *Point Mode*, select with the left mouse button the type of line (in the *Lines to Intersect* group box) you would like to add a point to. With the left mouse button, click on a location on the line to place the point, the brown cursor (*Cur.)* will appear. After the *Separate Line with Cur. Point* button is selected, a new point will appear and two separate lines will replace the original line.

For the second option and in *Point Mode*, select with the left mouse button the type of line (in the *Lines to Intersect* group box) you would like to add a point to. With the right mouse button, select an existing point. After the *Separate Line with Selected Point* button is selected, a new point will appear and two separate lines will replace the original line.

3.2.3.3 Adding and deleting lines

When the *Line* radio button of the *Left Mouse Mode* is selected (*Line Mode*), a line can be created by connecting two points. There are five different types of lines available for selection with the *Drain* line type radio button being selected in Figure 3.14. These line types define:

- the shape of the Gravity Dam by the selection of the radio button with the *Concrete* line type labeled in green;
- the radio buttons for the *Upstream* and *Downstream* ground surfaces (labeled in pink and brown);
- the radio button for the *Drain* labeled in red; and
- the radio button for all rock *Joint Reaches* labeled in black.

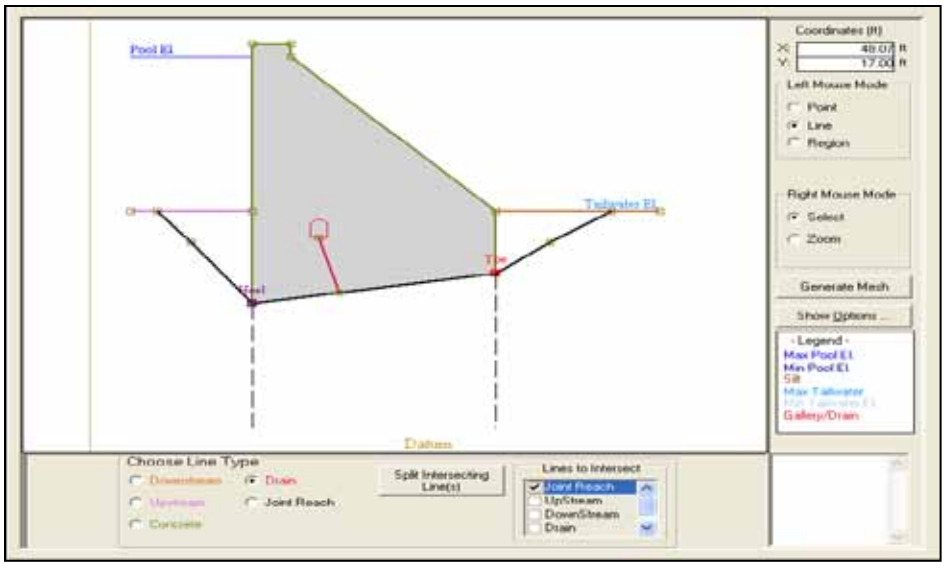

Figure 3.14. Adding or modifying lines.

To remove a line, select the line by holding the right mouse button and drawing a small window over it. The line will be highlighted in light blue, then hit the *Delete* key of the keyboard. The line will be deleted but the points connecting the line will remain.

3.2.3.4 Split intersecting lines

A line can be used to intersect multiple lines in order to separate these lines and create new points. An example would be the line of drains (in red) that intersect the base of the dam as in Figure 3.14. One way will be to draw the drain line from the floor of the gallery past the base of the dam. Select with the left mouse button the type of line (in the *Lines to Intersect* group box) you would like the drain line to intersect. In this case it is the *Joint Reach*. Select the drain line (will be highlighted in blue) then select the *Split Intersecting Line(s)* button. A point will appear at the intersection of the line of drains and the joint reach at the base of the dam. This joint reach is now replaced by two reaches on either side of the line of drains. Deselect the drain line and remove the node and line beneath the reach at the base of the dam. This will produce the line of drains in Figure 3.14.

3.2.3.5 Creating and modifying regions

Regions are created for classifying the properties of various rocks in the study. When the *Region* button of the *Left Mouse Mode* group of radio buttons is selected (*Region Mode*), an instruction panel appears as shown at the base of Figure 3.15. Regions are created from new points or from existing points which was described in Sections 3.2.3.1 and 3.2.3.2. The *Start Another Region* button must be selected in order to initiate a region. Keyboard characters like “S” for snapping to a point; “U” to go back to the previous line drawn; “C” to close or complete the region; and the “<ESC>” key to cancel previous edits are the key sequences used to create regions.

The *Accept* and *Cancel* buttons keep and cancel changes respectively during the creation of a region. Once a region is created it will be highlighted in blue as in Figure 3.15 which shows a total of three regions. After the completion of a region, a new region can be created by selecting the *Start Another Region* button. The *Remove all Regions* button will remove all regions. Once this button is selected, all regions will be gone. The *Exit Region Edit*” button is only used to exit this sub window for region creation.

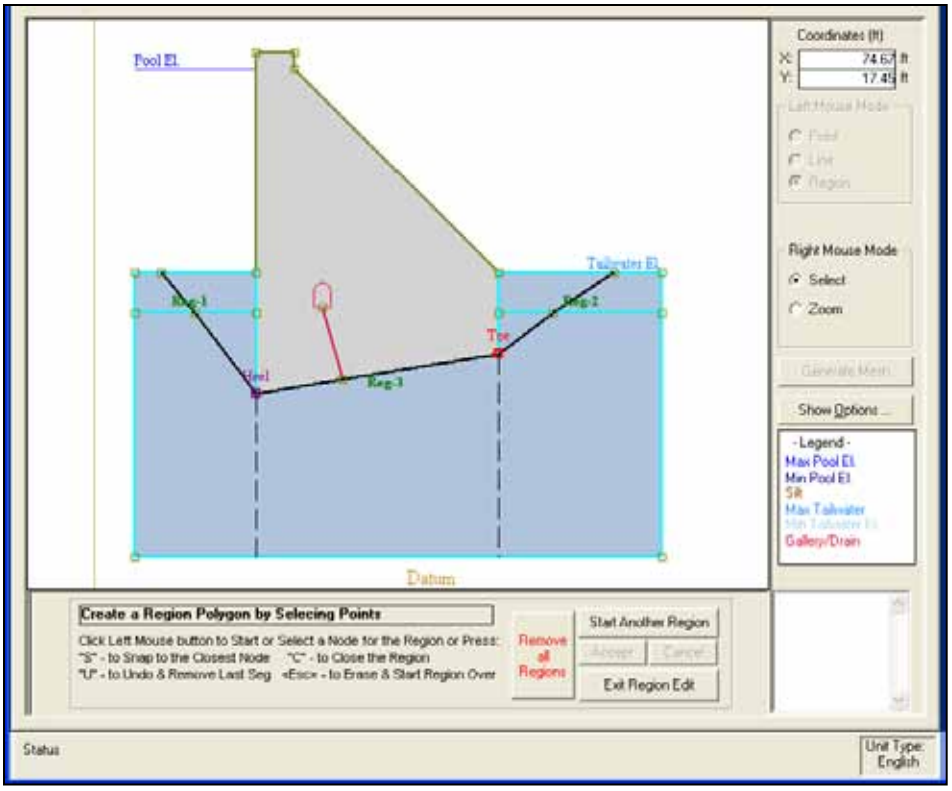

Figure 3.15. Adding and modifying regions.

3.2.4 The Right Mouse Mode

The Right Mouse Mode group of radio buttons located at the center right hand side of Figure 3.15 is used in conjunction with the creation of points, lines or regions that specify material properties.

3.2.4.1 The Select Mode

The Select radio button of the Right Mouse Mode (*Select Mode*) of Figure 3.15 has to be selected before any points, lines or regions can be created or deleted. This radio button is usually selected in conjunction with the Left Mouse Mode group of radio buttons.

3.2.4.2 The Zoom Mode

The Zoom radio button of the Right Mouse Mode (*Zoom Mode*) of Figure 3.16 is used to zoom in on locations of interest. The ability to keep zooming into the image is an option; however, the capability to zoom out is currently not available. There is only one general way to zoom out and it is the Extents button which redraws the image to its original size and limits.

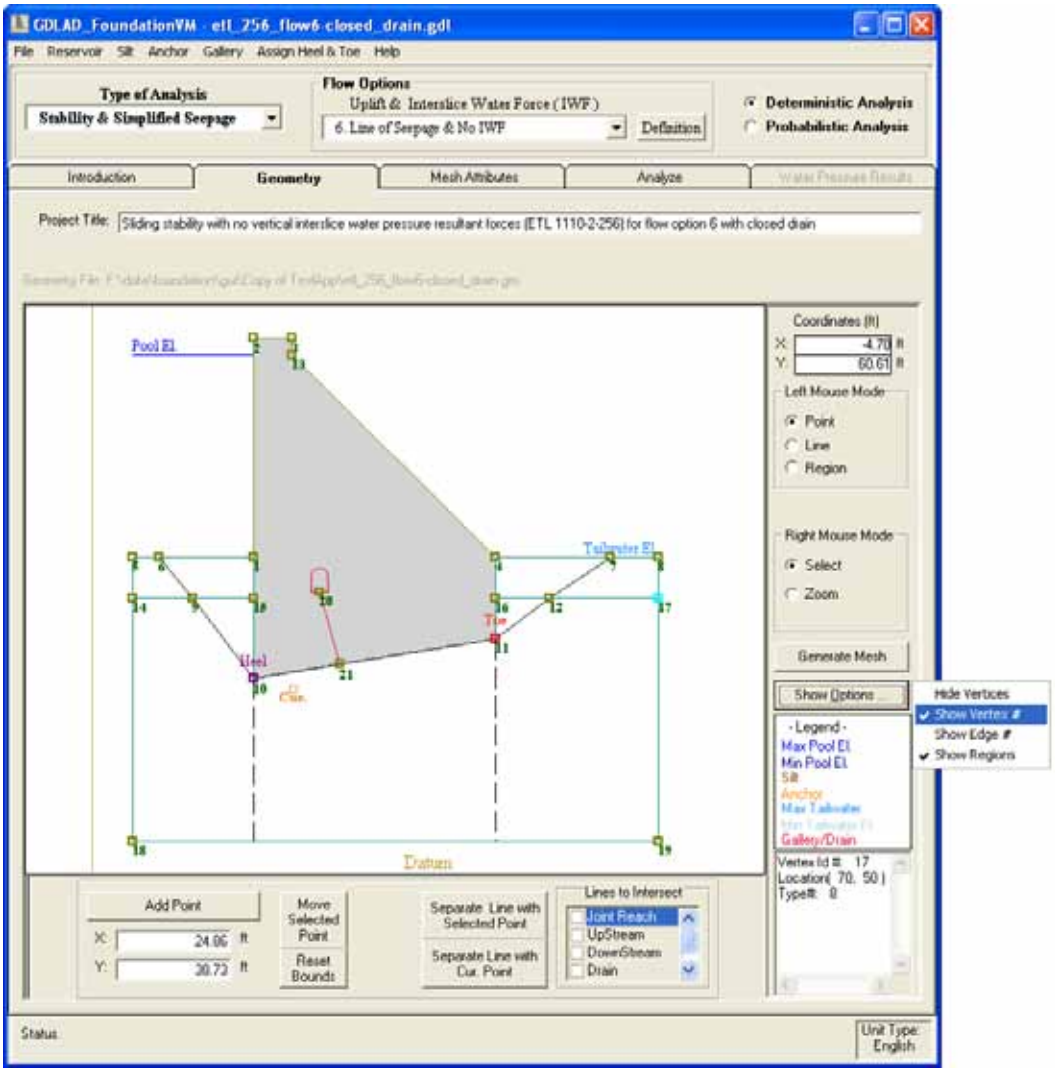

Figure 3.16. Right side menu functions of the Geometry tab.

3.2.5 Generate Mesh

When all additions and modifications of regions, lines and nodes are finalized and accepted, the next step is to generate a mesh in order to assign relevant attributes to the joint reaches, drain and regions. This is also true when the Potential Sliding Plane is defined and Wedges formed. The *Generate Mesh* button is located at the center right of Figure 3.16.

3.2.6 Show Options

The *Show Options...* button is shown selected in Figure 3.16 with the four options available. The "*Show Vertex #*" (highlighted in blue) and the "*Show Regions*" options have both been selected and designated by a check mark. These options will show the I.D. numbers of the points and also display the

outlines of the regions as seen in the image area of Figure 3.16. The other two options not selected are "*Hide Vertices*" which removes the brown squares identifying the locations of points in the image and the "*Show Edge #*" that labels the I.D. numbers of line segments relating to regions (RG-*id*), upstream ground surface (US-*id*), downstream ground surface (DS-*id*), drain (D-*id*), the edges of the gravity dam (E-*id*) and the sub surface joint reaches(R-*id*).

3.2.7 Legend and geometry information

The "- *Legend* -"window located directly below the "*Show Options…*" button of Figure 3.16 identifies the legends for the Pools, tailwater, Silt and Gallery/Drain, and Anchor. If these items are selected the image will display them in their specific color.

The text window located below the "- *Legend* -"window gives geometric information about the point or lines that are selected. Figure 3.16 shows that point ID=17 has been selected (the highlighted blue square). This information is shown in the geometry text window together with the *X:*, *Y:* coordinate of the point. If in *Line Mode*, the selected line would be highlighted and the line ID would be listed as well as the *X:*, *Y:* coordinates of the two nodes connecting the line and its length.

3.2.8 The Menu Bar

The Menu Bar is located below the window title of Figure 3.11. It consists of seven items, *File, Reservoir, Silt, Anchor, Gallery, Assign Heel & Toe,* and *Help*.

3.2.8.1 File menu item

The first item on the left hand side of the menu bar of Figure 3.17 is the *File* item which is highlighted in blue. Once selected, the drop-down menu shows the various file selections which are explained in Section 3.1.2.1. The only additional item is the *Print* item which is highlighted in blue. Selection of *Print* sends the image of the window (with the white background which includes the concrete gravity dam) to the printer.

Figure 3.17. Creating and updating project, geometry and mesh files.

3.2.8.2 *Reservoir menu item*

The *Reservoir* item of the menu bar of Figure 3.18a is highlighted in blue. When selected a list of three options are displayed. The options include:

1. *Pool* elevation (Figure 3.18b)
   Data can be entered for a Minimum Pool elevation, a Maximum Pool elevation, and the Increment which is used for generating intermediate pool levels and is used in a probabilistic analysis (discussed in Chapter 7).
2. *Tailwater* elevation (Figure 3.18c)
   This is the option for a constant tailwater elevation or a variable tailwater elevation. Figure 3.18c shows that a constant tailwater has been selected for all pool levels. Selection of a variable tailwater requires 4 input parameters

   a. Minimum tailwater elevation
   b. Minimum corresponding limiting pool elevation
   c. Maximum tailwater elevation
   d. Maximum corresponding limiting pool elevation

   The minimum and maximum tailwater elevations are associated with corresponding lower and upper pool elevations. When the pool elevation is less than or equal to the specified limiting lower pool elevation, the minimum tailwater (elevation) value is used. When the pool elevation is greater than or equal to the specified limiting upper elevation, the maximum tailwater (elevation) value is used. However, if the pool elevation is in between the lower and upper limiting pool values, the tailwater elevation is calculated by linearly interpolating between the minimum and maximum values.
3. *Show pools* (Figure 3.18d)
   To preview all pool elevations calculated from the minimum and maximum values entered, select Show Pools. These pool and tailwater elevations are described within Group 7 of Appendix D and provided as (ASCII) input to GDLAD_Foundation (FORTRAN).

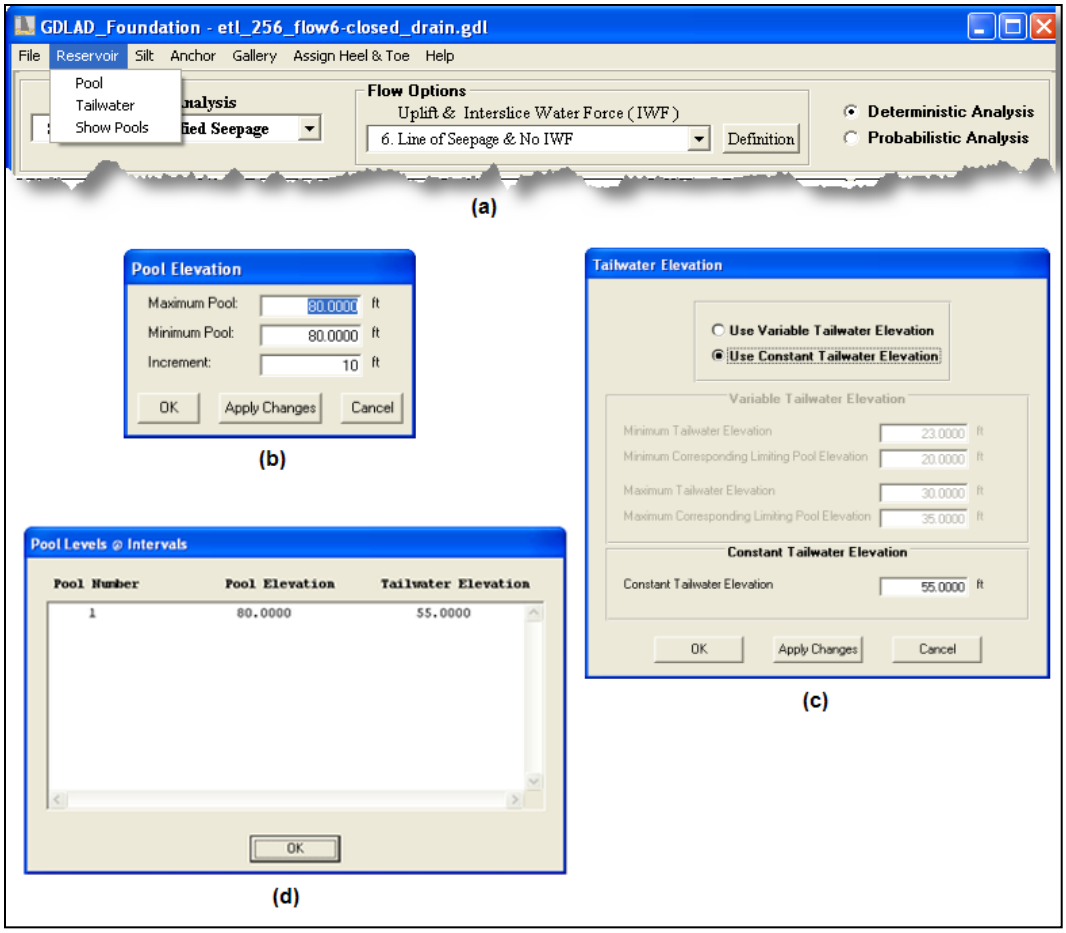

Figure 3.18. Reservoir input information. (a) Reservoir menu item, (b) Pool elevations, (c) Tailwater elevations, and (d) Reservoir and tailwater levels.

If the analysis is for a single pool, the Minimum Pool and Maximum Pool values should be equal, with a constant tailwater value entered. There should only be one pool elevation displayed when the Show Pools option is selected as in Figure 3.18d.

3.2.8.3 Silt menu item

This menu item describes the Silt characteristics when Silt pressures in the pool are significant and will be added to the horizontal force acting on the two-dimensional cross-section of the concrete gravity dam as shown in Figure 3.19. (Note that the weight of silt is also included in the stability analysis) Specific data within this menu is provided as input to GDLAD_Foundation FORTRAN and described within ASCII Group 5 data input of Appendix D. Silt parameters can be entered into the display Silt Parameters window. The following silt parameters available for user input are listed (note that items 5 and 6 will only be displayed for a probabilistic analysis):

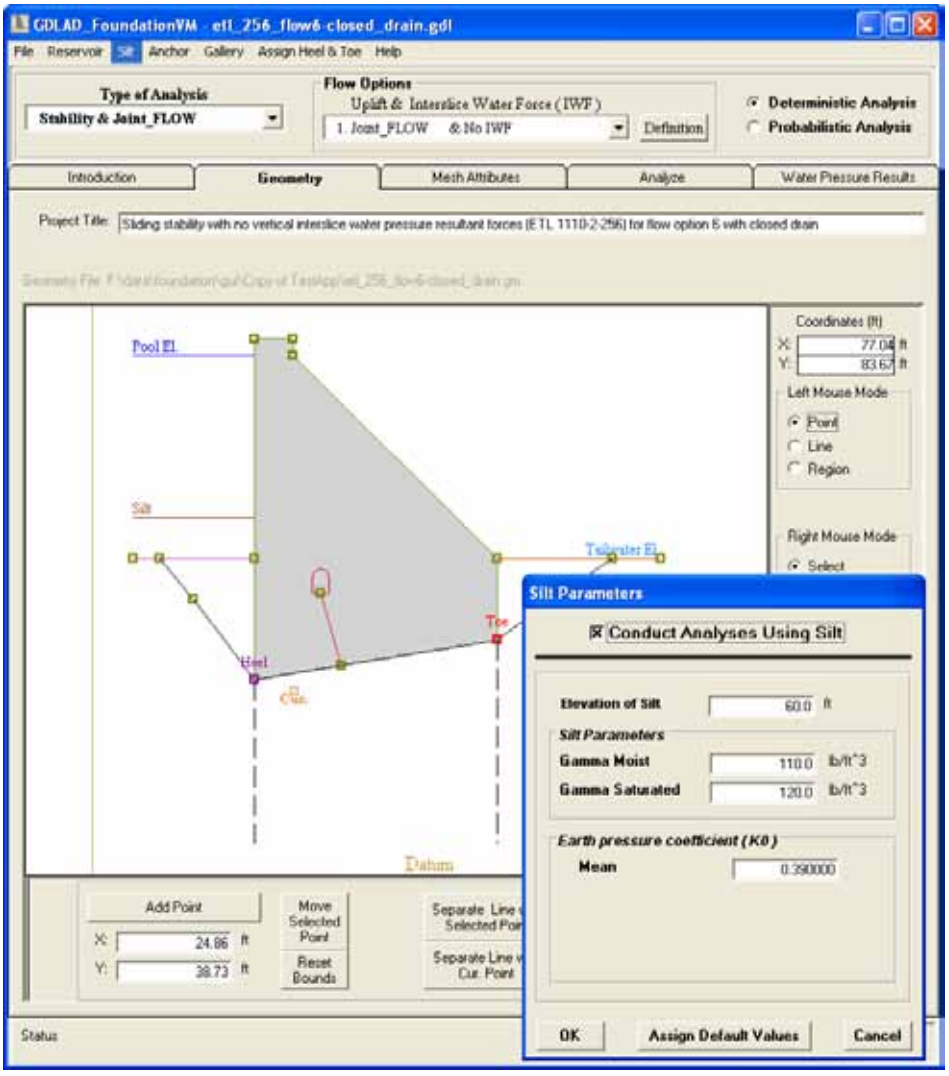

Figure 3.19. Silt parameters.

1. γ_{Moist}
   the moist unit weight of the silt in pounds per cubic foot
2. $\gamma_{Saturated}$
   the saturated unit weight of the silt in pounds per cubic foot
3. H_{Silt}
   the vertical distance from point a (of Figure 3.19) to the top of the Silt
4. K_o (Mean)
   the at-rest lateral pressure coefficient or the mean value
5. Standard deviation
6. Probability distribution type

EM 1110-2-2100, 1 December 2005, "Stability Analysis of Concrete Structures", states that horizontal silt pressure is assumed to be equivalent to that of a fluid weighing 85 pcf.

It also states that vertical silt pressure is determined as if silt were a soil having a wet density of 120 pcf. This results in a value of K_O equal to 0.39 which is provided as the default. If variable K_O is uncertain or random, a standard deviation and probability distribution type will be expected from the user. However, if K_O is a constant and not considered random then the standard deviation should be set to zero and the distribution type will be ignored.

For a K_O distribution, a mean of 0.39 and standard deviation of 0.0975 are the default values when using *Bounded Normal* and *Lognormal* distributions. When using Uniform distribution, a minimum of 0.29 and maximum of 0.49 are the default values. The *Assign Default Values* button is available to allow the user to select preset values as input.

The *OK* button assures that the edits will be saved and the *Cancel* button will not save any new data entered.

3.2.8.4 Anchor menu item

This *Anchor* menu describes the Anchorage features when Anchor force is considered for improving sliding stability of the gravity dam (Figure 3.20). Specific data within this worksheet is provided as input to GDLAD_Foundation and described within Group 4 of Appendix D. Relative data concerning post-tensioned anchors may be entered. The first six input variables and two optional buttons are defined as follows:

1. *Anchor Pt 1* From Toe (2 input values)
   x-, *y*- coordinates of the center of the Anchor Group on the downstream side at the top of dam
   The *Use Cursor Pnt* button below updates the *X*1 and *Y*1 coordinates with the position of the *Cur*. (brown cursor point) that is placed directly on the line defining the side of the dam.
2. *Anchor Pt 2* From Toe (2 input values)
   x-, *y*- coordinates of center of the Anchor Group at the base of the dam

The *Use Cursor Pnt* button below updates the *X*2 and *Y*2 coordinates with the position of the Cur. (brown cursor point) that is placed directly on the line defining the base of the dam.

3. Number of Anchors per Group
4. Spacing of Anchor Groups along the length of the dam

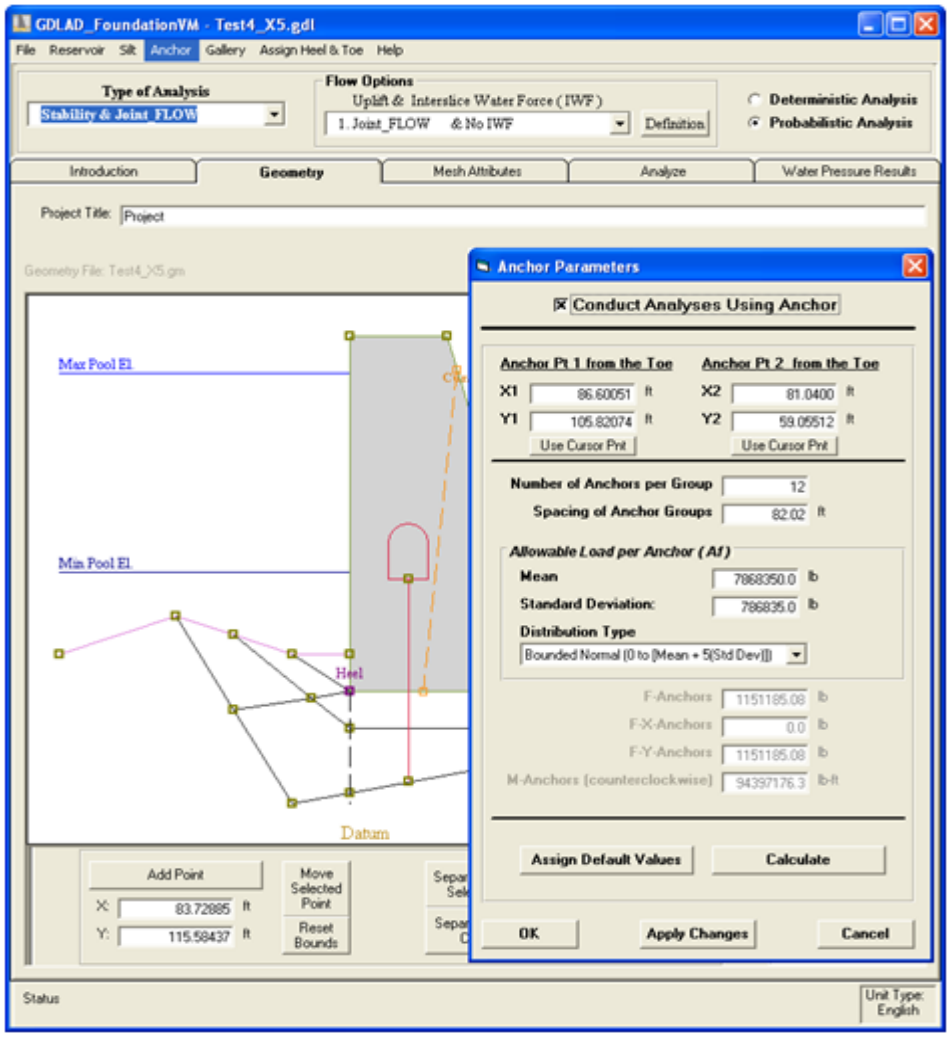

Figure 3.20. The *Anchor* menu item provides graphical presentation of Anchor positions relative to the concrete gravity dam and additional information relating to these post-tensioned anchors.

The next three input values provide information regarding the uncertainty in the allowable load per Anchor and thereby Anchor force. If the variable, load per anchor (A_f), is considered deterministic, a constant or the mean for the Anchor load should be entered and the Standard deviation set to zero. Distribution type will be ignored if the variable is deterministic. If the Anchor Load is random, then the mean, standard deviation and distribution type must be provided.

1. A_f(Mean)
   Load per individual Anchor
2. Standard deviation
3. Probability distribution type

The *Calculate* button is optional and can be selected in order to preview the resultant, horizontal and vertical Anchor forces and moment (about the toe) due to the Anchor forces. For an Anchor force distribution, a mean load per anchor of 35,000 lb and standard deviation of 3,500 lb are the default values when using *Bounded Normal* and *Lognormal* distributions. When using a *Uniform* distribution, a minimum of 31,500 lb and maximum of 38,500 lb are the default values. The *Assign Default Values* button is available to allow for preset values as input.

The *Apply Changes* button located at the center bottom of the *Anchor Parameters* window of Figure 3.20 allows any changes made to be saved in memory and the image of Figure 3.20 will be updated automatically.

The *Cancel* button located at the right hand bottom corner of the *Anchor Parameters* window of Figure 3.20 allows any changes made to be disregarded only since the last execution of the *Apply Changes* button, and exits out of the *Anchor Parameters* window.

The *OK* button located at the left hand bottom corner of the *Anchor Parameters* window of Figure 3.20 saves any changes in memory and exits out of the *Anchor Parameters* window.

The *OK* button assures that the edits will be saved and the *Cancel* button will not save and new data entered.

3.2.8.5 Gallery menu item

The distances that define the Height and Base of the Gallery as well as designating a dome on the Gallery is determined here. This is also the place where one can specify whether this is an open or closed drainage system. Figure 3.21 shows the *Drainage and Gallery Information* window when the Gallery menu item is selected. Values for $X_{W\text{-}Gallery}$, $Y_{B\text{-}Gallery}$ and L_{Drain} are among the values that are calculated by the VM internally from the points and lines (introduced in Section 3.2.3.1 to 3.2.3.4) that were added to create the Concrete Gravity Dam, the Gallery and line of drains.

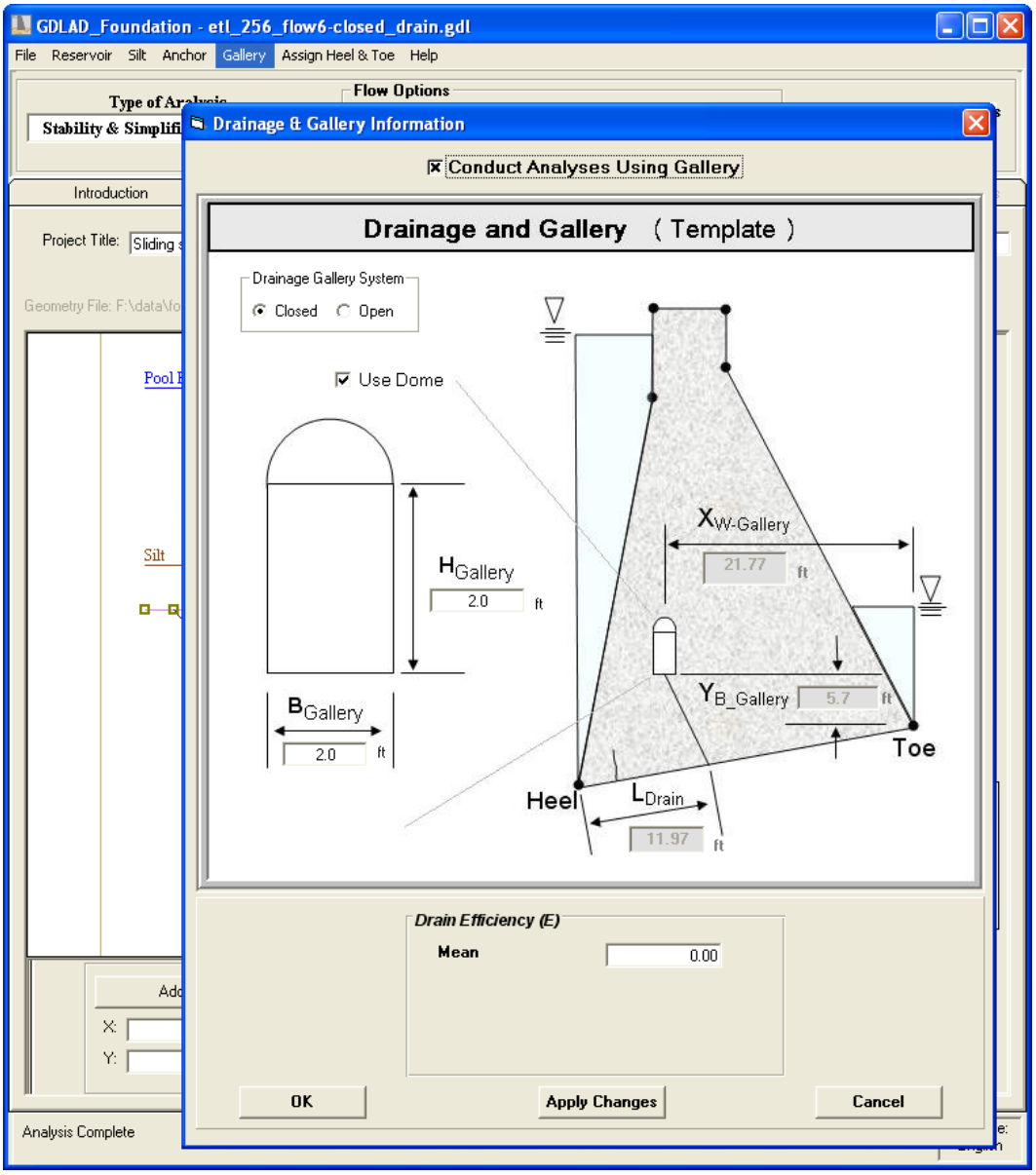

Figure 3.21.The Drainage and Gallery system.

Uplift pressures play an important role in the sliding stability of the concrete gravity dam. Two options are available that can describe this phenomena, i.e. the non-site specific uplift pressures that is described extensively in Chapter 6 (for Flow Options 4, 5 and 6) and the site specific uplift pressures provided by the program Joint_FLOW for flow options 1, 2, and 3 and presented in Chapter 4.

A non-site specific approach for describing the uplift pressure normal to the sloping dam-rock foundation interface is the efficiency of the drain (*E*). The next three input values provide information regarding the uncertainty

in the allowable Drain Efficiency[1]. The values entered in the *Mean* value field in decimal percentage will be used as a constant in a deterministic analysis. For a probabilistic analysis, the mean, standard deviation and distribution type are required.

A mean of 0.375 and standard deviation of 0.1 are the default values. The three distribution types that are available for *E* are the *Bounded Normal*, the *Bounded Lognormal*, and *Uniform*. The default type is *Bounded Normal*. A *Bounded Normal* distribution is a normal distribution that is only sampled between two specific values (0 and 1 in this case). A *Bounded Lognormal* distribution is a lognormal distribution that is also sampled between two specified values (0 and 1).

The *Apply Changes* button located at the center bottom of Figure 3.21 allows any changes made to be saved in memory and the image of Figure 3.21 will be automatically updated.

The *Cancel* button located at the right hand bottom corner of Figure 3.21 allows any changes made, since the last execution of the *Apply Changes* button, to be disregarded and exits out of the *Drainage and Gallery Information* window.

The *OK* button located at the left hand bottom corner of Figure 3.21 saves any changes in memory and exits out of the *Drainage and Gallery Information* window.

3.2.8.6 Assign Heel and Toe menu item

After the construction of the concrete gravity dam, the locations of the heel and the toe can be assigned. Selection of the "*Assign Heel & Toe*" Menu Item highlighted in blue in Figure 3.22 generates the "*Assign Structure Heel & Toe*" widow at the bottom of the figure. It is a relatively easy procedure:

1. Select a point by depressing and holding the right mouse button until point is selected. The selected point will be highlighted in light blue.
2. Choose the *HEEL* button. The text "*Heel*" will be displayed above the selected point.

[1] Recall EM 1110-2-2100 provides guidance on the assigned E value.

3. Select another point for assigning the Toe and follow the same procedures as (1) and (2) above.

Select the *Done* button to return to the *Geometry* window.

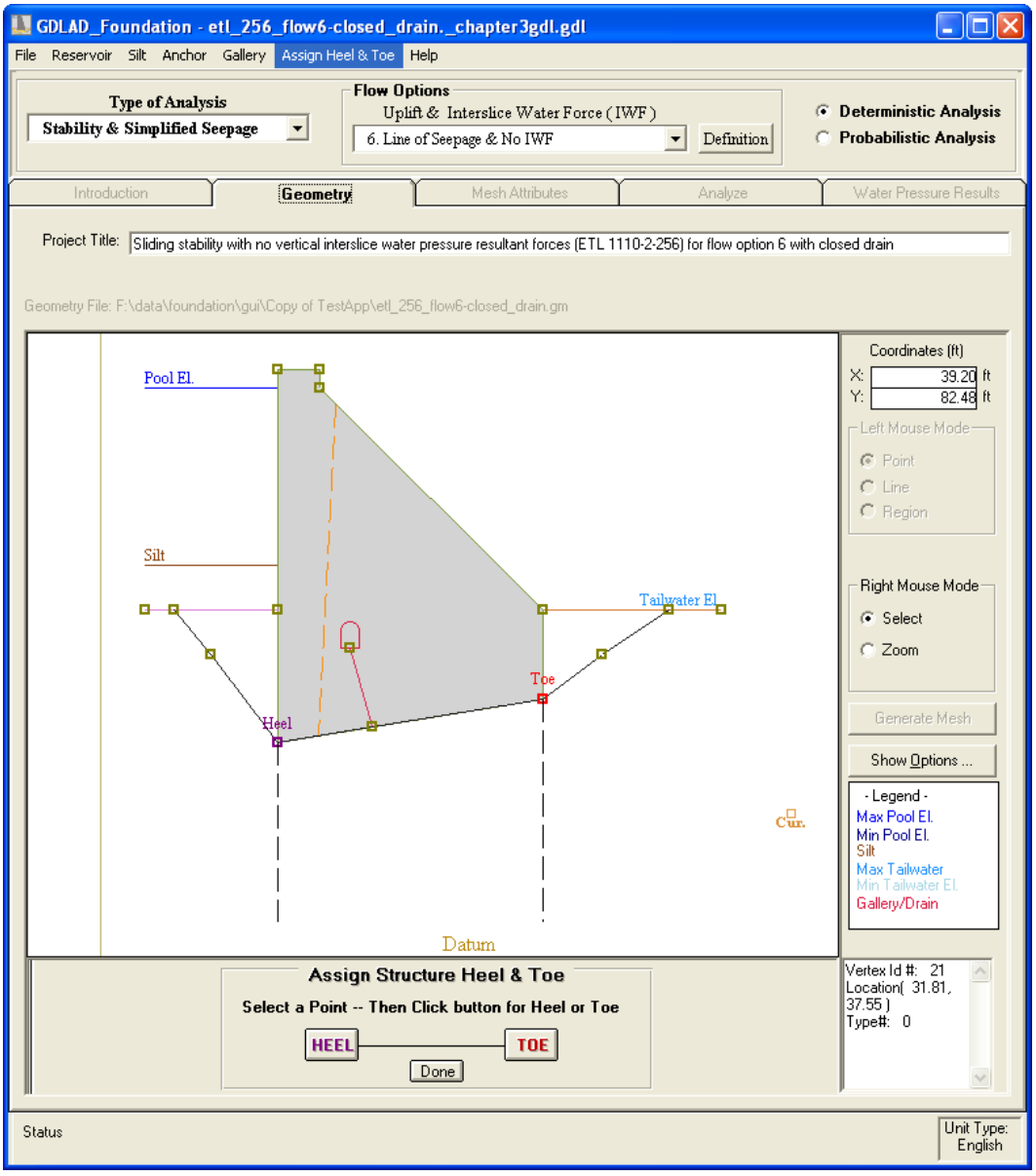

Figure 3.22. Assigning the location of Heel and Toe.

3.2.8.7 Help menu item

The last item on the menu bar of Figure 3.23 is the *Help* menu item which is highlighted in blue. Once selected, a drop-down menu shows the available help options which are explained in Section 3.1.2.2.

Figure 3.23. Guidance to GDLAD_Foundation.

3.3 The Mesh Attributes tab

The Mesh Attributes tab allows the user to define attributes and properties of lines and regions of the geometry that has been created for a concrete gravity dam embedded within rock. Figure 3.24 is a presentation of the mesh when either the Mesh Attributes tab is selected or when the mesh is generated from the geometry with the *Generate Mesh* button from the *Geometry* tab. After the Mesh is generated from the created or modified geometry (Section 3.2.5), a new nomenclature is established for points which are now labeled as nodes and lines are now considered as reaches. These are shown in The *Left Mouse Mode* group of radio buttons located below the *x*-, *y*-coordinates on the right hand side of Figure 3.24. The *Node* radio button will always be enabled and its functionality if selected would be to display selected node information in the geometry text window. Note that extra nodes and lines can be introduced to the newly created Mesh. This occurs at points where lines intersect regions. A node will be created and the original line will be replaced by two lines connected at the new node (node 2 and node 7 of Figure 3.24). The same is true of the two vertical dashed lines starting from the Heel and starting from the Toe of Figure 3.24. Any lines intersecting these two vertical dashed lines in the geometry will cause a node to be created as well as two new lines replacing the original line. The right hand side menu items of Figure 3.24 function basically the same as those shown in the Geometry tab except for the *Assign Attributes* button which will provide a variety of input options depending on the selection of the radio buttons in the *Left Mouse Mode* and the "*Joint Attributes*" items of the menu bar. The three types of analyses: "Stability & Joint_FLOW", "Stability & Simplified Seepage", and "Joint_FLOW Only" previously discussed in Section 3.1.1 will be addressed in this section.

3.3.1 The Project Title

The Project Title is located above the image window of Figure 3.24 and is a very important feature that allows one to convey information about the project. A total of 512 characters can be used to express the project. This

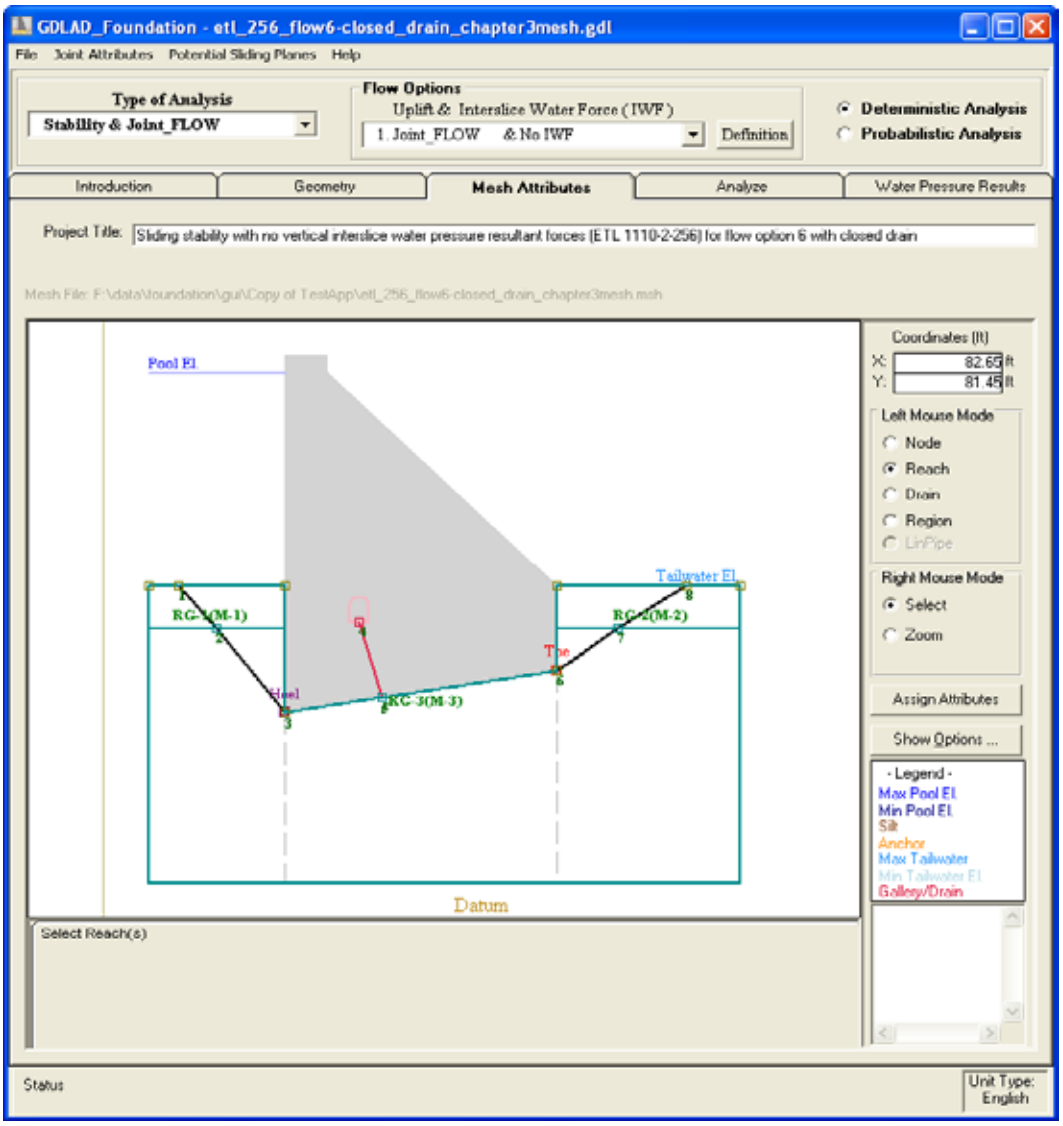

Figure 3.24. Generated mesh of a Stability & Joint_FLOW analysis.

project title is visible and can be accessed by all the tabs except when the Introduction tab is selected.

3.3.2 The Menu Bar

The Menu Bar is located below the window title of Figure 3.24. It consists of four items, *File, Joint Attributes, Potential Sliding Plane,* and *Help*.

3.3.2.1 File menu item

The first item on the left hand side of the menu bar of Figure 3.25 is the *File* item which is highlighted in blue. Once selected, a drop down menu offering various file options can be selected. These items are explained in Section 3.2.8.1.

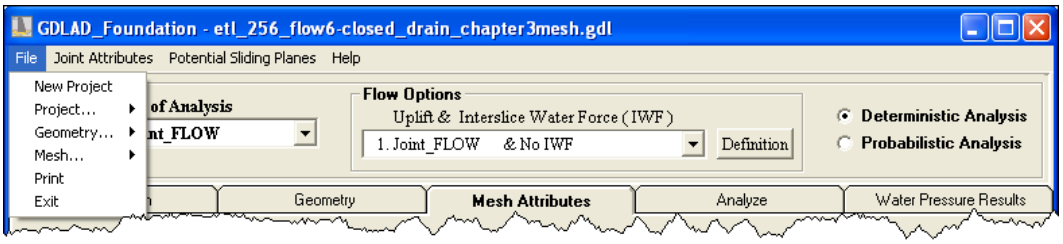

Figure 3.25. Guidance to GDLAD_Foundation.

3.3.2.2 Joint Attributes menu item

The second item from the left corner of the menu bar of Figure 3.26 is the "*Joint Attributes*" menu item and is highlighted in blue. There are three items listed in the drop down menu. These are the *Aperture type*, the *Drain type,* and *LinPipe* type. Each of these options will lead to further selections.

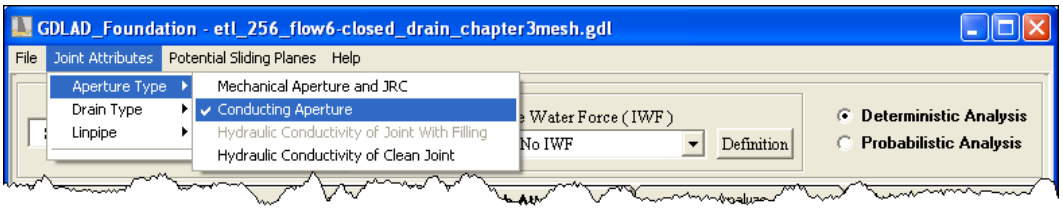

Figure 3.26. Aperture type menu item.

3.3.2.2.1 Aperture type

The *Aperture type* consists of three types of apertures available for selection; the Mechanical Aperture and JRC, the Conducting Aperture and the Hydraulic Conductivity of a Clean Joint. The Conducting Aperture highlighted in blue in Figure 3.26 is currently selected by the assignment of a check mark. These types of rock joint apertures are discussed in detail in Chapter 1.

3.3.2.2.2 Drain type

When a gallery or drain is specified for a project, the option for a *Drain type* in Figure 3.27 will be enabled only for a *Stability and Joint_FLOW*

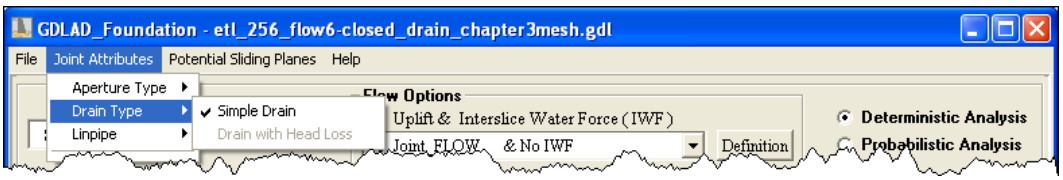

Figure 3.27. Drain type menu item.

and a "*Joint_FLOW Only*" type of analysis. This option will be disabled (grayed out) for "*Stability and Simplified Seepage*" type of analysis. When the D*rain type* is enabled, it can be selected as shown in Figure 3.27. At present, the Simple Drain procedure for simulating a drain is the only option available.

3.3.2.2.3 LinPipe type

The selection of *LinPipe* allows the user to use an alternative calculation of Head Loss in rock joint flow within a pipe network. This option is further described in Appendix C. Figure 3.28 shows the option to select a *LinPipe* type of procedure.

Figure 3.28. LinPipe Menu Item.

3.3.2.3 Potential Sliding Planes menu item

The third item on the menu bar shown in Figure 3.29 is the *Potential Sliding Planes* menu item which is highlighted in blue. Once selected, a potential sliding plane frame (frame) consisting of a group of buttons below the image window appears. This allows the user to *Add*, *Show,* and *Delete* a sliding plane[s] as well as to show wedges above the sliding plane. Note that sliding plane and slip plane are used interchangeably throughout the report.

The button on the upper left of the frame is the *Add Plane* button. Use the right mouse button to select all reaches that define a slip plane. Then select the *Add Plane* button. A "1" will be shown in the Choose Plane to Display drop down menu if there were no previous slip planes selected. If there were other slip planes, this number would be incremented by 1.

The *Show All Planes* button and the *Show Current Plane* button are located in the center of frame and are self explanatory. When selected, the potential sliding plane will appear highlighted in light blue as shown in Figure 3.29. They will both produce the same result if only 1 plane is defined.

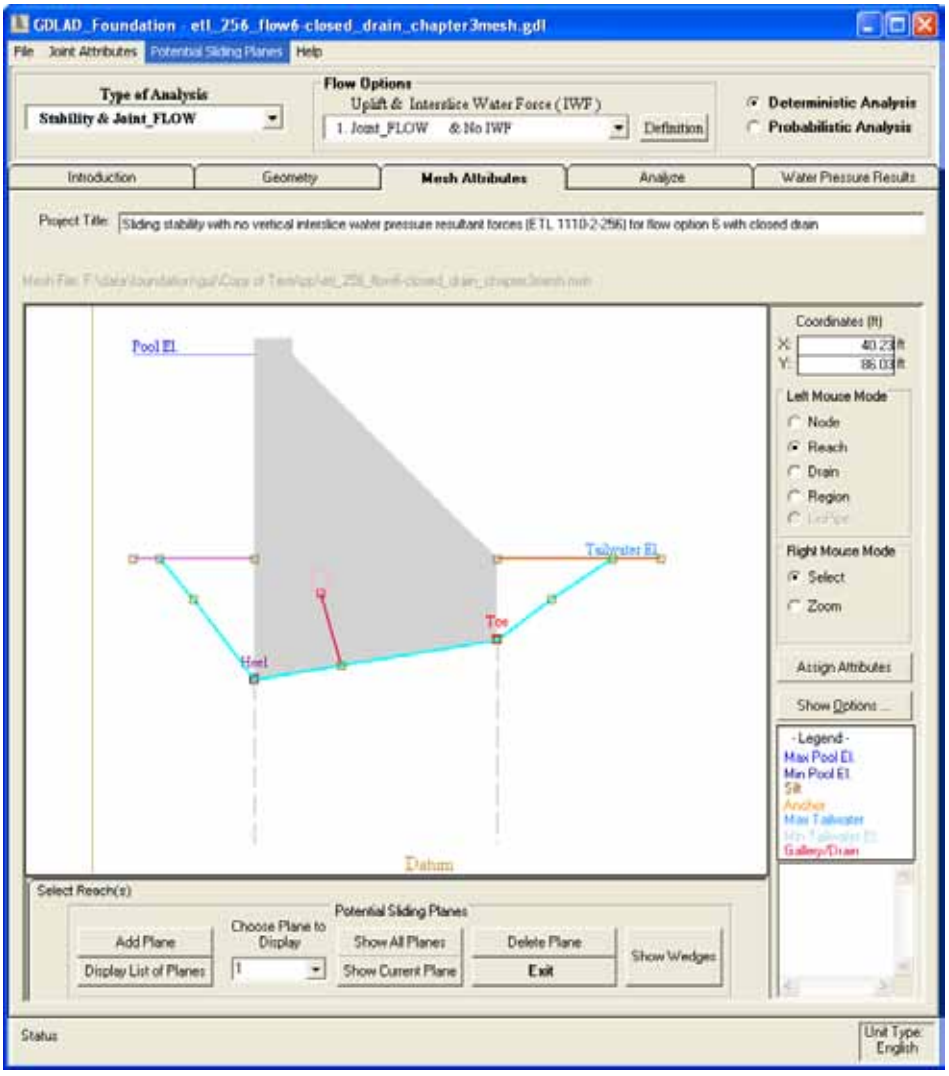

Figure 3.29. A Potential Sliding Plane.

The *Delete Plane* will delete the current plane selected. There will be a warning for confirmation of the deletion.

The *Show Wedges* button of Figure 3.29 above will draw all the wedges for the current slip plane. Wedge numbers are identified by "W-id" and the sub-wedges of each wedge are numbered from the sliding plane upwards as seen in Figure 3.30. The *Clear Wedge Display* button is selected to exit and the original image and Figure 3.29 will reappear.

The selection of the *Display List of Planes* button will produce a window like Figure 3.31. A total of five lines of text will be displayed for each plane. The first line lists the sliding plane number; the second line gives the number of elements which is followed by a list of element id numbers in

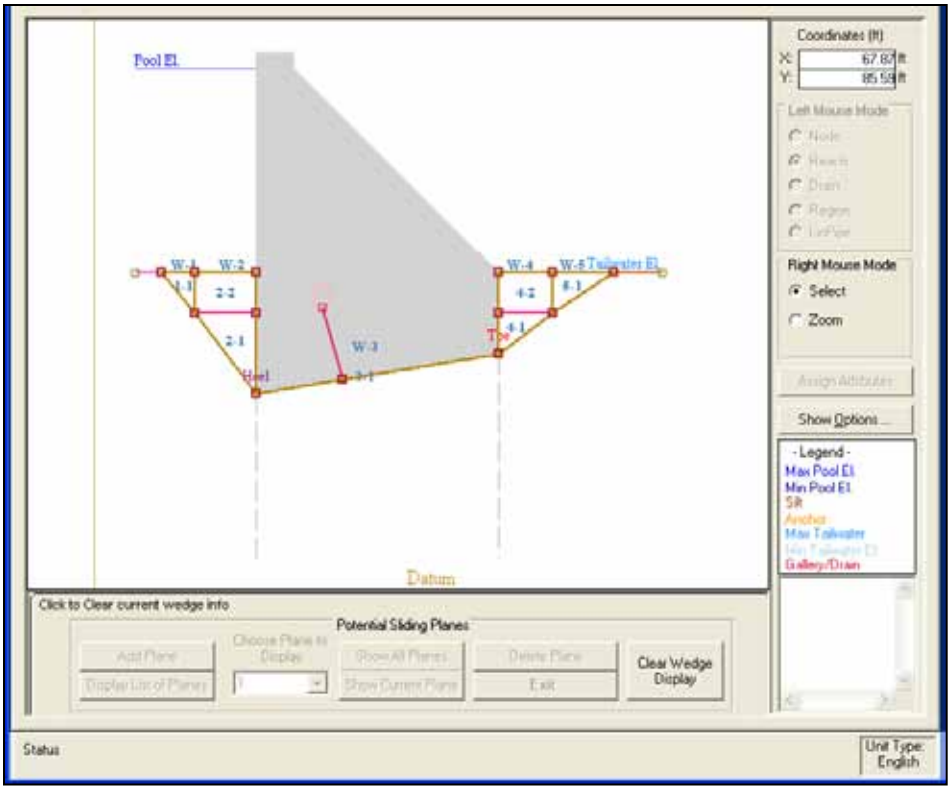

Figure 3.30. Display Wedge information.

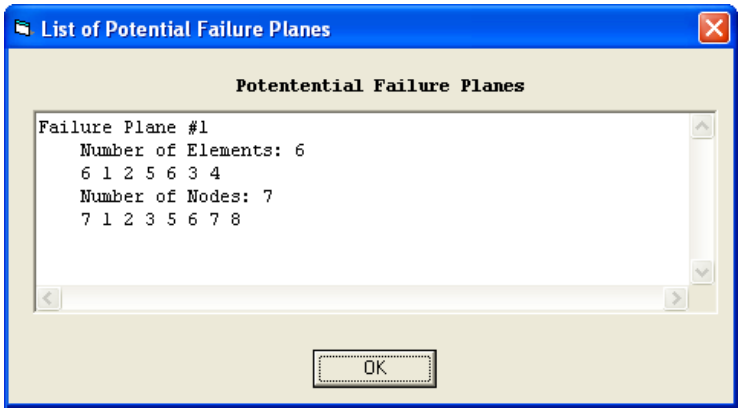

Figure 3.31. List of Sliding Planes.

the third line. The fourth line provides the number of nodes and this is followed by the node id numbers on the fifth line. If there are multiple planes, a set of five lines for each plane will be displayed below the previous set. This can be useful for checking purposes. Select the *OK* button to return to the *Potential Sliding Planes* menu of Figure 3.29.

The *Exit* button is used to exit out of the *Potential Sliding Planes* menu.

3.3.2.4 Help menu item

The last item on the menu bar of Figure 3.32 is the *Help* menu item which is highlighted in blue. Once selected, a drop-down menu shows the available help options which are explained in Section 3.2.8.7.

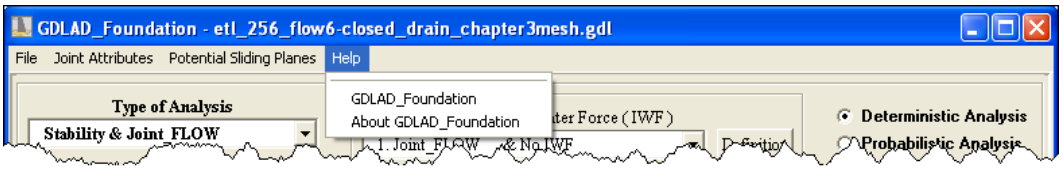

Figure 3.32. Guidance to GDLAD_Foundation.

3.3.3 Type of analysis menu

Depending on the type of analysis selected, the Joint Attributes items of the menu bar in Section 3.3.2 will change as well as the availability of the options within the *Left Mouse Mode* group of radio buttons. The three types of analysis are defined in greater detail in Section 3.1.1. The following sub-sections describe how the selection of each of the three types of analyses, namely Stability and Joint_FLOW, Stability and Simplified Seepage, and Joint_FLOW Only determine the assignment of rock joint attributes and rock strength properties.

3.3.3.1 Stability and Joint_FLOW type of analysis

A simplified concrete gravity dam embedded within rock with a rock foundation drain has been generated to describe the Stability and Joint_FLOW type of analysis. There will be no difference between assigning attributes for Flow Options 1, 2, or 3. As shown in Figure 3.33, the *Left Mouse Mode* group of radio buttons comprise of the *Node*, *Reach, Drain*, *Region,* and *LinPipe* buttons are active for selection. Note that the *LinPipe* (alternative method to calculate head loss discussed in Chapter 5) input options are discussed in Section 3.3.2.2.3.

3.3.3.1.1 Joint Attributes menu item

For a Stability and Joint_FLOW type of analysis, the three Joint Attributes will be active (i.e. not grayed out), as seen in Figure 3.34.

Each option has been described in Section 3.3.2.2. Each of these attributes is listed in Figure 3.35 with selected options preceded by a check mark. For this example, a conducting aperture with a simple drain and the *LinPipe* calculations of Head loss will be considered.

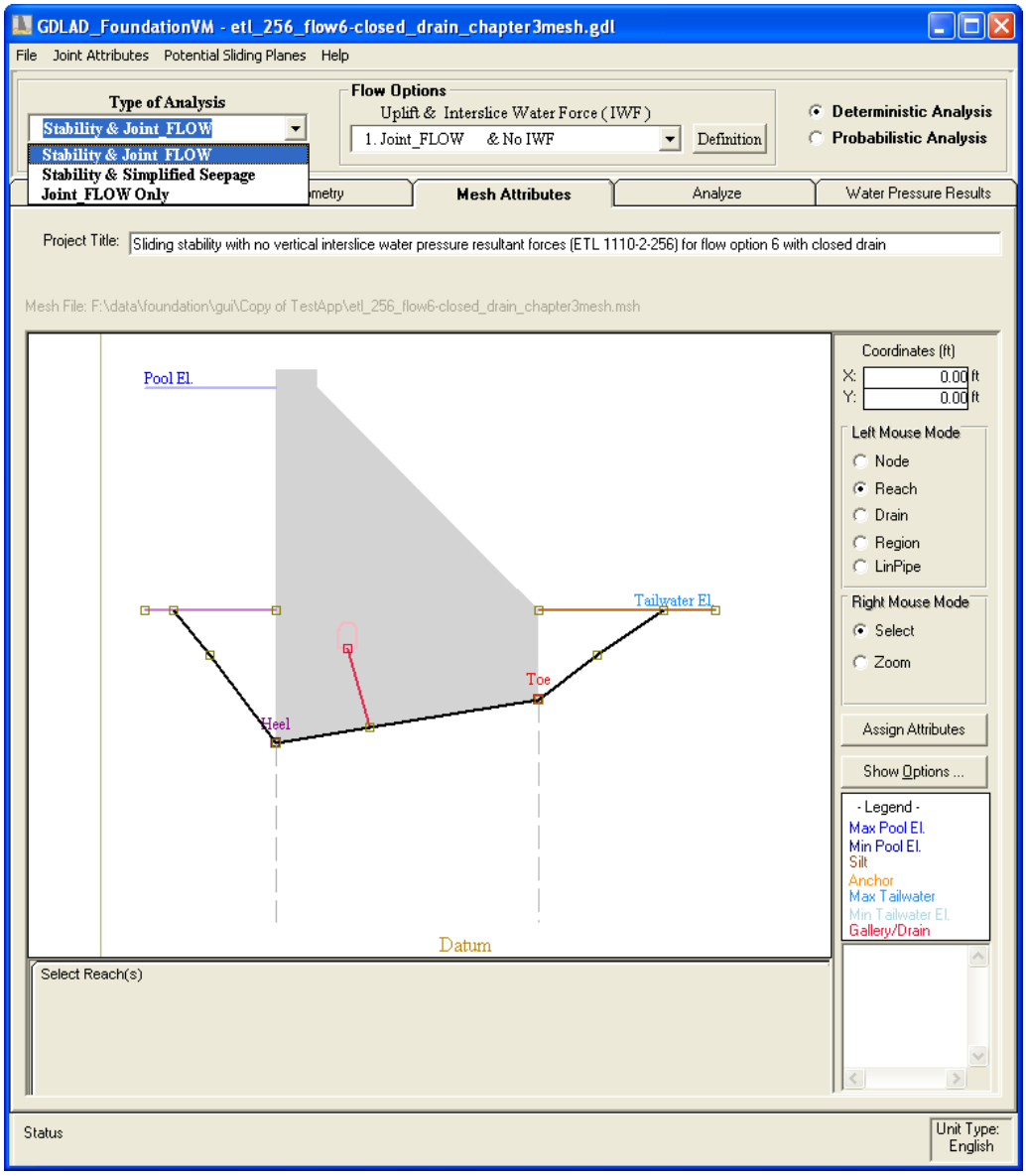

Figure 3.33. Stability & Joint_FLOW type of analysis.

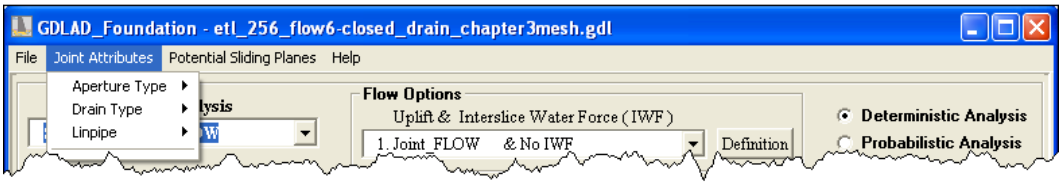

Figure 3.34. Joint Attributes for a Stability and Joint_FLOW type of analysis.

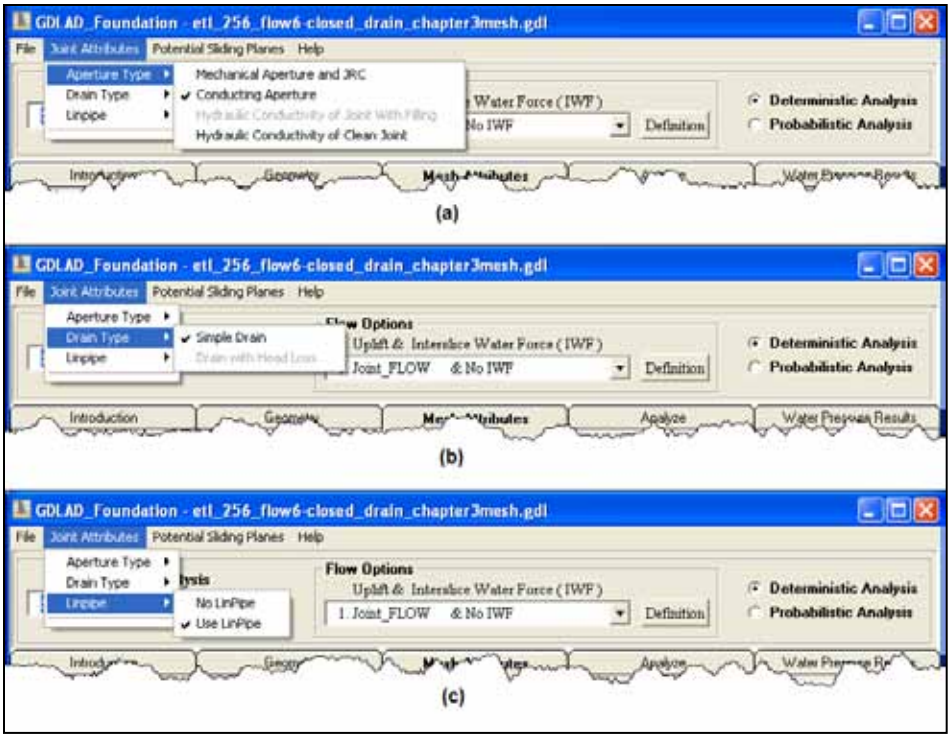

Figure 3.35. Joint Attributes (a) Aperture Type, (b) Drain Type and (c) LinPipe.

3.3.3.1.2 Potential Sliding Planes menu item

The third item on the menu bar of Figure 3.36 is the *Potential Sliding Planes* menu item which is highlighted in dark blue. Once selected, a frame consisting of a group of buttons below the image window appears. This allows the user to *Add*, *Show,* and *Delete* a sliding plane[s] as well as to display wedges above the sliding plane. Section 3.3.2.3 gives further detail of this menu item.

3.3.3.1.3 Assign Attributes

The following sub-sections describe each of the attribute tables for the active radio buttons on the *Left Mouse Mode* frame. Each corresponding radio button has to be selected before assigning attributes. As mentioned earlier, the *Node* radio button lists node id numbers in the message window and does not have an effect on the *Assign Attributes* button.

3.3.3.1.3.1 Reach Mode

In *Reach Mode* all relevant reaches have to be selected first before the *Assign Attributes* button can be selected. Figure 3.37 shows the assignment of the conducting aperture values for each reach. The table headings include

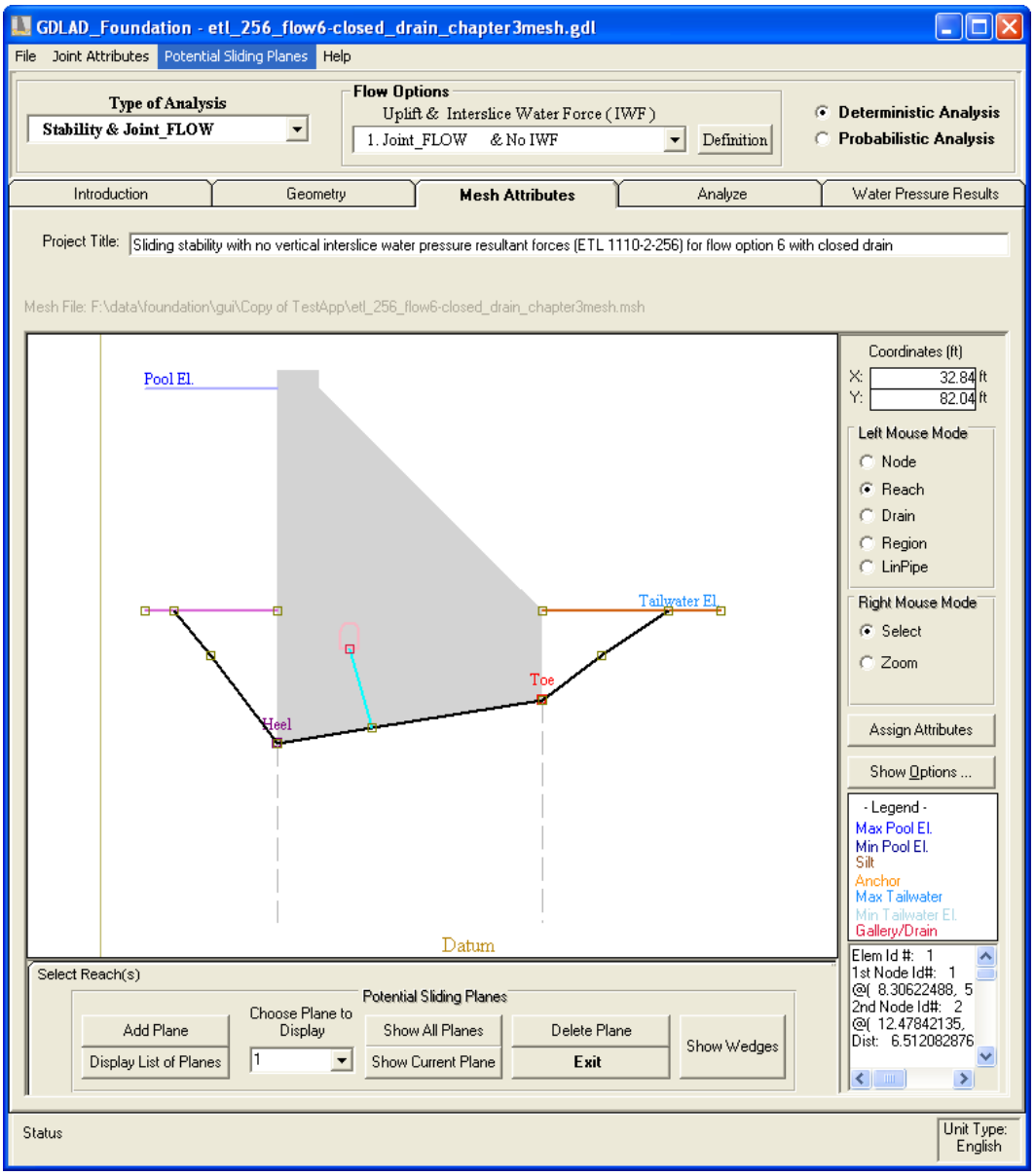

Figure 3.36. Potential Sliding Planes menu item for Stability and Joint_FLOW type of analysis.

the reach number, the starting node number (id) and ending node id, the material id, the starting value of the conducting aperture, the ending value of the conducting aperture and the number of elements per reach. As each reach number is selected, a green line on the original image will show the current reach selected. From the values provided, a uniform aperture has been selected and one element is assigned for each reach with a total of 6 elements and 6 reaches ("elevator" bar allows viewing of reach number 6 and beyond in Figure 3.37).

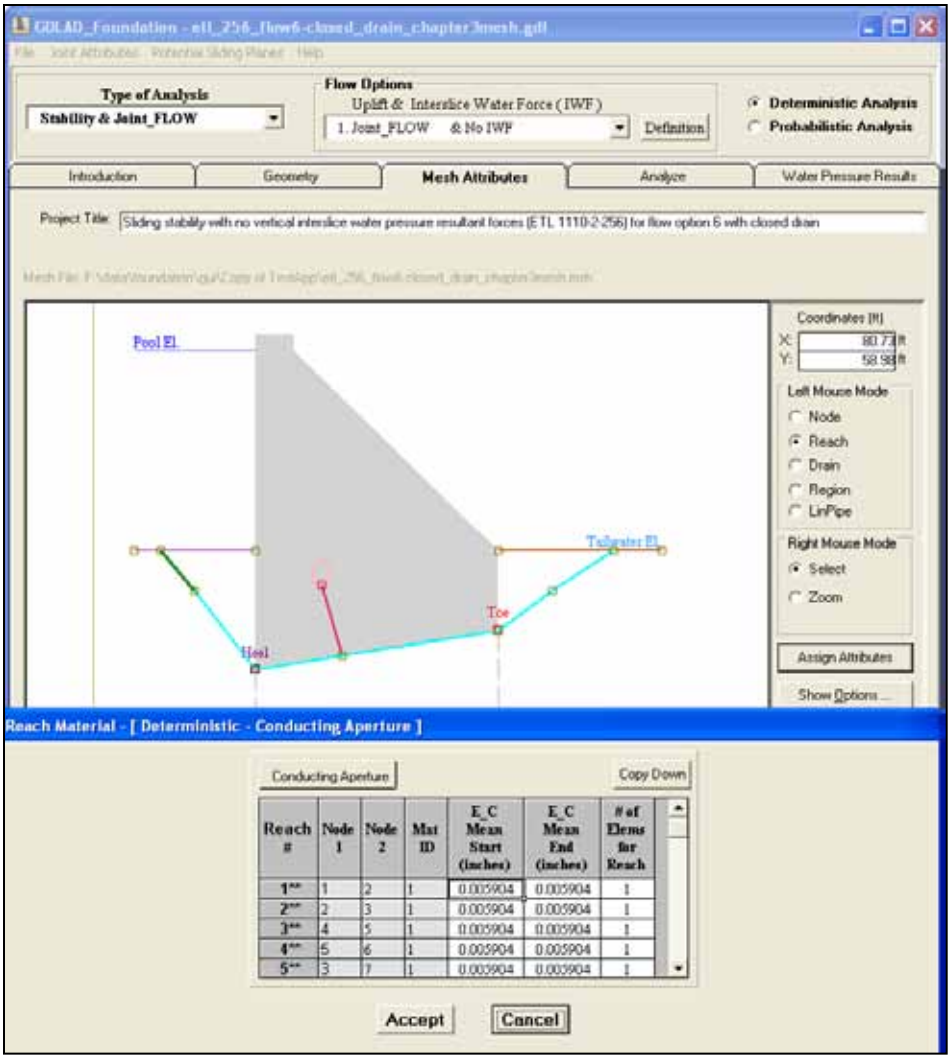

Figure 3.37. Conducting Aperture with one element per reach.

The *Copy Down* button provides a way to populate similar column items in the table. Just highlight the cells in a column and the first value will be copied to the other cells after the selection of the *Copy Down* button. As an alternative method of copying, since this table functions in some ways to a spreadsheet, a small plus sign will appear at the right base of the selected cell. Selection of this small sign with the left mouse button and dragging down to the chosen last cell will also accomplish this task (i.e. copying the same values).

Entering a greater-than-one value in the "*# of Elems for Reach*" in any/all cells in the column will cause the VM to internally create new nodes and modify reaches.

The *Accept* button will save any additions and modifications and then exit.

The *Cancel* button will not save any edits and only exit out of this window.

On exit, the original background image of Figure 3.37 will be displayed.

In *Reach Mode* and for a probabilistic analysis of a Stability and Joint_FLOW type of Analysis, please see section 3.6.1.

3.3.3.1.3.2 Drain Mode

Before the *Assign Attributes* button is selected, the drain segments (in red) have to be selected. Figure 3.38 shows the assignment of the drain values for the drain segments. The table headings are the Drain Reach number, the starting node id, the ending node id, the drain diameter, the spacing between drains (Interval), and the number of elements per reach. As each drain segment id is selected, a green line will appear over the original drain segment. From the values provided, a one element drain line with a drain diameter of 5 in. at 20 ft intervals (along the gallery of the dam) has been assigned.

The *OK* button will save any additions and modifications and then exit.

The *Cancel* button will not save any edits and only exit out of this window.

On exit, the original background image of Figure 3.38 will be displayed.

3.3.3.1.3.3 Region Mode

In *Region Mode* all the region areas must be selected first before the *Assign Attributes* button can be selected. Figure 3.39 shows the selection of all three regions. The table beneath the image shows the input of the unit weight of concrete of 150 pcf and unit weight of water of 62.4 pcf. Three material properties have been created. When copying cells within a column in a table, begin by selecting a cell. A small plus sign will appear at the right base of the selected cell. Selection of this small sign with the left mouse button and dragging down to a chosen last cell will copy the top value to every selected cell. The unit weight for each of the three rock materials are assigned, with cohesion (*C*) set to zero and the internal angle of friction (*Phi*) defined individually for each rock material[1]. In the Map Material to Regions table, material 1 is mapped to region 1, material 2 is mapped to region 2 and material 3 is mapped to region 3.

[1] Effective stress shear strength parameters.

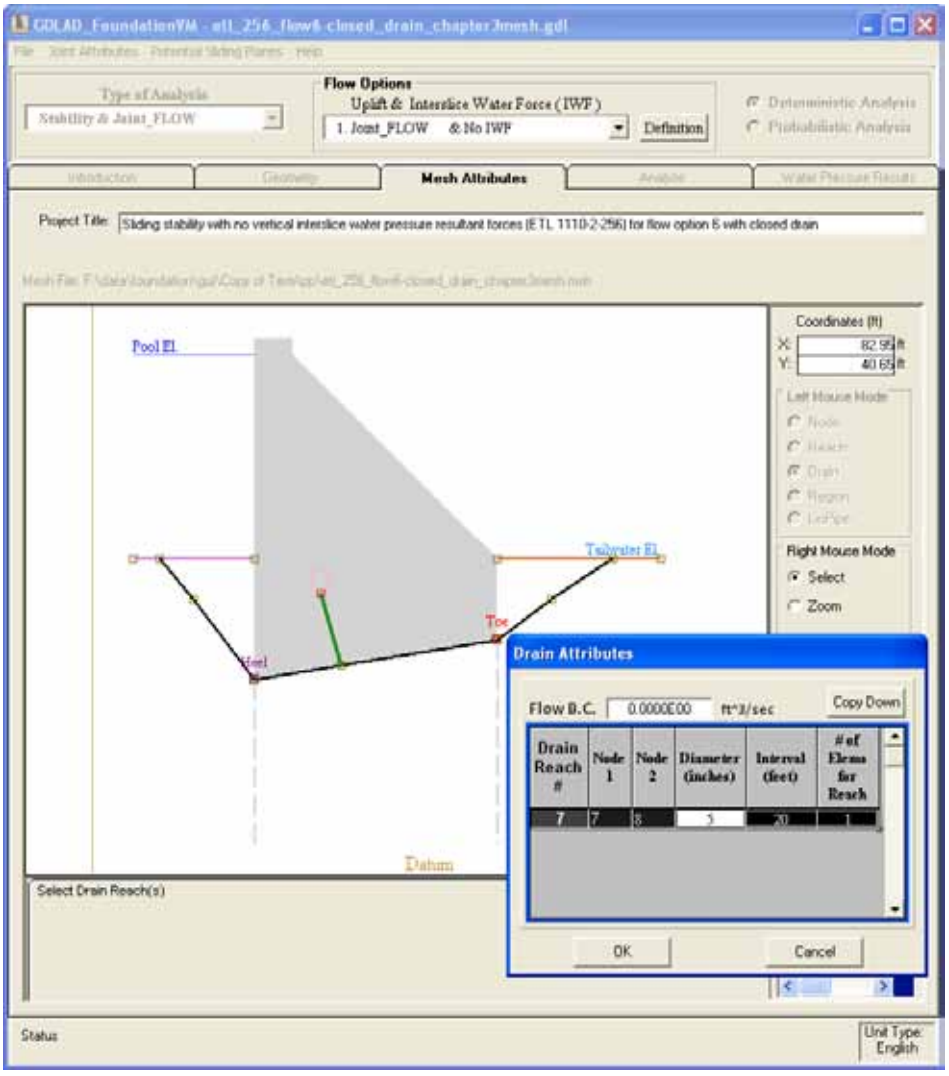

Figure 3.38. Drain with one element per reach.

The *Exit* button will save any additions and modifications and then exit.

The *Cancel* button will not save any edits and only exit out of this window.

On exit, the material attributes table will close and the original image of Figure 3.39 with all regions selected will be displayed.

In *Region Mode* and for a probabilistic analysis of a Stability and Joint_FLOW type of Analysis, please see section 3.6.2.

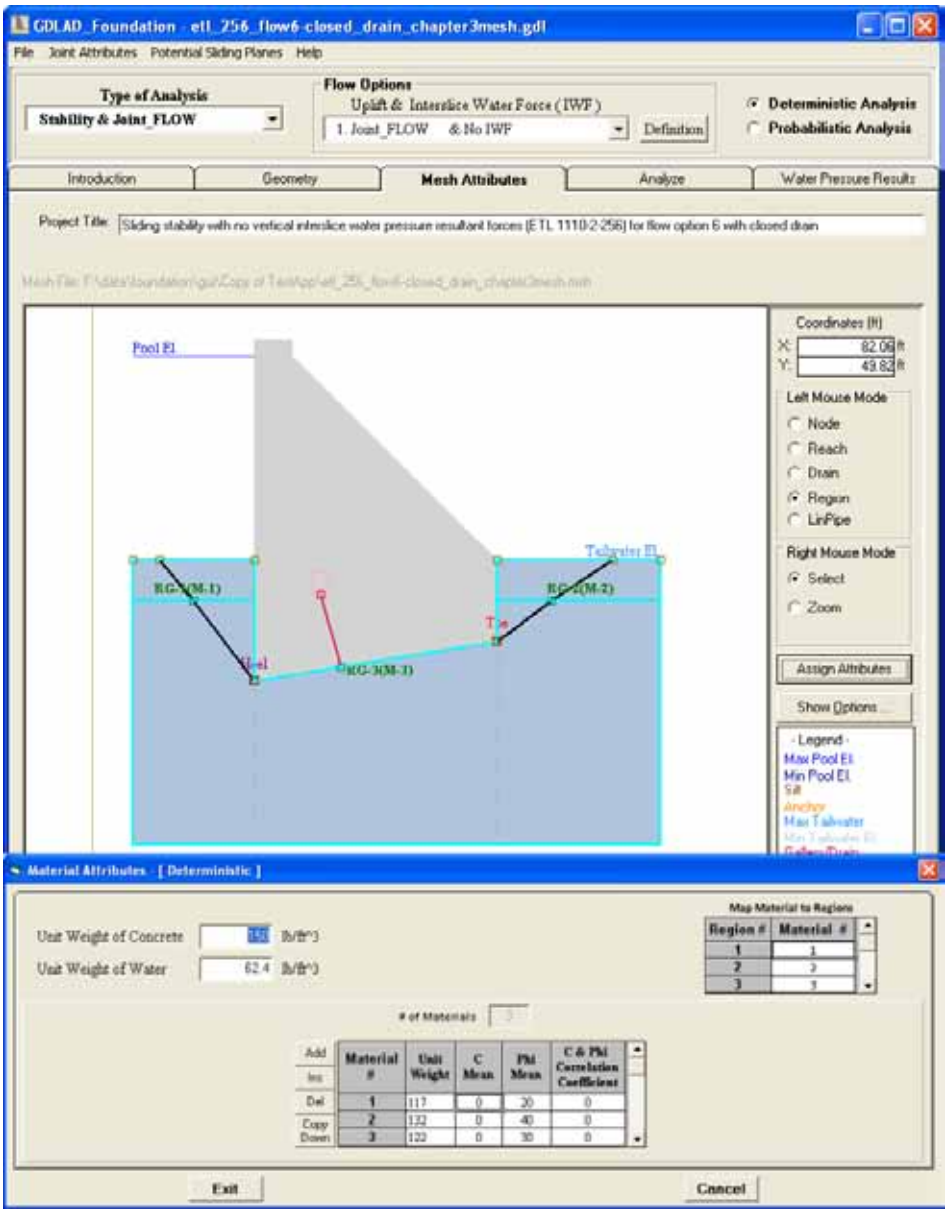

Figure 3.39. Material properties and regions.

3.3.3.1.3.4 LinPipe Mode

With the *LinPipe* radio button enabled, all reaches and drain elements will be included in the analysis automatically and it will not be necessary to select any reaches nor drain segments. In this example, there are two elements assigned to each reach. As mentioned earlier, in *Reach Mode* Section 3.3.3.1.3.1, the assignment of more than one element per reach will cause the VM to create new nodes and modify reaches. However, these additional nodes are not displayed on the image of Figure 3.40 but only on the image of Figure 3.41a which is in *LinPipe Mode*.

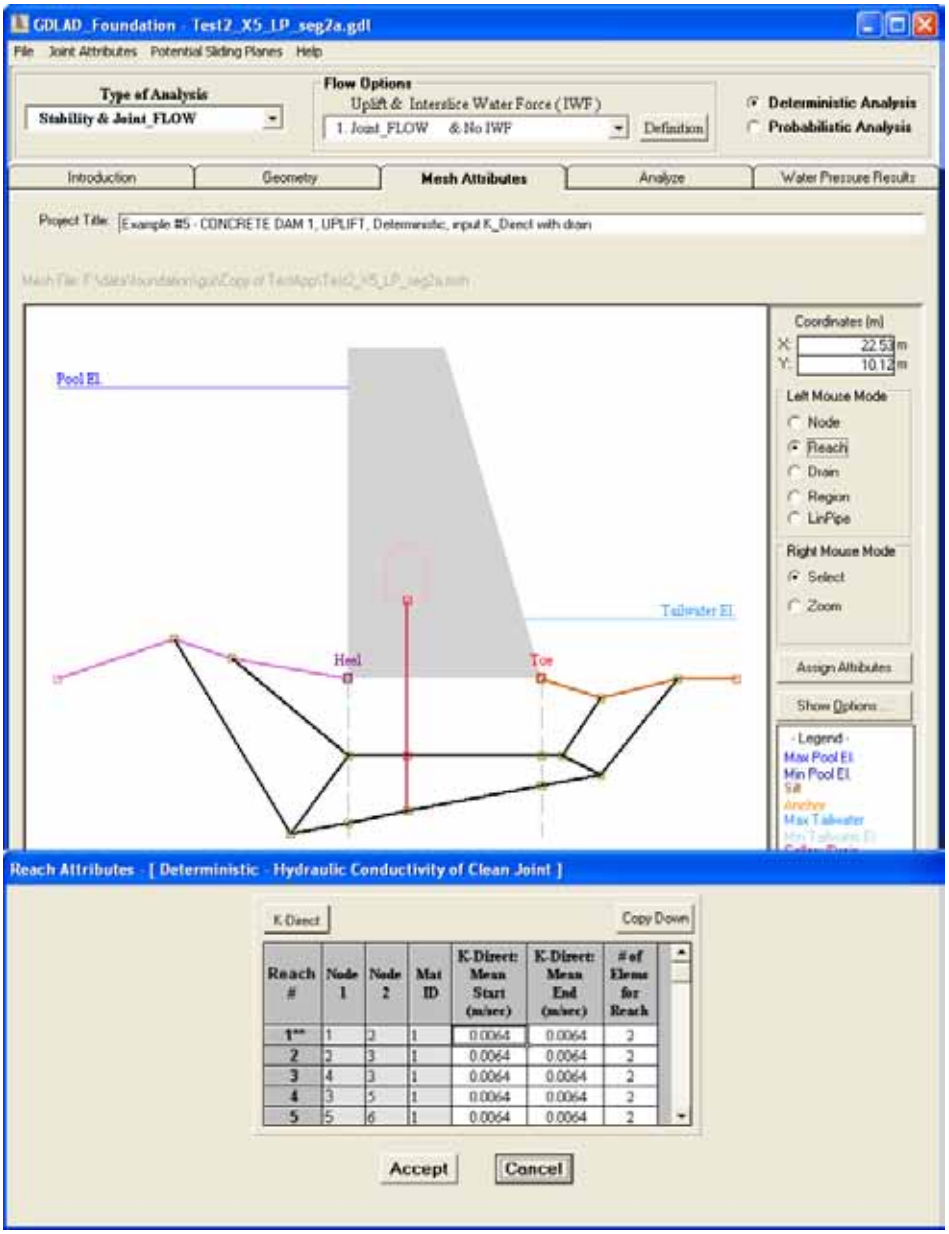

Figure 3.40. An image of rock joints in *Reach Mode*.

This is shown in the images of Figure 3.41a, where there are now two elements per reach, instead of the original one element per reach as shown on the image in Figure 3.40.

Figure 3.41a shows a network of reaches and a two segment rock drain. When the *Assign Attributes* button is selected, Figure 3.41b will appear.

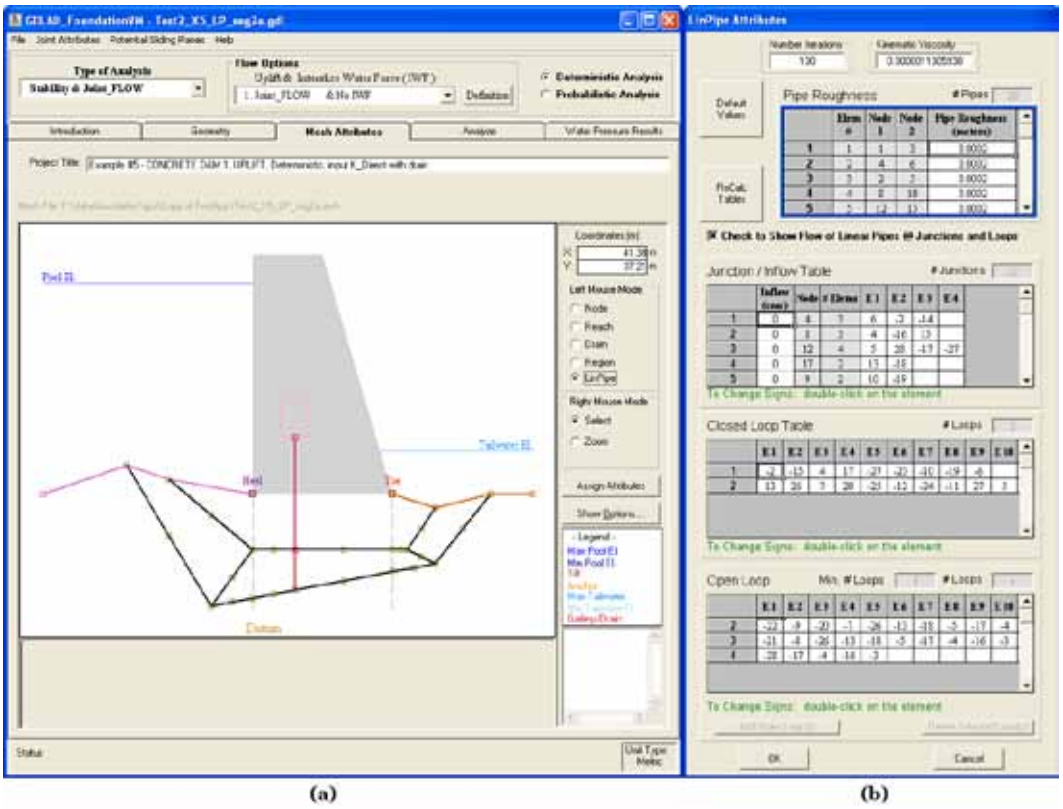

Figure 3.41. LinPipe assignments (a) Image of network of rock joints (b) LinPipe attributes table.

Default values have been provided for the number of iterations, the Kinematic Viscosity and Pipe Roughness for each element. The three tables have been assigned element numbers that follow a particular flow pattern. The upper table, the Junction/Inflow Table, shows flows at a particular junction or node. The lower two tables show flows along a path. The signs of the elements indicate the direction of flow and can be changed by double-clicking a particular cell. The LinPipe methodology and element assignments are explained in detail in Chapter 5 and Appendix C.

The *Default Values* button will re-enter the default parameters for the Number of Iterations, the Kinematic Viscosity, and Pipe Roughness of all elements.

The *ReCalc Tables* button will re-enter the default elements in all three tables.

The *OK* button at the bottom of Figure 3.41b will save any additions and modifications and then exit.

The *Cancel* button at the bottom of Figure 3.41b will not save any edits and only exit out of the *LinPipe Attributes* window.

If the *Check to Show Flow of Linear Pipes @ Junctions and Loops* check box is selected as in Figure 3.41b, flow directions will be drawn on the image when a particular row in any one of the three lower tables is selected. Otherwise, only the path will be highlighted in light blue.

The following three figures show the flow patterns at a junction and of both closed and open loop flows. For a row selected in the Junction/Inflow Table, only the nodes will be highlighted within the image. The selected rows of the other two tables indicate the highlighted paths in light blue within the images.

Figure 3.42 shows that the highlighted row 3 of the Junction/Inflow Table will have its elements represented by directional flow at a particular node or junction. Flow leaving the junction is positive and drawn in blue. Flow entering the junction is negative and drawn in red.

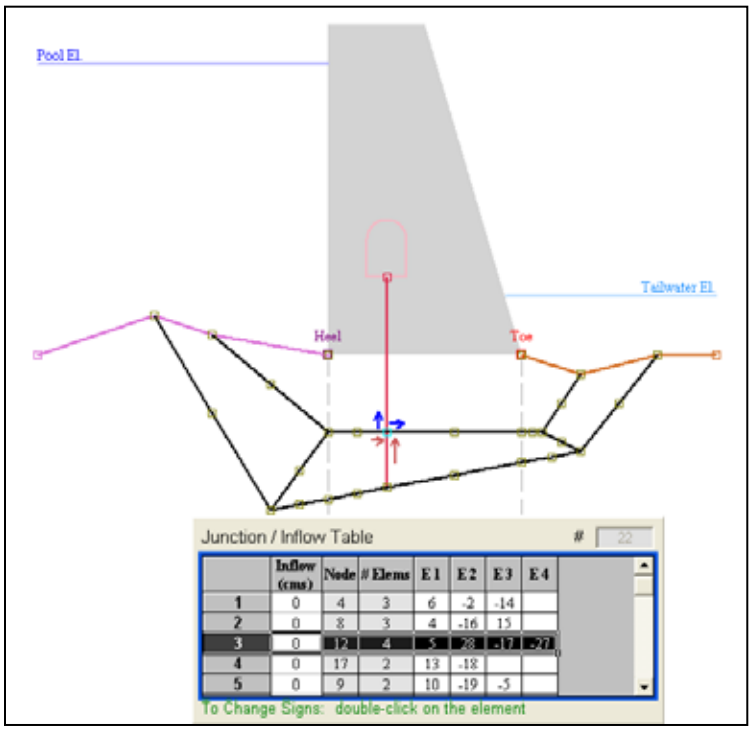

Figure 3.42. Negative flow into a junction (red) and positive flow out of the junction (blue) are drawn to signify direction of flow at a junction after row 3 of the Junction/Inflow Table has been selected.

Figure 3.43 shows that the highlighted row 2 of the closed loop table will have its elements represented by directional flow patterns. Clockwise flow around the closed loop is positive and is represented as blue arrows. Counter-clockwise flow around the closed loop is negative and is represented as red arrows.

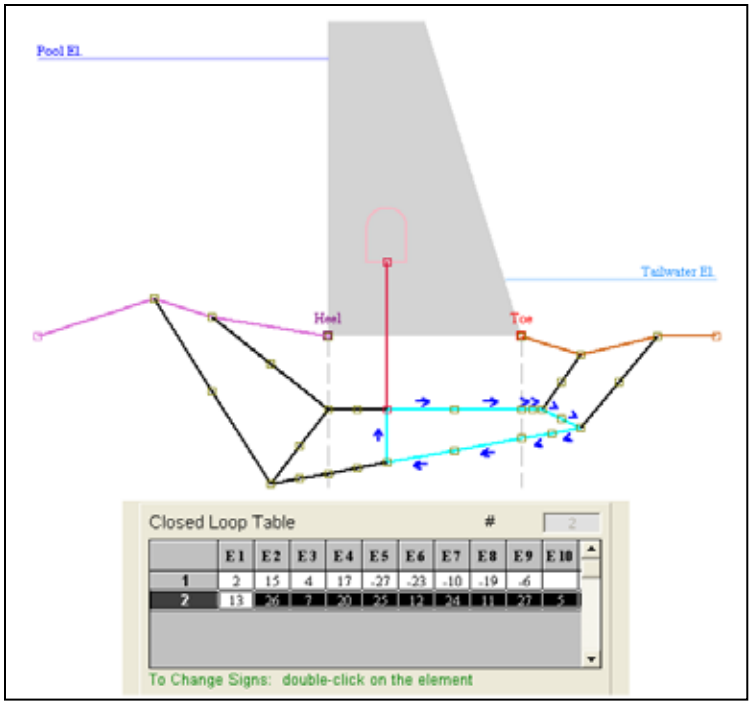

Figure 3.43. A positive (clockwise) flow pattern after row 2 of the Closed Loop Table has been selected.

Figure 3.44 shows the directional flow patterns of the elements of the highlighted row 1 of the open loop table.

For the Open Loop table there is the option to add a loop or remove a loop. Counter-clockwise flow of the open loop is negative and represented as red arrows.

When the *Delete Selected Loop(s)* button is selected, one or more rows of the Open Loop table that have been selected (highlighted) will be removed.

The *Add Open Loop(s)* button will add an open loop to the table. First select the *Add Open Loop(s)* button. Then with the *Control* button depressed, use the right mouse to select all reaches in order to create a new open loop. A light blue line should appear on every selected reach. Next select the *Add Loop* button to add this loop to the table. Repeat this procedure until all new loops have been added. Select the *Done* button when finished.

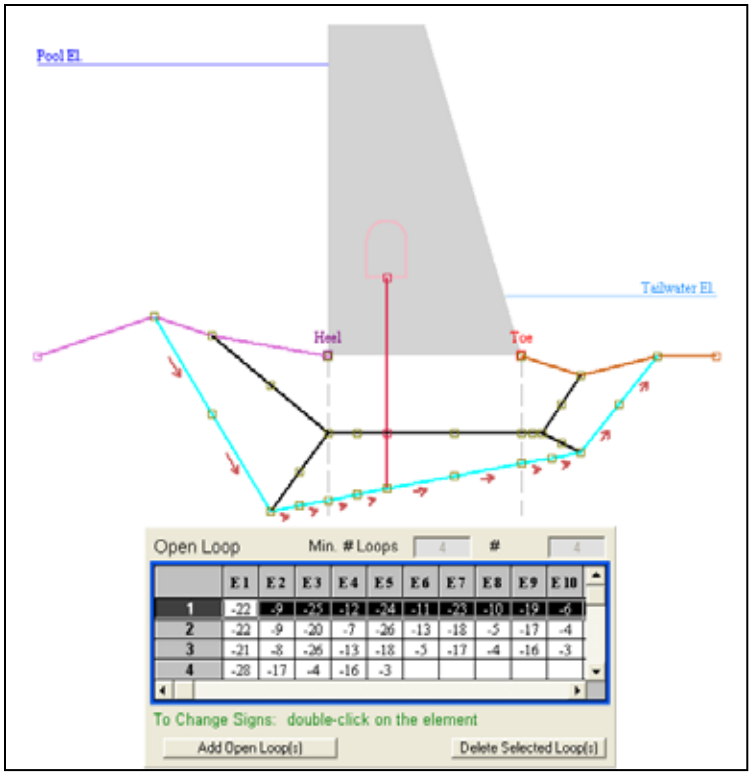

Figure 3.44. A negative (counter-clockwise) flow pattern after row 1 of the Open Loop Table has been selected.

On exit of the *LinPipe Attributes* window, the image of either Figure 3.39 or Figure 3.40a will be displayed depending on whether the *Reach Mode* or *LinPipe Mode* radio button is selected.

The LinPipe method uses pipe networking technology where flow distribution is analyzed by obtaining the continuity equation at each junction and the conservation of the energy equation around any closed loop. To obtain a solution for the number of elements defined, the same number of equations must exist. An inspection of the images in Figures 3.33 and 3.44 shows that there are 2 closed loops (closed polynomial of elements) and 22 junctions (nodes that are connected by more than 1 element) and a total of 28 elements (both rock joints and drain segments) or pipes. We need 28 equations but we only have 24 (22 junctions + 2 closed loops). The open loops are necessary for the 4 extra equations needed. This methodology is further discussed in Chapter 5.

3.3.3.2 Stability and Simplified Seepage Type of Analysis

The second option listed in the *Type of Analysis* drop-down menu is the Stability & Simplified Seepage and pertains to the second three types of

flow options (namely 4, 5, and 6). These are listed in the *Flow Options* drop-down menu with flow option 4 highlighted in blue in Figure 3.45. This option is relevant to the Uplift and Interslice Water Pressure Resultant Force calculations which are explained in greater detail in Section 6.2 of Chapter 6.

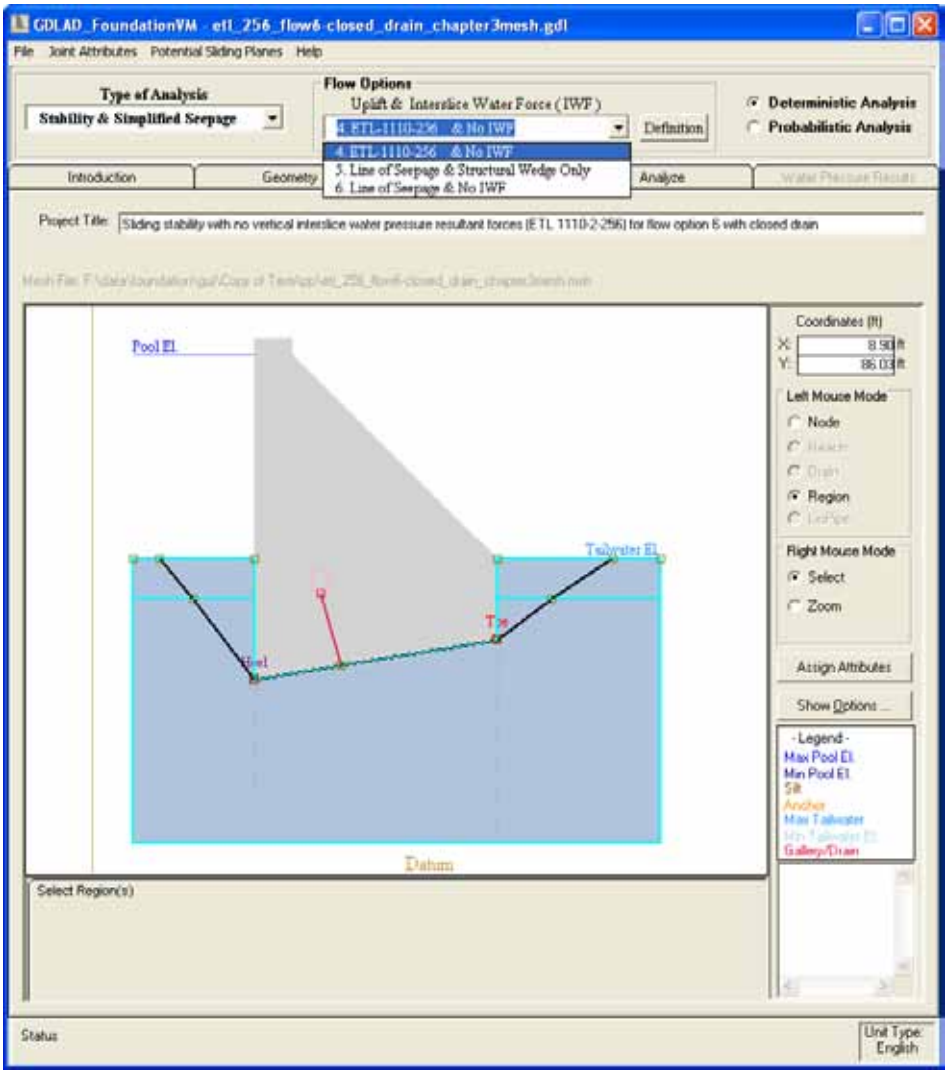

Figure 3.45. Stability & Simplified Seepage type of analysis.

A simplified concrete gravity dam embedded within rock with a rock foundation drain has been generated to describe the Stability and Simplified Seepage type of analysis. There is no difference assigning attributes when accessing Flow Options 4 and 5 but there will an additional step for Flow Option 6 which will be discussed in Section 3.3.3.2.3. Note that the *Left Mouse Mode* group of radio buttons comprise of only the *Node* and *Region* buttons in Figure 3.45.

3.3.3.2.1 Joint Attributes menu item

For a Stability and Simplified type of analysis, the three Joint Attributes are not active, as seen in Figure 3.46. These attributes are not used in a Stability and Simplified type of analysis.

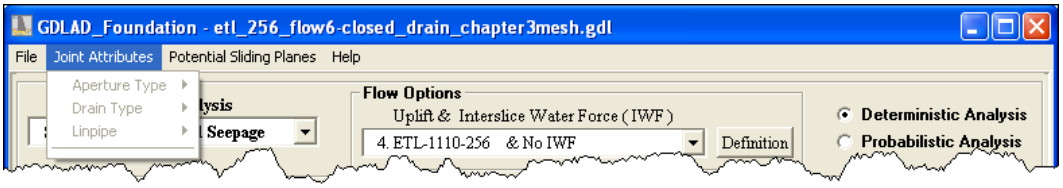

Figure 3.46. Joint Attributes for a Stability and Simplified Seepage type of analysis.

3.3.3.2.2 Potential Sliding Planes menu item

The third item on the menu bar of Figure 3.47 is the *Potential Sliding Planes* menu item which is highlighted in blue. Once selected, a frame consisting of a group of buttons below the image window appears. This allows the user to *Add*, *Show,* and *Delete* a sliding plane[s] as well as to show wedges created above the sliding plane. Section 3.3.2.3 gives further detail of this menu item.

3.3.3.2.3 Assign attributes (Region Mode only)

The only option available in a Stability and Simplified Seepage type of analysis is the *Region active* radio button on the *Left Mouse Mode* frame. As mentioned earlier, the *Node* radio button lists node id numbers in the geometry information window and does not have an effect on the *Assign Attributes* button.

In *Region Mode* all the region areas must be selected before the *Assign Attributes* button can be selected. Figure 3.48 shows the selection of all three regions. The table beneath the image shows the input of the unit weight of concrete with 150 pcf and unit weight of water with 62.4 pcf. Three material properties have been created. When copying cells within a column in the table, a small plus sign will appear at the right base of the selected cell. Selection of this small sign with the left mouse button and dragging down to the chosen last cell will copy the top value to all the selected cells. Next, the unit weight for each of the three rock materials are assigned, with cohesion (*C*) set to zero and the internal angle of friction (*Phi*) defined individually for all rock joint contained within each rock material. In the Map Material to Regions table, material 1 is mapped to region 1, material 2 is mapped to region 2 and material 3 is mapped to region 3.

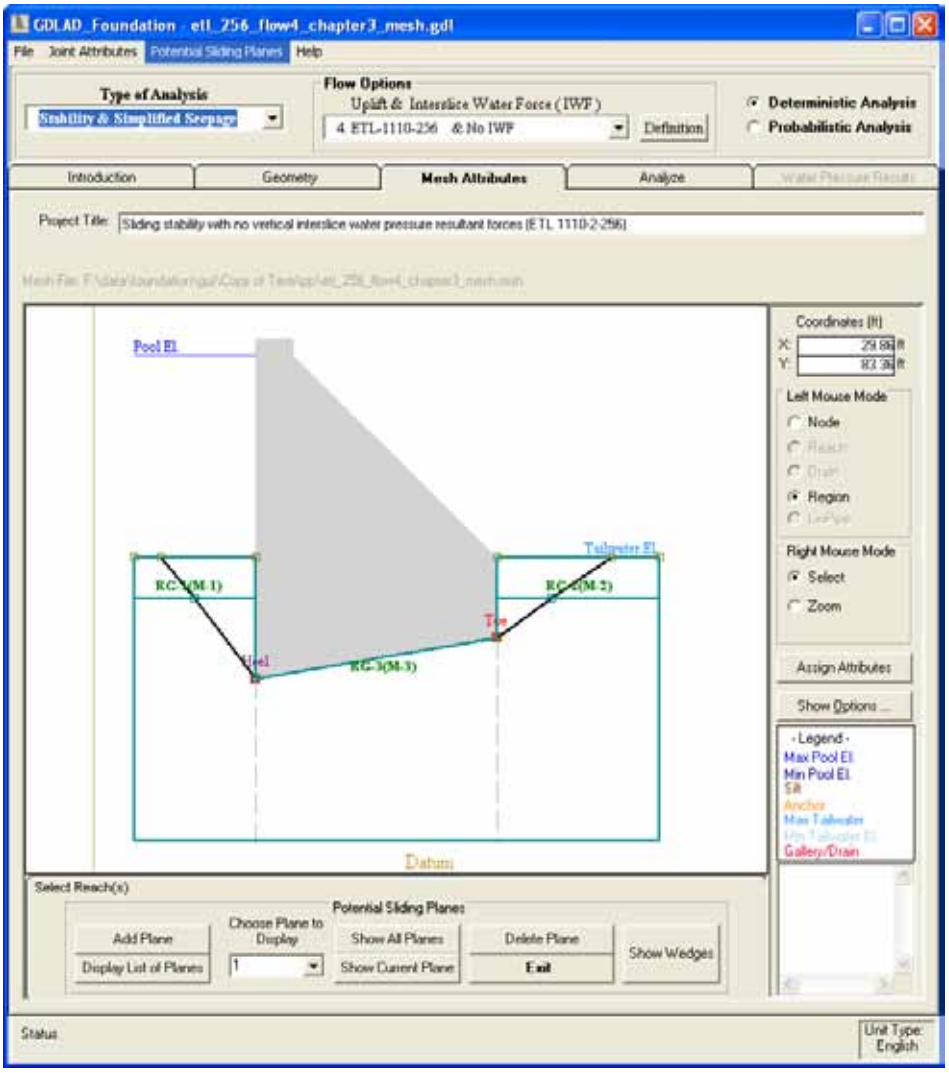

Figure 3.47. Potential Sliding Planes menu item.

This section so far centered on discussions regarding parameter values for flow options 4 and 5. As mentioned earlier there is other necessary information required when flow option 6 is selected. For the Line of Seepage Methodology, the rock joint attributes must be considered. Figure 3.49a displays the extra button that was disabled in Figure 3.48, i.e. the *Assign Joint Attributes to Potential Sliding Plane* button. This button is enabled only for Flow option 6. Upon selection, the window of Figure 3.49b will appear and the starting and ending values of Conducting Aperture information will be entered for each rock joint.[1] The number of elements for each rock joint reach can also be entered.

[1] The double asterisk for the rock reaches denotes the fact that the rock reach is part of the potential slip plane.

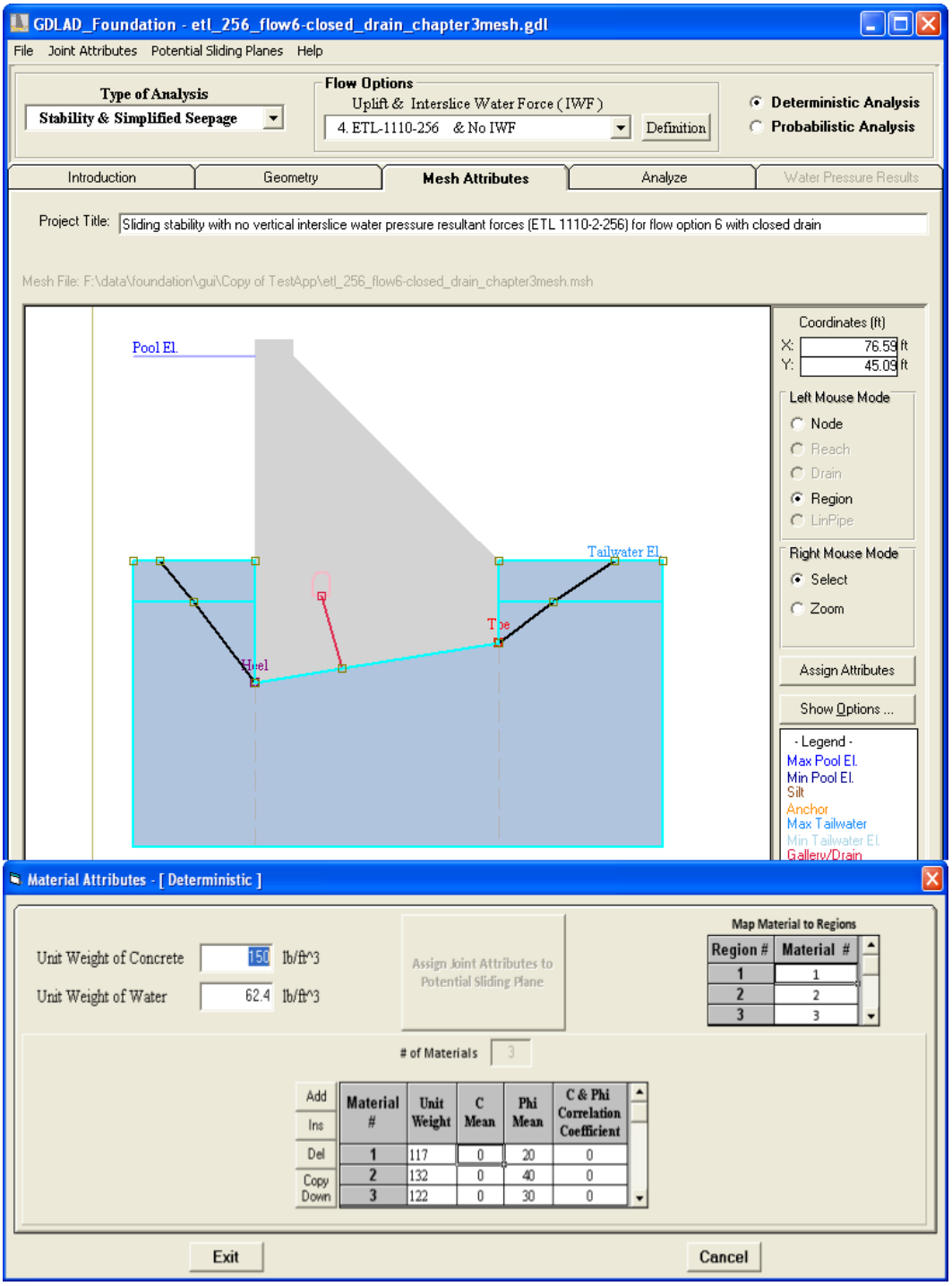

Figure 3.48. Material Properties and Regions.

The *Accept* button of Figure 3.49b will save any additions and modifications and then exit.

The *Cancel* button of Figure 3.49a will not save any edits and only exit out of this window.

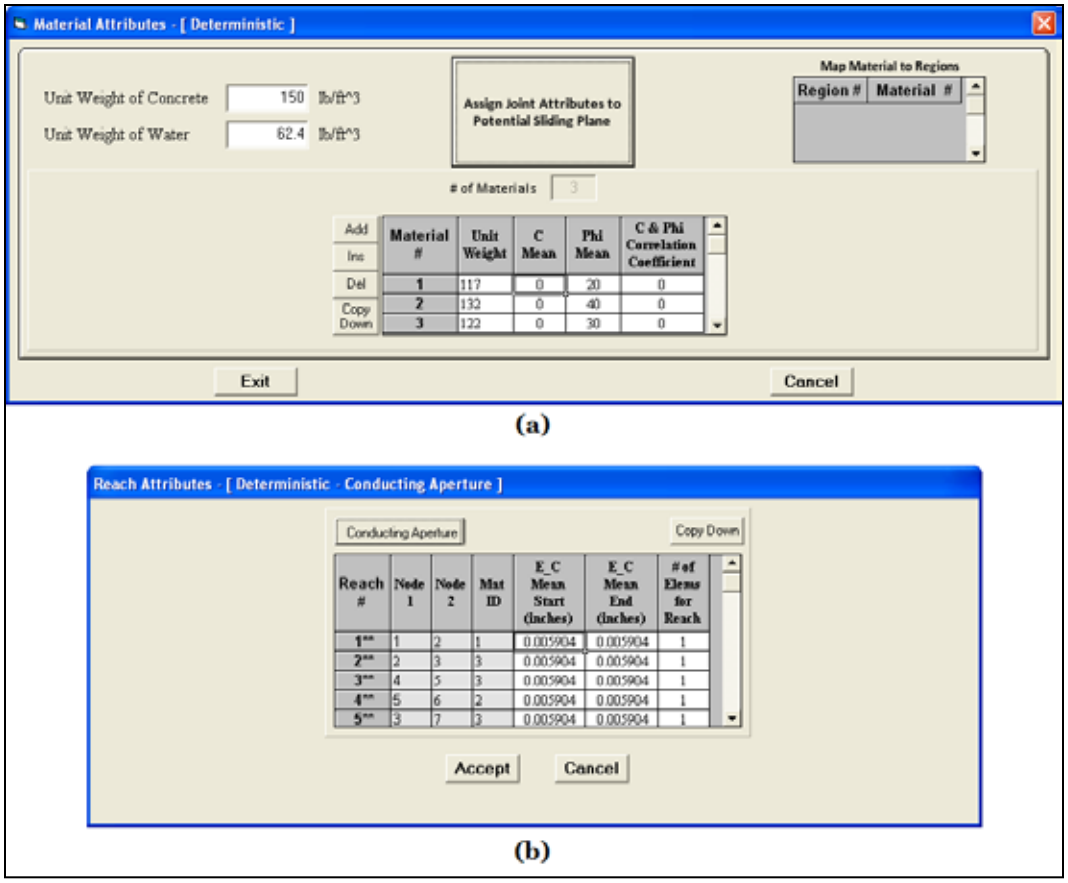

Figure 3.49. Attribute tables for (a) Material Properties and (b) Rock Joint attributes.

After the window (Figure 3.49b) has exited, Figure 3.48a will be the window remaining.

The *Exit* button of Figure 3.49a will save any additions and modifications and then exit.

The *Cancel* button of Figure 3.49a will not save any edits and only exit out of this window.

On exit, the material attributes table will close and the original image of Figure 3.45 with all regions selected will be displayed.

In *Region Mode* and for a probabilistic analysis of a Stability and Simplified Seepage type of Analysis for Flow Option 6, please see section 3.6.3.

3.3.3.3 *Joint_FLOW only type of analysis*

The third option listed in the *Type of Analysis* drop-down menu is for a *Joint_FLOW Only* type of analysis. Figure 3.50 shows this selection where nodal point water pressures and resultant uplift water pressure forces will be calculated by the software Joint_FLOW.

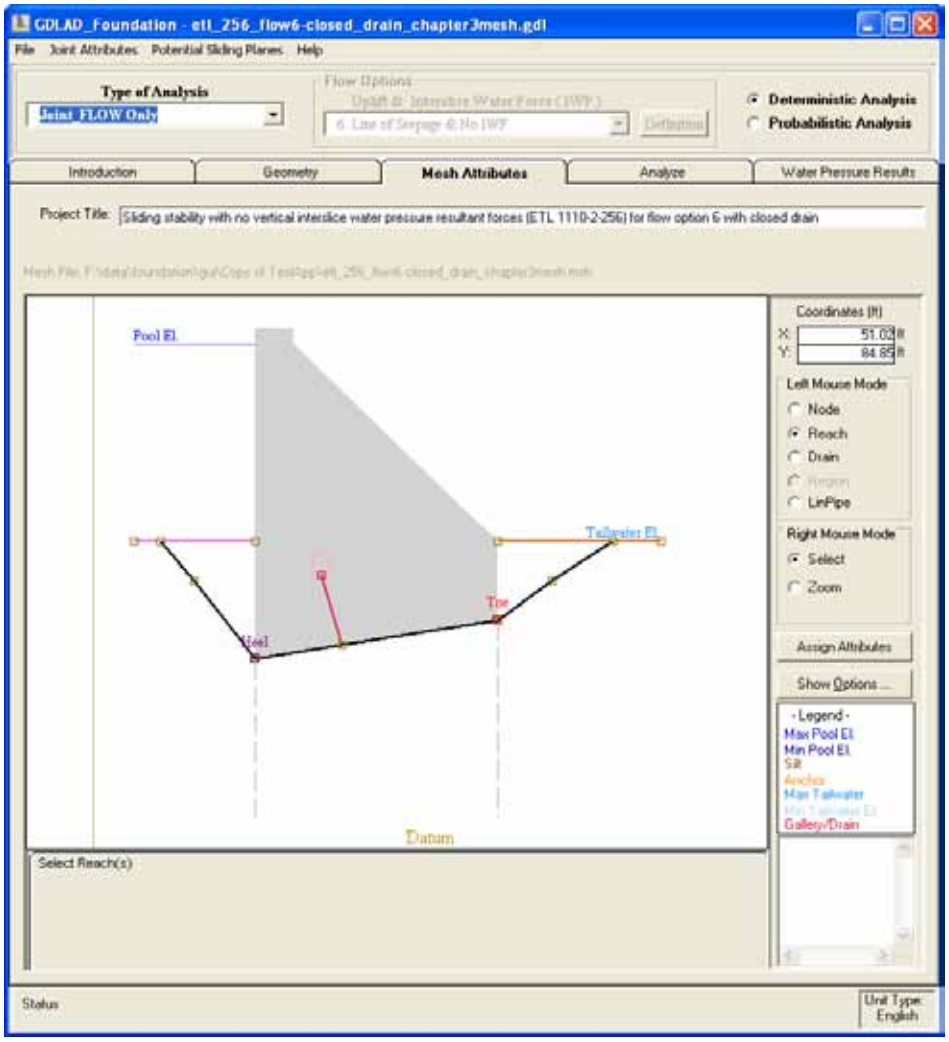

Figure 3.50. Selection Joint_FLOW only.

A simplified concrete gravity dam embedded within rock with a rock foundation drain has been generated to describe the Joint_FLOW Only type of analysis. There are no flow options available for the Joint_FLOW Only type of analysis. As shown in Figure 3.50, the *Left Mouse Mode* groups of radio buttons comprise of the *Node, Reach, Drain,* and *LinPipe* buttons and are active for selection. Note that *LinPipe* (alternative method to calculate head loss discussed in Chapter 5) input information is discussed in Section 3.3.2.2.3.

3.3.3.3.1 Joint Attributes menu item

The second item from the left corner of the menu bar is the "*Joint Attributes*" menu item shown in Figure 3.51. There are three items listed in the drop down menu. These are the *Aperture Type*, the *Drain Type,* and *LinPipe*. Each of these options will lead to further selections.

Figure 3.51. Aperture type in the Joint Attributes menu item.

3.3.3.3.1.1 Aperture Type

The *Aperture Type* consists of three types of apertures available for selection; the Mechanical Aperture and JRC, the Conducting Aperture and the Hydraulic Conductivity of a Clean Joint. The Conducting Aperture highlighted in blue in Figure 3.52 is currently selected by the assignment of a check mark. These types of rock joint apertures are discussed in detail in Chapter 1.

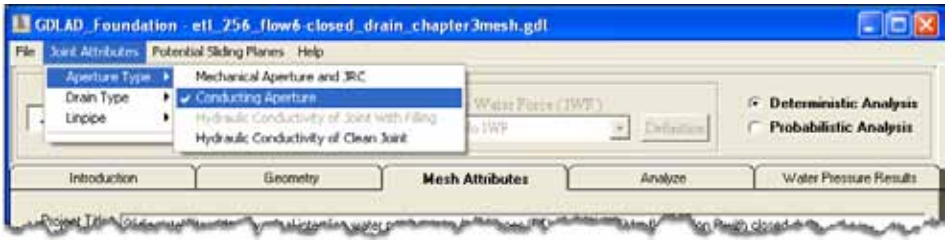

Figure 3.52. Aperture Type of a Rock joint.

3.3.3.3.1.2 Drain Type

When a Gallery or drain is specified for a project, this menu option will only be enabled for a "Stability and Joint_FLOW" and a "Joint_FLOW Only" type of analysis. This option will be disabled (grayed out) for the Stability and Simplified Seepage type of analysis. When *Drain Type* is enabled, it can be selected as shown in Figure 3.53. At present, the Simple Drain procedure for simulating a drain is the only option available.

Figure 3.53. Drain Type.

3.3.3.3.1.3 LinPipe type

The selection of *LinPipe* allows the user to use an alternative calculation of Head Loss in rock joint flow within a pipe network. This option is further described in Appendix C. Figure 3.54 shows the option to select *LinPipe*.

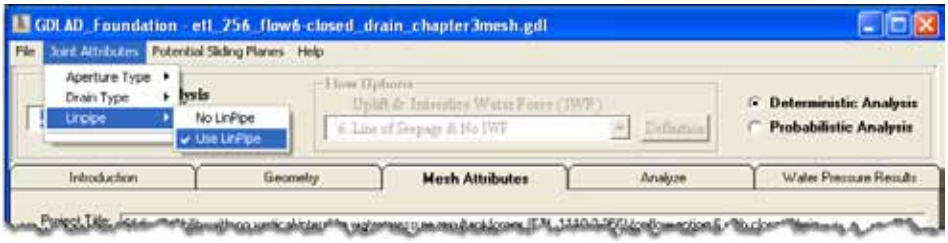

Figure 3.54. LinPipe.

3.3.3.3.2 Potential Sliding Planes menu item

The third item on the menu bar of Figure 3.55 is the *Potential Sliding Planes* menu item which is highlighted in dark blue. Once selected, a frame consisting of a group of buttons below the image window appears. This allows the user to *Add*, *Show*, and *Delete* a sliding plane[s] as well as to show wedges above the sliding plane. Section 3.3.2.3 gives further detail of this menu item.

3.3.3.3.3 Assign attributes

The following sub-sections describe each of the attribute tables for the active radio buttons on the *Left Mouse Mode* frame. As mentioned earlier, the *Node* radio button lists node id numbers in the message window and does not have an effect on the *Assign Attributes* button.

3.3.3.3.3.1 Reach Mode

In *Reach Mode* all relevant reaches must be selected before the *Assign Attributes* button can be selected. For each reach that is selected, the reach id would be listed as well as the *X*-, *Y*-coordinates of the two nodes

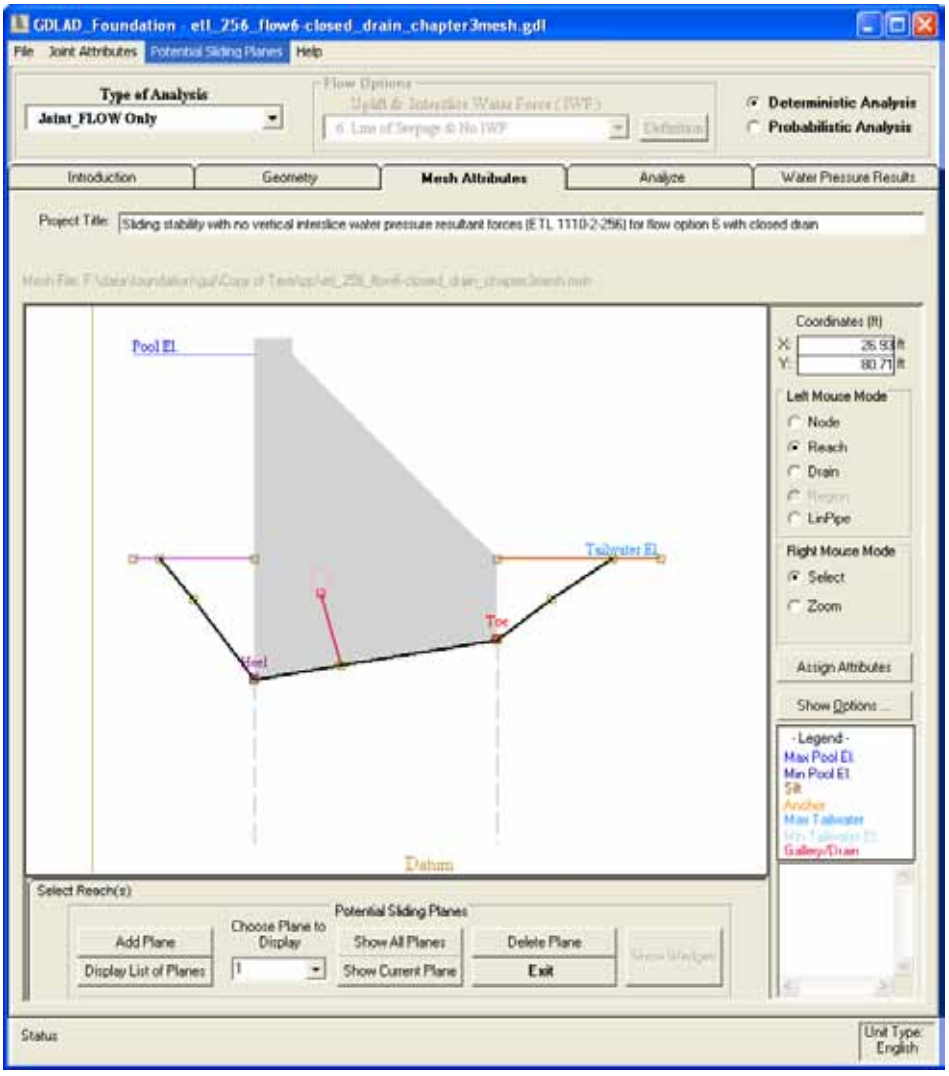

Figure 3.55. Potential Sliding Planes menu item.

connecting the reach and its length will be displayed in the *Geometry Text* window (refer to Section 3.27). Figure 3.56 shows the assignment of the hydraulic conductivity values for each reach. The table headings are the reach number, the starting node number (id), the ending node id, the material id, the starting value of the hydraulic conductivity, the ending value of the hydraulic conductivity and the number of elements per reach. As each reach number is selected, a green line on the original image will show the current reach selected. From the values provided, a uniform aperture has been designed and one element is assigned for each reach with a total of 6 reaches ("elevator" bar allows viewing of reach number 6 in Figure 3.56).

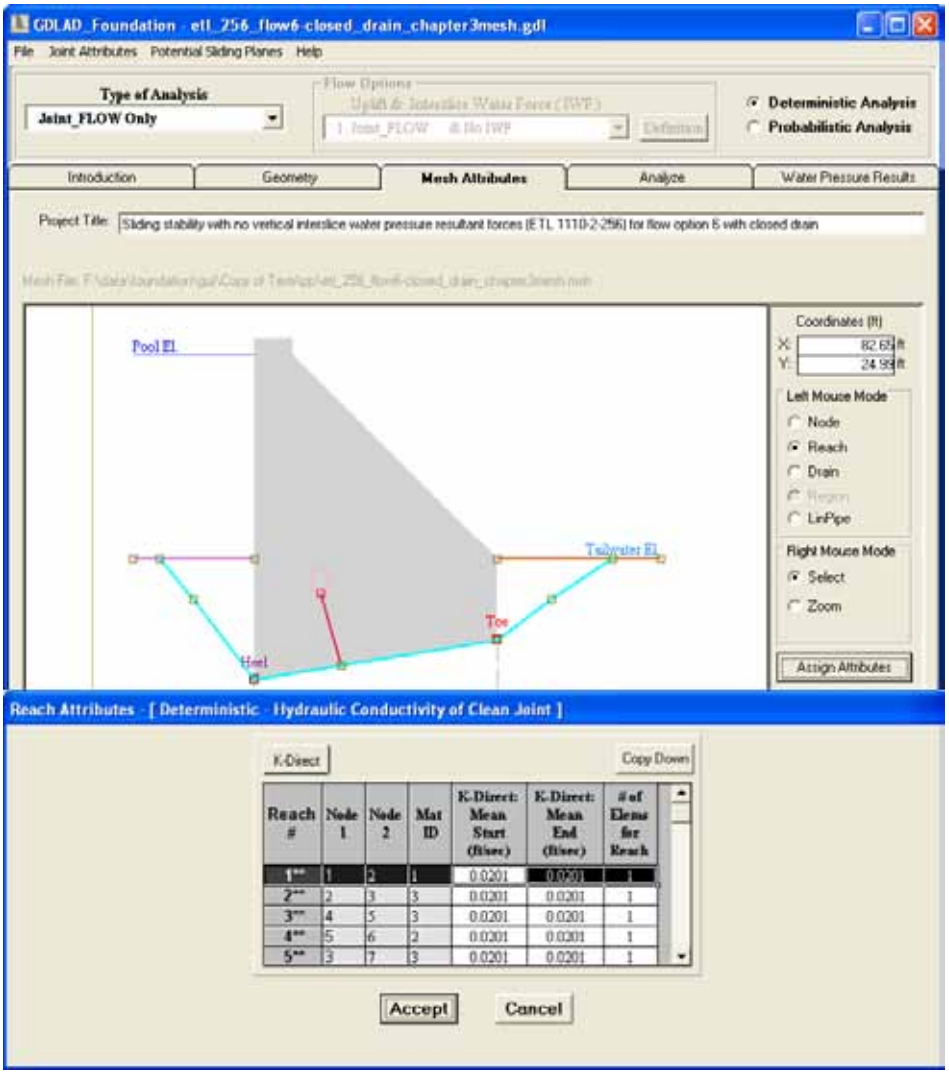

Figure 3.56. Hydraulic conductivity values with one element per reach.

The *Copy Down* button of the *Reach Attributes* window of Figure 3.56 provides a way to populate similar column items in the table. Just highlight the cells in a column and the first value will be copied to the other cells after the selection of the *Copy Down* button. As an alternative, since this table has a few functions similar to a spreadsheet, a small plus sign will appear at the right base of the selected cell. Selection of this small sign with the left mouse button and dragging down to the last cell of interest will also accomplish this task (i.e. copying the same values).

Entering a value greater than 1 in the *# of Elems for Reach* in any/all cells in the column (i.e. number of elements per reach) will cause the VM to internally create new nodes and modify reaches.

The *Accept* button will save any additions and modifications and then exit.

The *Cancel* button will not save any edits and only exit out of this window.

On exit, the original image of Figure 3.56 will be displayed.

In *Reach Mode* and for a probabilistic analysis of a Joint_FLOW Only type of Analysis, please see section 3.6.1.

3.3.3.3.3.2 Drain Mode

Before the *Assign Attributes* button is selected, the drain segment[s] (in red in Figure 3.56) must be selected. Figure 3.38 of Section 3.3.3.1.3.2 gives a full description of the variables and shows the assignment of the drain values of the drain segments.

3.3.3.3.3.3 LinPipe Mode

With the *LinPipe* radio button enabled, all reaches and drain elements will be included in the analysis automatically and it will not be necessary to select any reaches nor drain segments. Figure 3.39 of Section 3.3.3.1.3.4 gives a full description of the assignment of LinPipe parameters.

3.3.4 Show Options

The "*Show Options…*" button is shown selected in Figure 3.57 with five options available. The functionality of this button is similar to the "*Show Options…*" button discussed in Section 3.2.6. The "*Show Reach #*" (highlighted in blue) and the "*Show Regions*" options have both been selected and designated by a check mark. These options will show the Reach numbers or id's of both the reaches (R-id) and drain segments (D-id) and also display the outlines of the regions and region id and its associated material id (RG-id (M-id)) as seen in the image area of Figure 3.57. The other three options not selected are "*Hide Nodes*" which removes the squares identifying the locations of nodes in the image (except for the Heel and Toe); the "*Show Node #*" that labels the I.D. numbers of line segments relating to regions, upstream ground surface, downstream ground surface, drain and the sub surface joint reaches; and the "*Show Wedges*" which draws vertical brown lines starting from the potential slip plane and delimiting all wedges with id numbers for both wedge and sub-wedges.

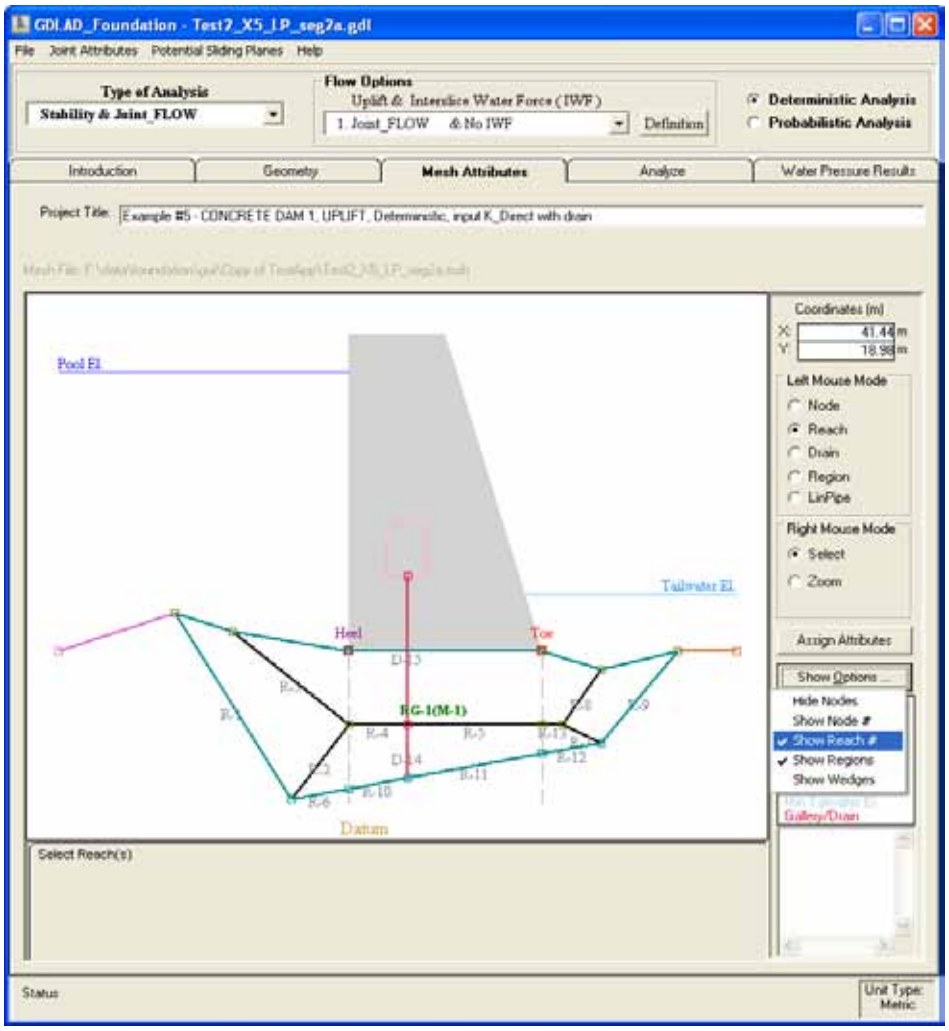

Figure 3.57. Show Options.

3.3.5 Legend and Geometry information

Both the "- *Legend* -"window located directly below the *Show Options…* button of Figure 3.57 and the text window located beneath the - Legend - window provide the same information as that described in the Legend and Geometry Information Section 3.2.7.

3.4 The Analyze tab

The Analyze tab allows the user to execute the project that was created or updated in the Geometry tab and Mesh Attributes tab. Figure 3.58 is a presentation of the various options available within the *Analyze* tab. A deterministic or probabilistic analysis is determined by the number of simulations provided; the *Stability Information* button that provides options for output generation; and most importantly, the viewing of results with the ability to save and print these as well.

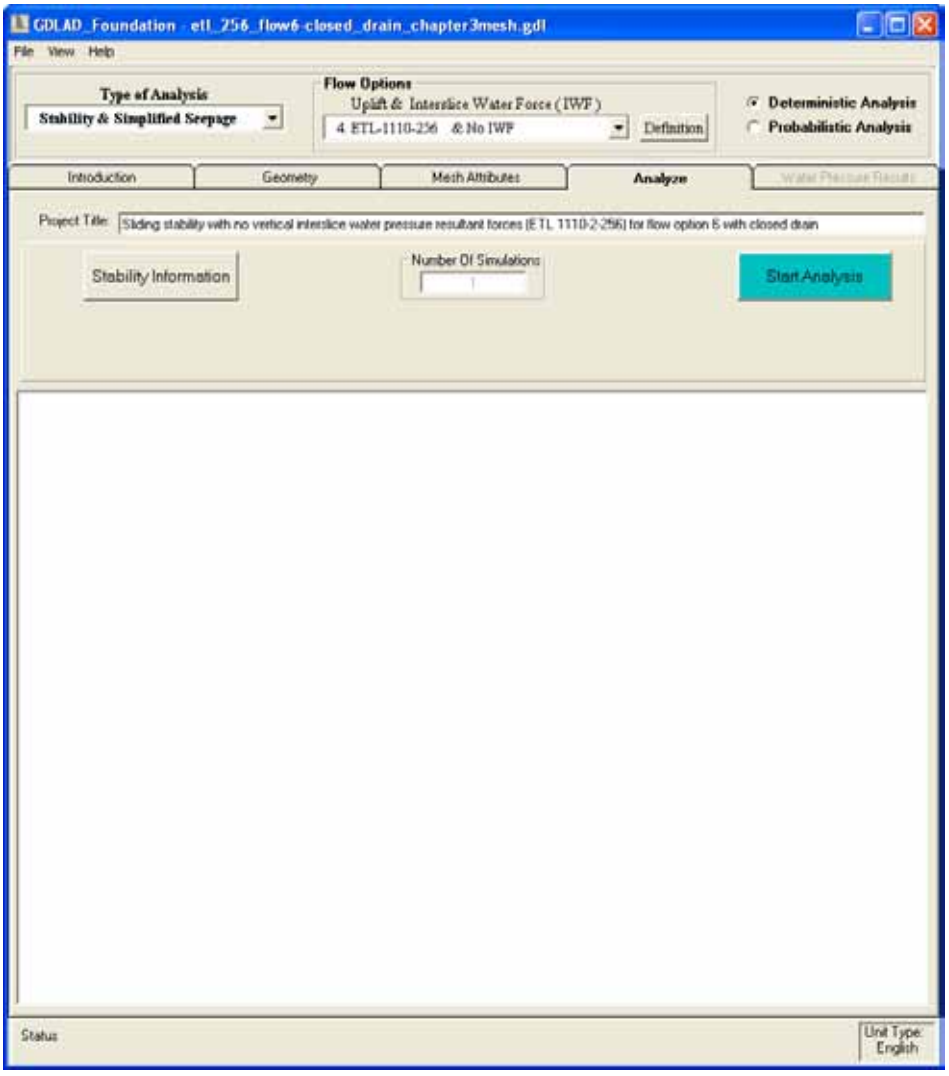

Figure 3.58. Generated mesh of a Stability & Joint_FLOW analysis.

3.4.1 The Type of Analysis

The *Type of Analysis* and *Flow Options* shown in Figure 3.58 were previously established either from within the Geometry tab or the Mesh Attributes tab. These options can also be changed, however, certain parameters would have to be added or modified within the Geometry and Mesh Attributes tab before any analysis can be performed. The *Type of Analysis* and *Flow Options* drop-down menus are described in detail within the Geometry tab section and Mesh Attributes tab section.

3.4.2 The project title

The project title is located directly beneath the various tabs of Figure 3.58 and is a very important feature that allows one to convey information

about the project. A total of 512 characters can be used to express the project. This project title is visible and can be accessed by all the tabs except when the Introduction tab is selected.

3.4.3 Number of Simulations

The *Number of Simulations* edit window allows the user to specify the number of Latin Hypercube simulations required to conduct a probabilistic analysis. The number of simulations mostly depends on the number of stochastic variables in the study. For a deterministic analysis, the number of simulations defaults to 1. The selection of either the *Deterministic* or *Probabilistic* radio buttons at the top right of the window will determine whether the *Number of Simulations* edit window will be enabled for input data. Figure 3.58 shows that the edit window is disabled and the Number of Simulations is set to 1 for a deterministic analysis.

3.4.4 Stability Information

The *Stability Information* button is located beneath the Project Title in Figure 3.58. This option determines how wedge force information will be generated for viewing, saving and printing. This button is enabled for both the Stability & Joint_FLOW and the Stability & Simplified Seepage types of analyses as this option is used specifically when calculations for stability are required. It will be disabled for a Joint_FLOW Only type of analysis. Figure 3.59 shows the options when the *Stability Information* button is selected. If the "*None*" check box is selected, there will be no output generated. Only one Pool elevation of information can be viewed or printed at a time. The drop down menu of the Pool Elevation allows for the selection of a particular Pool elevation. The first selection is always the Maximum Pool Elevation and it is 80 ft in this case. The next three radio buttons specify the condition of how often to provide output, i.e. at convergence, at specified iterations or at every iteration. It is not recommended to use the last option as it can be very time consuming and create an especially large file. The most often used and the default is the output of wedge forces at *Convergence Only*.

The *OK* button saves any edits and exits out of the *Stability Information* window.

The *Cancel* button just exits without saving.

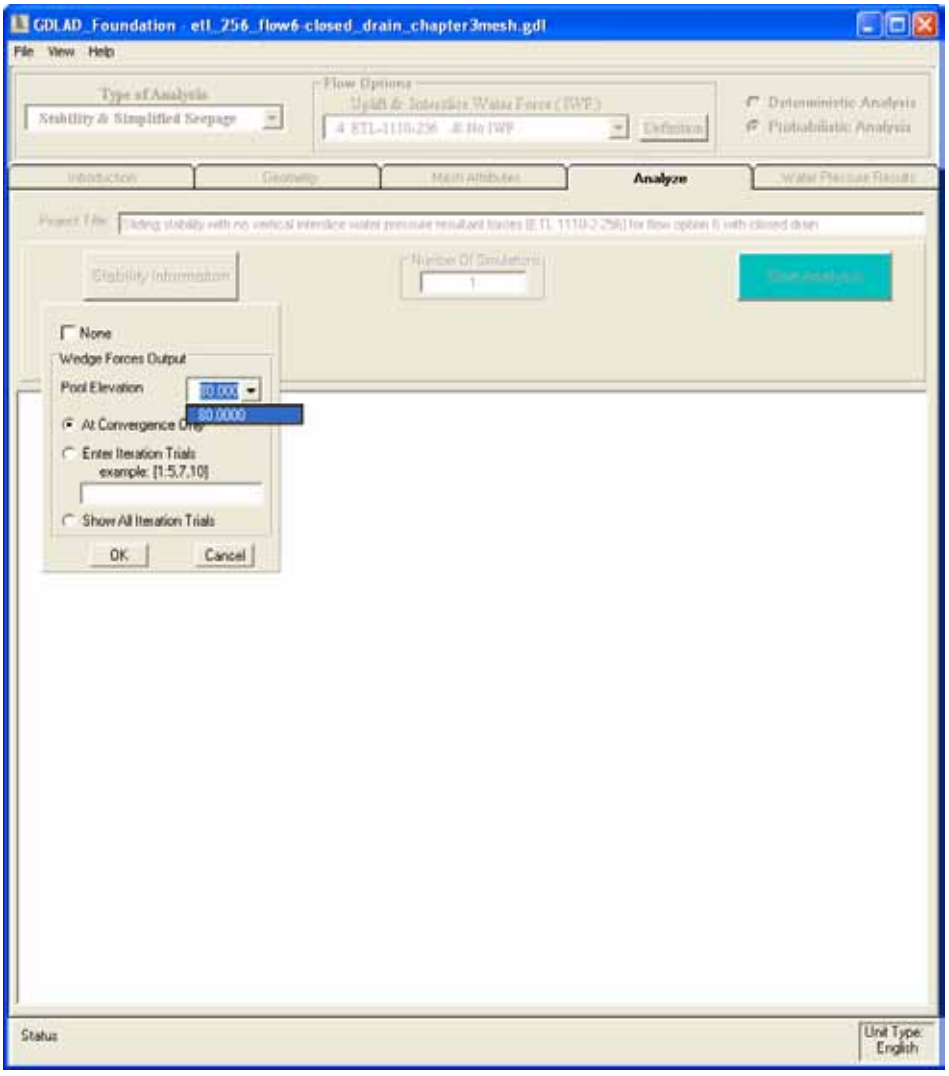

Figure 3.59. Stability output selection.

3.4.5 Start Analysis

After all parameters have been identified, entered and saved, it is now time to execute the program. The selection of the *Start Analysis* button (in green) will cause the VM to start the simulation of multiple programs. Each program will provide some form of run-time information while the user is waiting for results. It is good to note the Status Bar during run time. Figure 3.60 shows the processes that appear during a run.

Upon completion, a system response curve will appear if this analysis is in *Probabilistic Mode* for either a Stability & Joint_FLOW or a Stability & Simplified Seepage type of analysis. Figure 3.61 shows a system response curve within the image window of a hypothetical example with 2000 simulations. To have legible labels in the *x*-axis, the button at the

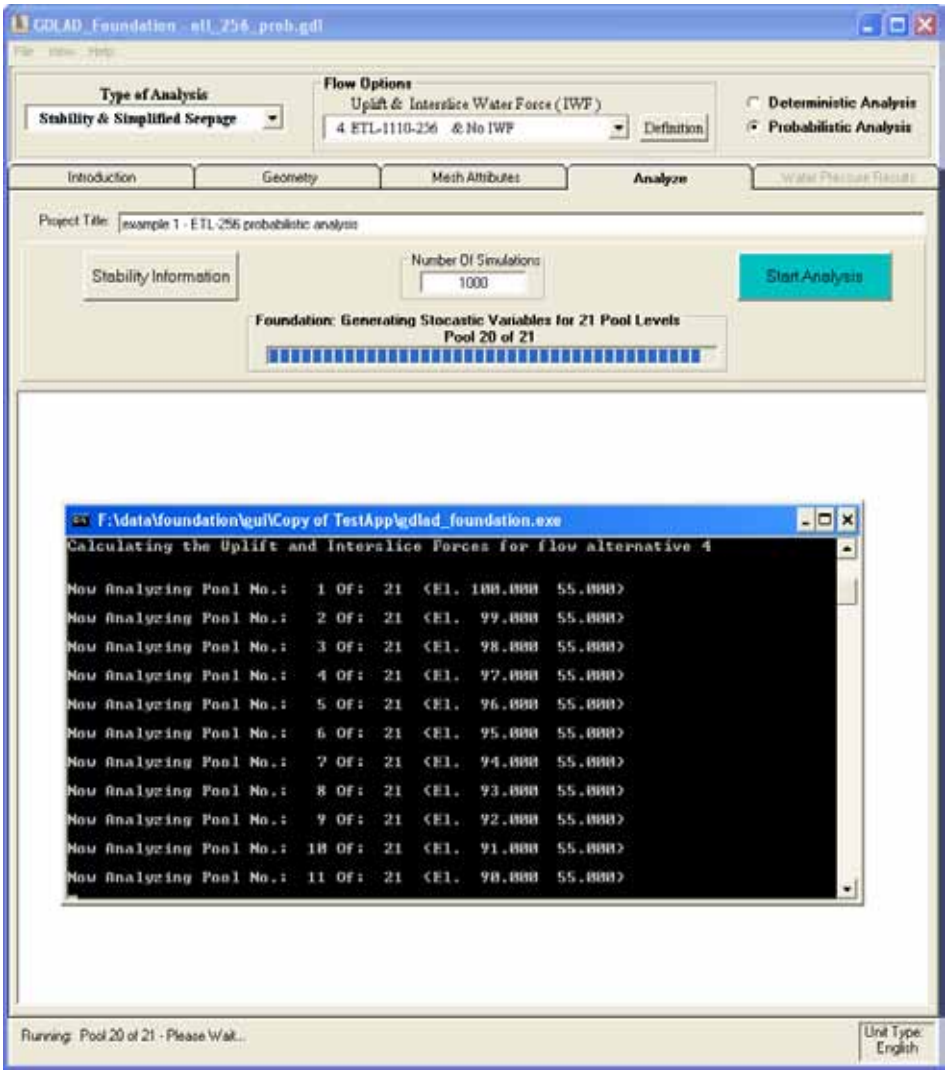

Figure 3.60. Run time information.

lower right hand corner of the image labeled *Edit X-axis* can be used to set the Interval Size which is the distance between elevations or gridlines and the "Increments/Interval" which sets the number of minor gridlines within each major gridline. Selecting the *Apply* button of the *Edit X-axis* window will accept the changes and update the image of Figure 3.61 and selecting the *Exit* button will close the "*Edit X-Axis*" window.

It is also a good time to look at the Menu Bar items for viewing, saving and printing output data.

3.4.6 The Menu Bar

The Menu Bar is located below the window title of Figure 3.62. It consists of three items, *File, View,* and *Help*.

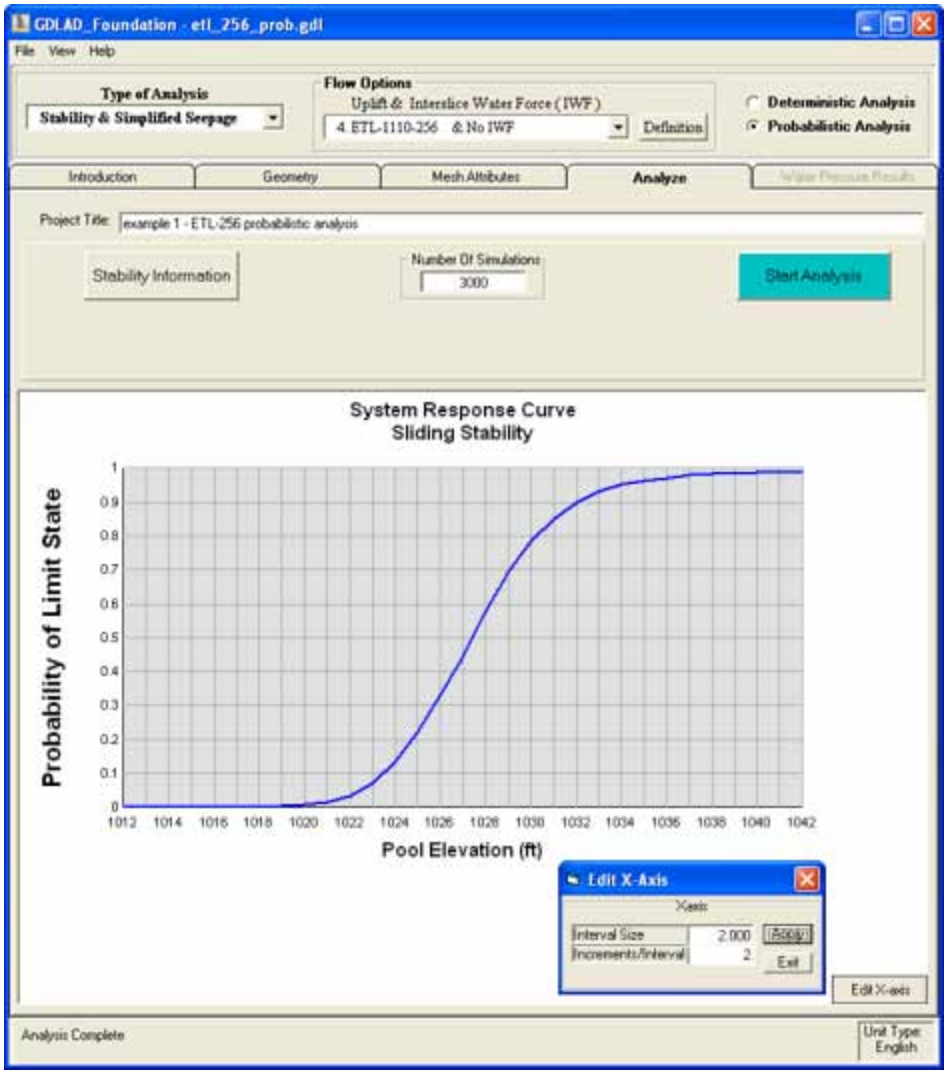

Figure 3.61. System response curve.

3.4.6.1 File Menu Item

The first item on the left hand side of the menu bar of Figure 3.62 is the *File* item which is highlighted in blue. Once selected, a drop down menu offering various file options can be selected. These items are explained in Section 3.2.8.1.

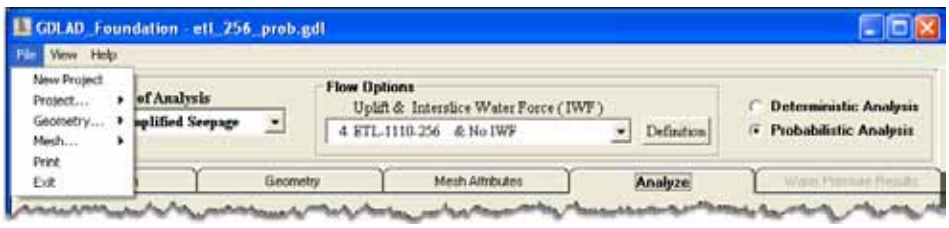

Figure 3.62. File menu item.

3.4.6.2 View menu item

The second item on the left hand side of the menu bar of Figure 3.63 is the *View* item which is highlighted in blue. Once selected, a drop down menu appears with two options for selecting a GDLAD_Foundation output and/or a Joint_FLOW output. Depending on the type of analysis selected, either one or both can be enabled. Figure 3.63 shows a GDLAD_Foundation probabilistic analysis with three files. If this was a deterministic analysis there would be two files listed.

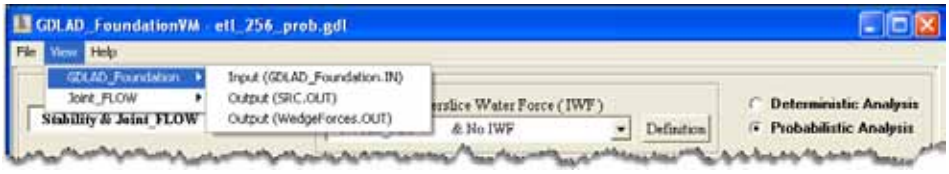

Figure 3.63. GDLAD_Foundation Input and Output file selection.

These data files are ASCII files provided by GDLAD_Foundation as input to the FORTRAN engineering program; SRC.OUT for a probabilistic analysis with system response curve; and WedgeForces.OUT with information regarding wedge forces. Examples of the three types of GDLAD_Foundation files are illustrated in Figures 3.64 through 3.66. All three figures have the option to save and print the information they contain. This can be done from the *File* item of the Menu Bar within each of the three figures.

Figure 3.64. GDLAD_Foundation input file.

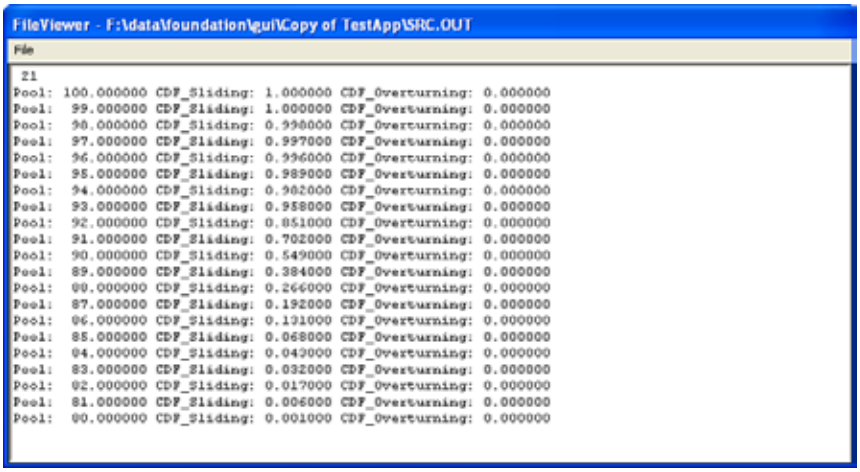

Figure 3.65. GDLAD_Foundation system response curve.

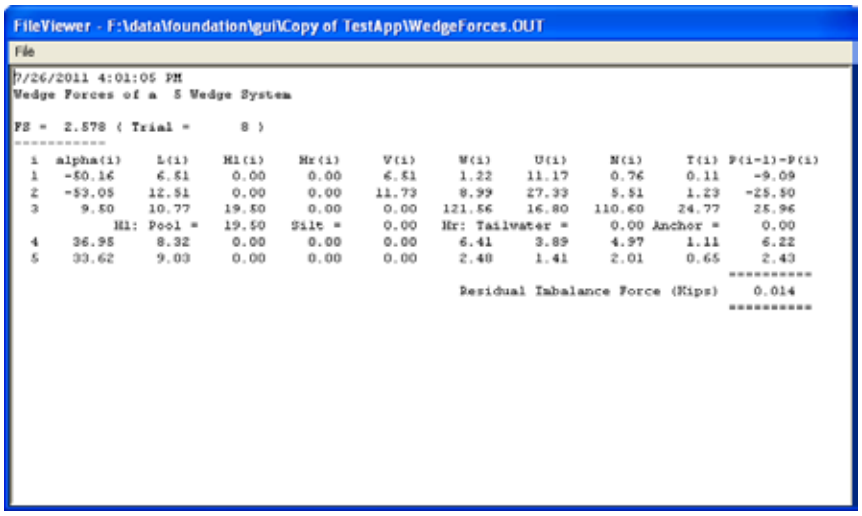

Figure 3.66. GDLAD_Foundation wedge forces.

The Joint_FLOW analysis in blue in Figure 3.67 will produce two ASCII files. Joint_FLOW.IN showing input information to the FORTRAN engineering program and Joint_FLOW.OUT with information of water pressures at the nodes and uplift water pressure forces normal to a wedge base.

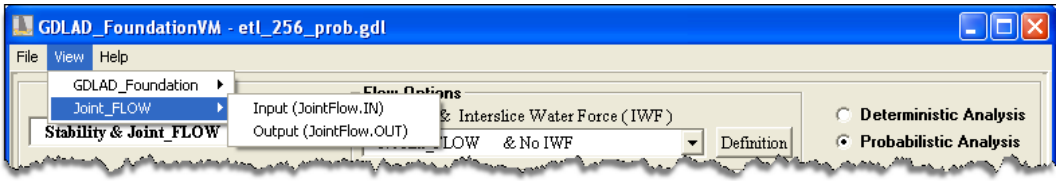

Figure 3.67. Joint_FLOW Input and Output.

Examples of the two Joint_FLOW files are illustrated in Figures 3.68 and 3.69.

Both figures have the option to save and print the information they contain. This can be done from the *File* item of the Menu Bar within each of the two figures.

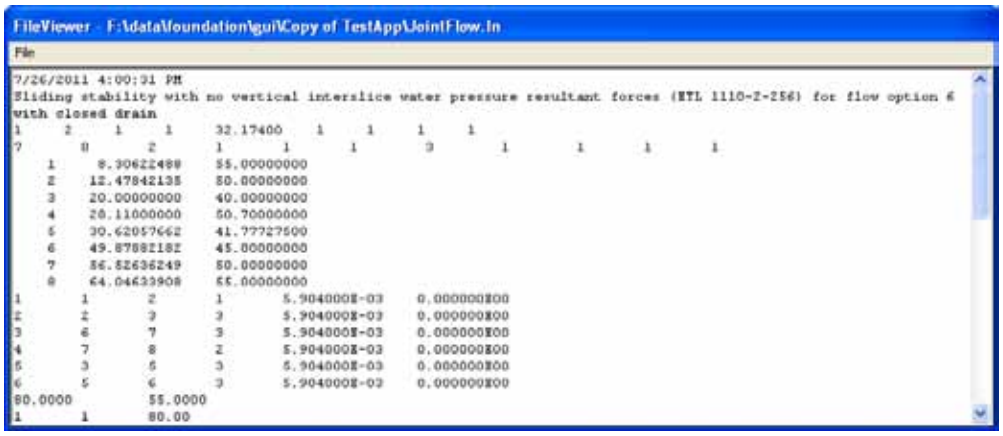

Figure 3.68. Joint_FLOW input.

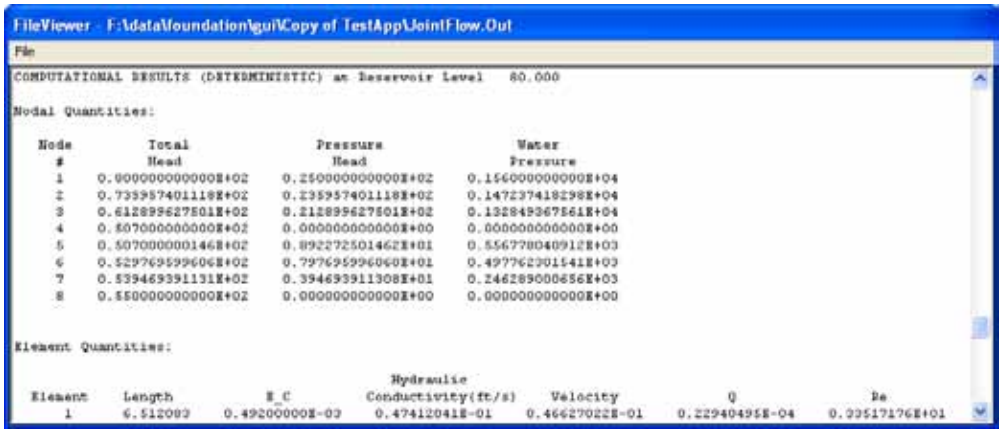

Figure 3.69. Joint_FLOW output.

3.4.6.3 Help menu item

The last item on the menu bar is the *Help* menu item which is highlighted in blue (Figure 3.70). Once selected, a drop-down menu shows the available help options which are explained in Section 3.2.8.7.

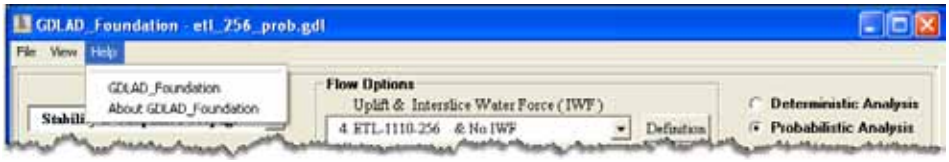

Figure 3.70. Guidance for GDLAD_Foundation.

3.5 View Pressure Results tab

The View Pressure Results tab allows the user to view results for either a *Stability & Joint_FLOW* type of analysis or a *Joint_FLOW Only* type of analysis. Figure 3.71 is an example where water pressure results at nodal points within rock joints are presented as solid circles. The mean values are represented by the size of the circles and the standard deviation values are represented by the color. Please see the legend in Figure 3.71 for approximate values. The mean maximum values are also provided in text boxes at the right side of Figure 3.71.

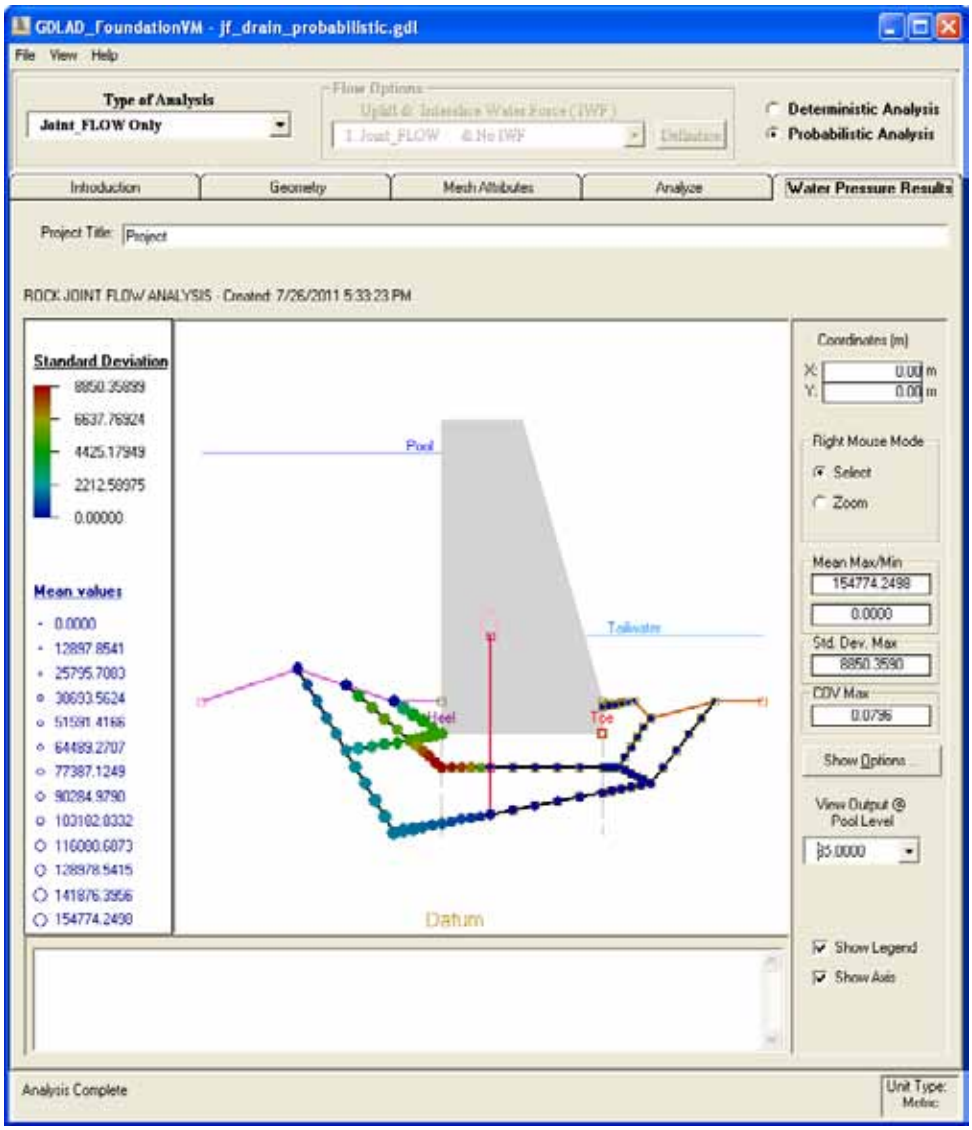

Figure 3.71. Probabilistic analysis with water pressures at nodal points.

3.5.1 The project title

The project title is located directly beneath the various tabs of Figure 3.71 and is a very important feature that allows one to convey information about the project. A total of 512 characters can be used to express the project. This project title is visible and can be accessed by all the tabs except when the Introduction tab is selected.

3.5.2 The Right Mouse Mode

The *Right Mouse Mode* group of radio buttons located at the center right side of Figure 3.72 is used for the selection of nodal points that represent water pressures within rock joints and drain segments.

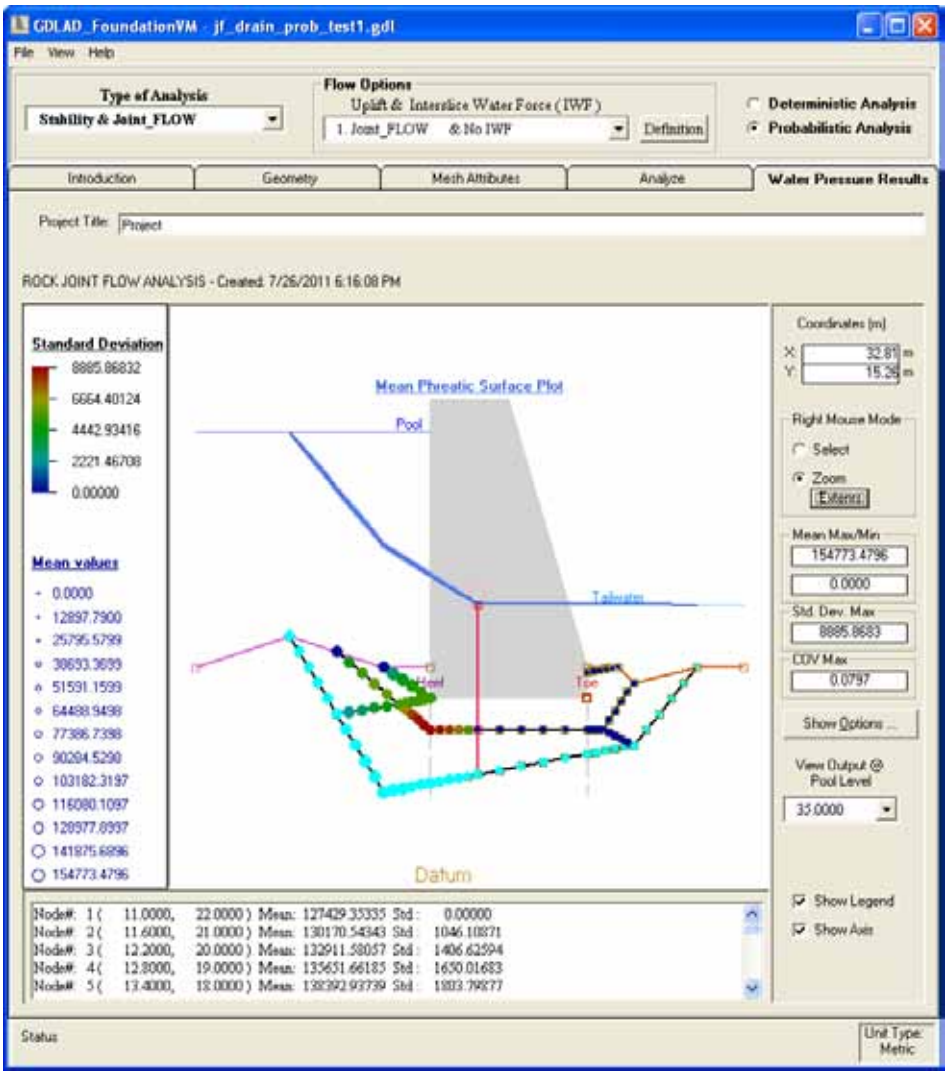

Figure 3.72. Mean Phreatic Surface at selected nodal points.

3.5.2.1 The Select Mode

The *Select* radio button of the *Right Mouse Mode* (*Select Mode*) of Figure 3.72 must be enabled before any nodes can be selected.

Figure 3.72 shows that all nodes along the potential slip plane have been selected. This is done by pressing the control key and simultaneously with the left mouse select all nodes that represent the potential slip plane. The selected nodes are shown in light blue. When each node is selected, the node number, *x*-, *y*-coordinates, mean value and standard deviation value are displayed at the bottom window beneath the legend and the image area representing the concrete gravity dam and rock joints. At the same instance, the mean phreatic surface is being drawn. This continuous line starts at the Pool, connects at the top of drain and terminates at the tailwater. Standard deviation values are also drawn.

3.5.2.2 The Zoom Mode

The *Zoom* radio button of the *Right Mouse Mode* (*Zoom Mode*) of Figure 3.72 is used to zoom in on locations of interest. The ability to keep zooming into the image is an option; however, the capability to zoom out is currently not available. There is only one general way to zoom out and it is the *Extents* button which redraws the image to its original size and limits.

3.5.3 Show Options

The "*Show Options…*" button when selected will display five options as shown in Figure 3.73. The functionality of this button is similar to the "*Show Options…*" button discussed in Section 3.2.6. None of the options have been selected in this example. The four options are *Hide Nodes* which removes the squares identifying the locations of nodes in the image; the "*Show Node #*" that labels the node numbers of all nodes; the "*Show Reach #*" and the "*Show Regions*" options will show the Reach numbers or id's of both the reaches (R-id) and drain segments (D-id) and also display the outlines of the regions and region id and its associated material id (RG-id (M-id)); and lastly the *Show Wedges* option will draw vertical brown lines from the base of the potential slip plane to the ground surface and define all wedges with id numbers for both wedge and sub-wedges.

3.5.4 Select pool elevation, legend and axis

The "*View Output@ Pool Level*" drop-down menu gives output results depending on the Pool level selected, i.e. a water pressures file is imported and the image is updated that corresponds to the Pool level selected. The *maximum pool level* is the first listed and always the default. In *Deterministic Mode*, there will only be one Pool level. The Pool level of 35.0 ft is shown highlighted in blue in Figure 3.73.

The "*Show Legend*" and "*Show Axis*" check boxes are both enabled and located at the lower right corner of Figure 3.73. Both these options will enable or disable the legend and axis individually.

Note that Figure 3.73 is a copy of the right vertical selection panel of Figure 3.72.

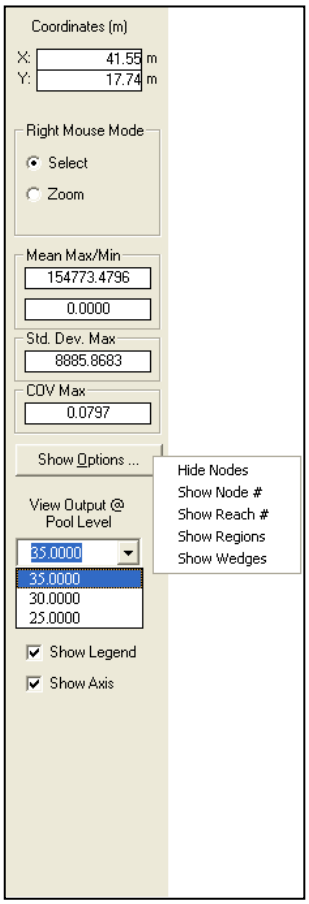

Figure 3.73. Right selection panel of water pressure results tab.

3.5.5 The Menu Bar

The Menu Bar is located beneath the window title bar. It consists of three items, *File, View,* and *Help*.

3.5.5.1 File menu item

The first item on the left hand side of the menu bar of Figure 3.74 is the *File* item which is highlighted in blue. Once selected, a drop down menu offering various file options can be selected. These items are explained in detail in Section 3.2.8.1.

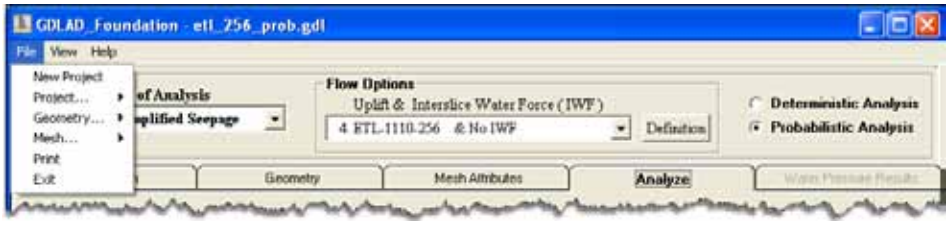

Figure 3.74. File menu item.

3.5.5.2 View menu item

The second item on the left hand side of the menu bar of Figure 3.75 is the *View* menu item which is highlighted in blue. Once selected, a drop down

menu appears with one option for selecting an *Output Plot* file that was created by the Joint_FLOW engineering program.

Figure 3.75. GDLAD_Foundation Input and Output file selection.

This *Output Plot* menu item when selected will list all the "*.plt" files available in the project directory. Figure 3.76 shows a standard window explorer file folder in list form for opening a file. Once the *Open* button is selected, the *GDLAD_FoundationVM* window will update all its data values and redraw the water pressures at the rock joints.

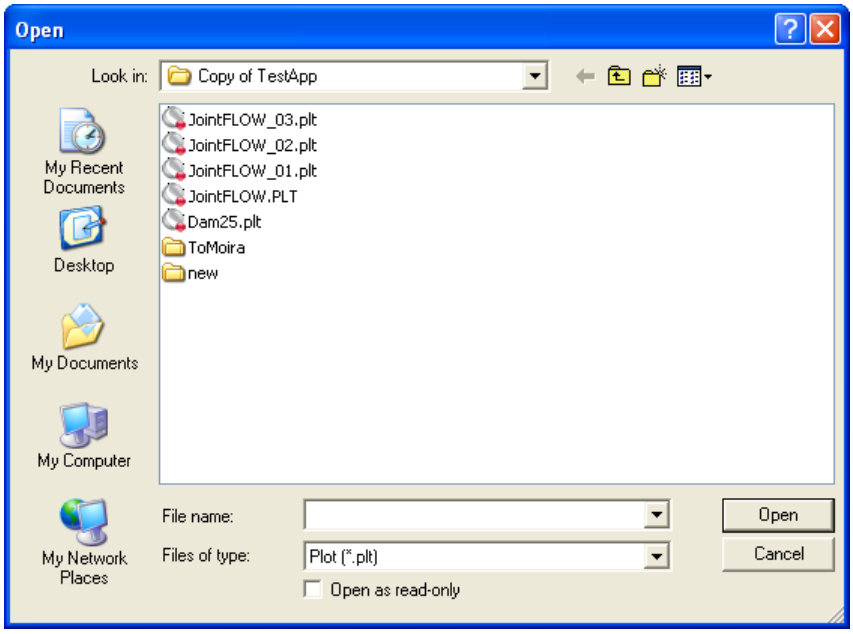

Figure 3.76. Selection of water pressure files.

3.5.5.3 *Help menu item*

The last item on the menu bar is the *Help* menu item which is highlighted in blue (Figure 3.77). Once selected, a drop-down menu shows the available help options which are explained in Section 3.2.8.7.

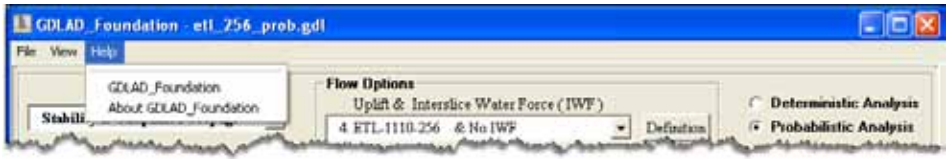

Figure 3.77. Guidance for GDLAD_Foundation.

3.6 Probabilistic supplementary material

Within the Mesh Attributes tab is the option to *Assign Attributes* when a reach, drain, or region option is selected within the *Left Mouse Mode* group of radio buttons (see Section 3.3 for more details). An example of the concrete gravity dam with multiple rock joints is shown in Figure 3.78.

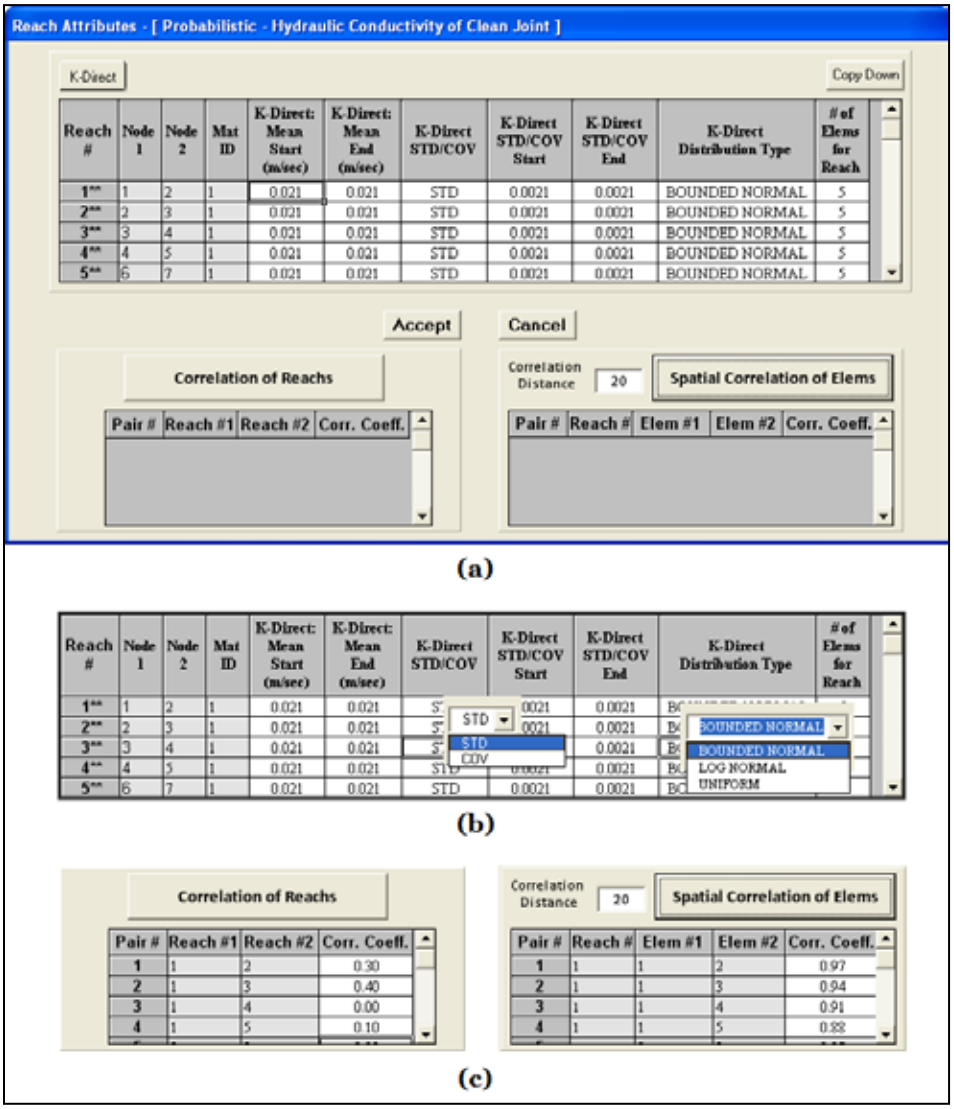

Figure 3.78. Reach Attributes for a Probabilistic Analysis (a) Table for K-Direct values (b) Std/Cov and Distribution type selection (c) correlation coefficient between elements.

3.6.1 Reach Mode (Stability and Joint_FLOW and Joint_FLOW Only)

After the selection of all reaches of interest and the *Assign Attributes* button is selected, the window of Figure 3.78a is displayed. For a probabilistic analysis there is the extra information besides providing the mean start and end hydraulic conductivity (K-Direct) values. There is also an option to enter either the standard deviation (Std.) or the coefficient of variation (Cov) values of K-Direct. This is accomplished by the selection of the cells representing each reach within the "K-Direct STD/COV" data column. After the cell is selected, double-click it and a pull-down menu will appear. Click the down arrow and the two options (STD and COV) will appear as in Figure 3.78b. Selection of either will close this option window. The cell should now have the value you selected. The next step would be to provide the start and end Std. or Cov K-Direct values for entry in column eight and nine of the table. Continue to make any other changes regarding columns 7 thru 9. Another item for a probabilistic analysis is the Distribution type which is also available for selection in column 10. Figure 3.78b shows that after double-clicking a cell, the three option pull-down menu will appear and the *Bounded Normal* distribution type highlighted in blue has been selected.

There are two options to define correlation between elements and both are represented by the lower two input tables of Figure 3.78a. The selection of either table depends on the last column which is the *# of Elems for Reach* column of the upper table (K-Direct).

If the number of elements per reach is equal to 1 then the *Correlation of Reaches* button (the left lower table of Figure 3.78a) can be used to enter correlation coefficient values for any pairs of elements that only have one element per reach.

If the number of elements per reach is greater than one, the *Spatial Correlation of Elems* button (the right lower table of Figure 3.78a) can be used to enter correlation coefficient values. It has the option of entering the correlation coefficient between each element by hand or the use of an automatic procedure to enter these values.

There is the possibility that both tables will be populated, especially when some reaches will have one element while some will have more than one element. Figure 3.78c shows the correlation coefficient values between pairs of elements on both tables.

In the automatic procedure that calculates the correlation coefficient between two elements (lower right table of Figure 3.78c), the Correlation Distance is first entered (default is 20). The *Spatial Correlation of Elems* button must then be selected and a triangular function will be used to calculate the correlation coefficient between any two elements. The Spatial Correlation (ρ) between elements within a rock joint is determined by the triangular function

$$\rho = 0.0, \quad abs\left[x'_{ele} - x'\right] \geq SP_{len} \tag{3.1}$$

otherwise,

$$\rho = 1.0 - \left[\frac{abs\left(x'_{ele} - x'\right)}{SP_{len}} \right] \tag{3.2}$$

where

SP_{len} = spatial correlation length
x'_{ele} = local x-coordinate of function at peak (mid-point) along the length of the rock joint reach
x' = local x-coordinate of the mid-point of all other elements within rock joint along the length of the rock joint reach

Equation 3.1 states that if the distance between two elements is larger than the given *Correlation Distance* than there is no correlation between these elements and the correlation coefficient will be set to zero. Otherwise Equation 3.2 will be used to determine the correlation coefficient values populated in the table.

The *Accept* button will save any additions and modifications and then exit.

The *Cancel* button will not save any edits and only exit out of this window.

3.6.2 Region Mode (Stability and Joint_FLOW and Stability and Simplified Seepage with flow option 4 and 5)

After the selection of all regions of interest and the *Assign Attributes* button is selected, the window of Figure 3.79a is displayed. In a probabilistic analysis there is extra information besides providing the mean values of both cohesion (*C*) and the internal friction angle (*Phi*) values. There is also an option to enter either the standard deviation (Std.) or coefficient of

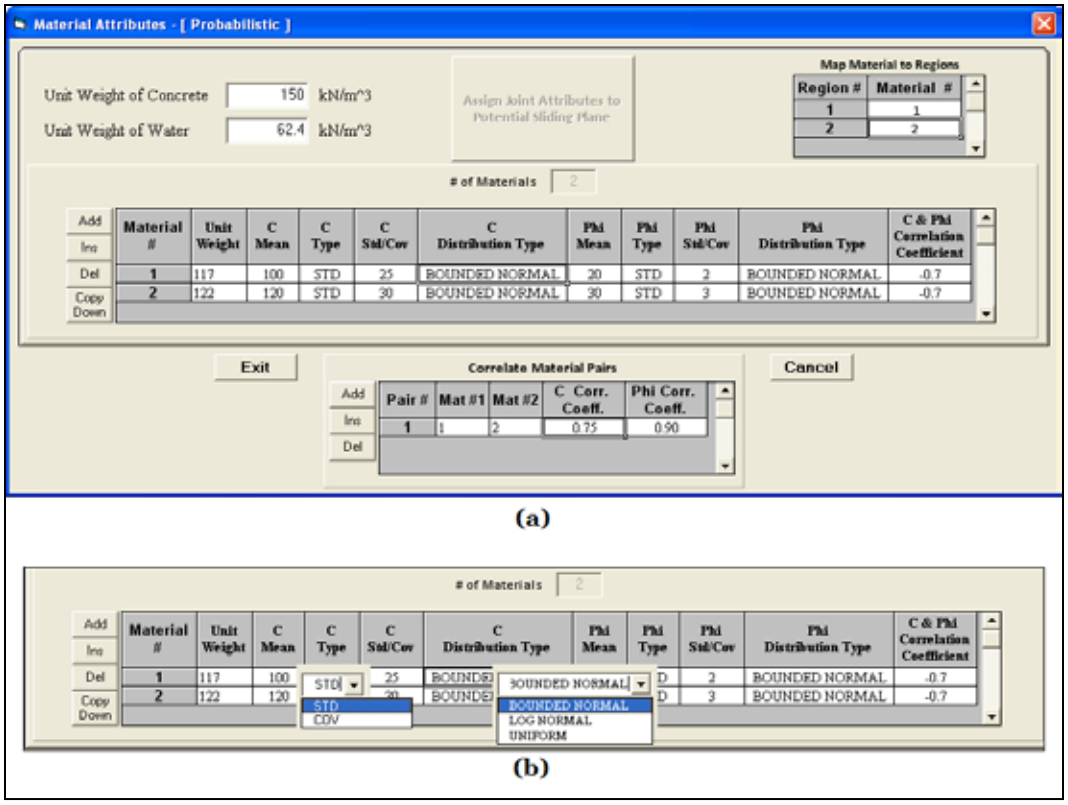

Figure 3.79. Region Attributes for a Probabilistic Analysis for flow options 4 and 5. (a) Material attributes table (b) Std/Cov and Distribution type selection.

variation (*Cov*) values for both *C* and *Phi*. This is accomplished by the selection of the cells representing each reach within the "*C Type*" and "*Phi Type*" data columns. When a cell is selected, double-click it and a pull-down menu will appear. Click the down arrow and the two options (*STD* and *COV*) will appear as in Figure 3.79b. Selection of either will close this menu window. The cell should now have the value you selected. The next step would be to provide the *C* values for either the *STD*. or *COV* for entry in column five of the materials table. The *PHI* values for either the *STD*. or *COV* can also be entered in column 9 of the materials table.

Another item for a probabilistic analysis is the Distribution type which is also available for selection in column 6 and 10 for *C* and *PHI* respectively. Figure 3.79b shows that after double-clicking of the cell, the three option pull-down menu will appear and the *Bounded Normal* distribution type highlighted in blue has been selected.

The final item in the materials table of Figure 3.79a is the correlation between *C* and *PHI* values which is entered in the last column. For this example, the *C* and *PHI* values of both rock materials are inversely

correlated and given a value of -0.7 (Evaluation of site specific data will be needed to quantify this value).

The last table at the bottom of Figure 3.79a is the *Correlate Material Pairs* table which establishes the correlation between the *C* values of two different material types as well as the correlation between the *PHI* values of the same two different material types. In the *Correlate Material Pairs* table of Figure 3.79a, there is a high positive correlation between the *PHI* values of both material 1 and material 2. While there is a 0.75 correlation between the *C* values of both material 1 and material 2.

The *Exit* button of Figure 3.79a will save any additions and modifications and then exit.

The *Cancel* button of Figure 3.79a will not save any edits and only exit out of this window.

3.6.3 Region with Reach Mode (Stability and Simplified Seepage with flow option 6)

In the Mesh Attributes tab after the selection of all regions of interest and the *Assign Attributes* button is selected, the window of Figure 3.80a is displayed. In a probabilistic analysis there is extra information in the materials table besides providing the mean values of both cohesion (*C*) and the internal friction angle (*PHI*) values. There is also an option to enter either the standard deviation (*STD.*) or coefficient of variation (*COV*) values for both C and PHI. This is accomplished by the selection of the cells representing each reach within the "*C Type*" and "*Phi Type*" data columns. When a cell is selected, double-click it and a pull-down menu will appear. Click the down arrow and the two options (*STD* and *COV*) will appear as in Figure 3.80b. Selection of either will close this drop-down menu window. The cell should now have the value you selected. The next step would be to provide the *C* values for either the *STD.* or *COV* for entry in column five of the materials table. The *PHI* values for either the *STD.* or *COV* can also be entered in column 9 of the materials table.

Another item for a probabilistic analysis is the Distribution type which is also available for selection in column 6 and 10 for *C* and *PHI* respectively. Figure 3.80b shows that after double-clicking of the cell, the three option pull-down menu will appear and the *Bounded Normal* distribution type highlighted in blue has been selected.

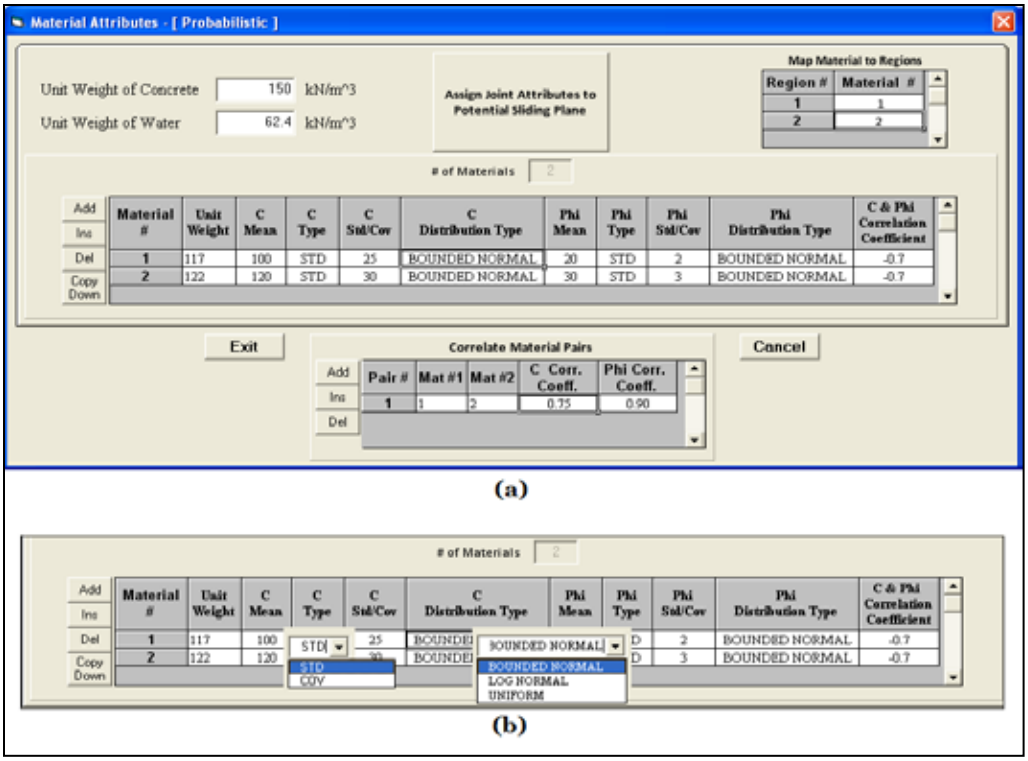

Figure 3.80. Region Attributes for a Probabilistic Analysis for flow option 6 (a) Material attributes table (b) Std/Cov and Distribution type selection.

The final item in the materials table of Figure 3.80a is the correlation between *C* and *Phi* values which is entered in the last column. For this example, the *C* and *Phi* values of both rock materials are inversely correlated and given a value of -0.7 (Further study will be needed to quantify this value).

The last table at the bottom of Figure 3.80a is the *Correlate Material Pairs* table which establishes the correlation between the *C* values of two different material types as well as the correlation between the *Phi* values of the same two different material types. In the "*Correlate Material Pairs*" table of Figure 3.80a, there is a high positive correlation between the *Phi* values of both material 1 and material 2. While there is a 0.75 correlation between the *C* values of both material 1 and material 2.

There is the *Assign Joint Attributes to Potential Sliding Plane* button located in the upper center of Figure 3.80a. This button is enabled only for Flow option 6 for a Stability and Simplified Seepage type of analysis. Upon selection, the window of Figure 3.81a will appear and the starting and ending values of the mean hydraulic conductivity values (K-Direct) will be entered for each rock joint reach that makes up the potential sliding plane. The number of elements for each rock joint can also be entered.

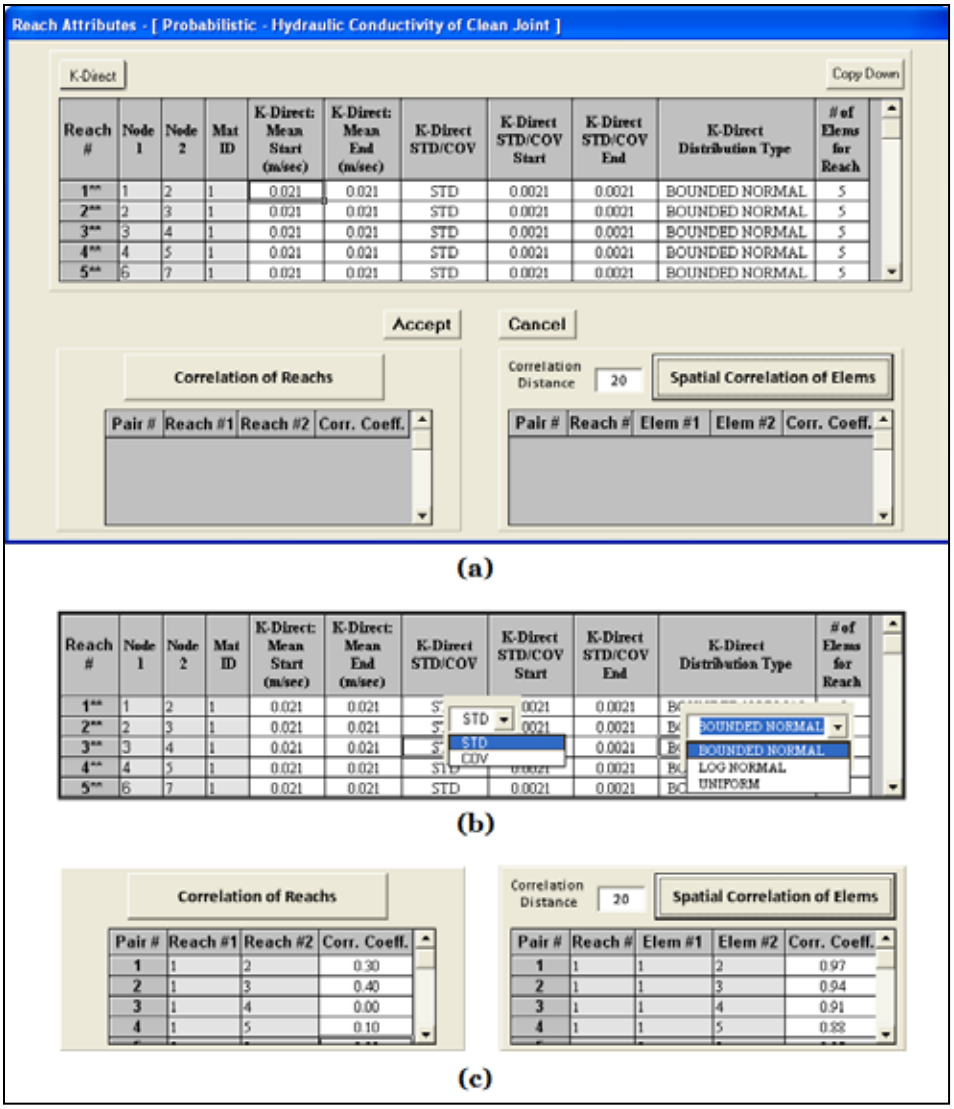

Figure 3.81. Reach Attributes for a Probabilistic Analysis of (a) Table for K-Direct values (b) Std/Cov and Distribution type selection (c) correlation coefficient between elements.

There is also an option to enter either the standard deviation (Std.) or coefficient of variation (*COV*) values of K-Direct. This is accomplished by the selection of the cells representing each reach within the "*K-Direct STD/COV*" data column. After the cell is selected, double-click it and a pull-down menu will appear. Click the down arrow and the two options (*STD* and *COV*) will appear as in Figure 3.81b. Selection of either will close this option window. The cell should now have the value you selected. The next step would be to provide the start and end *STD*. or *COV* K-Direct values for entry in column eight and nine of the reach attributes table. Continue to make any other changes regarding columns 7 thru 9.

Another item for a probabilistic analysis is the distribution type, which is also available for selection in column 10. Figure 3.81b shows that after double-clicking the cell, the three option pull-down menu will appear and the *Bounded Normal* distribution type highlighted in blue has been selected.

There are two options to define correlation between elements and both are represented by the lower two input tables of Figure 3.81a. The selection of either table depends on the last column, the "*# of Elems for Reach*" column of the upper table (K-Direct).

If the number of elements per reach is equal to one then the *Correlation of Reaches* button (the left lower table of Figure 3.81a) can be used to enter correlation coefficient values for any pairs of elements have contain one element per reach.

If the number of elements per reach is greater than one, then the *Spatial Correlation of Elems* button (the right lower table of Figure 3.81a) can be used to enter correlation coefficient values. There is the option of entering the correlation coefficient between each element by hand or the use an automatic procedure to enter these values.

There is the possibility that both tables will be populated, especially when some reaches will have one element while some will have more than one element. Figure 3.81c shows the correlation coefficient values between pairs of elements on both tables.

In the automatic procedure that calculates the correlation coefficient between two elements (lower right table of Figure 3.81c), the Correlation Distance is first entered (default is 20). The *Spatial Correlation of Elems* button must then be selected and a triangular function will be used to calculate the correlation coefficient between two elements. The Spatial Correlation, ρ, between elements within a rock joint is determined by the triangular function

$$\rho = 0.0, \quad abs\left[x'_{ele} - x'\right] \geq SP_{len} \qquad \text{(bis 3.1)}$$

otherwise,

$$\rho = 1.0 - \left[\frac{abs\left(x'_{ele} - x'\right)}{SP_{len}} \right] \quad \text{(bis 3.2)}$$

where

SP_{len} = spatial correlation length
x'_{ele} = local x-coordinate of function at peak (mid-point) along the length of the rock joint reach
x' = local x-coordinate of the mid-point of all other elements within rock joint along the length of the rock joint reach

Equation 3.1 states that if the distance between two elements is larger than the given *Correlation Distance* than there is no correlation between these elements, and the correlation coefficient will be set to zero. Otherwise, Equation 3.2 will be used to determine the values populated in the table.

The *Accept* button of Figure 3.81a will save any additions and modifications and then exit.

The *Cancel* button of Figure 3.81a will not save any edits and only exit out of this window.

4 Fluid Flow Along Rock Joints

4.1 Introduction

Fluid flow along rock joints can be characterized as laminar flow between a pair of flat parallel plates so long as the fluid velocity satisfies the range in validity of Darcy's law, which is expressed by using the Reynolds number criterion (refer to Chapter 1). The physical separation distance of the "walls" of a rock joint are described in terms of its mechanical aperture, *E*. Table 1.1 (refer to Chapter 1) provides general guidelines regarding the magnitude of the "size" of a rock joint opening and its associated opening "class" (i.e., very tight, tight, partially open, open, moderately wide, and wide). Rock joints with "small" apertures contribute to "lower" flow velocities which cause the smooth and steady fluid flow known as laminar flow. Besides establishing the distribution of flow, the distribution of joint dimension along a joint reach, specifically joint aperture, also influence the corresponding uplift pressures as will be shown using three examples discussed in section 4.2. Networks of various-levels of rock joint reaches are also examined in section 4.3 to establish their influence on the distributions of uplift pressures.

4.2 Fluid flow along a single reach rock joint with three different tapered rock joints

Laminar flow through a single permeable joint within a rock foundation is considered in this subsection, along with the effect a tapered aperture (i.e. a constant change in taper with distance along the rock joint) has on the distribution of permeability and uplift pressures. The following introductory discussion summarizes background material contained in Ebeling et al. (1997) and in Murphy et al. (2002).

Laminar flow occurs when fluid flows between two smooth parallel plates separated by a constant distance. This distance is the joint opening or conductive aperture, *e*. The flow rate per unit width of joint, *Q*, is given by

$$Q = \frac{\gamma_w e^2}{12\mu_w} \cdot \left(\frac{\partial h}{\partial l}\right) \cdot e \qquad \text{(bis 1.14)}$$

where γ_w is the unit weight of water (lb/ft^3), *e* is the conducting aperture (ft), μ_w is the dynamic viscosity (lb-s/ft^2), and the term within the

parenthesis (the ratio of the change in total head to length of joint), is the hydraulic gradient (ft/ft). The above equation is known as the cubic law and is described in section 1.3.1. By analogy, the relationship of hydraulic conductivity to flow rate in an open joint was established with Darcy's law; therefore, the equation for a single joint can be rewritten (Ebeling and Pace, 1996a)

$$Q = K_{RJ} \cdot (i) \cdot A_{flow} \quad \text{(bis 1.15)}$$

where K_{RJ} is the hydraulic conductivity of a single rock joint, i is the hydraulic gradient, and A_{flow},

$$A_{flow} = e \quad \text{(bis 1.16)}$$

The area of flow at any point along the single joint is equal to the conductive aperture, e times unit width into the cross-section for this two-dimensional joint flow model. The joint hydraulic conductivity K_{RJ} can be expressed as (Ebeling and Pace, 1996b)

$$K_{RJ} = \left(\frac{\gamma_w}{12 \cdot \mu_w} \right) \cdot e^2 \quad \text{(bis 1.17)}$$

where e is the conducting aperture in units of length.

While the hydraulic conductivity, K_{RJ}, is the quantifiable ability of a medium to transmit a fluid under a pressure gradient, the permeability, k, is the ability of soil or rock to transmit fluid under a hydraulic gradient. Hydraulic conductivity considers the properties of both fluid and medium transmitting the fluid (i.e., the rock joint) and has units of length per time (length L/time T), where "true" permeability does not consider the properties of the fluid and has units of length squared (L^2). As a side note, the hydraulic conductivity, K_{RJ} is related to the permeability, k

$$K_{RJ} = k \left(\frac{\gamma_w}{\mu_w} \right) \quad (4.1)$$

Equation 1.17 is derived from the permeability equation $k = C(d^2)$, where d is the pore size medium and C is a dimensionless shape factor (Freeze and Cherry, 1979; Davis and DeWiest, 1966). From this basic relationship, Snow (1968) showed that for a single planar joint of conducting aperture e,

the permeability can be defined as $k = e^2/12$ (see Murphy et al. 2002, for an explanation of Snow's equation). Substituting Snow's equation for k into Equation 4.1 yields Equation 1.17. It is important to recognize that hydraulic conductivity, K_{RJ}, of Equation 1.17 is the basic parameter specified in Joint_FLOW seepage analyses and not the permeability, k.

Equations 1.15 and 1.17 can be used to compute steady state flow and distribution of uplift pressures from known values of γ_w, μ_w, the heads at the joints, and the variation in aperture e with distance along the joint.

Laminar flow conditions may be predicted by examining the Reynolds number, Re, given by

$$R_e = \frac{2Q}{\upsilon_w} \tag{4.2}$$

Equation 4.2 is analogous to Equation 1.13 where the flow rate, Q, is equal to the Darcian velocity times the conductive aperture (v^*e), with υ_w, the kinematic viscosity of water, given by

$$\upsilon_w = g\frac{\mu_w}{\gamma_w} \tag{4.3}$$

with g the gravitational constant, μ_w, the dynamic viscosity of water and, γ_w, the unit weight of water. In our examples, the dynamic viscosity of water, υ_w, at 51.76 degrees Fahrenheit has been determined to be 2.654880e-05 lb-s/ft2 (US customary units) or 1.270667e-03 N-s/m2 (SI units), with the kinematic viscosity, υ_w, calculated from Equation 4.3 as 1.368880e-05 ft2/s (US customary units) or 1.271236e-06 m2/s (SI units).

The Barton et al.1985 inter-relationship between the conducting aperture, the mechanical aperture and joint roughness shows that the roughness of the joint walls and the magnitude of the measured joint opening (expressed as the mechanical aperture) control the "smoothness" of flow through the joint.

$$e = \frac{(JRC^{2.5})}{\left(\frac{E}{e}\right)^2} \tag{bis 1.19}$$

or

$$e = \frac{E^2}{JRC^{2.5}} \tag{4.4}$$

where e is the conducting aperture, E is the mechanical aperture and JRC is the joint roughness coefficient of Barton (1973). Equations 1.19 and 4.4 are valid for SI units and only for values of $E \geq e$ and within a range of aperture of 1 to 1,000 μm (Ebeling et al. 1997). Observe by Equation 4.4 that the higher the roughness of the rock joint and/or the higher magnitude of the mechanical aperture, the higher the conducting aperture of the rock joint. Values of JRC range from 0 for smooth joints to 20 for rough joints with many asperities. Citing Barton et al. (1985), Ebeling et al. (1997) state that 15 is a typical upper value for JRC. For a given mechanical aperture and JRC, the conducting aperture and flow can be determined from Equations 4.4 and 1.19 respectively.

In the special case of a tapered joint, there is a linear variation in aperture with distance x along the rock joint. The equation for the conducting aperture e is given as,

$$e(x) = \left(\frac{e_{out} - e_{in}}{L}\right)x + e_{in} \tag{4.5}$$

and from Equation 1.17, the hydraulic conductivity, K_{RJ}, can now be defined at any point x, varying in proportion to the square of e

$$K_{RJ}(x) = \left(\frac{\gamma_w}{12\mu_w}\right) \ [e(x)]^2 \tag{4.6}$$

In a two-dimensional analysis, the area of flow per unit width, A_{flow}, at any point x, along the joint can be defined as

$$A_{flow} = e(x) \tag{4.7}$$

Ebeling et al. 1997 showed that given head boundary conditions on either side of the rock joint with flow values of $Q_{in} = Q_{out} = Q(x)$, as shown in Figure 4.1, the following closed form equations (Equations 4.8 through 4.10) can be obtained when Equations 4.5 thru 4.7 are introduced into Equation 1.14

$$Q = 2\left(\frac{\gamma_w}{12\gamma_w}\right) e_{in}^{\ 2} \cdot \left(\frac{h_{in} - h_{out}}{L}\right) \cdot \left(\frac{e_{out}^{\ 2}}{e_{out} + e_{in}}\right) \tag{4.8}$$

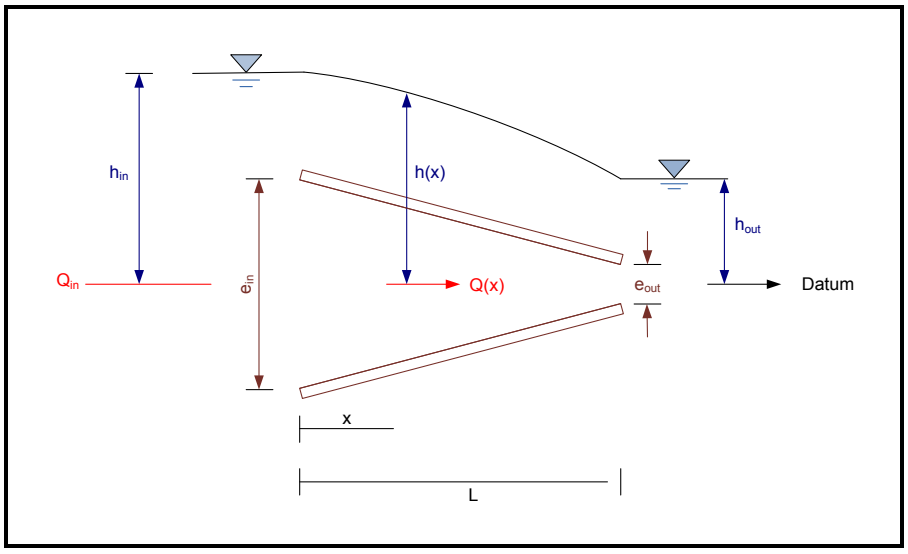

Figure 4.1. Variation of head along a tapered joint.

with the total head, h, at any point x, varying along the rock joint

$$h(x) = h_{in} - \left\{\left(\frac{h_{in} - h_{out}}{L}\right) \cdot \left(\frac{e_{out}^{\ 2}}{e_{out} + e_{in}}\right) \cdot \left[\frac{mx^2 + 2xe_{in}}{(mx + e_{in})^2}\right]\right\} \tag{4.9}$$

with

$$m = \frac{e_{out} - e_{in}}{L} \tag{4.10}$$

Equation 4.9 shows that the variation in head along a tapered joint is defined by the reservoir head, the tailwater head, the length of the joint, and the conducting apertures at both ends of the rock joint.

According to the Bernoulli equation for ideal flows, i.e. steady, frictionless, incompressible flows, the total head, H, at any point can be determined by taking the sum of the pressure head, h_p, the velocity head, h_v, and the elevation head, h_z

$$H = h_p + h_v + h_z \tag{bis 1.3}$$

where the pressure head is defined as the ratio of the water pressure to the unit weight of water ($h_p = u/\gamma_w$), the velocity head is the ratio of velocity squared to twice the gravitational constant ($h_v = V^2/2g$), and the elevation head is the elevation with respect to the datum ($h_z = z$). The total head can therefore be represented as

$$H = \frac{u}{\gamma_w} + \frac{V^2}{2g} + z = \text{constant} \quad \text{(bis 1.4)}$$

As previously mentioned, lamina flow occur at very low velocities along rock joints; the velocity head, in this case is negligible, with the total head

$$H = h_p + h_z \quad \text{(bis 1.5)}$$

In our applications, we apply the simplified hydrostatic Bernoulli's equation, Equation 1.5, in order to determine the pressure head, $h_p = H - h_z$, and consequently water pressure at a specified point within a rock joint

$$u = \gamma_w (H - h_z) \quad \text{(bis 1.6)}$$

In this report, water pressure, u, at a point within a rock joint is sometimes referred to as uplift pressure.

Consider the case of a single horizontal rock joint located below the base of a concrete monolith for the case of a 150 ft pool and 0.0 ft tailwater. Figure 4.2 shows the hypothetical dam to be 300 ft high and 235 ft wide. It was assumed that jointing within the rock foundation was simplistic, i.e., a single rock joint parallel to and immediately below the dam-to-foundation interface. This rock joint is made up of 20 elements with constant conducting aperture of 100 microns (1 ft = 0.305 m). Assume a datum at el 0. Since the single rock joint is located at an elevation of 0.0 ft, the elevation head, h_z, will be zero and the total head, H, equal to the pressure head, h_p. Equation 1.5 is further simplified

$$H = h_p \quad \text{(bis 1.7)}$$

and the water pressure, u, simplified to

$$u = \gamma_w \cdot h_p \quad \text{(bis 1.8)}$$

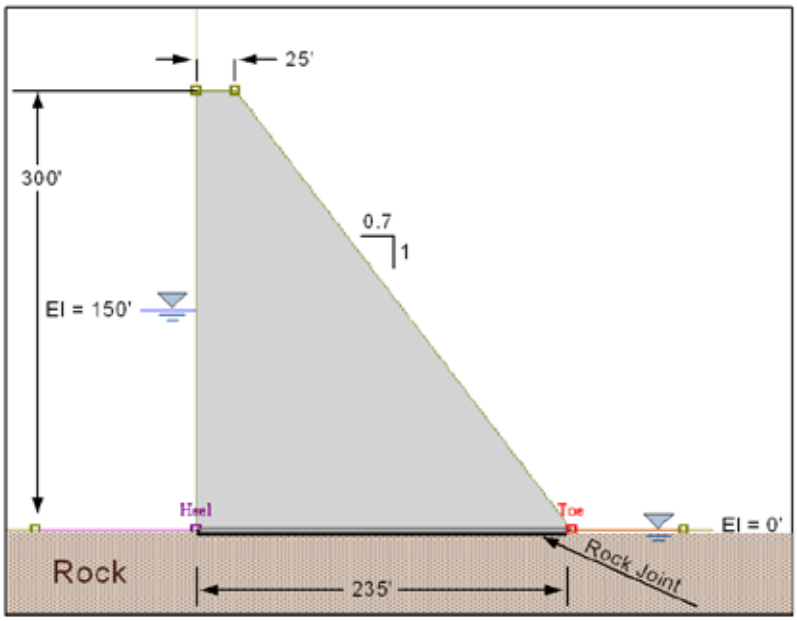

Figure 4.2. Geometry of dam used in three example problems.

Three example problems will demonstrate the computation of uplift pressure along a single rock joint reach for the three cases of varying apertures; for uniform joint aperture ($e_{in} = e_{out}$); for a joint aperture with a taper downstream ($e_{in} > e_{out}$); and for a joint aperture with a taper upstream ($e_{in} < e_{out}$). By assigning the datum to be the center line of the horizontal rock joint (Figure 4.2), the uplift pressure at any point is equal to the total head at the point times the unit weight of water (with elevation head equal to zero and velocity head negligible). These analyses will demonstrate the influence that rock joint aperture has on the distribution of uplift pressures and on the magnitude and point of application of the resultant uplift pressure force acting upwards normal to the dam.

4.2.1 Problem 4: Fluid flow along a uniform rock joint; a single horizontal reach joint at the dam-to-foundation interface

A deterministic analysis of the provided dam geometry from Figure 4.2 was conducted for a Joint_FLOW only analysis with a uniform conductive aperture (5.904×10^{-3} in.) for the single rock joint (Figure 4.3). This uniform rock joint with constant conducting aperture of 100 microns is characterized as a "tight" joint according to Table 1.1.

The resultant water pressures approximated at each of the 20 elements is shown in Figure 4.4. This figure shows the decrease in water pressures at the 21 nodes along the rock joint.

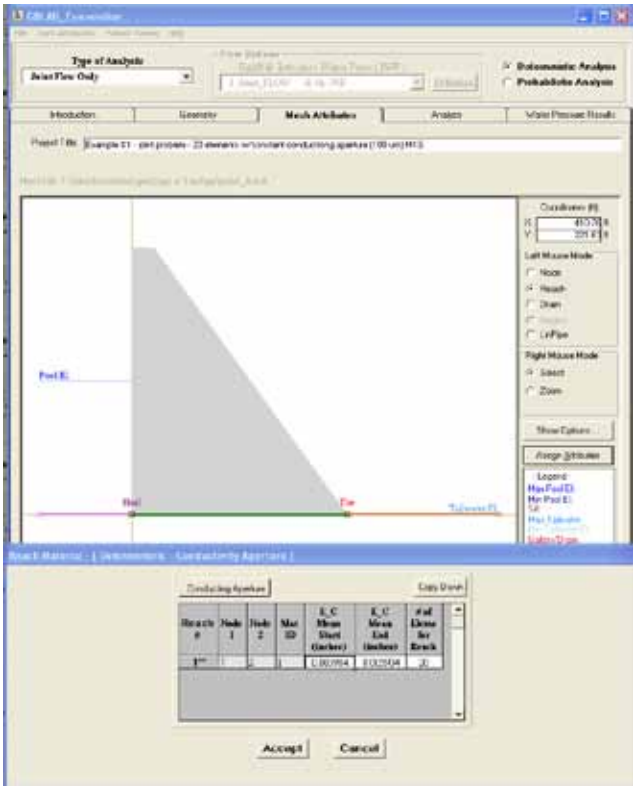

Figure 4.3. Geometry of dam with a single horizontal rock joint of twenty elements with uniform conductive aperture.

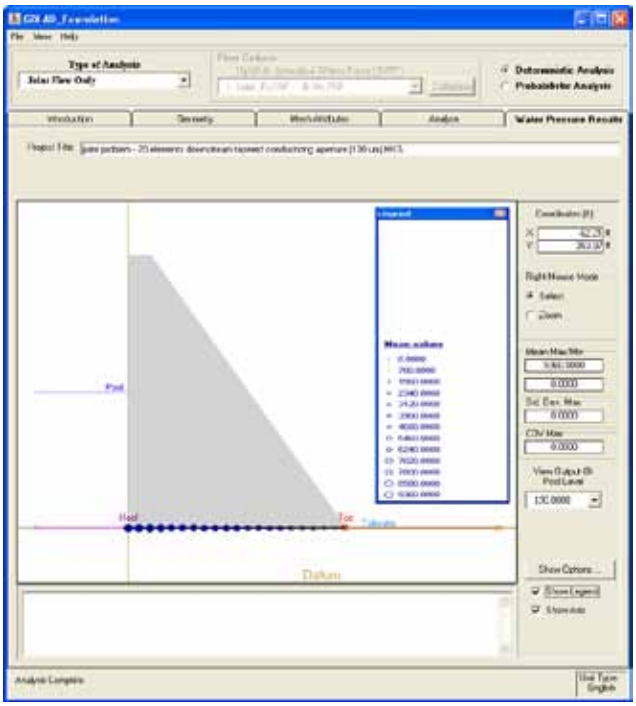

Figure 4.4. Water pressures at specific locations along a single horizontal rock joint of 20 elements with uniform conductive aperture.

Joint_FLOW computational results were compared with calculated values for the flow rate, Q, (Equation 4.8), the total head, H, (Equation 4.9), the hydraulic conductivity, K_{RJ}, (Equation 4.6), and Reynolds number, Re, (Equation 4.2) with identical results. Since the velocities calculated were found to be low at 0.030 ft/sec, the velocity head was considered negligible and Equation 1.8 was used to calculate water pressures.

The variation in total head and uplift pressure along the single rock joint is further illustrated in the scatter plot of Figure 4.5. This figure shows the uplift pressures varying linearly along the uniform rock joint. Since the total head is approximately equal to the pressure head (Equation 1.7), the uplift pressure by Equation 1.8 differs from the total head by a constant, i.e. the unit weight of water. This is shown in Figure 4.5, with the total head and uplift pressure displayed on opposite vertical axes with values superimposed over each other.

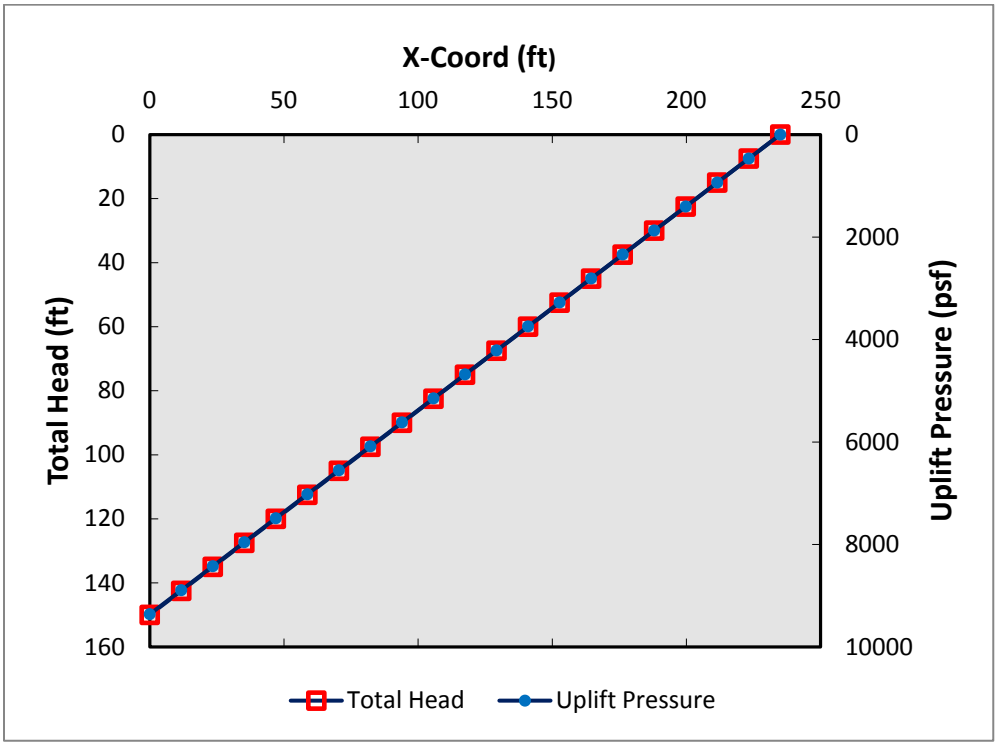

Figure 4.5. Variation in total head and uplift pressure along a uniform, horizontal rock joint.

Values for the resultant uplift force, the moments about the toe and heel, and the distance from the toe and heel, X_{Toe} and (L - X_{Toe}), at which the resultant uplift force is applied at, are recorded in Table 4.1. Three sources of data are used to validate the results. The first source is described by

(*Source ID*=1.1) integrating previously defined equations and (*Source ID*=1.2) from applying a triangular uplift distribution (first two rows of Table 4.1). The second source (*Source ID*=2 of Table 4.1) provides calculated values at the nodes and the third source (*Source ID*=3 of Table 4.1) show where the uplift pressures and resultant forces are calculated at the point of action measured from the right-hand end point of reach respectively. From observations of Table 4.1, all values have been validated with (L - X_{Toe}) equal to difference between the length of the rock joint and X_{Toe}.

Table 4.1. Uniform aperture.

Source ID	Source of data	Resultant Uplift Force (kips)	Moment		L - X_{Toe} (ft)	X_{Toe} (ft)
			About Heel (kip-ft)	About Toe (kip-ft)		
1.1	Uplift water pressure by Equations 4.9, 1.7, and 1.8	1,099.8	86,151		78.33	
1.2	Uplift water pressure and resultant force (using triangular uplift distribution)	1,099.8	86,151		78.33	
2	Joint_FLOW results of calculated water pressures at 21 nodes.	1,099.8		172,302		156.67
3	Joint_FLOW resultant uplift water pressure force for each of the 20 reaches (i.e. elements and its point of action measured from the right-hand end point of reach.	1,099.8		172,302		156.67

4.2.2 Problem 5: Fluid flow along a tapered downstream rock joint; a single reach, horizontal joint at the dam-to-foundation interface tapered in the direction of flow

A deterministic analysis of the provided dam geometry from Figure 4.2 was conducted for a Joint_FLOW only analysis with a tapered downstream conductive aperture (upstream at 5.904×10^{-3} in. and downstream at 2.952×10^{-3} in.) for the single rock joint of Figure 4.6. The resultant water pressures approximated at each of the 20 elements is shown in Figure 4.7. This figure shows a decrease in water pressures at the 21 nodes along the rock joint as the distance from the heel is increased. Joint_FLOW computational results were compared with calculated values for the flow rate, Q,

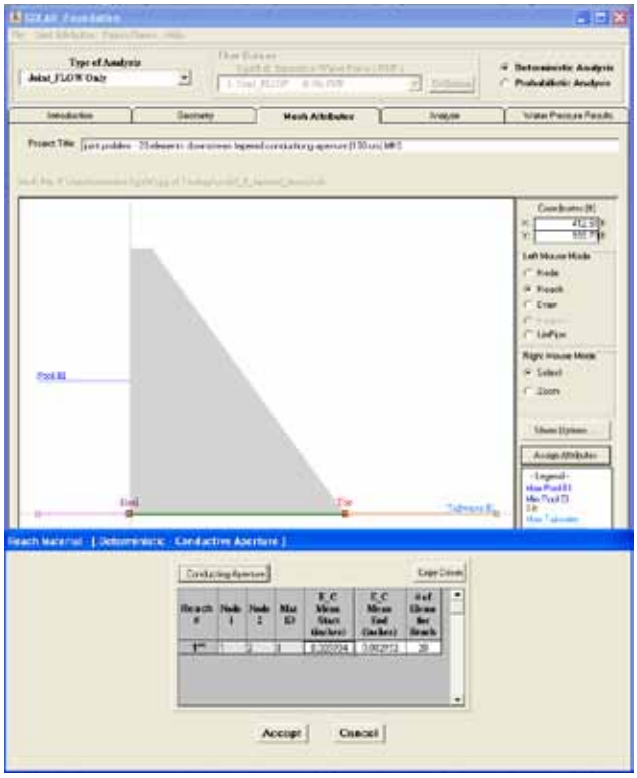

Figure 4.6. Geometry of dam with a single horizontal rock joint of twenty elements with tapered downstream conductive aperture; $e_{in} = z \cdot e_{out}$.

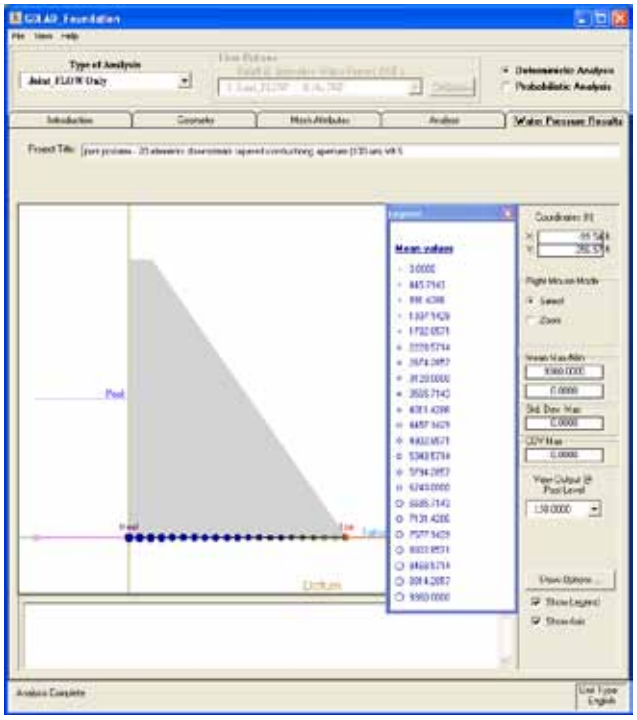

Figure 4.7. Water pressures at specific locations along a single horizontal rock joint of 20 elements with tapered downstream conductive aperture.

(Equation 4.8), the total head, H, (Equation 4.9), the hydraulic conductivity, K_{RJ}, (Equation 4.6), and Reynolds number, R_e, (Equation 4.2) with percent differences of less than 0.08. Since the velocities calculated were found to be low, maximum value at 0.020 ft/sec, the velocity head was considered negligible and Equation 1.8 was used to calculate water pressures.

The variation in total head and uplift pressure along the single rock joint is further illustrated in the scatter plot of Figure 4.8. This figure shows the exponential decline of the uplift pressures along the tapered downstream rock joint. Since the total head is approximately equal to the pressure head (Equation 1.7), the uplift pressure by Equation 1.8 differs from the total head by a constant, i.e. the unit weight of water. This is shown in Figure 4.8, with the total head and uplift pressure displayed on opposite vertical axes with values superimposed over each other.

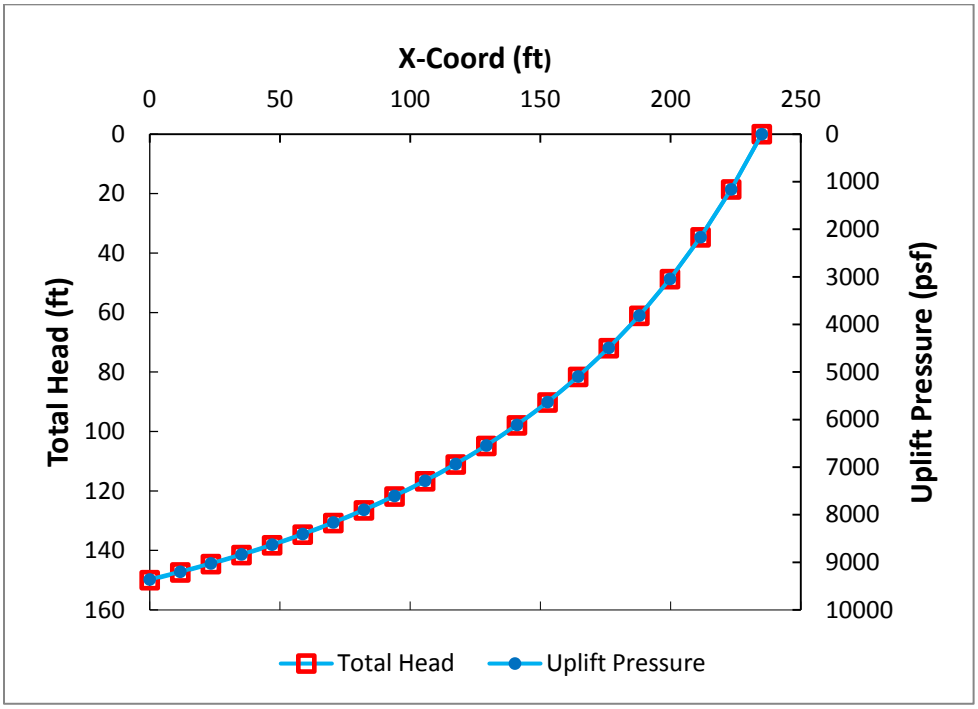

Figure 4.8. Variation in total head and uplift pressure along a tapered downstream, horizontal rock joint; $e_{in} = z \cdot e_{out}$.

Values for the resultant uplift force, the moments for the resultant uplift force about the toe and heel, and the distance from the toe and heel, X_{Toe} and (L - X_{Toe}), at which the resultant uplift force is applied at, are recorded in Table 4.2. Three sources of data are used to validate these results. The first source is described by integrating previously defined equations (*Source ID*=1 of Table 4.2). The second source (*Source ID*=2 of Table 4.2) provides calculated resultant uplift force values calculated for each joint

Table 4.2. Tapered downstream aperture; $e_{in} = z \cdot e_{out}$.

Source ID	Source of data	Resultant Uplift Force (kips)	Moment		$L - X_{Toe}$ (ft)	X_{Toe} (ft)
			About Heel (kip-ft)	About Toe (kip-ft)		
1	Uplift water pressure by Equations 4.9, 1.7, and 1.8	1,466.4	-137,131.72		93.52	141.48
2	Joint_FLOW results of calculated water pressures at 21 nodes.	1,465.33		211,413.52		144.28
3	Joint_FLOW resultant uplift water pressure force for each of the 20 reaches (i.e. elements and its point of action measured from the right-hand end point of reach.	1,465.33		211,413.67		144.28

element at the nodes and the third source (*Source ID*=3 of Table 4.2) show that the uplift pressures and resultant forces are calculated at the point of action measured from the right-hand end point of each reach respectively. From observations of Table 4.2, the resultant uplift force calculated from sources two and three have a 0.01 percent difference and source one differs by 0.08 percent.

The calculated moment about the heel in Table 4.2 for source one is negative which suggests that the calculated x-location of the uplift force is at the negative x-axis; taking the absolute value of the distance from the x-location to the origin, puts this distance in the positive x-axis. The distance from the toe is calculated by taking the difference between the rock joint length and the previously calculated distance (= X_{Toe}). Sources two and three give approximately equal moments about the toe with equivalent distances as measured from the toe.

From the discussed observations regarding Table 4.2, values of resultant uplift force and X_{Toe} have been validated. Consequently, the value for (L - X_{Toe}), equal to difference between the length of the rock joint and X_{Toe}, has also been validated.

4.2.3 Problem 6: Fluid flow along a tapered upstream rock joints; a single reach, horizontal joint at the dam-to-foundation interface tapered in the direction opposite to flow

A deterministic analysis of the provided dam geometry from Figure 4.9 was conducted for a Joint_FLOW only analysis with a tapered upstream

conductive aperture (upstream at 2.952 x10-3 in. and downstream at 5.904 x 10-3 in.) for the single rock joint of Figure 4.9. The resultant water pressures approximated at each of the 20 elements is shown in Figure 4.10. This figure shows a decrease in water pressures at the 21 nodes along the rock joint as the distance from the heel is increased. Joint_FLOW computational results were compared with calculated values for the flow rate, Q, (Equation 4.8), the total head, H, (Equation 4.9), the hydraulic conductivity, K_{RJ}, (Equation 4.6), and Reynolds number, R_e, (Equation 4.2) with percent differences of less than 0.08. Since the velocities calculated were found to be low, maximum value at 0.020 ft/sec, the velocity head was considered negligible and Equation 1.8 was used to calculate water pressures.

The variation in total head and uplift pressure along the single rock joint is further illustrated in the scatter plot of Figure 4.11. This figure shows the exponential decline of the uplift pressures along the tapered upstream rock joint. Since the total head is approximately equal to the pressure head (Equation 1.7), the uplift pressure by Equation 1.8 differs from the total head by a constant, i.e. the unit weight of water. This is shown in Figure 4.11, with the total head and uplift pressure displayed on opposite vertical axes with values superimposed over each other.

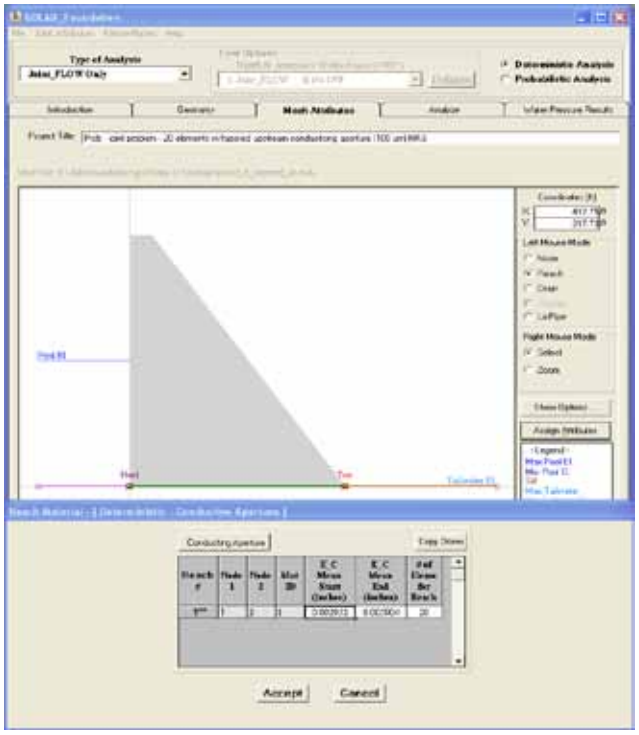

Figure 4.9. Geometry of dam with a single horizontal rock joint of twenty elements with tapered upstream conductive aperture; $z \cdot e_{in} = e_{out}$.

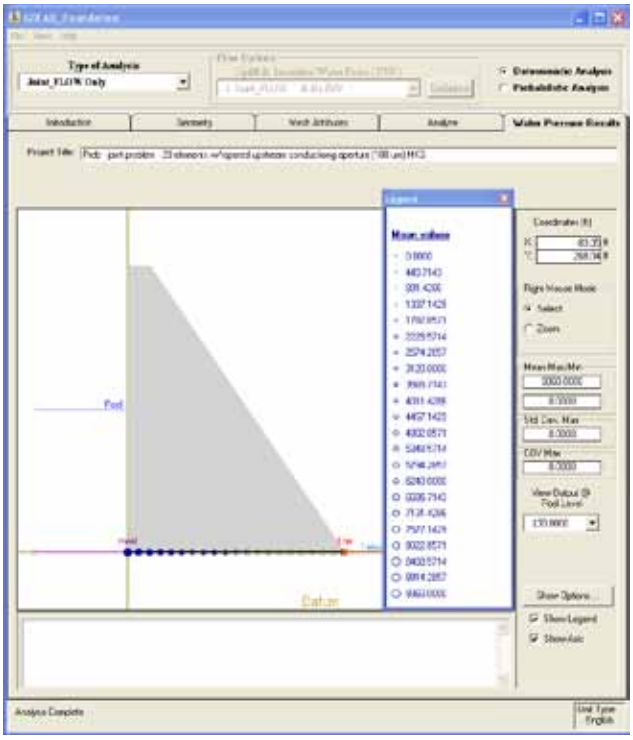

Figure 4.10. Water pressures at specific locations along a single horizontal rock joint of 20 elements with tapered upstream conductive aperture.

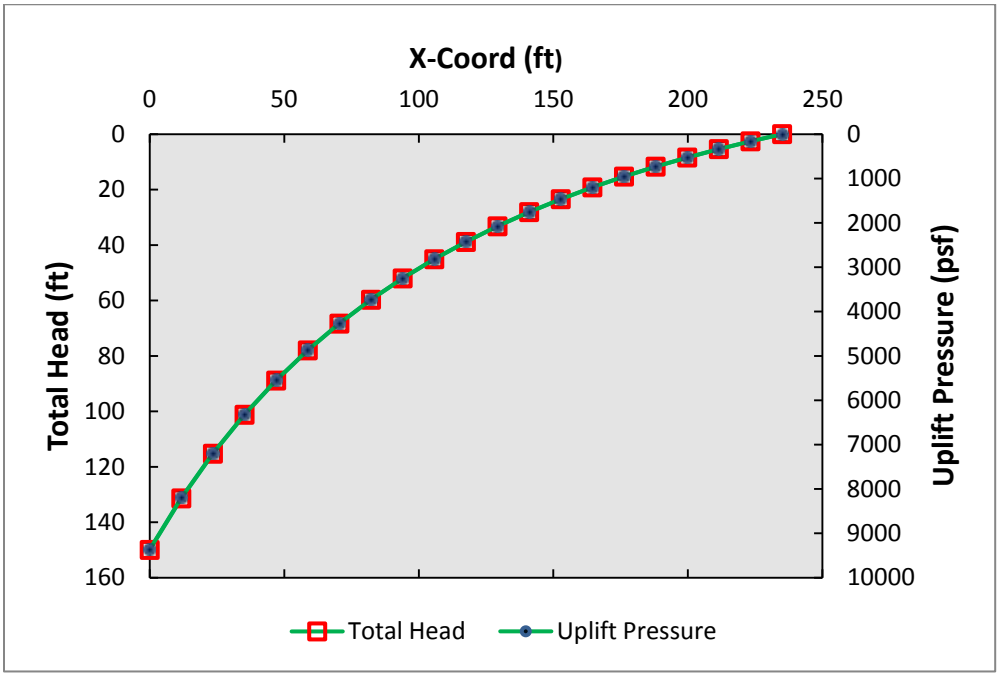

Figure 4.11. Variation in total head and uplift pressure along a tapered upstream horizontal rock joint; $z \cdot e_{in} = e_{out}$.

Values for the resultant uplift force, the moments of the resultant uplift force about the toe and heel, and the distance from the toe and heel, X_{Toe} and (L - X_{Toe}), at which the resultant uplift force is applied at, are recorded in Table 4.3. Three sources of data are used to validate these results. The first source is described by integrating previously defined equations (*Source ID*=1 of Table 4.3). The second source (*Source ID*=2 of Table 4.3) provides

Table 4.3. Tapered upstream aperture; $z \cdot e_{in} = e_{out}$.

Source ID	Source of data	Resultant Uplift Force (kips)	Moment		$L - X_{Toe}$ (ft)	X_{Toe} (ft)
			About Heel (kip-ft)	About Toe (kip-ft)		
1	Uplift water pressure by Equations 4.9, 1.7, and 1.8	733.20	-223,282.72		69.53	165.47
2	Joint_FLOW results of calculated water pressures at 21 nodes.	734.27		125,513.66		170.94
3	Joint_FLOW resultant uplift water pressure force for each of the 20 reaches (i.e. elements and its point of action measured from the right-hand end point of reach.	734.27		125,513.58		170.94

calculated values at the nodes and the third source (*Source ID*=3 of Table 4.3) show that the uplift pressures and resultant forces are calculated at the point of action measured from the right-hand end point of reach respectively. From observations of Table 4.3, the resultant uplift force calculated from sources two and three have a 0.02 percent difference and source one differs by 0.17 percent.

The calculated moment about the heel in Table 4.3 for source one is negative which suggests that the calculated x-location of the uplift force is at the negative x-axis; taking the absolute value of the distance from the x-location to the origin, puts this distance in the positive x-axis. Since this distance is larger than the length of the rock joint, the length of the joint is subtracted, resulting in the distance measured from the heel that is reported in the table. The distance from the toe is then calculated by taking the difference between the rock joint length and the previously calculated distance (= X_{Toe}). Sources two and three give approximately equal moments about the toe with equivalent distances as measured from the toe, which differ from the *Source ID*=1 value by 3.3 percent. From the discussed observations

regarding Table 4.3, values of resultant uplift force and X_{Toe} have been validated.

4.2.4 Comparison of results for a single reach with three different tapered rock joints

For the specified Dam geometry of Figure 4.2, deterministic analyses were completed for laminar flow along a single horizontal rock joint for three distinctive types of tapered apertures. These analyses were conducted with the assumptions that:

1. a linear water pressure distribution existed between nodes, and
2. the developed mesh is sufficiently refined to substantiate assumption 1.

Comparison of computed against closed form solutions for each of the three Joint_FLOW analyses have substantiated the assumption that 20 elements are sufficient for the Figure 4.2 problem of a 235 ft long horizontal joint of (a) constant (i.e., uniform) conducting aperture, with (b) taper downstream conducting aperture, and with (c) taper upstream conducting aperture.

Joint_FLOW results for the three types of rock joint tapered apertures were collected in a single figure to show the influence of joint taper on uplift pressures and total heads. Figure 4.12 shows the influence of the three spatial distributions in conducting apertures by establishing the resultant total head and uplift pressures with respect to *x*-location within the single rock joint reach, as measured from heel to toe for the Figure 4.2 gravity dam cross-section. This figure shows the uplift pressure and total head relationships with distance to be a function of apertures. This figure is derived by superposition of Figures 4.5, 4.8, and 4.11 results.

Observations:

1. Figure 4.12 shows that a uniform conducting aperture results in a linear variation in uplift pressures along the rock joint and the tapering of rock joint apertures illustrate the nonlinearity of the uplift pressures.
2. A taper downstream reach results in a larger uplift pressure when compared to the uplift pressure of the uniform aperture.
3. A taper upstream reach results in smaller uplift pressure when compared with the uniform aperture.

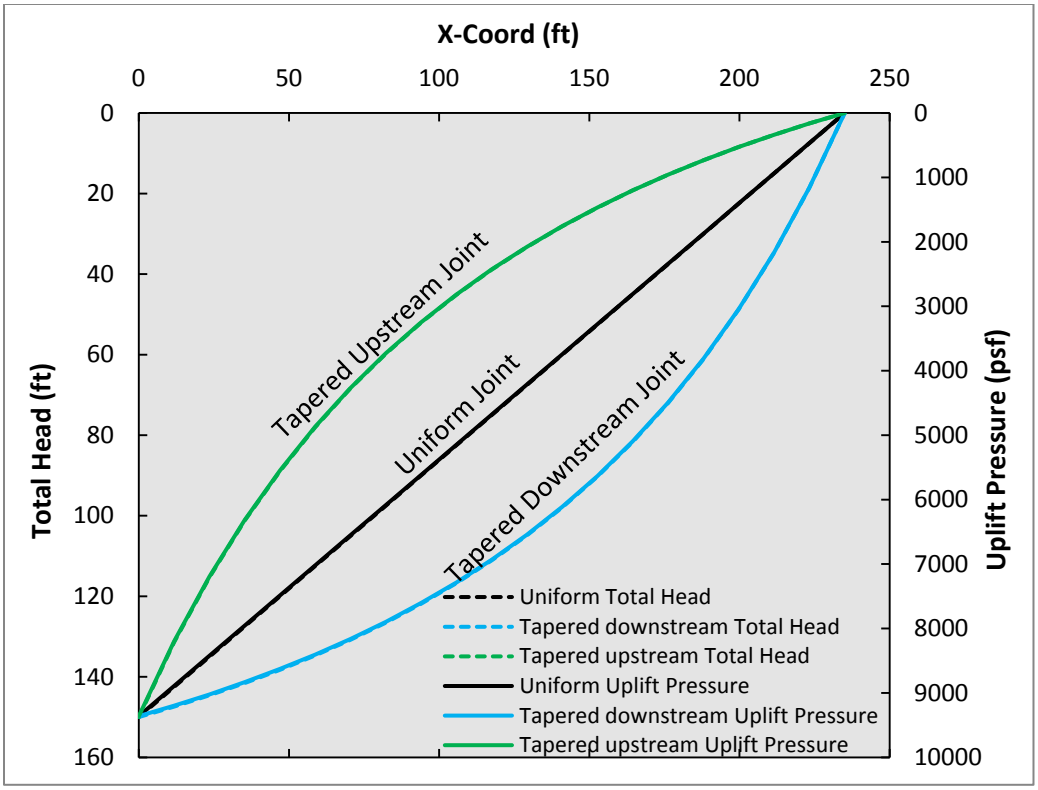

Figure 4.12. Variations in head and uplift pressures along a single reach, horizontal rock joint.

Table 4.4 gives the resultant uplift force and moments of the three types of tapered apertures. This shows that the taper downstream reach results in a higher resultant uplift force (1,465.33 kips) when compared to the uniform aperture (1099.80 kips) and the taper upstream reach results in a lower resultant uplift force (734.27 kips) when compared to the uniform aperture.

Table 4.4. Resultant uplift force and bending moments of variable apertures.

Aperture	Subsection	Resultant Uplift Force (kips)	Moment About Toe (kips)	X_{Toe} (ft)
Uniform	4.2.1	1,099.80	172,302.00	156.67
Taper Downstream (e_{in} = 2 e_{out})	4.2.2	1,465.33	211,413.52	144.28
Taper Upstream (2 e_{in} = e_{out})	4.2.3	734.27	125,513.66	170.94

Observations:

1. Among the three aperture distributions, a taper downstream in conducting joint aperture results in the most unfavorable uplift water pressure

distribution acting normal to the base of the Figure 4.2 gravity dam cross-section. It is viewed unfavorable in terms of Figure 4.12 uplift pressure distribution as well as in terms of Table 4.4 resultant uplift force and in terms of the moment about the toe.

2. Among the three aperture distributions, a taper upstream in conducting joint aperture results in the most favorable uplift water pressure distribution acting normal to the base of the Figure 4.2 gravity dam cross-section. It is viewed favorable in terms of Figure 4.12 uplift pressure distribution as well as in terms of Table 4.4 resultant uplift force and in terms of the moment about the toe.

4.3 Fluid flow along multi-reach rock joints contained within the rock foundation

Laminar flow along multi-reach permeable joints within a rock foundation is examined and the influence a network of connected rock joints can have on the distributions of total head and uplift pressures. Seven network configurations have being considered with the first six cases incorporating the effects of a rock foundation drain and the last without the effects of a drain. These cases are listed as follows:

Case 1: zero-level single-reach network (a continuous sequence of rock joint reaches that are joined together, extending from one water source to another, that form a potential sliding plane),

Case 2: zero-level multi-reach network (two potential sliding planes with no connectivity, i.e. they are physically separated within the foundation),

Case 3: one-level multi-reach network with two-upstream sources (two potential sliding planes, i.e. Case 2, with interconnectivity between the sliding planes),

Case 4: one-level multi-reach network with multi-upstream sources (two potential sliding planes, i.e. Case 2, with interconnectivity between the sliding planes and upstream sources),

Case 5: multi-level network with two-sources (a multi-level multi-reach network with interconnectivity between the rock joint reaches),

Case 6: multi-level network with multi-sources (a multi-level multi-reach network with interconnectivity between the rock joint reaches and upstream sources, see Figure 4.13), and

Case 7: zero-level single-reach network (a potential sliding plane, i.e. Case 1, without a drain).

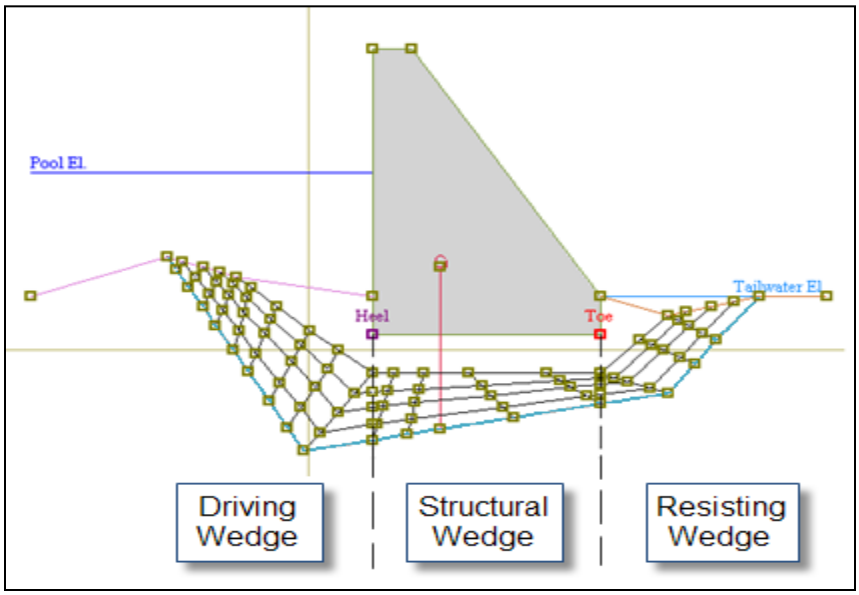

Figure 4.13. Multi-reach network of permeable joints within a rock foundation with one rock foundation drain.

These seven cases of various networks of rock joints beneath a non-overflow gravity dam section embedded in rock are considered. Figure 4.13 represents Case 6 where the hypothetical dam is 347 ft high and 235 ft wide with a 216 ft Pool and 65.6168 ft tailwater. All rock joints have a uniform conducting aperture of 5.904×10^{-3} in. (150 microns) and a rock foundation drain diameter of 5 in. with a drain spacing of 15 ft along the gallery within the gravity dam. These rock joints would be categorized as "tight" joints according to Table 1.1. Parts of the primary upstream-to-downstream joint reach network geometry of Figure 4.13 forms the basis for all joint reach geometry in these seven problems being analyzed in this section using Joint_FLOW. The distributions of total head and uplift water pressures are calculated at the nodes that define the potential sliding plane which is designated by the solid blue line in Figure 4.13. Each rock joint consists of 1 element, and from the blue line in Figure 4.13, there are 10 elements on the upstream side, noted as the Driving Wedge; 4 elements beneath the dam foundation or the structural wedge; and 4 elements at the downstream side or the resisting wedge. This indicates that a total of 18 elements will be used to describe the potential sliding plane. The determination of accuracy in the number of elements used will be discussed later in this section.

Subsection 4.3.1 through 4.3.3 introduces the seven different rock joint networks that were analyzed using Joint_FLOW. Total heads and uplift

water pressures along the same interconnecting reaches are compared in subsection 4.3.4 for these seven analyses of rock foundations with seven different joint network distributions. The selected interconnecting reaches for which the uplift water pressures and total head distributions corresponds to a potential slip plane that an engineer would have investigated if the analysis were extended to the next phase of a stability evaluation.

4.3.1 Problem 7: A single potential sliding plane

A deterministic analysis of the provided dam geometry from Figure 4.13 was conducted for a Joint_FLOW only analysis. Two cases that were introduced in section 4.3 have been selected when considering a single potential sliding plane.

The first case, a zero-level single-reach network, consists of a potential sliding plane with a rock foundation drain. The resultant total heads (nodes in light blue), approximated at each of the joint reaches, is shown in Figure 4.14. This figure shows a steep decrease in head from the pool to the drain at the gallery and then a small gradient from the drain to the tailwater.

Case 7 listed in the introductory section 4.3 is a zero-level single-reach network that consists of a single potential sliding plane within a rock foundation. This geometry is the same as Case 1, except that it has no drain. The resultant total heads (nodes in light blue), approximated at the nodes of each joint reach, is shown in Figure 4.15. This figure shows an almost linear decrease in head from the Pool to the tailwater.

4.3.2 Problem 8: Multiple potential sliding planes

A deterministic analysis of the provided dam geometry from Figure 4.13 was conducted for a Joint_FLOW only analysis. Three cases from section 4.3 have been selected when considering multiple potential sliding planes.

Case 2 listed in the introductory section 4.3 is a zero-level (no connection between potential sliding planes) multi-reach network which consists of two potential sliding planes within the rock foundation and a rock foundation drain. As can be seen in Figure 4.16, there are no reaches connecting the two potential sliding planes except at the drain. The resultant total heads (nodes in light blue), approximated at each joint reach, show a steeper decrease in head from the pool to the drain at the gallery and then a small gradient from the drain to the tailwater.

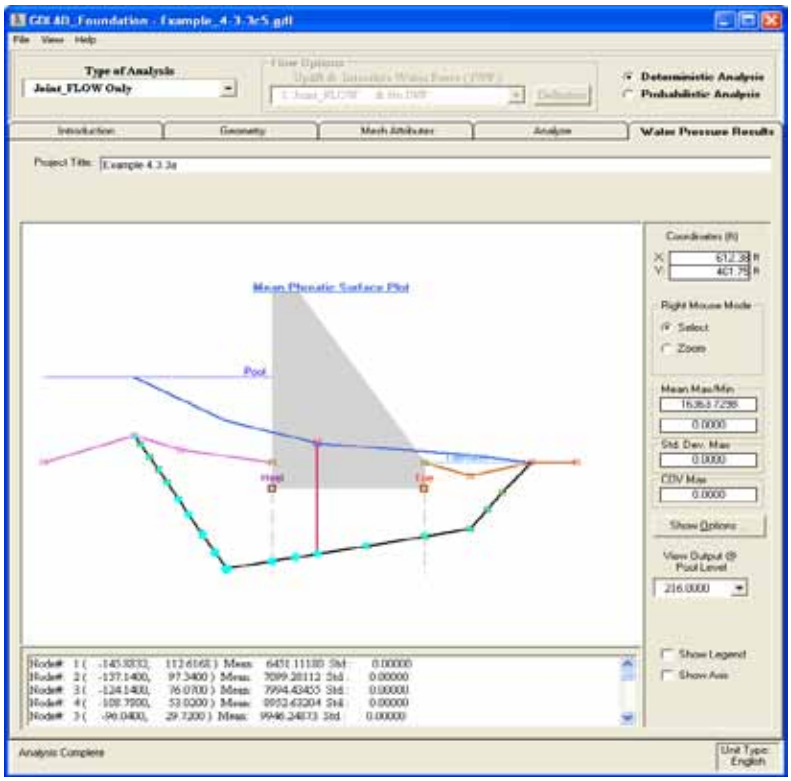

Figure 4.14. Zero-level single-reach network of permeable joints within a rock foundation with one rock foundation drain (Case 1).

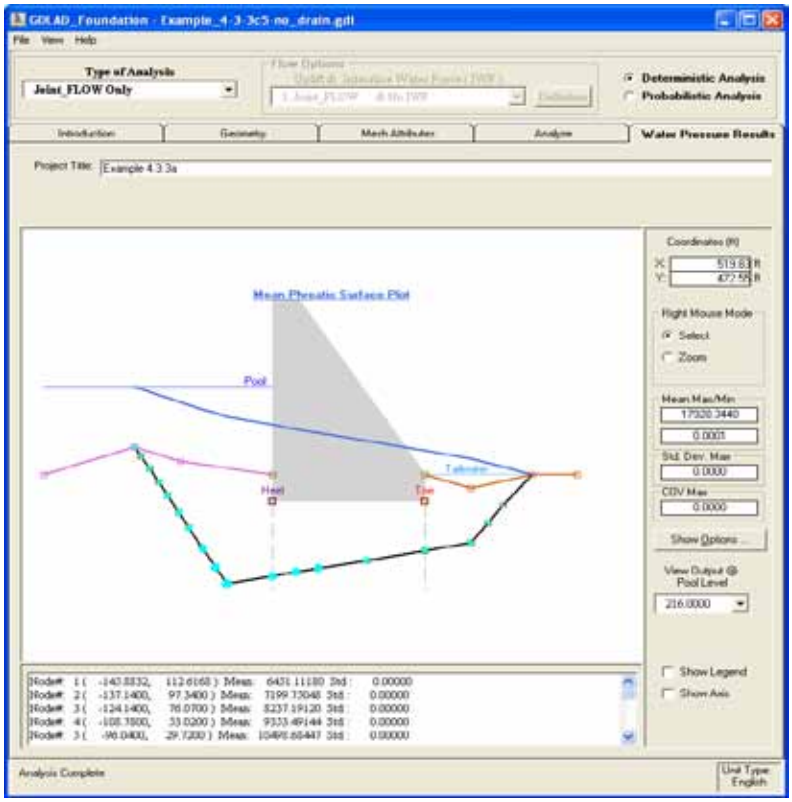

Figure 4.15. Zero-level single-reach network of permeable joints within a rock foundation with no rock foundation drain (Case 7).

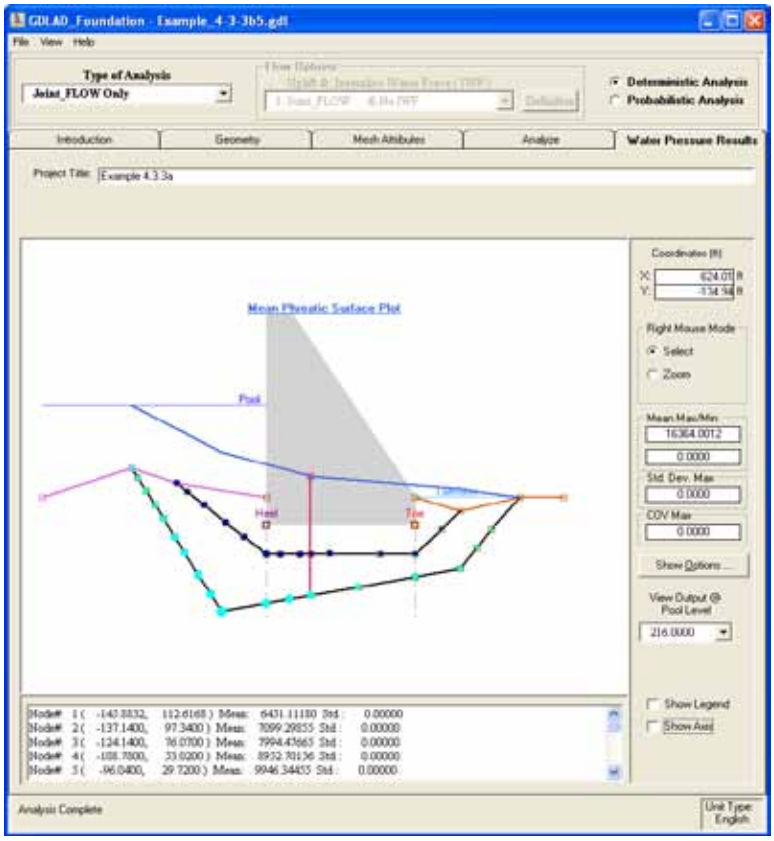

Figure 4.16. Zero-level multi-reach network of permeable joints within a rock foundation with one rock foundation drain (Case 2).

Case 3 listed in the introductory section 4.3 is a one-level multi-reach network with two sources (two upstream head boundary condition values) which consists of two potential sliding planes within the rock foundation with interconnectivity between the two potential sliding planes and a rock foundation drain. As can be seen in Figure 4.17, there are reaches connecting the two potential sliding planes and at the drain. The resultant total heads (nodes in light blue), approximated at each of the joint reaches, show the decrease in head from the pool to the drain at the gallery and then a small gradient from the drain to the tailwater.

Case 4 listed in the introductory section 4.3 is a one-level multi-reach network with multi-sources (multiple upstream head boundary condition values) and a rock foundation drain that consists of multiple potential sliding planes within a rock foundation. As can be seen in Figure 4.18, there are reaches connecting the two potential sliding planes and at the drain. The resultant total heads (nodes in light blue), approximated at each of the joint reaches, show a steep decrease in head from the pool to the drain at the gallery and then a small gradient from the drain to the tailwater.

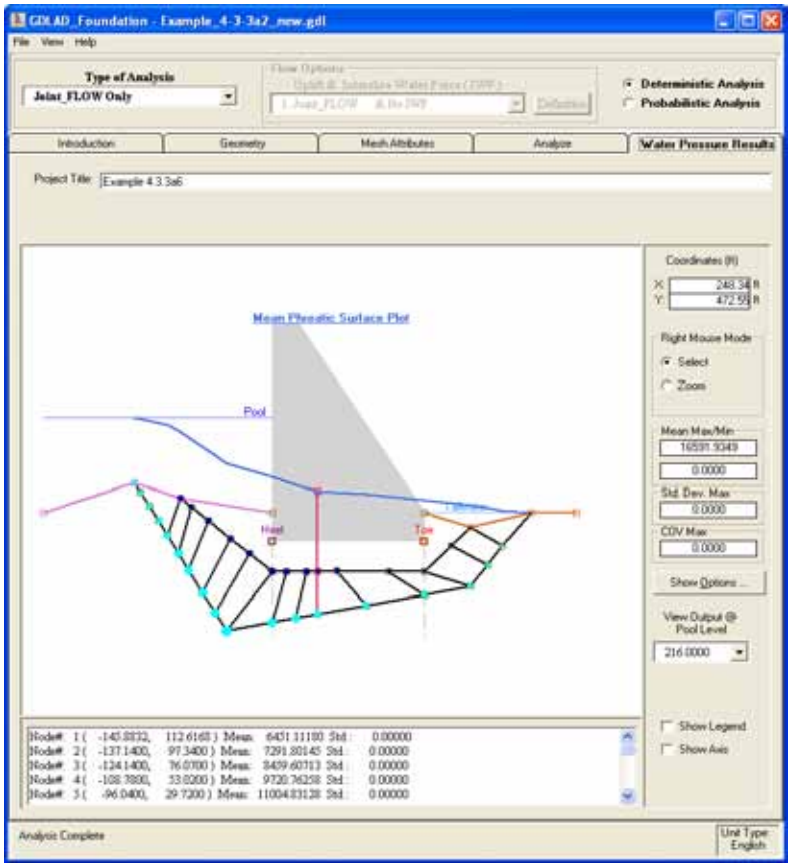

Figure 4.17. One-level multi-reach network with two upstream sources of permeable joints within a rock foundation with one rock foundation drain (Case 3).

4.3.3 Problem 9: Network of inter-connected rock joints with multiple potential sliding planes

A deterministic analysis of the provided dam geometry from Figure 4.13 was conducted for a Joint_FLOW only analysis. Two cases from introductory section 4.3 have been selected when considering multiple potential sliding planes.

Case 5 listed in the introductory section 4.3 is a multi-level multi-reach network with two sources (two upstream head boundary condition values) which consists of many potential sliding planes within the rock foundation with interconnectivity between the potential sliding planes and a rock foundation drain. As can be seen in Figure 4.19, there are reaches connecting all potential sliding planes and at the drain. The resultant total heads (nodes in light blue), approximated at each of the joint reaches, show the decrease in head from the pool to the drain at the gallery and then a small gradient from the drain to the tailwater.

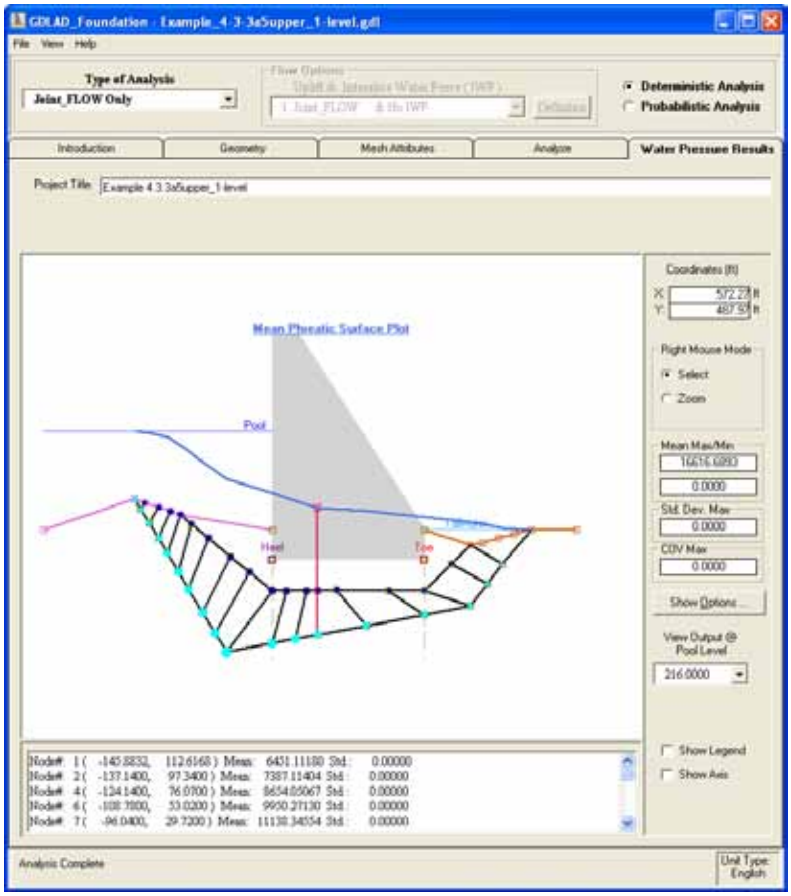

Figure 4.18. One-level multi-reach network with multi-upstream sources of permeable joints within a rock foundation with one rock foundation drain (Case 4).

Case 6 listed in the introductory section 4.3 is a multi-level multi-reach network with multi-sources (five upstream head boundary condition values) which consists of numerous potential sliding planes within the rock foundation with interconnectivity between all potential sliding planes and a rock foundation drain. As can be seen in Figure 4.20, there are reaches connecting all potential sliding planes and at the drain. The

resultant total heads at a potential sliding plane (nodes in light blue), approximated at each of the joint reaches, show a decrease in head from the pool to the drain at the gallery and then a small gradient from the drain to the tailwater.

4.3.4 Discussion of results for multiple-reach rock joints with multiple potential sliding planes

For the specified dam geometry of Figure 4.13, Joint_FLOW only, deterministic analyses were completed for laminar flow along rock joint

networks for the six joint network configurations containing the potential sliding plane(s) within a rock foundation containing a rock foundation drain and of the seventh case without a drain. These analyses were conducted with the assumptions that (1) there is a linear water pressure distribution existing between nodes, and (2) the developed mesh is sufficiently refined to substantiate the assumption above.

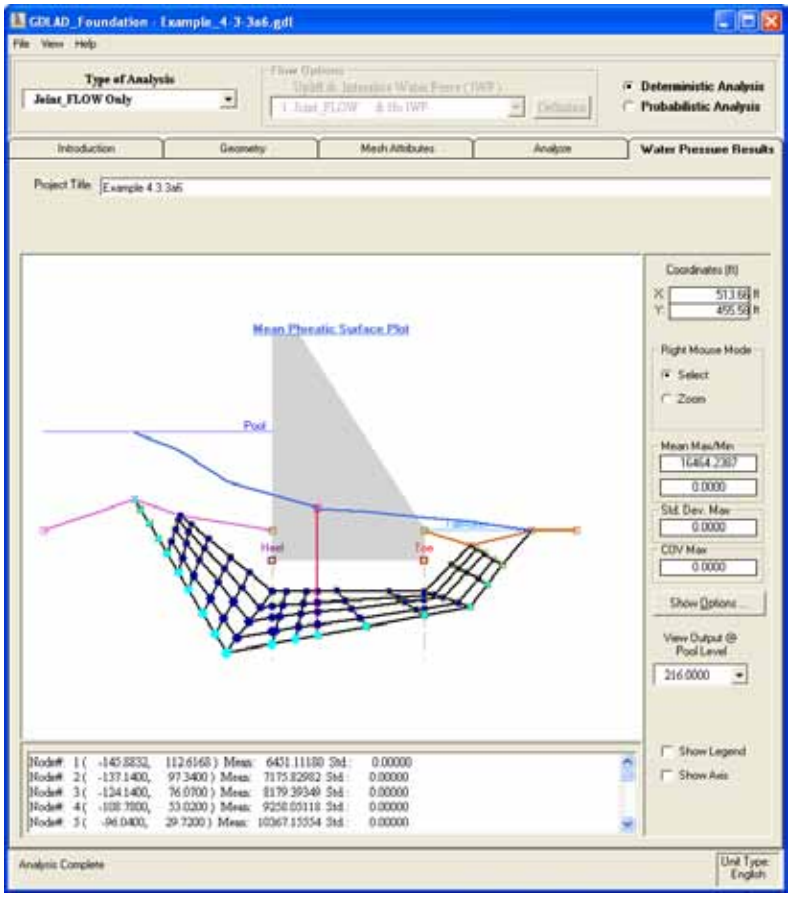

Figure 4.19. Multi-level multi-reach network with two-upstream sources of permeable joints within a rock foundation with one rock foundation drain (Case 5).

The resultant total head values computed for the various rock joint networks of subsections 4.3.1 thru 4.3.3 have been extracted along a sequence of joint reaches that form a single potential slip plane. This potential slip plane is the deepest of the Figure 4.13 upstream-to-downstream continuous joint reach paths that could form a potential slip plane. The distribution of computed total heads along this potential slip plane from Case 1 (Figure 4.14) and Case 2 (Figure 4.16) analyses are approximately the same. In view of the fact that there is no rock joint connectivity between the two upstream-to-downstream continuous joint

reach paths of Case 2, the resultant total head values calculated at this deeper (ie., lower elevation) sliding plane were equal to that for the upstream-to-downstream continuous joint reach path of Case 1. Observe that the Case 1 potential sliding plane is the same as the deeper potential sliding plane of Case 2. Therefore, the Case 2 results are represented in the following two figures by Case 1 results.

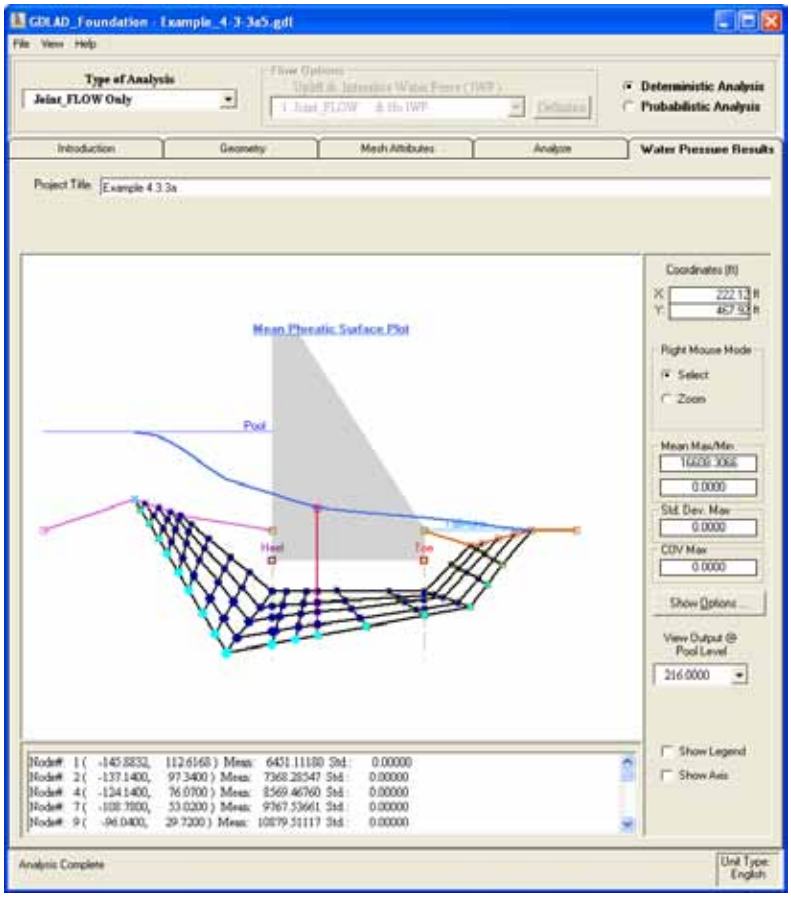

Figure 4.20. Multi-level multi-reach network with multi-upstream sources of permeable joints within a rock foundation with one rock foundation drain (Case 6).

The distribution of total head along the deepest upstream-to-downstream continuous joint reach path for all cases from section 4.3 (except for Case 2 since it mirrors Case 1 results, as explained previously) have been super-imposed and displayed in Figure 4.21. The authors of this report observe:

1. For Cases 1,3,4,5, and 6, the total head starts at the value corresponding to the Pool and then decreases steeply in value as one progresses with distance along the joint reaches due to the drawdown of the drain. After the position of the drain is passed, the reduction in total head is gentler (to

tailwater). The most noticeable is Case 7, where there is no rock foundation drain. It possesses a nearly linear variation in total head with distance along the flow path (i.e., a constant gradient) from Pool entrance to its exit into tailwater.

2. For the case where there is one potential sliding plane and a drain (Case 1), the distribution is almost linear from the Pool to the drain and then to the tailwater.

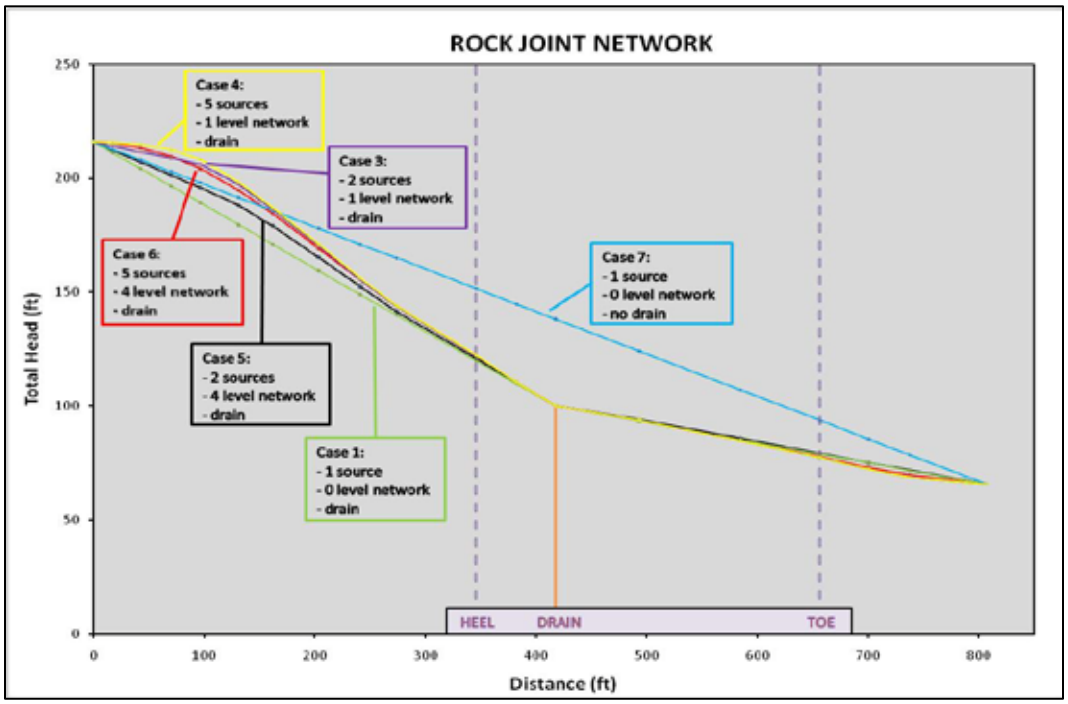

Figure 4.21. Variations in head along a potential sliding plane for various rock joint networks.

3. The higher the level of networks that is used to define the mesh, which indicates that the mesh is more refined and therefore more paths for flow, will result in lower head values as observed when comparing Case 4 with Case 6 and Case 3 with Case 5 in Figure 4.21
4. An increase in the number of sources to the upstream pool will produce higher head values. This can be observed in Figure 4.21 when comparing Case 4 with Case 3 as well as Case 5 with Case 6.

The resultant water pressures of the various rock joint networks of sections 4.3.1 thru 4.3.3 are presented in Figure 4.22. All the various cases of section 4.3 have been reviewed and the resultant water pressures follow the same trends when compared with resultant total head values at the same nodal positions.

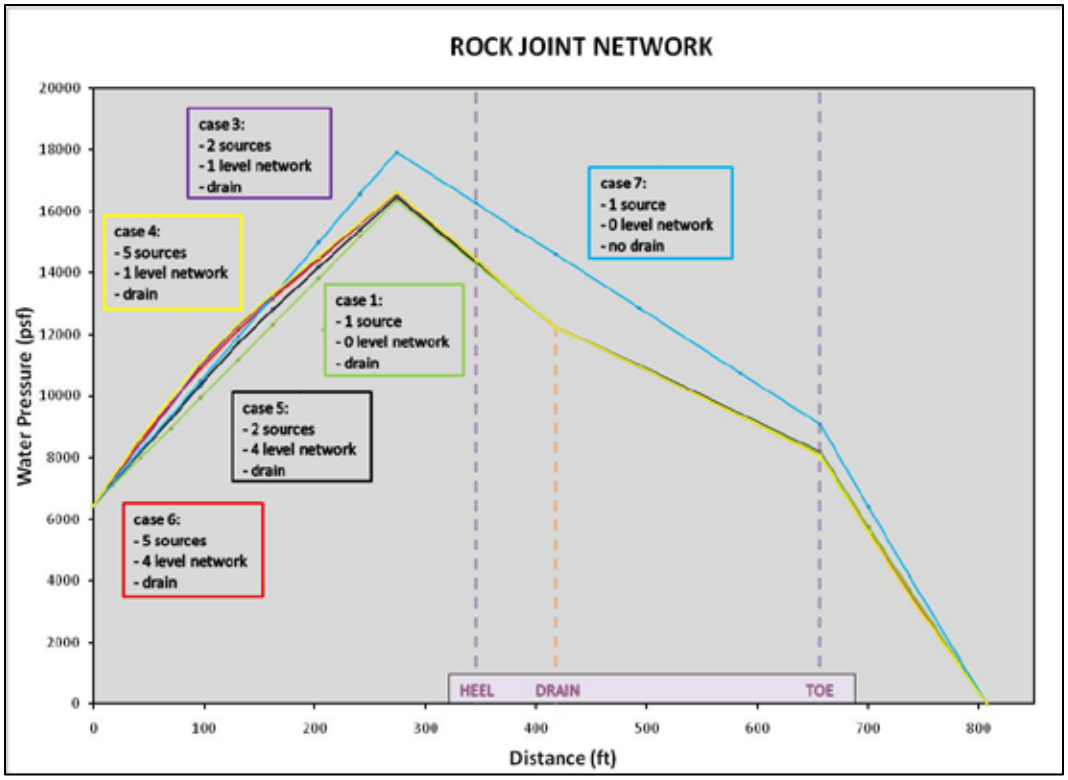

Figure 4.22. Variations in uplift pressures along a potential sliding plane with various rock joint networks.

An important feature to be addressed is the accuracy of the mesh that needs to be configured to provide optimum results. To perform the accuracy test, Case 5 was selected for its nested level of networks and two upstream pool sources. A new mesh of Case 5 was created with the addition of 3 elements per rock joint on all rock joints that were parallel to the potential sliding plane (light blue nodes) as defined in Figure 4.23. All additional elements were given the same uniform conducting aperture values and a deterministic analysis was performed on this new refined mesh in order to compare the results of total head and uplift water pressure distributions.

The resultant total head is compared to the total head of the original Case 5 in Figures 4.24 and 4.25 for total head and uplift water pressures values respectively. The refined mesh results are displayed in brown with the original Case 5 mesh in black. For every black point, there are two brown points between; this signifies that each reach was replaced by three reaches. With no difference in results for the Case 5 original and refined meshes, the authors of this report conclude that that original Case 5 mesh has a sufficient number and distribution of nodes to obtain accurate results.

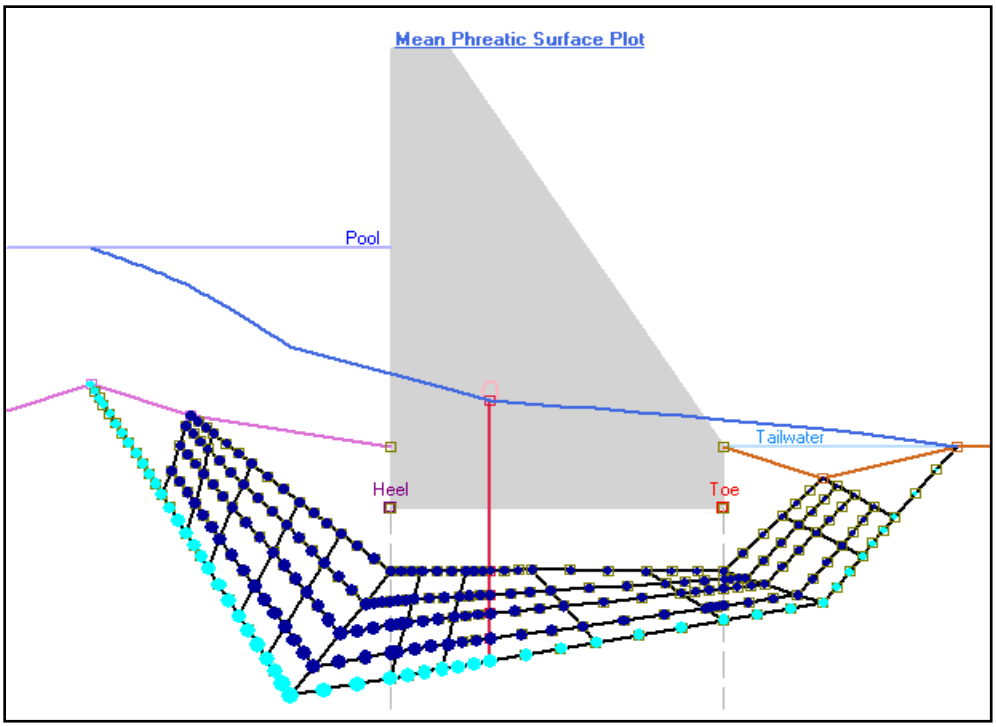

Figure 4.23. Refined mesh of Figure 4.19 for multi-level multi-reach network with two-upstream sources of permeable joints within a rock foundation with one rock foundation drain (Case 5).

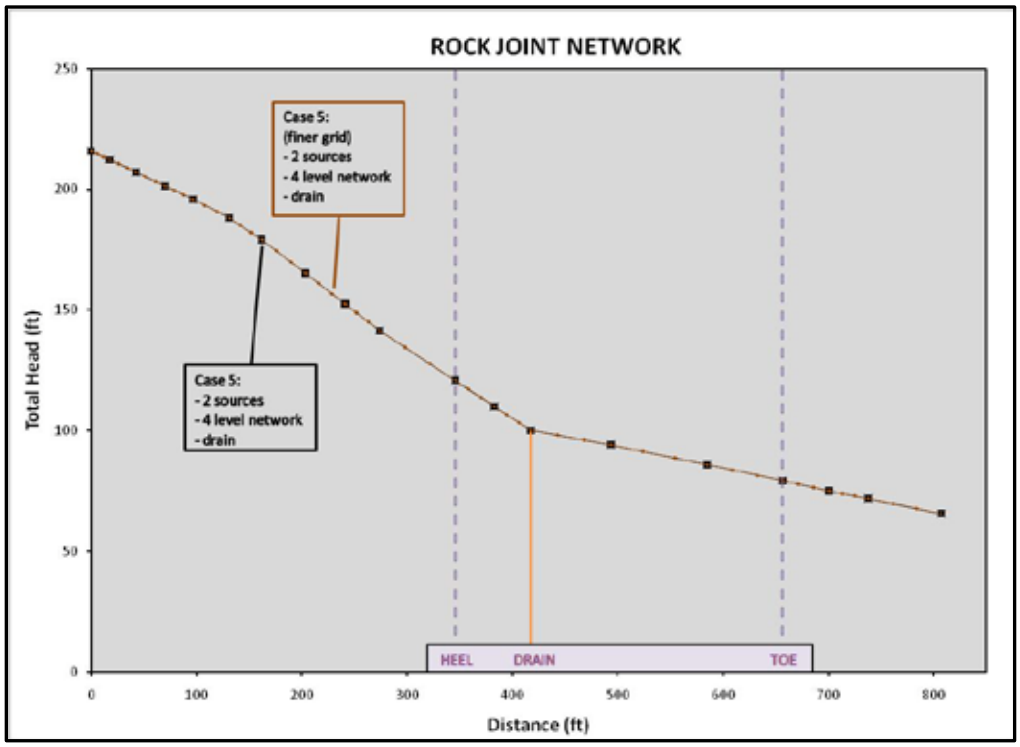

Figure 4.24. Variation in head along a potential sliding plane of Case 5 and its refined mesh.

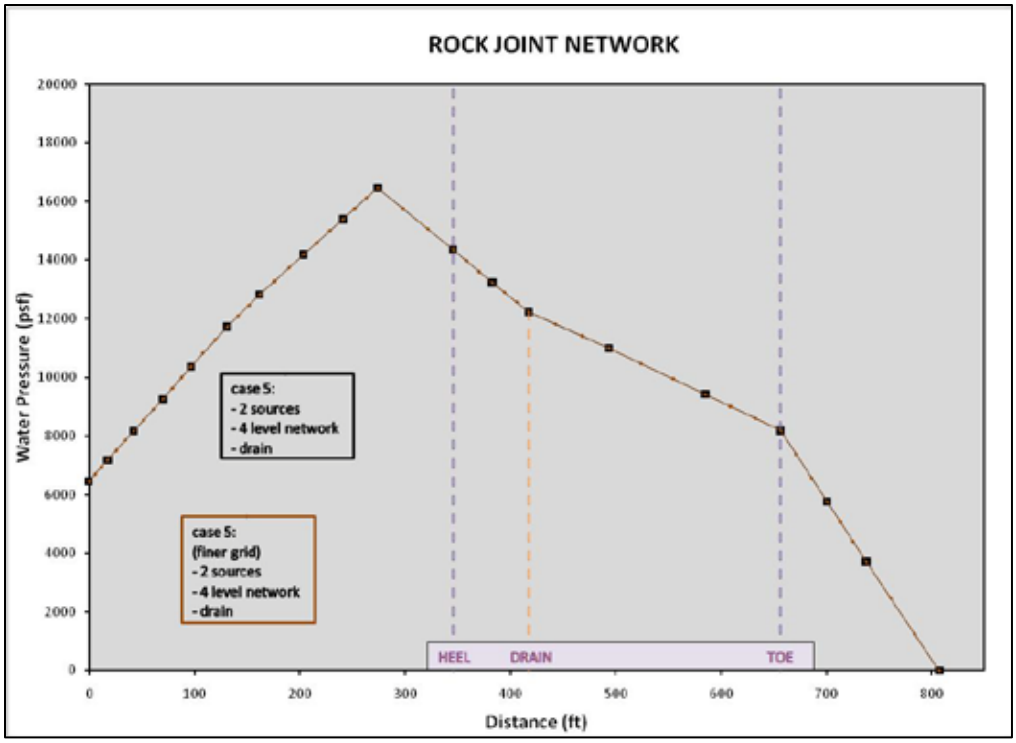

Figure 4.25. Variations in uplift pressures along a potential sliding plane for Case 5 and its refined mesh.

The results from these seven Joint_FLOW laminar flow seepages analyses of the Figure 4.13 based rock joint network configurations demonstrate that:

1. Rock joint network connectivity impacts the total head and uplift pressure distributions within the network of rock joints.
2. The impact of the joint network is more pronounced within the upstream joint reaches between the joints in contact with the Pool and the rock foundation drain.
3. The more joint reaches in communication with the pool (i.e., the number of sources) has more of an adverse impact on uplift water pressures (i.e., with greater water pressures) within the region between the pool and the line of drains than do the number of networks.
4. The lack of a rock foundation drain results in higher uplift water pressures and higher total heads within the rock joint reaches.

4.4 Summary and conclusions

This chapter discusses the result from two sets of Joint_FLOW analyses:

1. Fluid flow along a single reach rock joint with three different tapered rock joints (Section 4.2).
2. Fluid Flow along multi-reach rock joints contained within the rock foundation (Section 4.3).

Validation of Joint_FLOW calculations for two tapered and one uniform rock joint distribution against the closed form solutions for these three problems were also discussed.

The Section 4.2 series of uniform and tapered joint analyses demonstrate:

1. Tapering of rock joint apertures will result in nonlinear uplift pressure distribution(s) along a joint reach. Similar effects can be obtained when there is a network of inter-connected reaches of different apertures, joint roughness (JRC) or different joint hydraulic conductivities.
2. A taper downstream reach results in a larger uplift pressure when compared to the uplift pressure of a uniform aperture. This is a less favorable situation when viewed with regards to the stability of the gravity dam.
3. A taper upstream reach results in smaller uplift pressure when compared with the uniform aperture. This is a more favorable situation when viewed with regards to the stability of the gravity dam.

The Section 4.3 series of joint network analyses demonstrate:

1. Rock joint network connectivity impacts the uplift pressure distributions within the network of rock joints and will need to be accounted for in the laminar flow analysis.
2. The more joint reaches in communication with the pool (i.e., the number of sources) has more of an adverse impact on uplift water pressures (i.e., with greater water pressures) within the region between the Pool and the line of drains than do the number of networks.
3. As anticipated, it has been demonstrated that the lack of a rock foundation drain results in higher uplift water pressures and higher total heads within the rock joint reaches. Functioning drains contained within the rock foundation below a gravity dam reduce uplift pressures and contribute to the stability of the gravity dam.

Combining the lessons learned from the taper joint analyses and the joint network analyses, the authors of this report speculate that a network of

joints within rock strata's of different types (i.e., that is, with different apertures, JRC's and joint hydraulic conductivities) will likely exhibit some of the features observed in the tapered joint results combined with other features observed in the network analyses results. Consequently, when assessing the distribution of uplift pressures acting along joints within a network of jointed rock, a Joint_FLOW analysis are recommended.

5 Head Loss in Rock Joints Using the Linear Method (Computed by LinPipe)

The behavior of flow through natural rock joint network is very similar to the behavior of flow through a pipe network. The technology that has developed for pipe network analysis can be very useful when analyzing flow through rock joint. Goodman et al. (1983) and Amadei et al (1989a, 1989b) make use of the Darcy-Weisbach equation in calculating the flow head loss in an angle rock joint connection and in the entrance and exit of a rock joint slot into a drain hole. These rock joint conditions that equate to head loss and the equations evaluating head loss is further discussed in Appendix C.

The LinPipe method uses pipe networking technology where flow distribution is analyzed by obtaining the continuity equation at each junction and the conservation of the energy equation around any closed loop. To obtain a solution for the number of rock joints or elements defined, the same number of equations must exist.

In a rock joint network of n joints, j junctions and l loops, Wood and Charles (1972) showed that the following identity holds:

$$n = j + l - 1 \tag{5.1}$$

Figure 5.1 shows a schematic diagram describing the relationship expressed in equation 5.1. There are six joints (n = 6), five junctions (j = 5), and two loops (l = 2).

An inspection of the image in Figure 5.2 of an example of multiple-reach rock joints show that there are 2 closed loops highlighted in blue that both include a portion of the drain shown in red (closed polynomial of elements), 9 junctions (rock joint and drain nodes that are connected by more than 1 element), and a total of 15 elements (both rock joints and drain segments) or pipes (refer to Table 5.1). Fifteen equations are needed but only eleven equations are available (9 junctions + 2 closed loops). Inclusions of the "open" loops are necessary in order to obtain the required additional four equations. This methodology and equation formulations have been described in Appendix C.

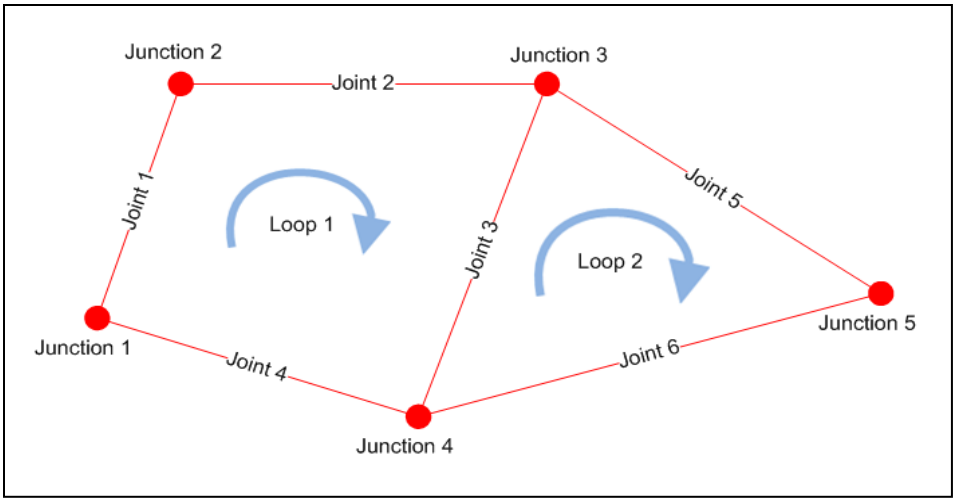

Figure 5.1. Schematic diagram describing relation 5.1.

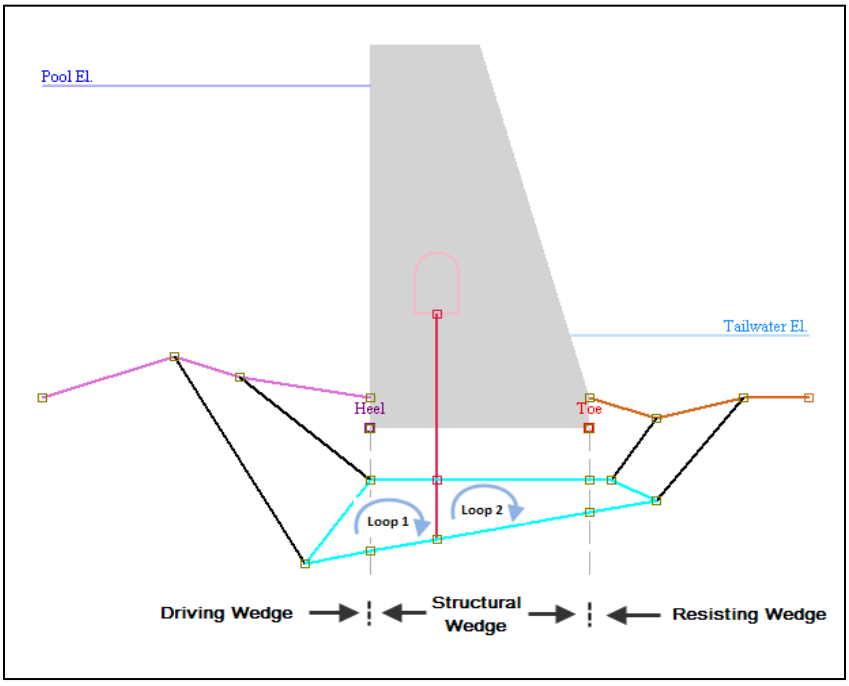

Figure 5.2. A hypothetical dam with segments of rock joints and a drain segment defining two potential inner loops.

Table 5.1. Number of elements comprising each of the three major wedges.

Wedge	Number of Elements
Driving Wedge	4
Structural Wedge (with Drain)	6
Resisting Wedge	5
Total	**15**

Instead of the Darcy-Weisbach equation, empirical equations are sometimes used to determine a head loss or a pressure drop. The most widely used are the Hazen-Williams and Manning equations. The values for the coefficient of roughness for these equations are listed in Table 5.2 for various types of pipe materials.

Table 5.2. Values of the Hazen-Williams Coefficient, C_{HW}, and the Manning Roughness Coefficient, n, for common pipe materials (after Jeppson, 1976).

Type of Pipe	C_{HW}	n
PVC Pipe	150	0.008
Very Smooth Pipe	140	0.011
New Cast Iron or Welded Steel	130	0.014
Wood, Concrete	120	0.016
Clay, New Riveted Steel	110	0.017
Old Cast Iron, Brick	100	0.020
Badly Corroded Cast Iron or Steel	80	0.035

For a linear pipe method of analysis, the number of rock joint and rock drain elements (or pipes); the number of junctions where these pipes intersect; the pipe roughness; and the elements that form a closed loop are among the parameters necessary to perform the analysis. The following section outlines the procedure by the presentation of an example problem.

Laminar flow along multi-reach permeable joints within a rock foundation with a rock foundation drain is examined with a comparison of the optional linear pipe method of flow to that of conventional flow along rock joints (as described in chapter 4). The distributions of total head will be used as a comparison.

5.1 Problem 10: Multiple-reaches of rock joints modeled as a pipe network and using the Linear Method to compute the distribution of total heads

A deterministic analysis of the provided dam geometry from Figure 5.3 was conducted for a Joint_FLOW Only analysis. A one-level multiple reach network (introduced in Chapter 4) with one potential slip plane is presented. Figure 5.3 shows the embedded dam with a pool elevation of 35.0 m and tailwater elevation of 23.0 m. Each rock joint has been assigned five elements, i.e., there are now five elements or rock joints

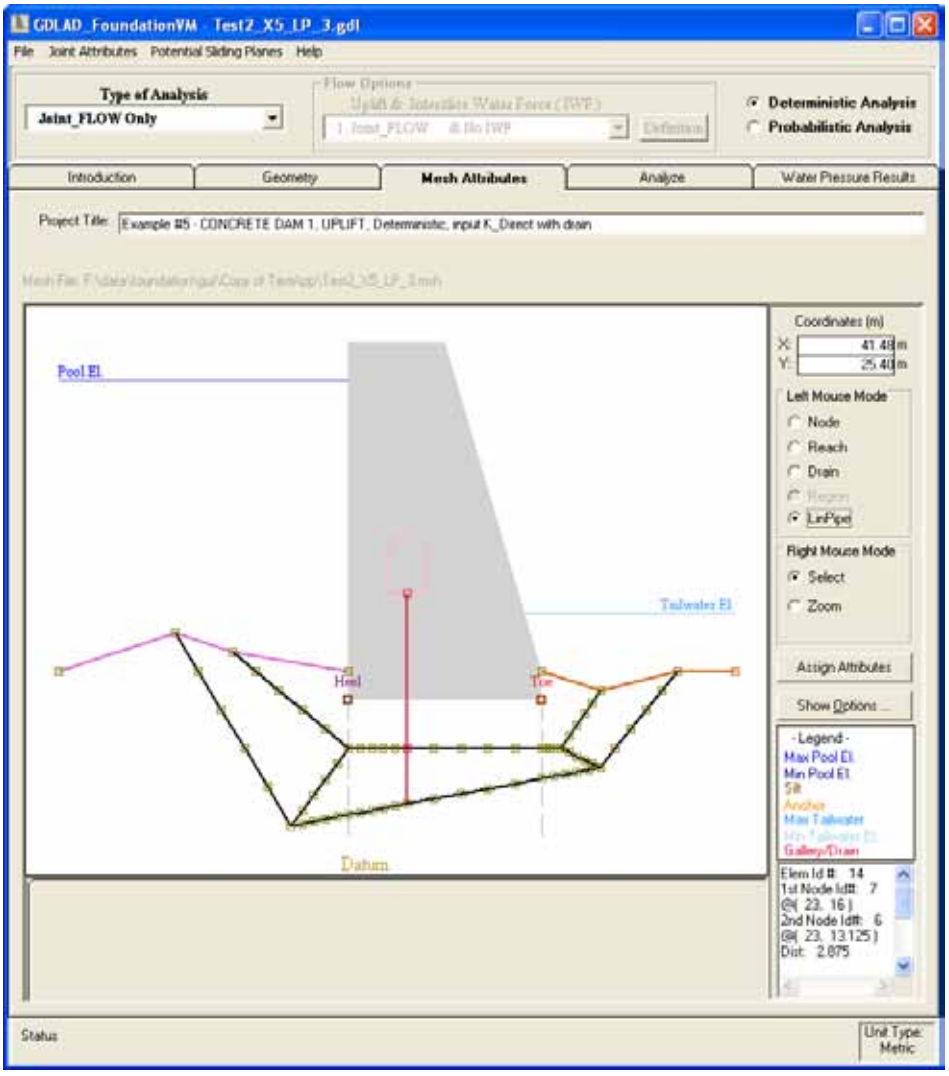

Figure 5.3. A hypothetical embedded dam with segments of rock joints and a rock foundation drain.

that describe each original longer rock joint. A brief comparison of rock joints between Figures 5.2 and 5.3 illustrate the additional rock joints which can be seen in Figure 5.3, which are connected by nodes (designated by small brown squares in this figure).

An inspection of the image in Figure 5.3 of multiple-reach rock joints show that there are a total of 67 elements (both rock joints and drain segments), 2 closed loops, and 61 junctions. Sixty seven equations are needed to conform to the continuity and energy equations, since there are only 63 equations (61 junctions + 2 closed loops) available, the open loops are necessary for the required 4 additional equations.

After selection of all reaches in *Reach Mode*, Figure 5.4 shows a constant hydraulic conductivity of 0.0064 m/sec for every rock joint with five elements per reach. Figure 5.5 shows a drain diameter of 0.127 m at 6.098 m intervals at both drain reach and the assignment of one element for each rock drain reach.[1] Entry of this data was made possible by the selection of all drain segments in *Drain Mode*. LinPipe element assignments are explained in detail in Chapter 3.

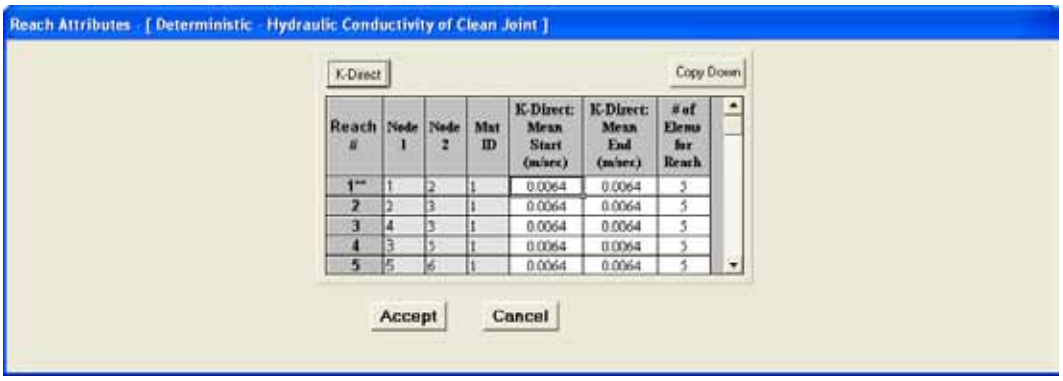

Figure 5.4. Reach attributes showing five elements per rock joint reach.

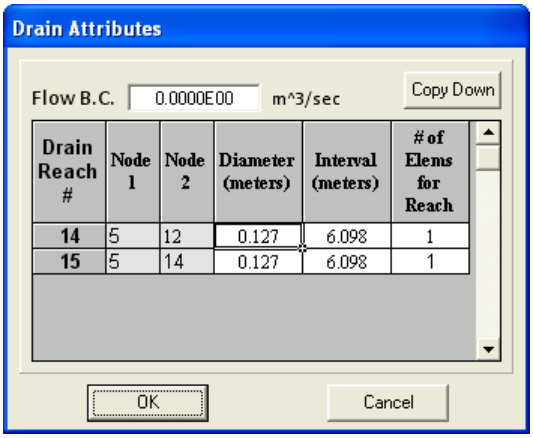

Figure 5.5. Drain Attributes showing one element per rock drain reach.

Figures 5.6 and 5.7 show the particular attributes that have been entered and selected for LinPipe. Figure 5.6 shows a total of 4 tables of input with a Kinematic Viscosity of 1.13059E-6 N-sec/m and a pipe roughness of 0.0002 assigned to all elements of the first table. Item number two of the "*Junction / Inflow Table*" (second table) of Figure 5.6 is a match to Figure 5.7a. Flow entering and leaving the junction is assigned a negative and positive value

[1] In an actual project analysis, each of these two large drain elements would be subdivided into several elements.

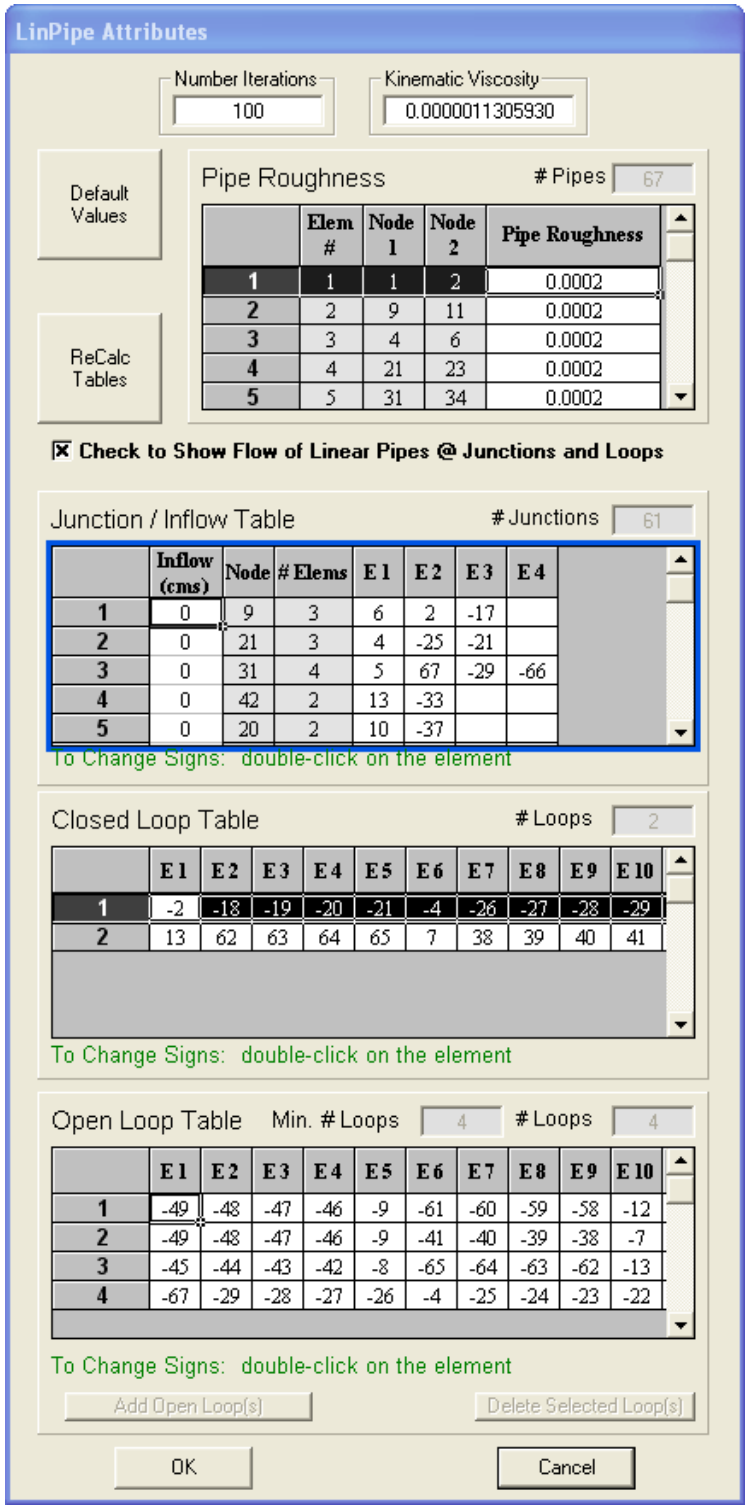

Figure 5.6. LinPipe Attributes.

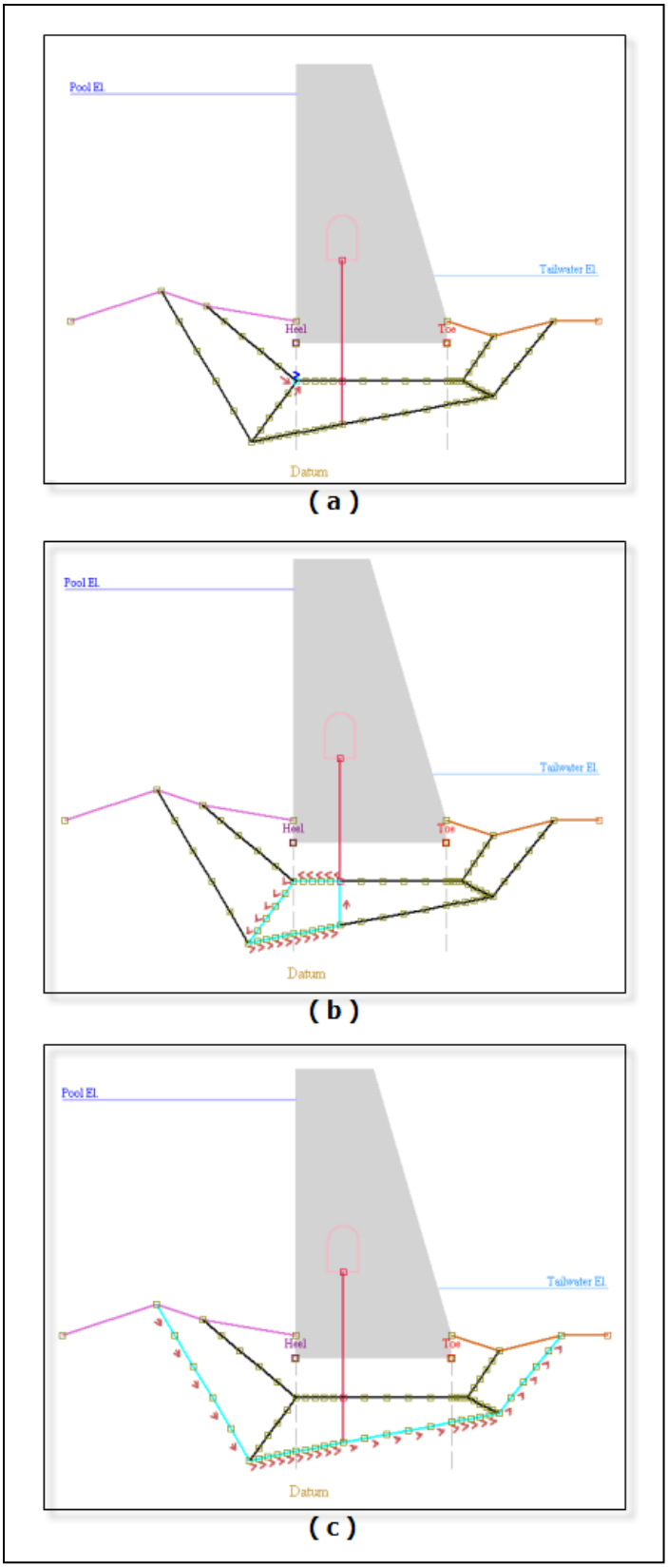

Figure 5.7. Flow directions (a) at a junction (b) closed loop (c) open loop.

and drawn in red and blue respectively. All element signs are negative in the first row of the "*Closed Loop Table*" (third table) of Figure 5.6 and are shown as red arrows in Figure 5.7b for a counter-clockwise direction of flow within the closed loop.[1] The last table in Figure 5.6 is the *Open Loop Table* (fourth table) with the first row showing negative signs for all elements. With the selection of any cell in this row, a counter-clockwise flow direction drawn in red is shown in the image of Figure 5.7c.

At the conclusion of this deterministic analysis, Figure 5.8 shows the resultant total heads (blue line extending from the pool to the tailwater) plotted above the nodes that are highlighted in light blue along the user selected assemblage of deepest rock joint reaches. This figure illustrates a decrease in head from the pool to the drain at the gallery and then with a lesser gradient from the drain to the tailwater. The magnitude of water pressures computed at all nodes is N/m^2 and also shown in this figure (recall the diameter of the circle reflects the magnitude of the water pressure according to the scale on the left-hand side of this figure).[2]

5.2 Comparison of total head results for flow along rock joints with and without the LinPipe methodology

For the specified Dam geometry of Figure 5.3, a deterministic analysis was completed for laminar flow along rock joints containing the potential sliding plane within a rock foundation with a rock foundation drain. This analysis was conducted with the assumptions that (1) there is a linear water pressure distribution existing between nodes, and (2) the developed mesh is sufficiently refined to substantiate the assumption above.[3]

The resultant total head values computed for the rock joint network has been extracted along a sequence of joint reaches that form a single potential slip plane (whose nodes are highlighted in light blue in Figure 5.8). This potential slip plane is defined by the "deepest" upstream-to-downstream continuous joint reach path. The distribution of computed total heads along

[1] Observe the sign is the same for all entries in each row. The user may have to adjust the signs to the entries to obtain the proper flow direction to complete the loop.

[2] At the bottom right hand corner of the GDLAD_Foundation Visual Modeler is listed the system of measurement, as Metric or English, for the current project. Dimensions of length, density, force, pressure and aperture are given in (m : ft); (N/m^3 : pcf); (N : lb); (N/m^2 : psf); (microns : inches) for (Metric : English) units respectively.

[3] The user can verify that sufficient refinement of the mesh has been achieved by observing no change in computed results when a subsequent mesh refinement results in no significant change in outcome.

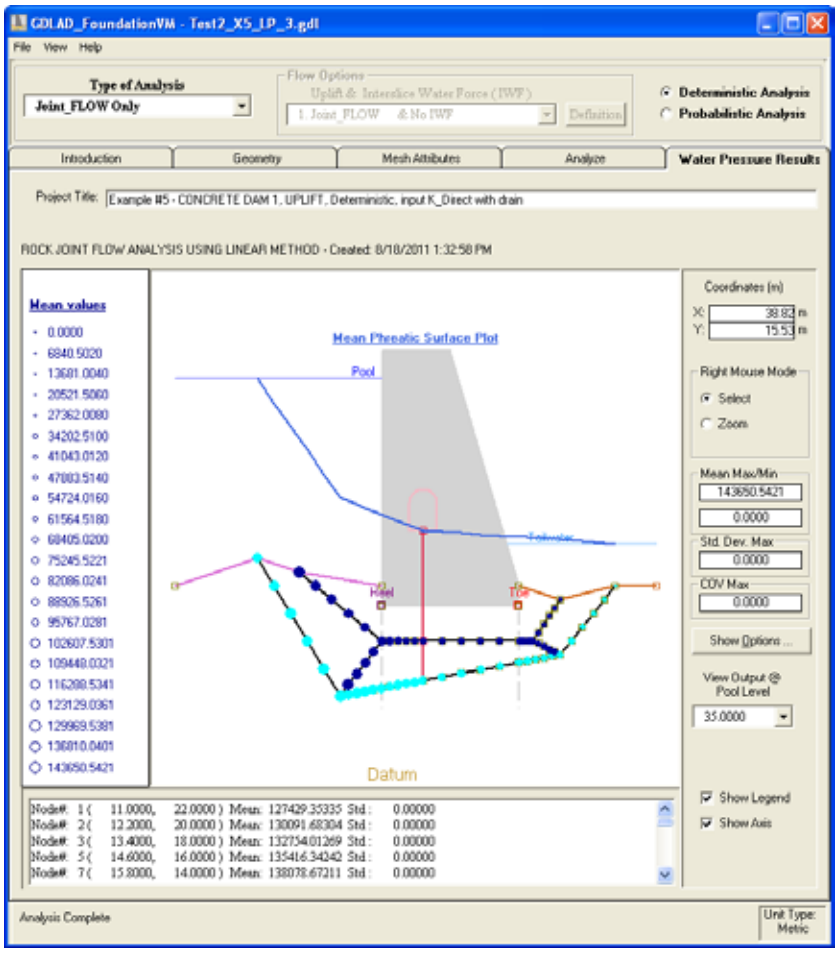

Figure 5.8. Water pressure results.

this potential slip plane is analyzed for both a Joint_FLOW analysis (with the hydraulic conductivity values listed in Figures 5.4 and 5.5) and by utilizing the linear pipe method, with the comparison as shown as a function of distance along this potential slip plane in Figure 5.9. Observe that the total head values differ at the upstream side and merge at the drain. There is a steeper descent at the upstream side for the analysis that uses the linear method with a maximum percent difference of 7.49 percent at the upstream side. This difference may be reduced by refinement of input to Joint_FLOW and to LinPipe analyses.

The resultant (Joint_Flow) water pressures of the deepest rock joint network of Figure 5.3 with one utilizing the linear method are plotted versus distance along the potential slip plane in Figure 5.10. The resultant water pressures follow the same trends when compared with resultant total head values at the same nodal positions.

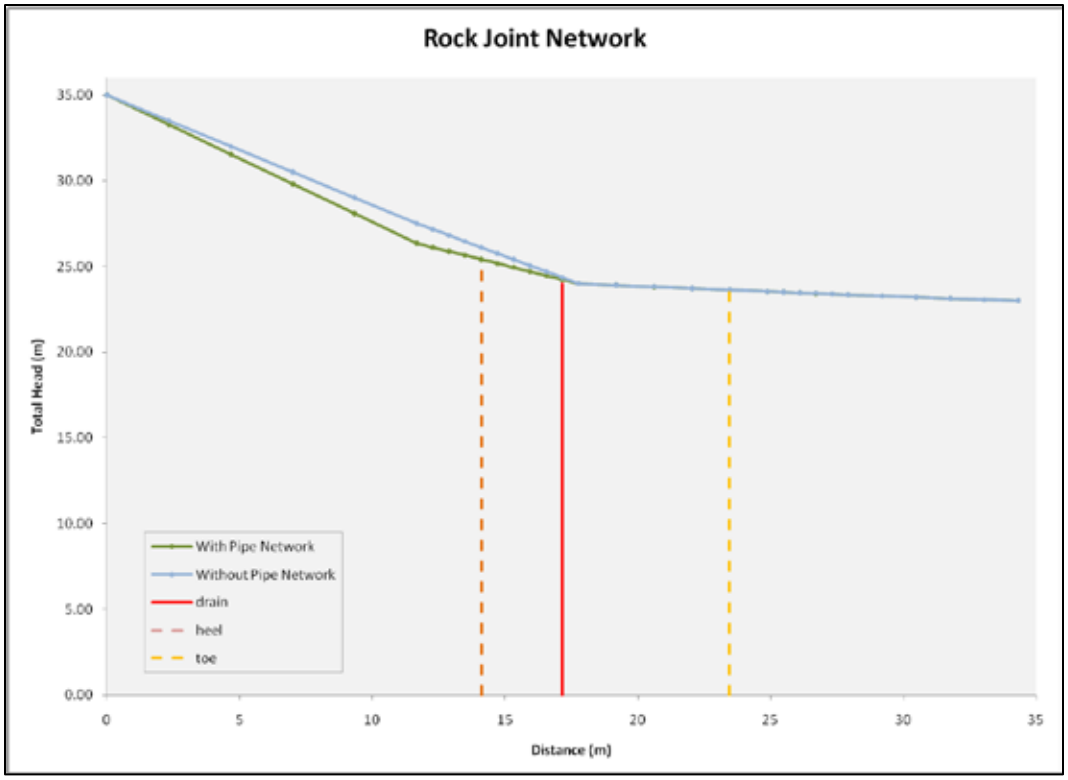

Figure 5.9. Variation in head along a potential sliding plane for a rock joint network.

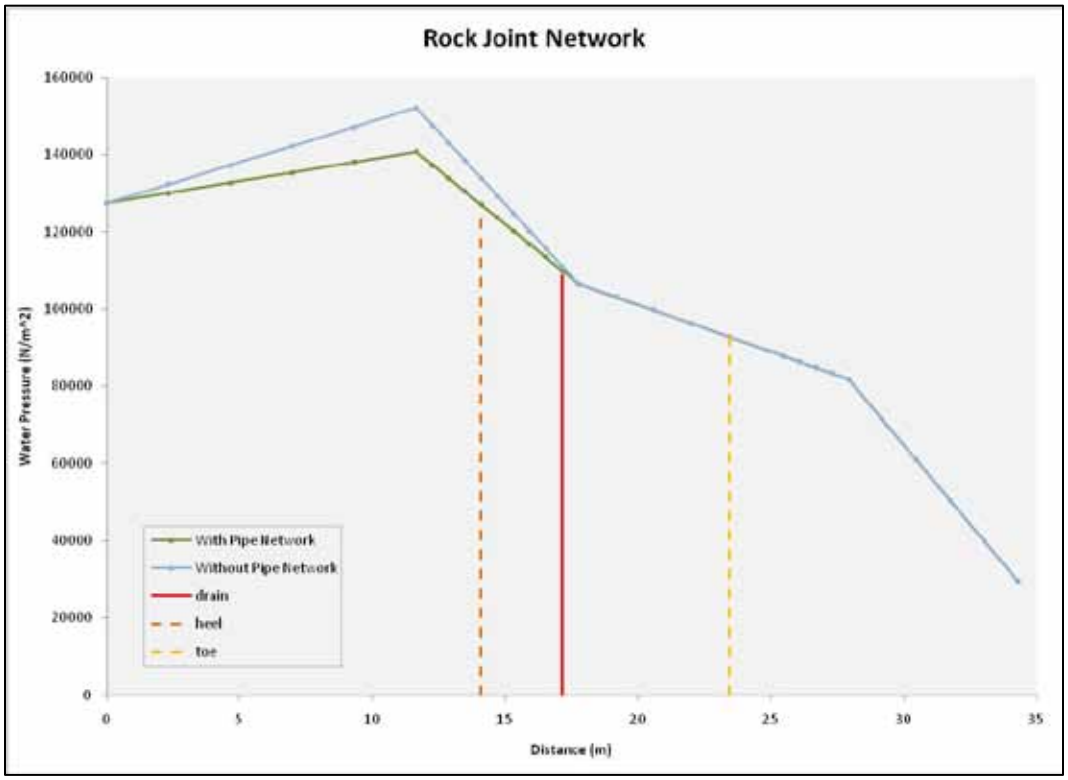

Figure 5.10. Variation in water pressures along a potential sliding plane for a rock joint network.

6 Stability with Simplified Seepage Analysis

6.1 Introduction to Limit Equilibrium Procedure and Procedure of Slices

The GDLAD_Foundation package has the ability to

1. assess the uplift pressures resulting from laminar flow within individual rock joints or networks of rock joints, and
2. assess the stability of a gravity dam cross-section embedded within a rock foundation.

This chapter focuses on the assessment of the stability of a non-overflow gravity dam cross-section model. Three simplified methods of establishing uplift water pressures that may be used in the stability analysis are also discussed. These simplified Flow Options, designated as options 4, 5 and 6, center on a formulation for a continuous series of connected rock joints from upstream to downstream of the gravity dam with fluid flow assumed along this singular joint path system. Note that these three simplified methods of analysis do not account for a network of interconnected rock joints as depicted and discussed in Section 4.3 of Chapter 4, which conducts Joint_FLOW only type of analyses.

The hypothetical non-overflow gravity dam cross-section used in ETL 1110-2-256 (1981) and shown in Figure 6.1 allows for a convenient introduction to the engineering process. The rock foundation consist of three rock types with the unit weights and Mohr-Coulomb effective shear strength parameter values listed in Table 6.1 for each of the three regions used to designate each type of rock as found in Figure 6.1. There is a 25 ft high pool above rock Region 1 on the upstream side of the gravity dam and the tailwater is at the top of rock Region 3. A user selected potential slip plane coincident with a continuous series of connected rock joints (from upstream to downstream of the dam) is also shown in this figure with the corresponding joint lengths and orientations defined in Table 6.2. A GDLAD_Foundation stability analysis will be conducted of this cross-section for this user selected potential slip plane. The GDLAD_Foundation Visual Modeler distinguishes among three types of wedges as labeled in

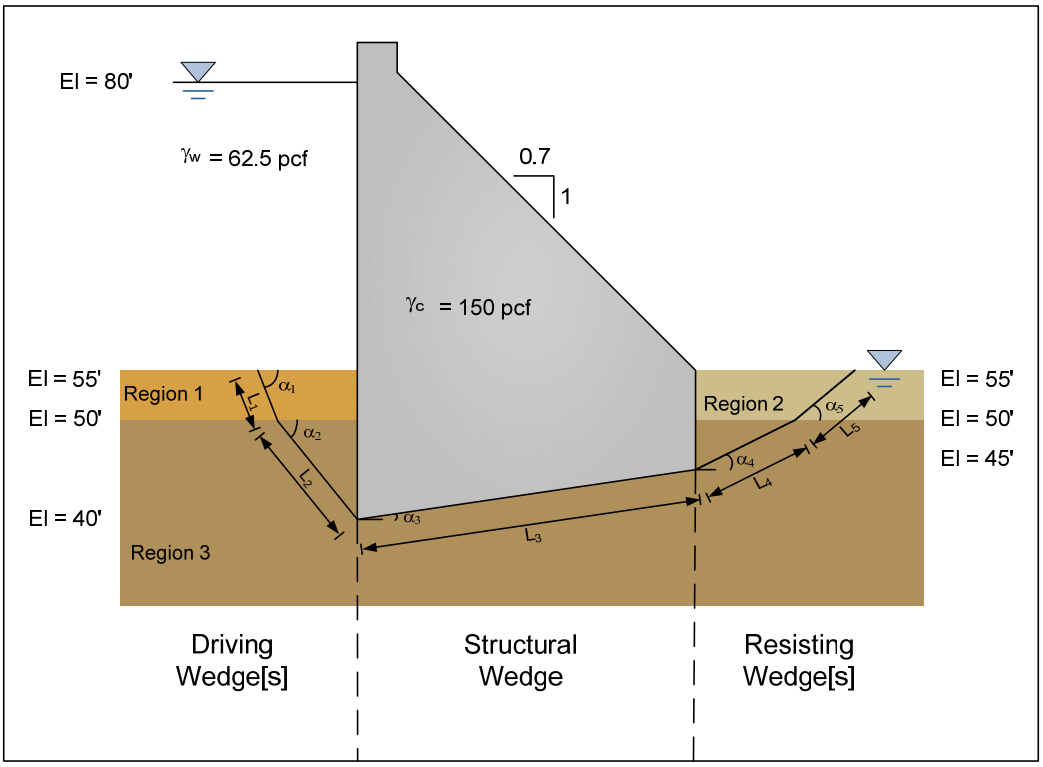

Figure 6.1. The ETL 1110-2-256 hypothetical gravity dam embedded in a rock foundation with no rock foundation drain.

Table 6.1. Categorization and mapping of unit weights and effective shear strength parameter values to the three rock regions.

Region	γ (pcf)	C' (psf)	ϕ' (deg)
Region 1	117	0	20
Region 2	132	0	40
Region 3	122	0	30

Table 6.2. Joint Lengths and Orientation along the base of each wedge/sub-wedge.

Wedge	L (ft)	α (deg)
1	6.51	-50.16
2	12.51	-53.05
3	30.3	9.50
4	8.33	36.95
5	9.03	33.62

Figure 6.1; the Driving Wedge(s), the Structural Wedge; and the Resisting Wedge(s). The Driving Wedge(s) consists of 2 wedges, the Structural Wedge has 1 wedge and the Resisting Wedge(s) has 2 wedges. From Figure 6.1 and Table 6.2, this five wedge system is defined by the joint lengths and the angle between the inclined potential slip surface and the horizontal. There are two sub-wedges contained within the driving wedge, a single structural wedge, and two sub-wedges contained within the resisting wedge.

The stability of a two-dimensional gravity dam cross-section against sliding is expressed in terms of the computed value for the Factor of Safety (*FS)*. The factor of safety (*FS)* is defined as the ratio of the Mohr-Coulomb shear strength, τ_F, divided by the shear stress required for equilibrium, τ,

$$FS = \frac{\tau_F}{\tau} \tag{6.1}$$

with the Mohr-Coulomb shear strength relationship τ_F defined by Equation 1.2. It is important to recognize that GDLAD_Foundation uses effective stresses to compute the frictional portion of the shear strength of the rock discontinuity being investigated as a potential sliding surface. The equilibrium shear stress is the shear stress required to maintain a stable driving-structural-resisting wedges system. Equation 6.1 may be re-written as

$$\tau = \frac{\tau_F}{FS} \tag{6.2}$$

This expression demonstrates that the equilibrium shear stress τ is equal to the shear strength divided by the Factor of Safety (*FS*). One can think of the term (1/*FS*) as a scale factor as suggested by Duncan and Wright (2005). They also observe that the Factor of Safety (*FS*) represents the factor by which the shear strength is reduced so that the shear strength is in equilibrium with the "applied" shear stress. That is to say, the driving-structural-resisting wedge is in a state of just-stable limiting equilibrium. Limiting equilibrium procedures as outlined in ETL 1110-2-256 are used in GDLAD_Foundation to perform the computation of the value for the Factor of Safety (*FS*) for the user selected potential sliding plane contained within the rock joint network(s). In a limiting equilibrium stability analysis such as that used by GDLAD_Foundation, the rock and gravity dam mass are divided into a number of vertical slices (Figure 6.2) and equilibrium

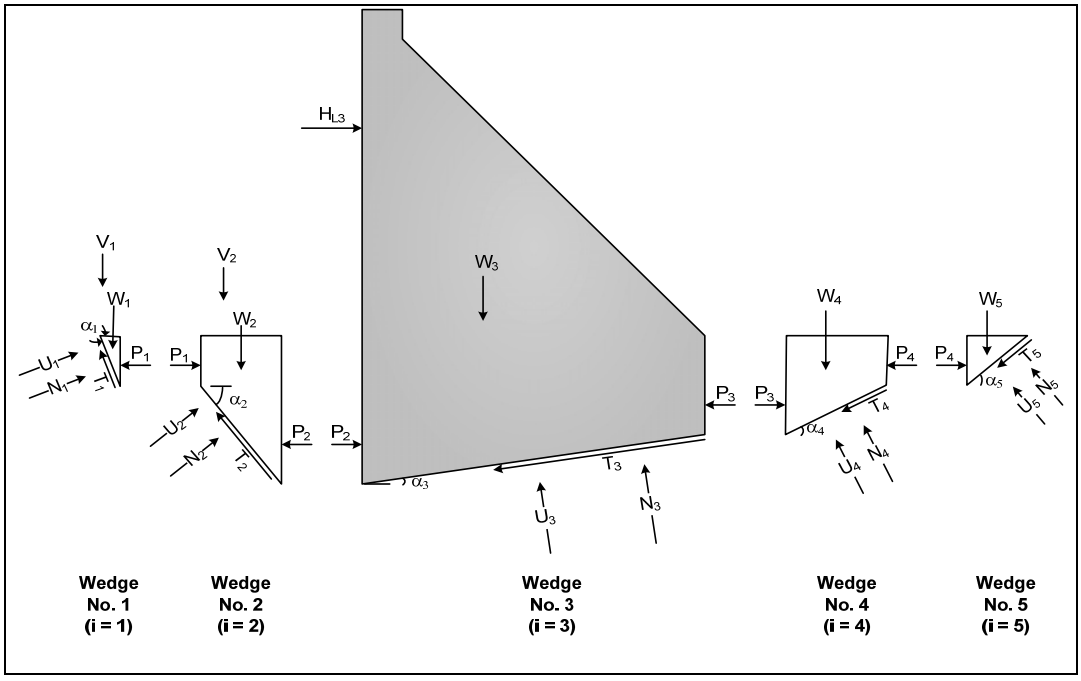

Figure 6.2. A Five wedge system for the ETL 1110-2-256 hypothetical gravity dam embedded in a rock foundation with no rock foundation drain.

equations are written and solved for each slice. The method of slices used by GDLAD_Foundation follows the procedure outlined in ETL 1110-2-256. It satisfies horizontal and vertical equilibrium. Equations for moment equilibrium are not evoked in the ETL 1110-2-256 method of slices.

Figure 6.2 shows the resulting five wedge system for the ETL 1110-2-256 hypothetical gravity dam embedded in a rock foundation with no rock foundation drain based on the user defined potential failure plane.[1] Recall that this plane corresponds to the interconnected reaches of the limited rock joints for this hypothetical site. This figure demonstrates that five wedges equates to four slices for the Figure 6.2 cross-section. Observe in Figure 6.2 that the shearing force parallel to the (vertical) interface of any two wedges is assumed negligible in this formulation.

Figure 6.3 outlines the distribution of pressures and resultant forces acting on a typical wedge and Figure 6.4 shows the free body diagram of the i^{th} wedge of the general wedge system. Observe that the wedge is designated as the i^{th} wedge. Referring to Figure 6.4; the total weight of the rock (or

[1] Although the ETL 1110-2-256 example problem has a potential slip plane below the dam-to-foundation interface, GDLAD_Foundation will accommodate a potential slip plane at any depth within the rock foundation.

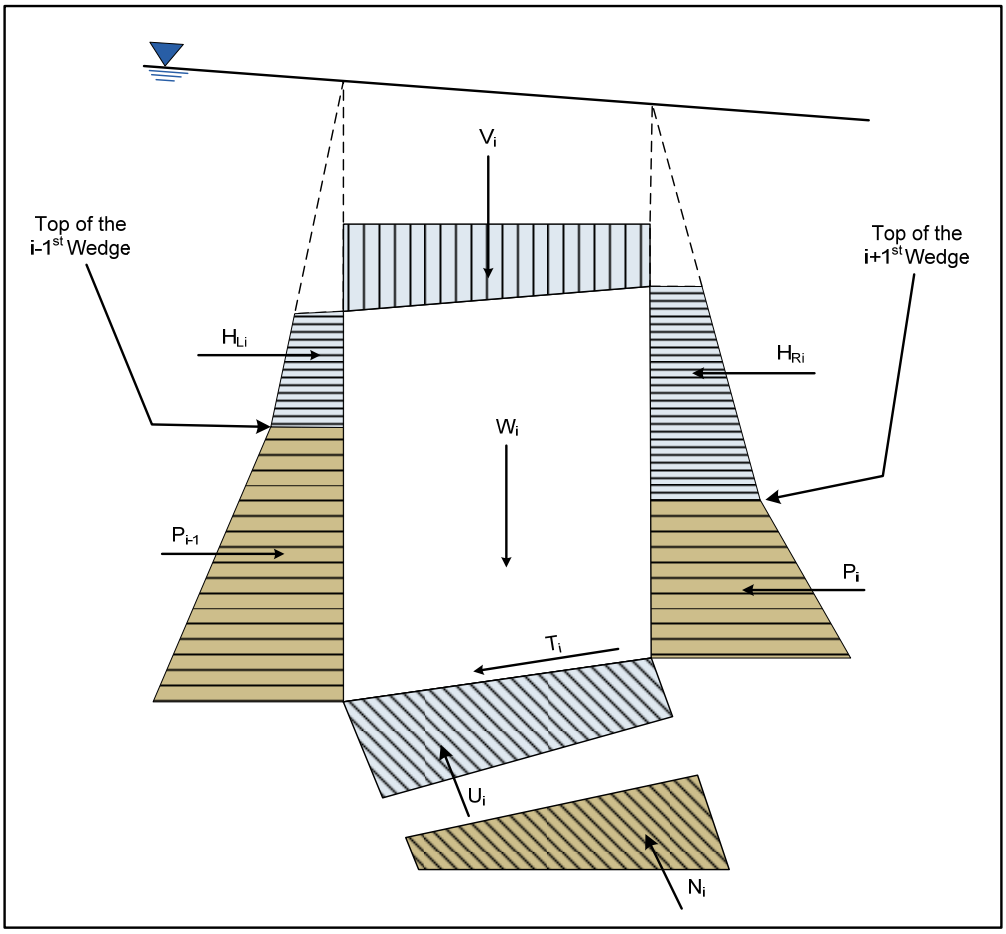

Figure 6.3. Distribution of pressures and resulting forces acting on a generalized wedge in the ETL 1110-2-256 formulation.

concrete and rock in the case of the structural wedge) is designated by the letter *W*; the horizontal interslice forces are designated by the letter *P*; the applied horizontal force (e.g., water pressure force should there be horizontal water pressure forces action normal to the interslice) is designated by the letter *H*; the overburden weight acting down on the wedge, such as the weight of the reservoir pool of water above wedge, is designated by the letter *V*; the shear force required for equilibrium along the user selected potential sliding wedge is designated by the letter *T*; the total force acting normal to the user selected potential sliding wedge is designated by the letter *N*; and the uplift water force acting normal to the user selected potential sliding wedge is designated by the letter *U*.

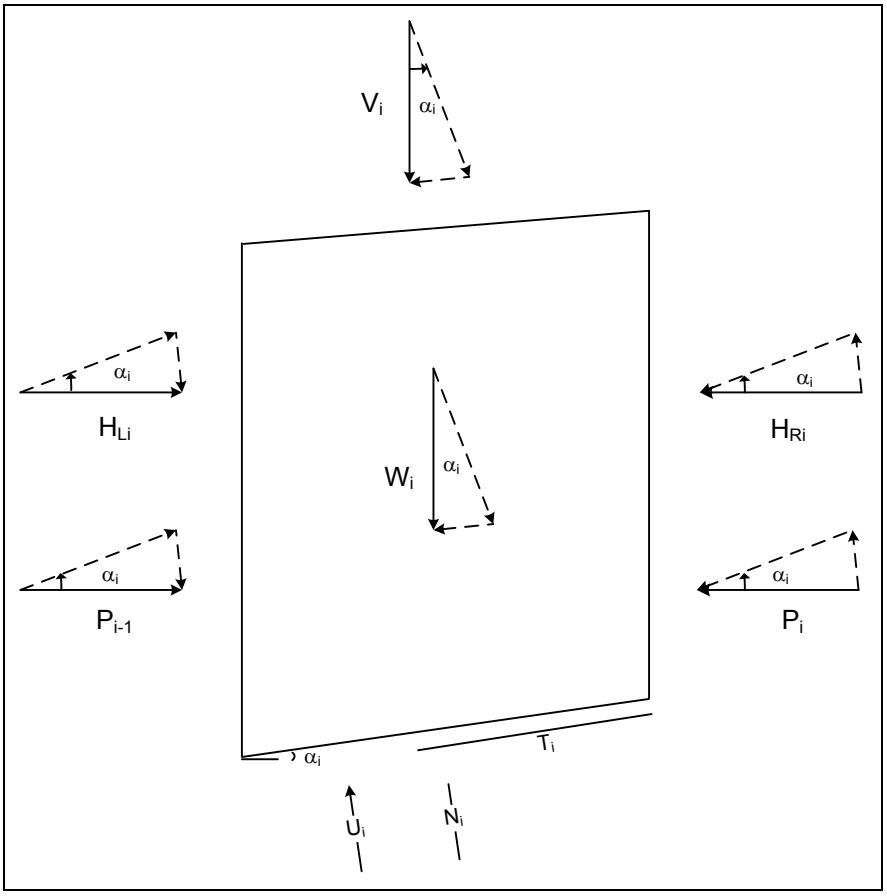

Figure 6.4. Free body diagram of the i^{th} wedge according to the ETL 1110-2-256 formulation.

The Factor of Safety (*FS)*, in this ETL 1110-2-256 limiting equilibrium formulation is defined in terms of the shear force at failure, T_F, divided by the Figure 6.4 shear force acting on the i^{th} wedge, T_i, of the general wedge system.

$$FS = \frac{T_F}{T_i} \tag{6.3}$$

For the Mohr-Coulomb failure criterion, the force T_F is defined as

$$T_F = c\varphi \cdot L_i + N_i \cdot \tan \varphi'_i \tag{6.4}$$

for the i^{th} wedge potential slip plane of length L_i. Re-arranging Equation 6.3 results in

$$T_i = \frac{T_F}{FS} \tag{6.5}$$

Equation 6.5 allows for the shear force T_i to be expressed in terms of the shear force at failure, T_F, divided by the Factor of Safety (*FS)*, in the equations of equilibrium for the i^{th} wedge (Figure 6.4) of the general wedge system (Figure 6.2), Equation 6.5 is used in the ETL 1110-2-256 solution of the limiting equilibrium equations for each slice. After algebraic manipulations of the equations of equilibrium for the Figure 6.2 wedges, the governing equation for the horizontal interslice forces ($P_{i-1} - P_i$) (see ETL 1110-2-256) is

$$(P_{i-1} - P_i) = \frac{\left[\left(W_i + V_i\right)\cos\alpha_i - U_i + \left(HL_i - HR_i\right)\sin\alpha_i\right]\frac{\tan\varphi_i}{FS_i} - \left(HL_i - HR_i\right)\cos\alpha_i + \left(W_i + V_i\right)\sin\alpha_i + \frac{c_i}{FS_i}L_i}{\left(\cos\alpha_i - \sin\alpha_i\frac{\tan\varphi_i}{FS_i}\right)} \quad (6.6)$$

An iterative solution is used to converge to the value for the Factor of Safety (*FS)*, in GDLAD_Foundation. The convergence is achieved when the sum of all interslice forces is minimized to a (small) tolerance of 100 lbs. The iterative solution is used to determine the factor of safety (*FS*) for sliding equilibrium. This procedure of wedge solution analysis is outlined in ETL 1110-2-256 (1981).

The free body diagram of Figure 6.5 idealizes the three forces acting on the potential sliding plane for the driving wedge (*D*), the structural wedge (*S*) and the resisting wedge (*R*). Recall that these three forces are the force normal to the potential slip plane, *N*, the resultant water pressure force, *U*, and the shear force required for equilibrium, *T*, respectively. Note that for an actual analysis, these three forces are defined for each of the sub-wedges within the driving and resisting wedges.

For sliding stability problems of the type shown in Figure 6.5 involving multiple reaches of rock joints, the user may select and investigate a single potential sliding plane at a time.

6.2 Uplift and interslice water pressure resultant forces for Flow Options 4, 5, and 6

The assessment of the uplift pressures at the slip plane and interslice forces at the vertical interfaces resulting from laminar flow within individual rock joints or networks of rock joints is further examined for certain conditions and categorized as Flow Options 4, 5, and 6. Table 6.3 lists the methods used for the calculations of uplift water pressures and

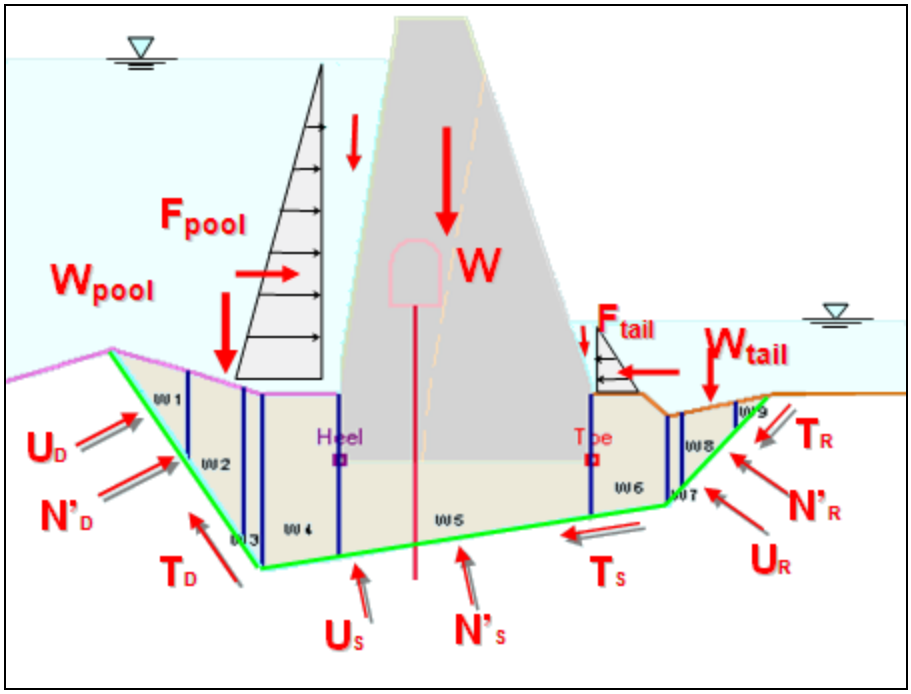

Figure 6.5. Free body diagram - Sliding stability analysis for a general wedge system.

Table 6.3. Classification of uplift and interslice water forces as flow options.

Flow Options	Wedge Features	Uplift and Interslice Water Force (IWF)	Driving Wedge	Structural Wedge	Resisting Wedge
4	Wedge Base	ETL-1110-256	Hydrostatic	Flow Along Slip Plane	Hydrostatic
	Vertical Interslice	No IWF	No Water Pressures	No Water Pressures	No Water Pressures
5	Wedge Base	Line of Seepage	Hydrostatic	Flow Along Slip Plane	Hydrostatic
	Vertical Interslice	Structural Wedge Only	No Water Pressures	Flow Along Interslice	No Water Pressures
6	Wedge Base	Line of Seepage	Flow Along Slip Plane	Flow Along Slip Plane	Flow Along Slip Plane
	Vertical Interslice	No IWF	No Water Pressures	No Water Pressures	No Water Pressures

Interslice water forces for these flow options. Note that these three Flow Options are simplified methods of analysis centering on a formulation for a continuous series of connected rock joints from upstream to downstream of the gravity dam with fluid flow assumed along this singular joint path system. These simplified methods of analysis do not account for a network

of interconnected rock joints as depicted in Section 4.3 of Chapter 4 and do not make use of the software Joint_FLOW.

6.2.1 Introduction to Flow Option 4

As an introduction to the assessment of uplift and interslice water forces by Flow Option 4, the Figure 6.1 hypothetical dam with its user defined slip plane is used. Figure 6.6 shows that this potential slip plane corresponds to a continuous series of connected rock joints from upstream to downstream of the gravity dam with a unique set of uplift pressures assumed along this singular joint path system. Interpreting the ETL 1110-2-256 (1981) uplift pressure assumptions for which this Flow Option is intended to represent, the authors of this report infer fluid flow within the singular, inter-connected jointed rock feature that is specified by the user to be a potential slip plane extending from upstream to downstream of the gravity dam cross-section embedded within a rock foundation.

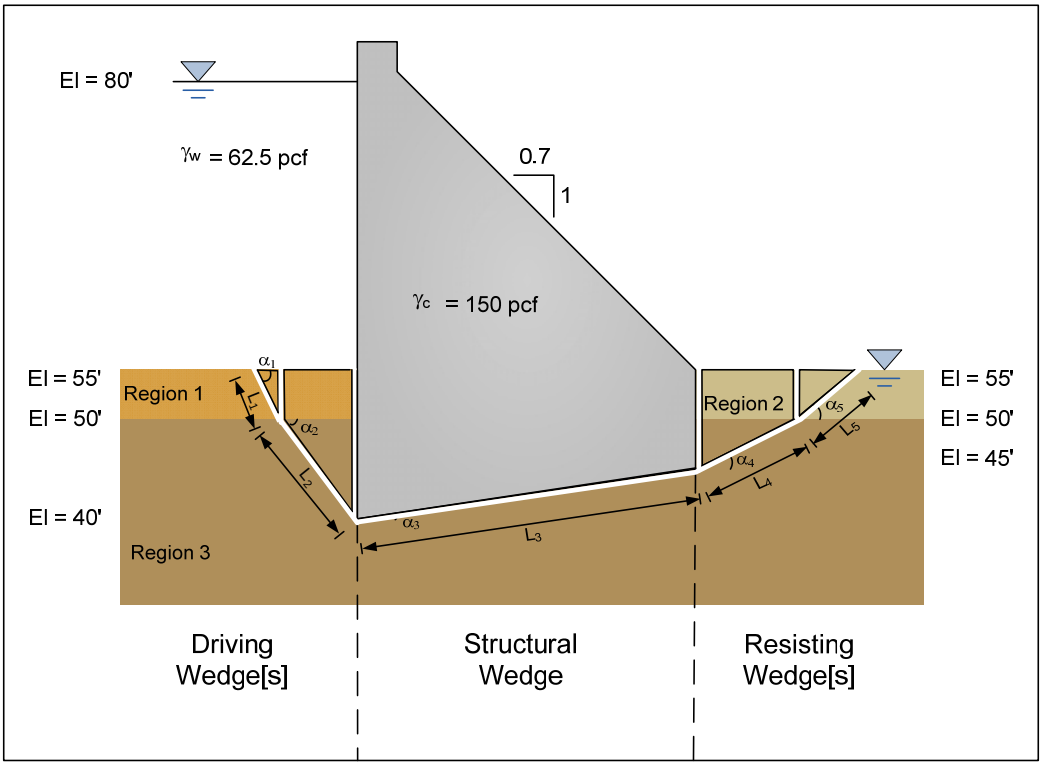

Figure 6.6. ETL 1110-2-256 hypothetical gravity dam embedded in a rock foundation with no rock foundation drain (Flow Option 4).

Recall that the weight of the reservoir pool of water above the two Figure 6.6 driving sub-wedges is accounted for in this formulation by the Figure 6.3 vertical force V_i acting down on the top of each of these two sub-wedges

(i = 1, 2), as noted in Figure 6.7. If a tailwater existed above the two downstream resisting sub-wedges, a vertical force V_i (with i = 4, 5) would act down on each of these sub-wedges 4 and 5 as well.

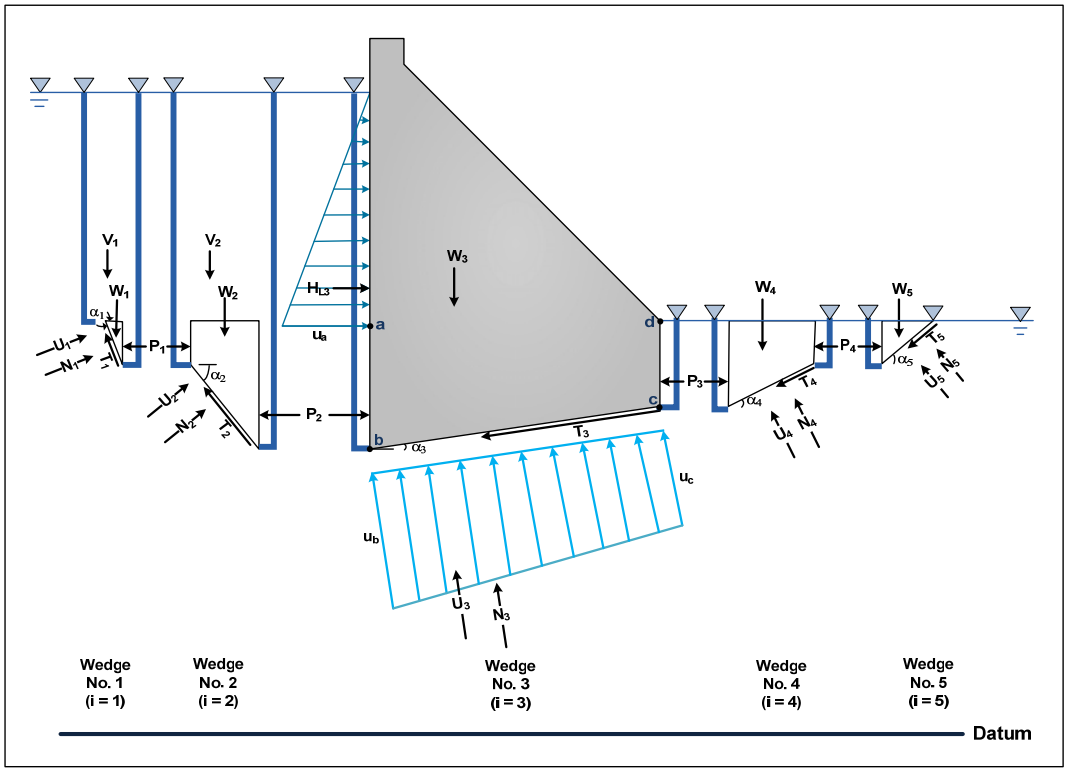

Figure 6.7. A Five wedge system for the ETL 1110-2-256 hypothetical gravity dam embedded in a rock foundation with no rock foundation drain (Flow Option 4).

Figure 6.7 depicts the water pressures in terms of pressure head acting at start and ending points along the base of each of the five wedges of the user defined potential slip plane. As Figure 6.7 shows (and Table 6.3 notes for this Flow Option 4), hydrostatic water pressures are assumed to act at the start and end points along the base of each pair of driving and resisting sub-wedges. For the two driving sub-wedges, a hydrostatic pool pressure head is assumed acting normal to the user defined potential slip plane. For the two resisting sub-wedges, a hydrostatic tailwater pressure head is also assumed. Given these two assumptions, all head losses are assumed to occur within the rock joint segment that corresponds to the potential slip plane below the structural wedge. The user specified potential slip plane below the structural wedge is defined by a starting point *b* immediately below the heel of the dam and an ending point *c* immediately below the toe of the dam. The pool's hydrostatic water pressure is assumed to act at point *b* and the tailwater's hydrostatic water pressure is assumed to act at point *c* (Figure 6.7). The height to each point as measured from the Figure 6.7 datum corresponds to

the elevation head. Recall by Bernoulli's Equation 1.5 (assuming a zero velocity head) that by adding the elevation head value to the pressure head value at each point identified in this figure, results in a value for total head. Considering the distribution of total heads for this problem, it is concluded that the head loss in joint fluid flow occurs along the portion of the potential slip plane that resides below the structural wedge in Flow Option 4. Since there is no drain in the ETL 1110-2-256 example problem, there is a linear variation in the water pressure acting normal to the base of the structural wedge between these two points (*b* to *c*).

For Flow Option 4, while there are water pressures acting normal to the bases of all wedges and sub-wedges comprising the potential slip plane, there are no vertical interslice water pressure forces being considered between each of the five Figure 6.7 sub-wedges/wedges. In other words, the four vertical slices between the five driving, structural and resisting sub-wedges/wedges do not contain (vertical) rock joints that allow for fluid flow nor contain a water pressure force acting normal to the faces of these four interslices. Consequently, there are no interslice water pressure forces acting normal to the four vertical interslices when using Flow Option 4, as noted in Table 6.3. Recall Flow Option 4 makes the same assumptions for computing water pressure acting on the driving, structural and resisting wedges and sub-wedges as are made in the ETL 1110-2-256 (1981) formulation.

Observe the pool's blue triangular horizontal distribution of water pressure acting normal to the upstream vertical face of the Figure 6.7 gravity dam (i.e., structural wedge i=3) extending to a depth of top of rock labeled as point *a*. These water pressures are hydrostatic pool pressures; with the water pressure u_a equal to γ_w times the difference in elevations of the pool and point *a*. Observe in this figure that there are no interslice water pressures acting below point a and along this interface (number I_2) between wedges 2 and 3. The resultant of this Figure 6.7 triangular water pressure distribution is designated as force H_{L3} and acts normal to its vertical upstream (left) face. This nomenclature is consistent with the Figures 6.3 and 6.4 notations of horizontal forces acting on the left face of the i^{th} wedge or sub-wedge. If tailwater was present, the horizontal component of a hydrostatic water pressure distribution would act on the right face of the structural wedge (wedge number 3) and would be designated as H_{R3}.

6.2.2 Introduction to Flow Option 5

As an introduction to the assessment of uplift and interslice water forces by Flow Option 5, the Figure 6.1 hypothetical dam with its user defined slip plane is used. Figure 6.8 shows that this potential slip plane corresponds to a continuous series of connected rock joints from upstream to downstream of the gravity dam with fluid flow along this singular joint path system. Also shown are the two driving sub-wedges, a structural wedge and two resisting sub-wedges. Recall that there is no foundation drain present in this problem.

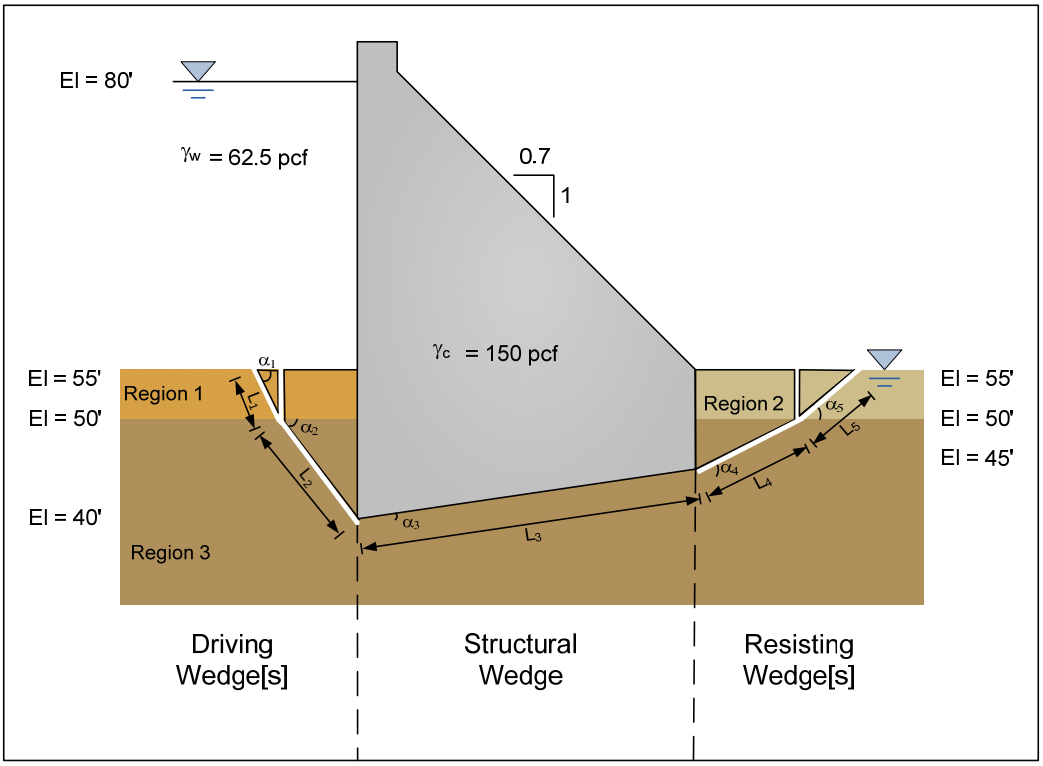

Figure 6.8. ETL 1110-2-256 hypothetical gravity dam embedded in a rock foundation with no rock foundation drain (Flow Options 5 or 6).

Recall also that the weight of the reservoir pool of water above the two Figure 6.8 driving sub-wedges is accounted for in this formulation by the Figure 6.3 vertical force V_i acting down on the top of each of these two sub-wedges (i = 1, 2), as noted in Figure 6.9. If a tailwater existed above the two downstream resisting sub-wedges, a vertical force V_i (with i = 4, 5) would act down on each of these sub-wedges 4 and 5 as well.

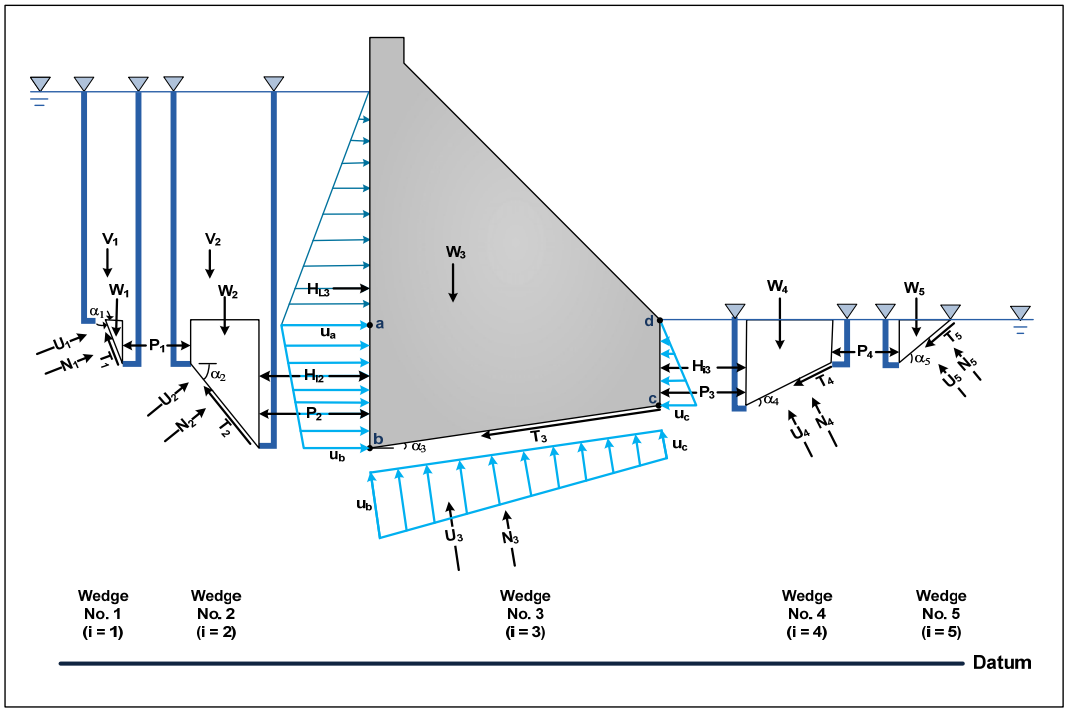

Figure 6.9. A Five wedge system for the ETL 1110-2-256 hypothetical gravity dam embedded in a rock foundation with no rock foundation drain (Flow Option 5).

Figure 6.9 depicts the water pressures in terms of pressure head acting at start and ending points along the base of each of the five wedges of the user defined potential slip plane. Figure 6.9 for Flow Option 5 is the same as Figure 6.7 for Flow Option 4 for the two driving sub-wedges and for the two resisting sub-wedges. It differs for the structural wedge in that Flow Option 5 assumes interslice water pressure forces while Flow Option 4 assumes no interslice water pressure forces. As Figure 6.7 shows (and Table 6.3 notes for this Flow Option 5), hydrostatic water pressures are assumed to act at the start and end points below each of the driving and resisting sub-wedges. For the two driving sub-wedges, a hydrostatic pool pressure head is assumed. For the two resisting sub-wedges, a hydrostatic tailwater pressure head is assumed. For the embedded portion of the structural wedge a steady state seepage in conjunction with a line of seepage methodology is used for a set of three rock joints extending from Figure 6.9 points *a* to *b*, from points *b* to *c* (along the potential slip plane at the base of the structural wedge), and from points *c* to *d*. This sequential rock joint flow path is used to establish the water pressure distribution acting on the upstream (left) and downstream (right) vertical faces of the structural wedge (i.e., wedge number 3) as well as normal to the base of the structural wedge (along the potential slip plane). A constant value for hydraulic conductivity is assumed within these three rock joint features when applying the line of seepage

methodology. The head loss in joint fluid flow occurs along the flow path *a* to *b*, *b* to *c* (corresponding to the potential slip plane below the structural wedge), and *c* to *d* due to the assumptions made in this Flow Option 5. With no foundation drain and for a constant value of rock joint hydraulic conductivity, the total head varies linearly along joint path *a* to *b*, *b* to *c*, and *c* to *d*. Bernoulli's Equation 1.5 (assuming a zero velocity head) in conjunction with Equation 1.8 allows for the calculation of water pressure along this series of joints. This aspect of the analysis is depicted in Figure 6.17b for the line labeled *E* = 0% (in Sub-section 6.4.1).

For Flow Option 5, while there are water pressures acting normal to the bases of all wedges and sub-wedges comprising the potential slip plane, there are no vertical interslice water pressure forces being considered between the driving sub-wedges and between the resisting sub-wedges. As Table 6.3 notes, only vertical interslice water pressures are assumed to act on both vertical (i.e., the upstream and downstream) slices defining the structural wedge, with equal but opposite horizontal water pressure forces acting on the adjacent driving wedge 2 (designated H_{I2}) and on resisting wedge 4 (designated H_{I3}). Recall that steady state seepage in conjunction with a line of seepage methodology with constant hydraulic conductivity for all three rock joints extending from Figure 6.9 points *a* to *b*, from points *b* to *c*, and from points *c* to *d*. And this sequential rock joint flow path establishes the water pressure distribution acting on the upstream (left) and downstream (right) vertical faces of the structural wedge (i.e., wedge number 3) as well as normal to the base of the structural wedge (along the potential slip plane).

Observe the pool's blue triangular horizontal distribution of water pressure acting normal to the upstream vertical face of the Figure 6.7 gravity dam (structural wedge *i*=3) to a depth of top of rock labeled as point *a*. These water pressures are hydrostatic pool pressures; with the water pressure u_a equal to γ_w times the difference in elevations of the pool and point a. The resultant of this triangular pressure distribution is designated as force H_{L3} and acts normal to its vertical upstream (left) face. This nomenclature is consistent with the Figures 6.3 and 6.4 notations of horizontal forces acting on the left face of the i^{th} wedge or sub-wedge. Note the interslice water pressure distribution extends from point *a* to point *b* in this figure for Flow Option 5. As discussed previously, vertical interslice water pressures are assumed to act on the upstream interface (*I2*) from points *a* to *b* that define the interface for wedge numbers 2 and 3. A similar situation of water

pressures exists along interslice *I3* between (structural) wedge number 3 and (resisting) sub-wedge number 4. If tailwater was present, the horizontal component of a hydrostatic water pressure distribution would act on the right face of the structural wedge (wedge number 3) and would be designated as H_{R3}. Because there are interslice water pressure forces acting from Figure 6.9 points *a* to *b* due to fluid flow down and around the structural wedge, there is an additional horizontal force H_{I2} that acts in addition to the H_{L3} hydrostatic horizontal pool force on the upstream face of the structural wedge. Fluid flow along the rock joint from point *c* to *d* results in the horizontal interslice force H_{I3} (for interslice *I3*). If tailwater were present, this horizontal force H_{I3} would act in addition to the H_{R3} hydrostatic horizontal tailwater force on the downstream (right) face of the structural wedge (i.e., wedge number 3).

6.2.3 Introduction to Flow Option 6

As an introduction to the assessment of uplift and interslice water forces by Flow Option 6, the Figure 6.1 hypothetical dam with its user defined slip plane is used. Figure 6.8 shows that this potential slip plane corresponds to a continuous series of connected rock joints from upstream to downstream of the gravity dam with fluid flow along this singular joint path system. Also shown are the two driving sub-wedges, a structural wedge and two resisting sub-wedges. Recall that there is no foundation drain present in this problem.

Recall also that the weight of the reservoir pool of water above the two Figure 6.8 driving sub-wedges is accounted for in this formulation by the Figure 6.3 vertical force V_i acting down on the top of each of these two sub-wedges (i = 1, 2), as noted in Figure 6.10. If a tailwater existed above the two downstream resisting sub-wedges, a vertical force V_i (with i = 4, 5) would act down on each of these sub-wedges 4 and 5 as well.

Figure 6.10 depicts the water pressures acting on the upstream face of the structural wedge (wedge number 3) and the forces acting on the five wedges of the user defined potential slip plane. The water pressures acting normal to the base of these five wedges are not depicted in this figure. For the driving, structural and resisting wedges/sub-wedges, steady state seepage in conjunction with a line of seepage methodology is used for the set of rock joints extending along the entire length of the Figure 6.10 potential slip

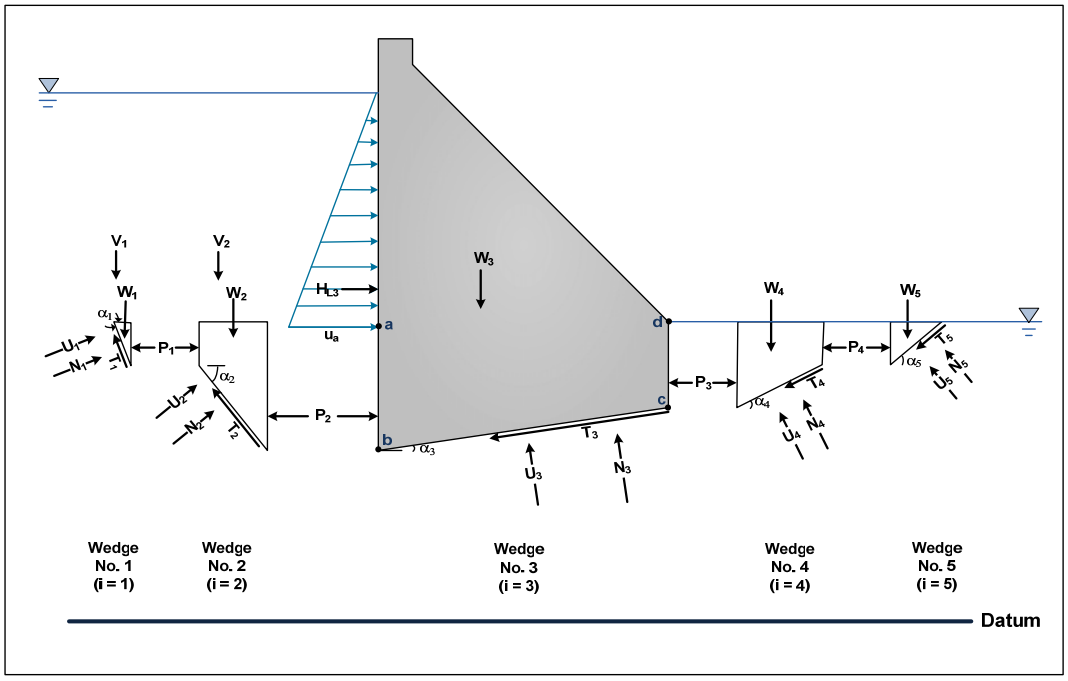

Figure 6.10. Five wedge system for the ETL 1110-2-256 hypothetical gravity dam embedded in a rock foundation with no rock foundation drain (Flow Option 6).

plane.[1] This sequential rock joint flow path is used to establish the water pressure distribution acting normal to the base of all five Figure 6.1 wedges. A constant value for hydraulic conductivity is assumed within the entire rock joint features when applying the Line of Seepage methodology. The head loss in joint fluid flow occurs along the entire length of the flow path corresponding to the potential slip plane due to the assumptions made in this Flow Option 6. With no foundation drain and for a constant value of rock joint hydraulic conductivity, the total head varies linearly along the entire path of interconnected rock joints. Bernoulli's Equation 1.5 (assuming a zero velocity head) in conjunction with Equation 1.8 allows for the calculation of water pressure along this series of joints. This aspect of the analysis is depicted in Figure 6.20b for the line labeled E = 0% (in Sub-section 6.5.1).

For Flow Option 6, while there are water pressures acting normal to the bases of all wedges and sub-wedges comprising the potential slip plane, there are no vertical interslice water pressure forces being considered between each of the five Figure 6.10 sub-wedges/wedges. In other words, the four vertical slices between the five driving, structural and resisting

[1] Refer to Appendix F for a description of the Line of Seepage Methodology used to define these water pressures.

sub-wedges/wedges do not contain (vertical) rock joints that allow for fluid flow nor contain a water pressure force acting normal to the faces of these four interslices. Consequently, there are no interslice water pressure forces acting normal to the four vertical interslices when using Flow Option 6, as noted in Table 6.3.

Observe the pool's blue triangular horizontal distribution of water pressure acting normal to the upstream vertical face of the Figure 6.10 gravity dam (structural wedge i=3) to a depth of top of rock labeled as point a. These water pressures are hydrostatic pool pressures; with the water pressure u_a equal to γ_w times the difference in elevations of the pool and point a. The resultant of this triangular pressure distribution is designated as force H_{L3} and acts normal to its vertical upstream (left) face. This nomenclature is consistent with the Figures 6.3 and 6.4 notations of horizontal forces acting on the left face of the i^{th} wedge or sub-wedge. If tailwater were present, the horizontal component of a hydrostatic water pressure distribution would act on the right face of the structural wedge (i.e., wedge number 3) and would be designated H_{R3}.

As stated earlier Flow Option 6 represents steady state seepage in conjunction with a line of seepage methodology of a potential slip plane that corresponds to a continuous series of connected rock joints from upstream to downstream of the gravity dam with fluid flow along this singular joint path system. Along each of the rock joints is the ability to define the particular type of aperture and thereby hydraulic conductivity it represents. For the example to be discussed in Section 6.5 a uniform constant aperture was established for the problem. A constant aperture for all joints reflects a constant hydraulic conductivity (Equation 1.17).

6.3 Problem 11: Sliding stability with no vertical interslice water pressure resultant forces for the ETL 1110-2-256 Gravity Dam example (Flow Option 4)

A deterministic analysis of typical static loading conditions for multiple wedge systems of the Figure 6.1 ETL 1110-2-256 Gravity Dam cross-section with no foundation drain is presented in Figure 6.11. Recall that Table 6.1 lists the values of unit weights and Mohr-Coulomb effective shear strength parameters for the three rock foundation Regions and that Table 6.2 summarizes the lengths and orientations of the base of each of the five wedges/sub-wedges. This analysis was conducted to demonstrate the application of the general wedge equation to the sliding analysis of multiple

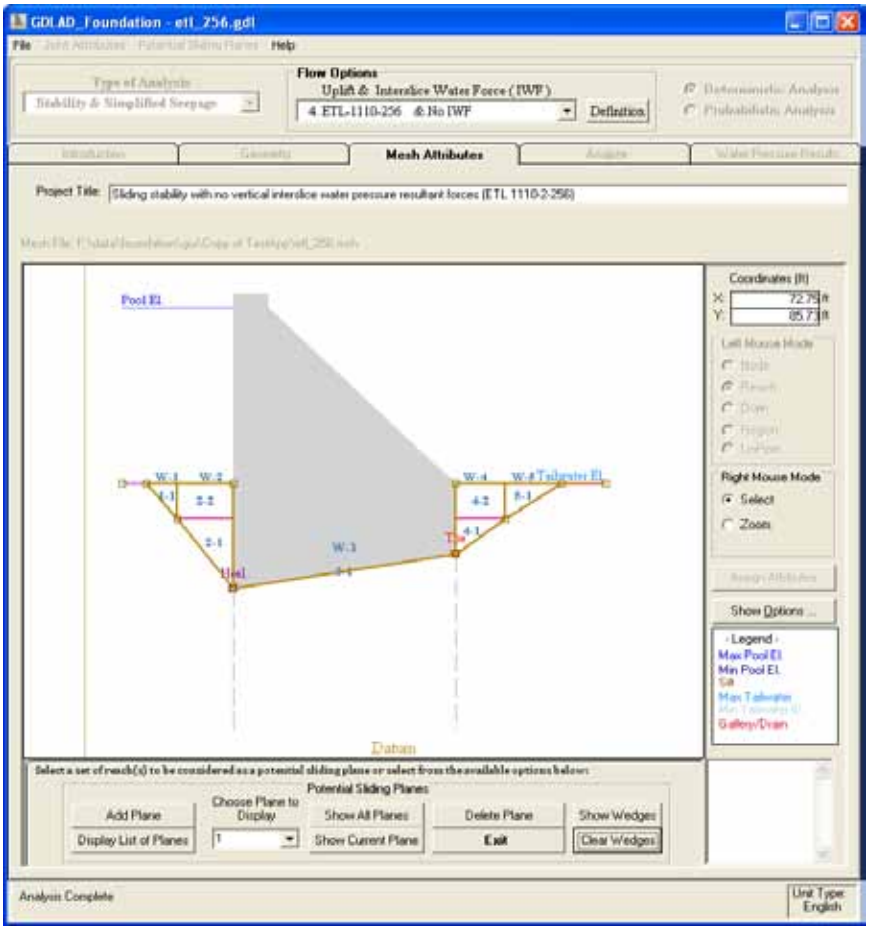

Figure 6.11. Geometry of dam with a five wedge system.

wedge systems. The case considered is for a pool at el 80 ft and tailwater at el 55 ft. Top of rock is at el 55 ft. This hypothetical embedded concrete gravity dam is 27 ft high above rock surface on the upstream side and approximately 30 ft wide. It is embedded 15 ft into rock at its heel and embedded 10 ft into rock at its toe. The five wedge system developed to analyze the stability of this system can be seen in the Figure 6.11 as the brown lines defining both wedges and sub wedges.

The first number in each triangular or rectangular geometric feature designates the wedge number, while the second number is a count of the geometric features comprising the particular sub-wedge. Three material regions were formed in the Geometry tab and three material properties were defined and mapped to the three regions in the Mesh Attributes tab (as defined in Chapter 3) and illustrated in Figure 6.12.

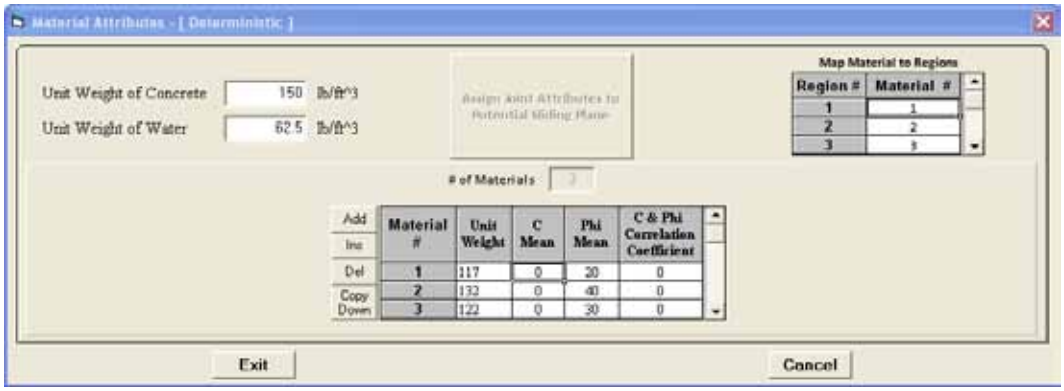

Figure 6.12. Table of properties of materials and the mapping of regions.

The resulting computed factor of safety (*FS*) against sliding for this multiple wedge system was found to be 1.992 with a residual imbalance Force of -0.01 kips after 9 iterations (see Figure 6.13). The matching of results was exceptional when compared with the example from ETL 1110-2-256 reporting a computed value of *FS*=2.0 and a residual imbalance of -0.18 kips with a tolerance for convergence of 100 lbs. Appendix A summarizes the results from these iterative hand-calculations given in ETL 1110-2-256.

6.3.1 Discussion of drain efficiency with Flow Option 4

An essential feature of gravity dams is the inclusion of a line of drains, i.e., individual drains spaced at regular intervals in plan along the axis of the dam (in Figure 6.14a), which extend from the gallery into the rock foundation. These drains serve the critical task of intersecting rock faults, fissures and/or joints within the rock foundation through which water flows beneath the footprint of the dam. Functioning drains play a vital role in the stability of the dam by relieving water pressures acting to uplift the dam.

One non-site specific approach used for characterizing the magnitude of the uplift pressure as well as quantifying the role the drains play in controlling the magnitude of the uplift pressures is by use of a parameter referred to as the efficiency of the drain (*E*). Drain efficiency, *E*, is expressed as a percentage ranging from 0 to 100. A value of *E*=100 corresponds to the case of the drains being fully effective and a value of *E*=0 corresponds to the case of the drains being fully clogged and ineffective. The authors of this report observe that Figure 1.2, taken from EM 111-2-2200, uses a lower case *e* to designate drain efficiency. This document uses a capital *E* to designate drain efficiency.

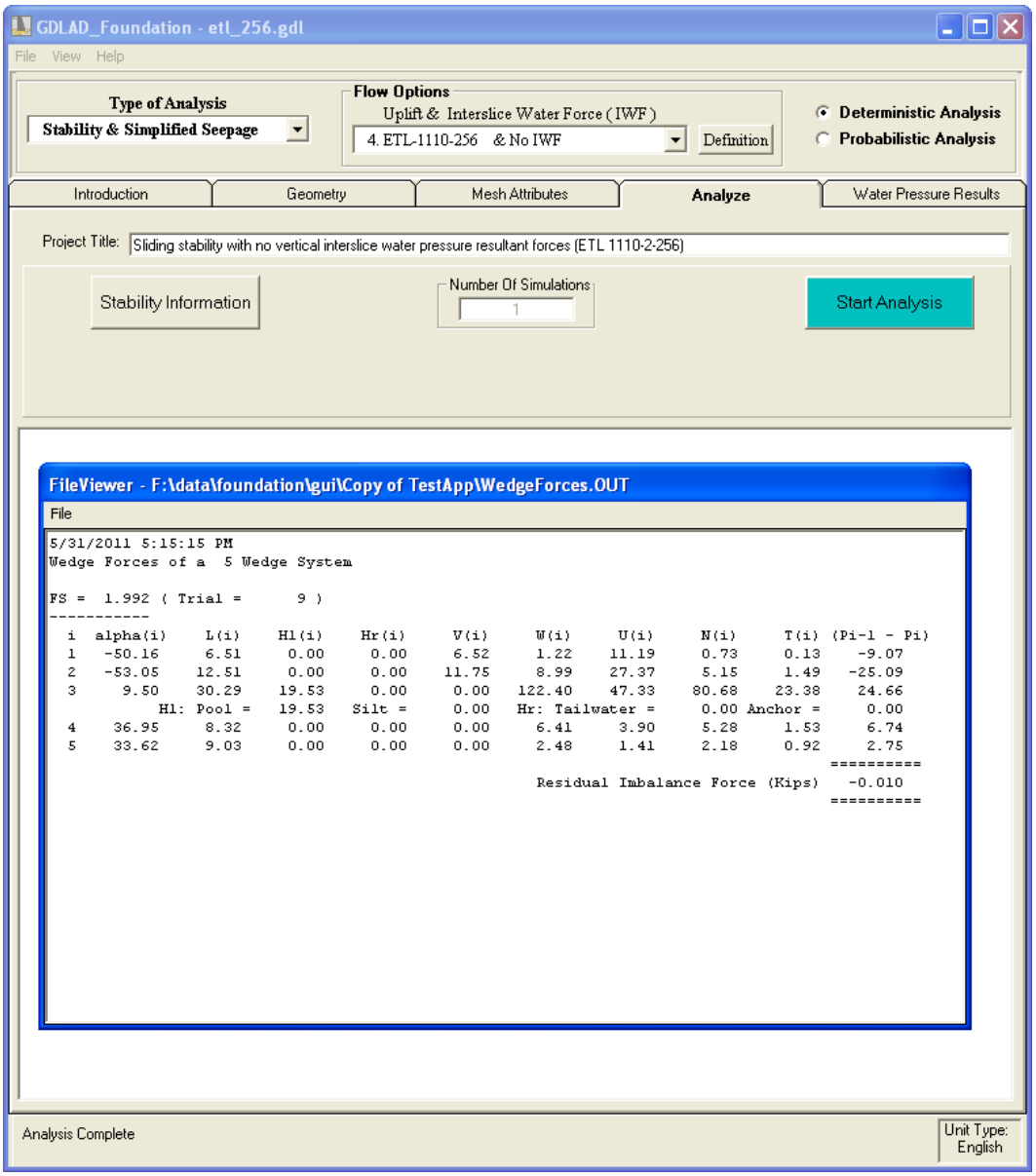

Figure 6.13. Resultant factor of safety with residual imbalance of a five wedge system with Flow Option 4.

Corps of Engineers Engineer Manuals 1110-2-2200, “Gravity Dam Design”, and 1110-2-2100, “Stability Analysis of Concrete Structures”, restrict the value of E to no greater than 50 percent (E=50). These manuals state that if foundation testing and flow analysis provide supporting justification, the drain efficiency can be increased beyond 50 percent. The analysis and/or design documentation must contain supporting data to justify the E value used.

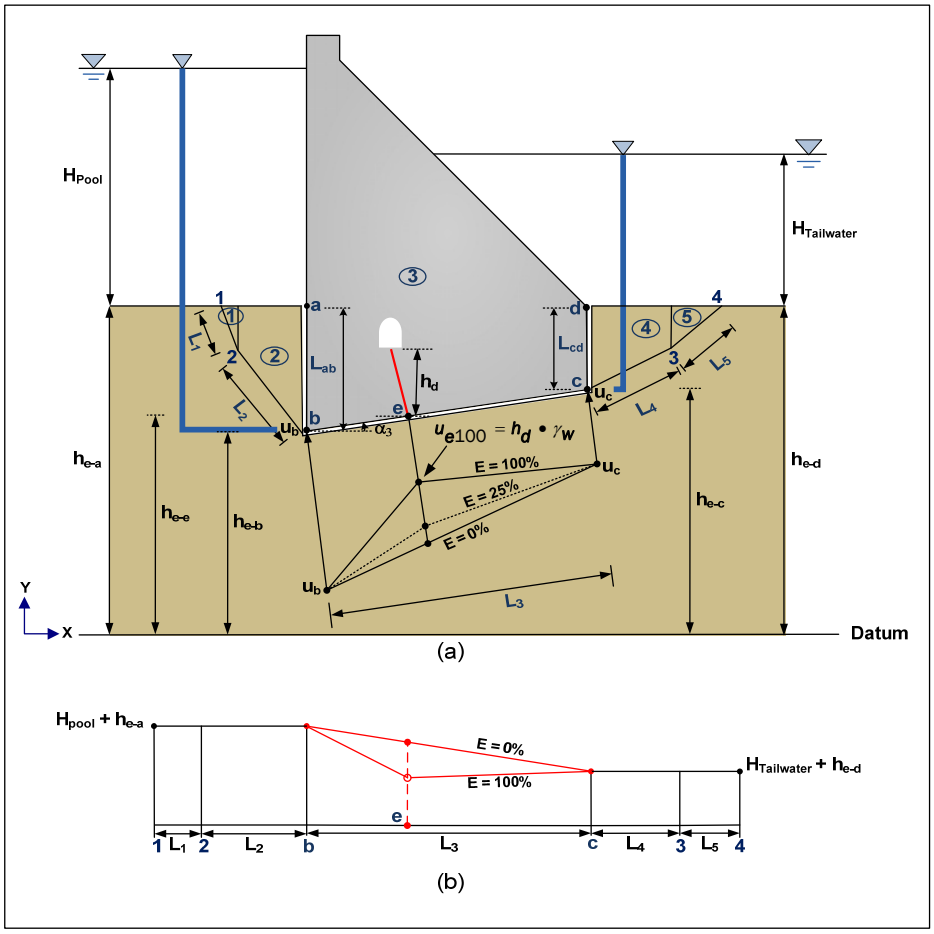

Figure 6.14. Drain efficiency of a closed drainage gallery system with Flow Option 4 (a) Wedge and uplift pressure diagram (water pressures not to scale) (b) Variation on total head along potential slip plane.

Recall that Flow Option 4 reflects the ETL 1110-2-256 (1981) uplift pressure assumptions that the authors of this report infer fluid flow within the singular, inter-connected jointed rock feature that is specified by the user to be a potential slip plane extending from upstream to downstream of the gravity dam cross-section embedded within a rock foundation. These assumptions are discussed in Subsection 6.2.1, using Figure 6.7.

6.3.1.1 Closed drainage gallery system

Figure 6.14a shows an idealized cross-section of the uplift pressure distribution for a closed drainage gallery system along a sloping base. The vertical distance from the base of the gallery to the point *e*, defined by the intersection of the line of drains (drawn in red) and the user defined potential slip plane is h_d. In this example, the user defined potential slip plane corresponds to the dam-to-rock foundation interface (i.e., the base

of the dam). For the closed drainage gallery system of Figure 6.14a, h_d < [($H_{Tailwater}$+$h_{e\text{-}d}$) – $h_{e\text{-}e}$].

Figure 6.14b displays total head versus distance measured along the user defined slip plane. Figure 6.14b shows a constant hydrostatic water pressure head from point 1 to point *b* (along the base of the two driving sub-wedges) with a total head of H_{pool}+$h_{e\text{-}a}$; and point c to point 4 (along the base of the two resisting sub-wedges) with a total head of $H_{Tailwater}$ + $h_{e\text{-}d}$. There is a linear variation between points *b* and *c* (along the base of the structural wedge) when the drain efficiency *E*=0 (i.e., the case for no drain or a fully clogged drain). At 100 percent drain efficiency, *E*=100, the vertical distance from point *e* up the red dash line to the red circle is comparable to the height (h_d) of Figure 6.14a. From this point, the 100 percent drain efficiency curve can be drawn by connecting a line to the point *b* and drawing a line to point *c*.

6.3.1.2 Open drainage gallery system

Figure 6.15a shows an idealized cross-section of the uplift pressure distribution for an open drainage gallery system along a sloping base. The vertical distance from tailwater to the point *e*, defined by the intersection of the line of drains (drawn in red) and user defined potential slip plane is h_d. For the open drainage gallery system of Figure 6.15a, $h_d = H_{Tailwater}$+ ($h_{e\text{-}d} – h_{e\text{-}e}$). In this example, the user defined potential slip plane corresponds to the dam-to-rock foundation interface (i.e., the base of the dam).

Figure 6.15b displays total head versus distance measured along the user defined slip plane. Figure 6.15b shows a constant hydrostatic water pressure head from point 1 to point *b* (along the base of the two driving sub-wedges) with a total head of H_{pool}+$h_{e\text{-}a}$; and point c to point 4 (along the base of the two resisting sub-wedges) with a total head of $H_{Tailwater}$ + $h_{e\text{-}d}$. There is a linear variation between points b and c (along the base of the structural wedge) when the drain efficiency *E*=0 (i.e., the case for no drain or a fully clogged drain). At 100 percent drain efficiency, *E*=100, the red circle is at the height ($H_{Tailwater}$ + $h_{e\text{-}d}$) of Figure 6.15a. From this point, the 100 percent drain efficiency curve can be drawn by connecting a line to the point *b* and drawing a horizontal line to point *c*.

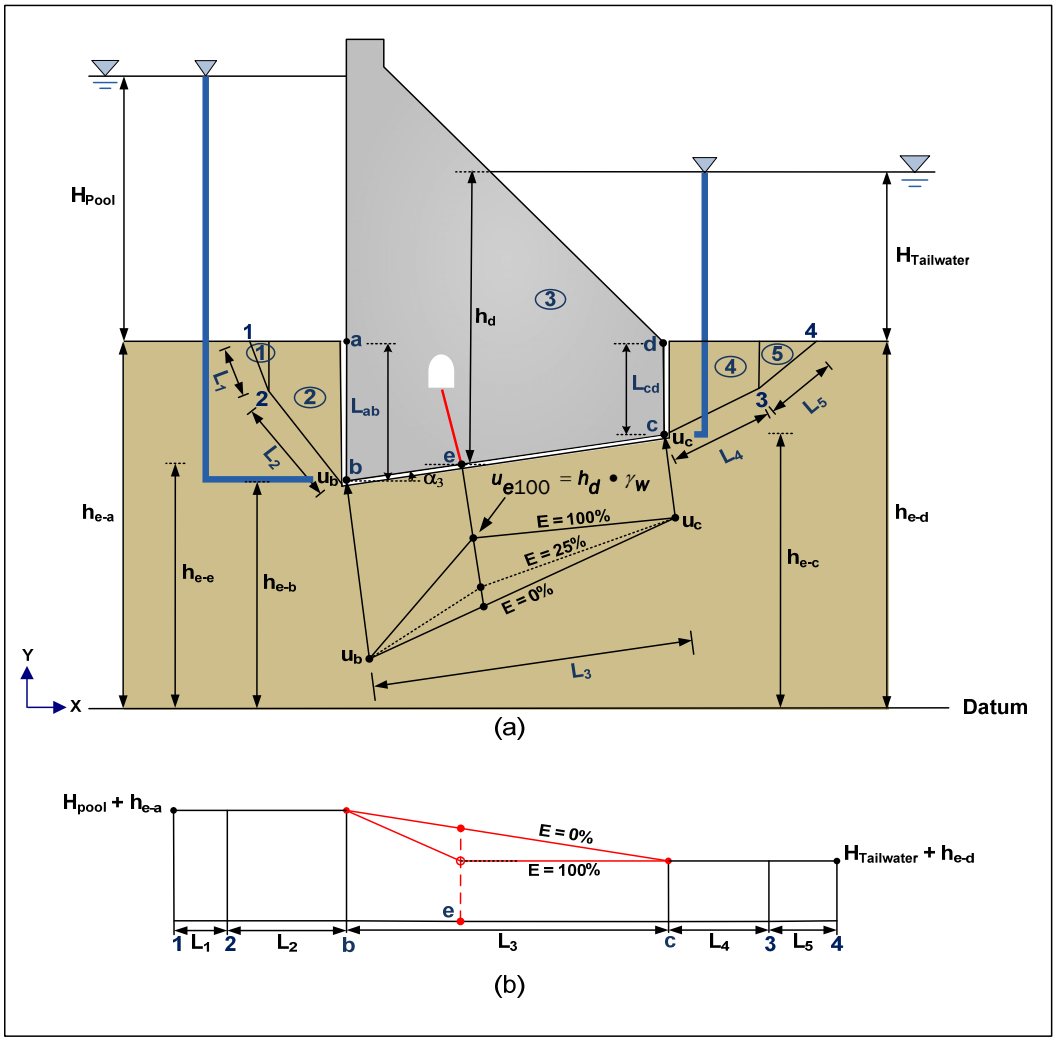

Figure 6.15. Drain efficiency of an open drainage gallery system with Flow Option 4 (a) Wedge and uplift pressure diagram (water pressures not to scale) (b) Variation on total head along potential slip plane.

6.3.2 Discussion of drain efficiency *E* value with Flow Option 4

In Flow Option 4 the uplift pressure below the structural wedge is defined by the value the user assigns to the drain efficiency *E*. Recall that drain efficiency, *E*, is expressed as a percentage ranging from 0 to 100. A value of *E*=100 corresponds to the case of the drains being fully effective and a value of *E*=0 corresponds to the case of the drains being fully clogged and ineffective. Corps of Engineers Engineer Manuals 1110-2-2200, "Gravity Dam Design", and 1110-2-2100, "Stability Analysis of Concrete Structures", restrict the value of *E* to no greater than 50 percent (*E*=50). These manuals state that if foundation testing and flow analysis provide supporting justification, the drain efficiency can be increased beyond 50 percent. The analysis and/or design documentation must contain supporting data to

justify the *E* value used. For the user specified value for *E*, the total head is first computed at point *e* for the Figure 6.14b case of a closed drainage gallery system or at point *e* for the Figure 6.15b case of a open drainage gallery system by linear interpolation (and measured downward from the *E* = 0 line). Bernoulli's Equation 1.5 (assuming a zero velocity head) in conjunction with Equation 1.8 allows for the calculation of water pressure at point *e*.

6.4 Problem 12: Sliding stability with simplified seepage Along the structural wedge (Flow Option 5)

A deterministic analysis of typical static loading conditions for multiple wedge systems of the Figure 6.1 ETL 1110-2-256 Gravity Dam cross-section with no foundation drain is presented in Figure 6.11. Recall that Table 6.1 lists the values of unit weights and Mohr-Coulomb effective shear strength parameters for the three rock foundation Regions and that Table 6.2 summarizes the lengths and orientations of the base of each of the five wedges/sub-wedges. This analysis was conducted to demonstrate the application of the general wedge equation to the sliding analysis of multiple wedge systems. In this section, steady state seepage in conjunction with the line of seepage methodology along the structural wedge is taken into account. The case of the hypothetical embedded concrete gravity dam considered is identical to the one in Section 6.3 for a pool at el 80 ft and tailwater at el 55 ft with top of rock at el 55 ft. The five wedge system developed to analyze the stability of this system can be seen in the Figure 6.11 as the brown lines defining both wedges and sub wedges. The first number in each triangular or rectangular geometric feature designates the wedge number, while the second number is a count of the geometric features comprising the particular sub-wedge. Three material regions were formed within the Geometry tab and three material properties were defined and mapped to the three regions in the Mesh Attributes tab (as defined in Chapter 3) and illustrated in Figure 6.12.

From the water pressure distributions illustrated in Figure 6.9 and described in Section 6.2, calculations were performed and the resulting computed factor of safety (*FS*) against sliding for this multiple wedge system was found to be 2.031with a residual imbalance force of 0.044 kips after 7 iterations with a tolerance for convergence of 100 lbs (see Figure 6.16).

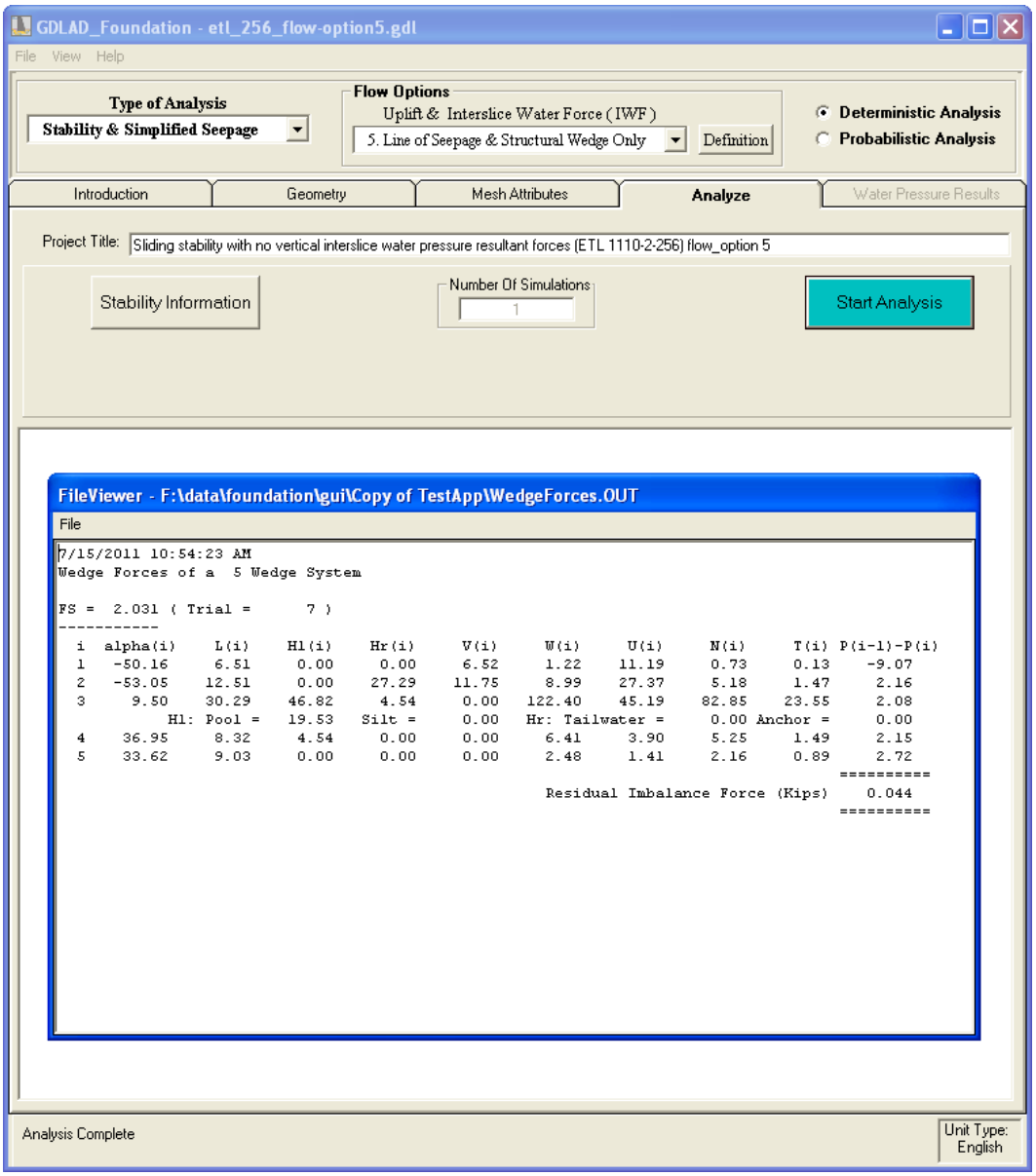

Figure 6.16. Resultant factor of safety with residual imbalance of a five wedge system with Flow Option 5.

The results from the Flow Option 5 sliding stability analysis indicate a (slightly) more stable Figure 6.1 non-overflow gravity dam cross-section than for the analysis using Flow Option 4; computing a Factor of Safety (*FS*) against sliding of 2.03 as compared to 1.99. This increase in computed value for the factor of safety (*FS*) is attributed to the fact that water pressures acting on the structural wedge resulting from the Flow Option 5 line of seepage analysis (Figure 6.9) along the perimeter of the structural wedge (wedge number 3) are less detrimental than the water pressures (resulting from the loss in head concentrated below the structural wedge) assumed for Flow Option 4 (Figure 6.7).

6.4.1 Discussion of drain efficiency with Flow Option 5

Flow Option 5 differs from Flow Option 4 by the fact that for the embedded portion of the structural wedge, a steady state seepage in conjunction with a line of seepage methodology is used for a set of three rock joints extending from Figure 6.9 points *a* to *b*, from points *b* to *c* (along the potential slip plane at the base of the structural wedge), and from points *c* to *d*. These assumptions are discussed in Subsection 6.2.2. It makes use of the U.S. Army Corps of Engineers non-site specific approach for characterizing the magnitude of the uplift pressure as well as quantifying the role the drains play in controlling the magnitude of the uplift pressures by the use of a parameter referred to as the efficiency of the drain (*E*). Recall that Drain efficiency, *E*, is expressed as a percentage ranging from 0 to 100. A value of *E*=100 corresponds to the case of the drains being fully effective and a value of *E*=0 corresponds to the case of the drains being fully clogged and ineffective.

6.4.1.1 Closed drainage gallery system

Figure 6.17a shows an idealized cross-section of the uplift pressure distribution for a closed drainage gallery system along a sloping base. The vertical distance from the base of the gallery to the point *e*, defined by the intersection of the line of drains (drawn in red) and the user defined potential slip plane is h_d. In this example, the user defined potential slip plane corresponds to the dam-to-rock foundation interface (i.e., the base of the dam). For the closed drainage gallery system of Figure 6.17a, $h_d < [(H_{Tailwater}+h_{e\text{-}d}) - h_{e\text{-}e}]$.

Figure 6.17b displays total head versus distance measured along the perimeter of the structural wedge that is embedded within the rock foundation. Figure 6.17b also shows a constant hydrostatic water pressure head at point *a* with a total head of $H_{pool}+h_{e\text{-}a}$, and at point *d* with a total head of $H_{Tailwater} + h_{e\text{-}d}$. There is a linear variation between points *a*, *b*, *e*, *c,* and *d* (i.e., along the embedded perimeter of the structural wedge) when the drain efficiency *E*=0 (i.e., the case for no drain or a fully clogged drain). At 100 percent drain efficiency, *E*=100, the vertical distance from point *e* up the red dash line to the red circle is comparable to the total head of $h_d+h_{e\text{-}e}$ of Figure 6.17a. From this point, the 100 percent drain efficiency curve can be drawn by connecting a line to the point *b* and to the point *c*.

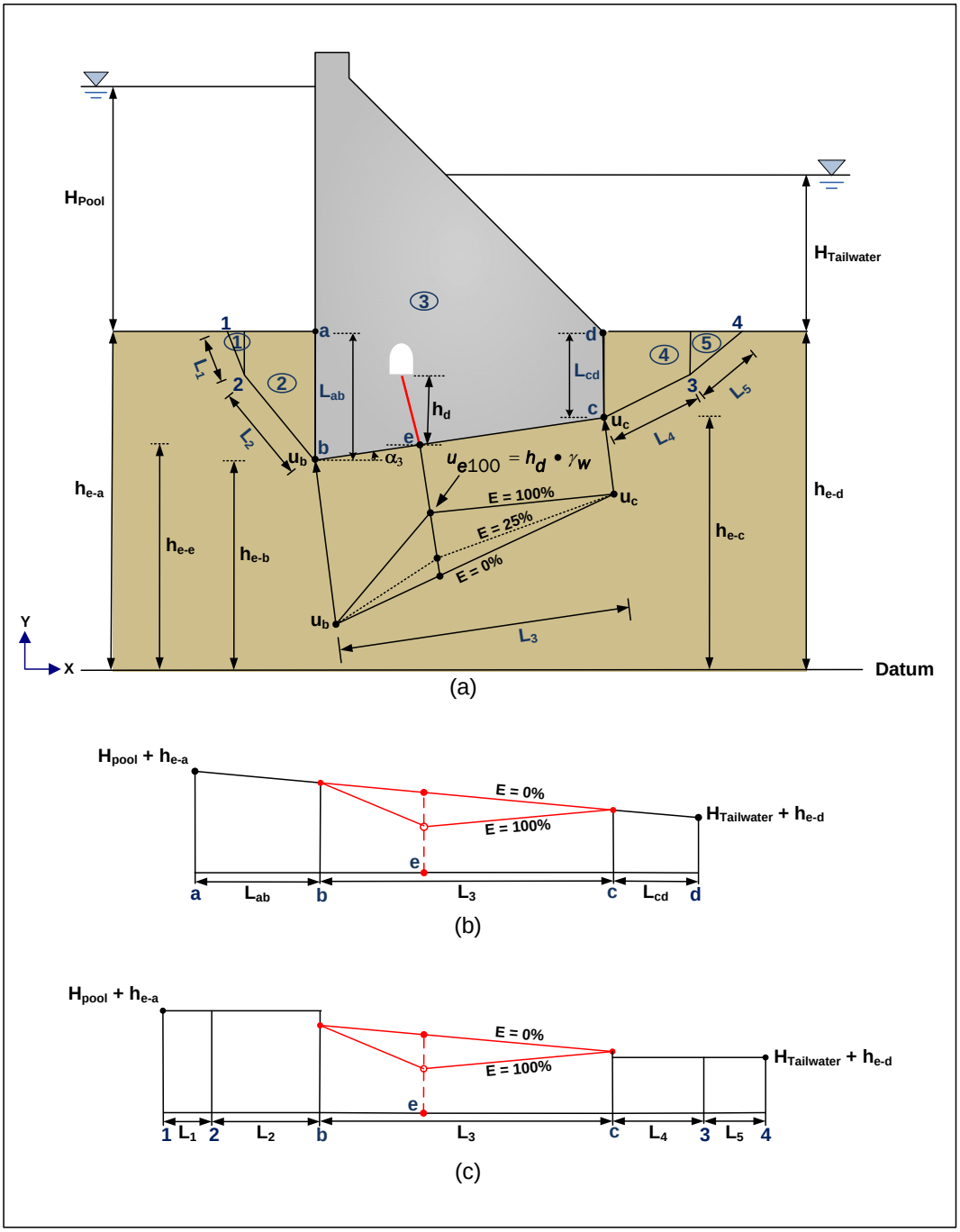

Figure 6.17. Drain efficiency of a closed drainage gallery system with Flow Option 5. (a) Wedge and uplift pressure diagram (water pressures not to scale) (b) Variation on total head along embedded part of the concrete gravity dam (c) Variation on total head along the slip plane.

Figure 6.17c displays total head versus distance measured along the user defined slip plane. Figure 6.17c also shows a constant hydrostatic water pressure head from point 1 to point 2 to point *b* (along the base of the two driving sub-wedges) with a total head of $H_{pool}+h_{e\text{-}a}$; and from point *c* to

point 3 to point 4 (along the base of the two resisting sub-wedges) with a total head of $H_{Tailwater} + h_{e\text{-}d}$. The total head distribution along the embedded portion of the structural wedge (i.e., *a*, *b*, *e*, *c,* and *d*) comes from Figure 6.17b.

6.4.1.2 Open drainage gallery system

Figure 6.18a shows an idealized cross-section of the uplift pressure distribution for an open drainage gallery system along a sloping base. The vertical distance from tailwater to the point *e*, defined by the intersection of the line of drains (drawn in red) and user defined potential slip plane is h_d. For the open drainage gallery system of Figure 6.18a, $h_d = H_{Tailwater} + (h_{e\text{-}d} - h_{e\text{-}e})$. In this example, the user defined potential slip plane corresponds to the dam-to-rock foundation interface (i.e., the base of the dam).

Figure 6.18b displays total head versus distance measured along the along the perimeter of the structural wedge that is embedded within the rock foundation. Figure 6.18b also shows a constant hydrostatic water pressure head at point *a* with a total head of $H_{pool}+h_{e\text{-}a}$; and at point *d* with a total head of $H_{Tailwater} + h_{e\text{-}d}$. There is a linear variation between points *a*, *b*, *e*, *c,* and *d* (i.e., along the embedded perimeter of the structural wedge) when the drain efficiency E=0 (i.e., the case for no drain or a fully clogged drain). At 100 percent drain efficiency, E=100, the vertical distance from point e up the red dash line to the red circle is comparable to the total head of $h_d+h_{e\text{-}e}$ of Figure 6.18a. From this point, the 100 percent drain efficiency curve can be drawn by connecting a line to the point *b* and to point *c*.

Figure 6.18c displays total head versus distance measured along the user defined slip plane. Figure 6.18c also shows a constant hydrostatic water pressure head from point 1 to point 2 to point *b* (along the base of the two driving sub-wedges) with a total head of $H_{pool}+h_{e\text{-}a}$; and from point *c* to point 3 to point 4 (along the base of the two resisting sub-wedges) with a total head of $H_{Tailwater} + h_{e\text{-}d}$. The total head distribution along the embedded portion of the structural wedge (i.e., *a*, *b*, *e*, *c,* and *d*) comes from Figure 6.18b.

6.4.2 Discussion of drain efficiency *E* value with Flow Option 5

In Flow Option 5 the uplift pressure below the structural wedge is defined by the value the user assigns to the drain efficiency *E*. Recall that Drain efficiency, *E*, is expressed as a percentage ranging from 0 to 100. A value of

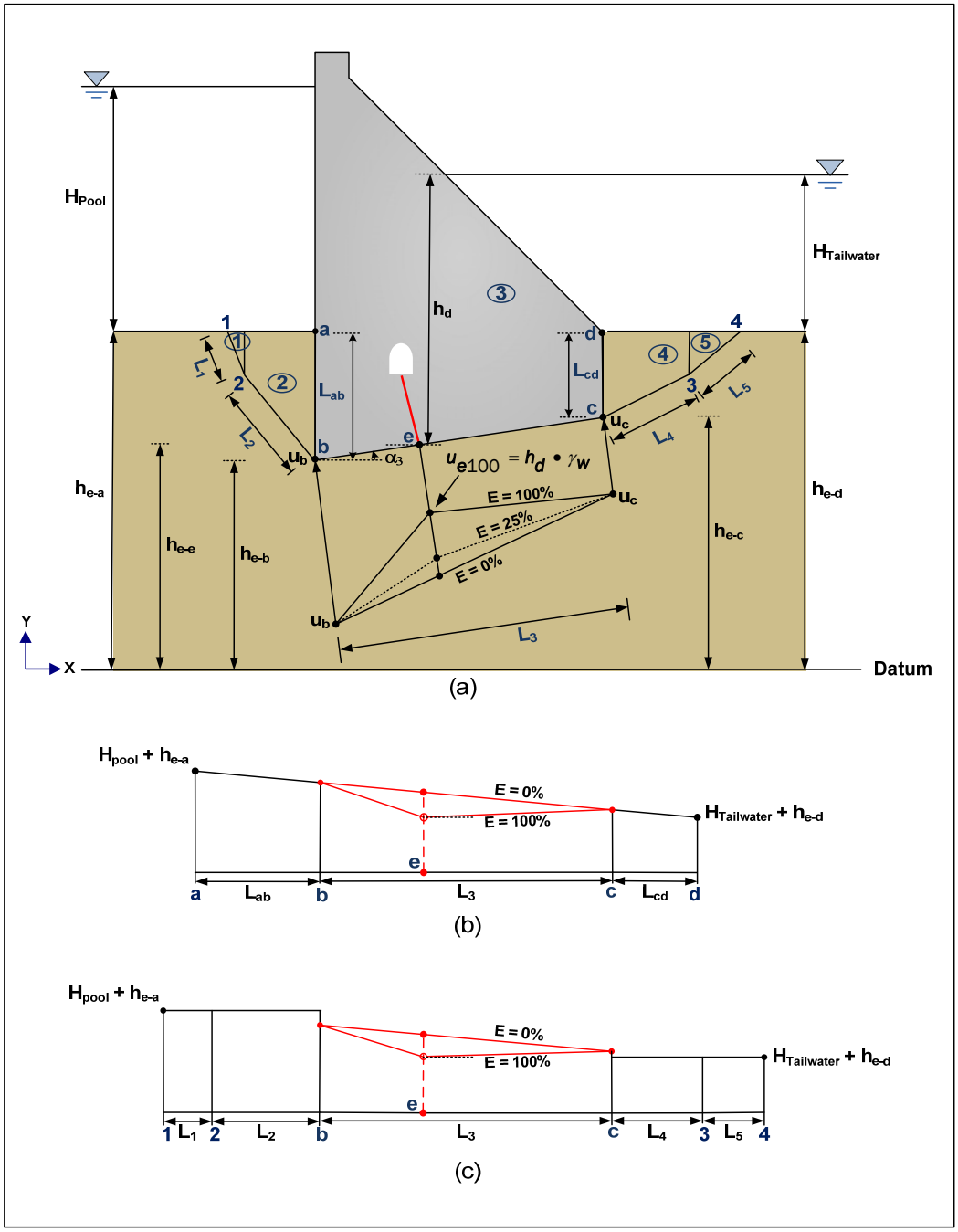

Figure 6.18. Drain efficiency of an open drainage gallery system with Flow Option 5. (a) Wedge and uplift pressure diagram (water pressures not to scale) (b) Variation on total head along embedded part of the concrete gravity dam (c) Variation on total head along the slip plane.

E=100 corresponds to the case of the drains being fully effective and a value of *E*=0 corresponds to the case of the drains being fully clogged and ineffective. Corps of Engineers Engineer Manuals 1110-2-2200, "Gravity Dam Design", and 1110-2-2100, "Stability Analysis of Concrete Structures",

restrict the value of *E* to no greater than 50 percent (*E*=50). These manuals state that if foundation testing and flow analysis provide supporting justification, the drain efficiency can be increased beyond 50 percent. The analysis and/or design documentation must contain supporting data to justify the *E* value used. For the user specified value for *E*, the total head is first computed at point *e* for the Figure 6.17b and c case of a closed drainage gallery system or at point *e* for the Figure 6.18b and c case of a open drainage gallery system by linear interpolation (and measured downward from the *E* = 0 line). Bernoulli's Equation 1.5 (assuming a zero velocity head) in conjunction with Equation 1.8 allows for the calculation of water pressure at point *e*.

6.5 Problem 13: Sliding stability using the line of seepage method with uniform permeability and no interslice water pressure resultant forces (Flow Option 6)

A deterministic analysis of typical static loading conditions for multiple wedge systems of the Figure 6.1 ETL 1110-2-256 Gravity Dam cross-section with no foundation drain is presented in Figure 6.11. Recall that Table 6.1 lists the values of unit weights and Mohr-Coulomb effective shear strength parameters for the three rock foundation Regions and that Table 6.2 summarizes the lengths and orientations of the base of each of the five wedges/sub-wedges. This analysis was conducted to demonstrate the application of the general wedge equation to the sliding analysis of multiple wedge systems. In this section, the line of seepage methodology along the entire length of the slip plane is considered and a uniform constant conducting aperture of 5.904E-3 in. was established for the problem. Recall that a constant aperture for all rock joints reflects a constant hydraulic conductivity (Equation 1.17).[1] The case of the hypothetical embedded concrete gravity dam considered is identical to the one in

[1] In Flow Option 6, different rock joints may be assigned different values for hydraulic conductivity. Appendix F discusses the Line of Seepage methodology used to compute uplift water pressure acting within a single flow path consisting of a series of rock joints for this flow option and to account for a variation in values of hydraulic conductivity among the rock joint features.

Assignment of value(s) for the hydraulic conductivity to the various joint reaches for Flow Option 6 starts with "Joint Attributes" item of the Menu bar, as shown in Figure 3.35(a). For a deterministic analysis, the rock "Joint Attributes" are assigned values to each reach number as shown in Figure 3.49(b). Observe that each reach along the potential sliding plane (six reaches for the example shown in this figure) receives a unique value of Mechanical Aperture (E) and JRC, value of conducting aperture (e), or values of hydraulic conductivity. GDLAD_Foundation does not require that the values assigned to all reaches be the same. For a probabilistic analysis, the rock joint reach attributes are assigned mean values and values characterizing the statistical dispersion for the data (expressed in terms of its standard deviation, STD, or its coefficient of variation, COV) to each reach number as shown in Figure 3.81, along with the designation of its distribution type (normal, lognormal, uniform, etc).

section 6.3 for a pool at el 80 ft and tailwater at el 55 ft with top of rock at el 55 ft. The five wedge system developed to analyze the stability of this system can be seen in the Figure 6.11 as the brown lines defining both wedges and sub wedges. The first number in each triangular or rectangular geometric feature designates the wedge number, while the second number is a count of the geometric features comprising the particular sub-wedge. Three material regions were formed within the Geometry tab and three material properties were defined and mapped to the three regions in the Mesh Attributes tab (as defined in Chapter 3) and illustrated in Figure 6.12.

By using the Appendix F Line of Seepage Formulation to determine the uplift pressure forces acting normal to the base of each wedge, stability calculations were performed. The resulting computed factor of safety (*FS*) against sliding for this multiple wedge system was found to be 1.969 with a residual imbalance force of 0.082 kips after 7 iterations with a tolerance for convergence of 100 lbs (see Figure 6.19).

6.5.1 Discussion of drain efficiency with Flow Option 6

Flow Option 6 differs from Flow Option 5 by the fact that for the entire length of potential slip plane and not just the embedded portion of the structural wedge, a steady state seepage in conjunction with a line of seepage methodology is used for the series of rock joints defining the potential slip plane. These assumptions are discussed in Subsection 6.2.3. It makes use of the U.S. Army Corps of Engineers non-site specific approach for characterizing the magnitude of the uplift pressure as well as quantifying the role the drains play in controlling the magnitude of the uplift pressures is by use of a parameter referred to as the efficiency of the drain (*E*). Recall that Drain efficiency, *E*, is expressed as a percentage ranging from 0 to 100. A value of *E*=100 corresponds to the case of the drains being fully effective and a value of *E*=0 corresponds to the case of the drains being fully clogged and ineffective.

6.5.1.1 Closed drainage gallery system

Figure 6.20a shows an idealized cross-section of the uplift pressure distribution for a closed drainage gallery system along a sloping base.[1] The

[1] A constant value for hydraulic conductivity is assumed within the entire rock joint features when applying the Line of Seepage methodology for this figure.

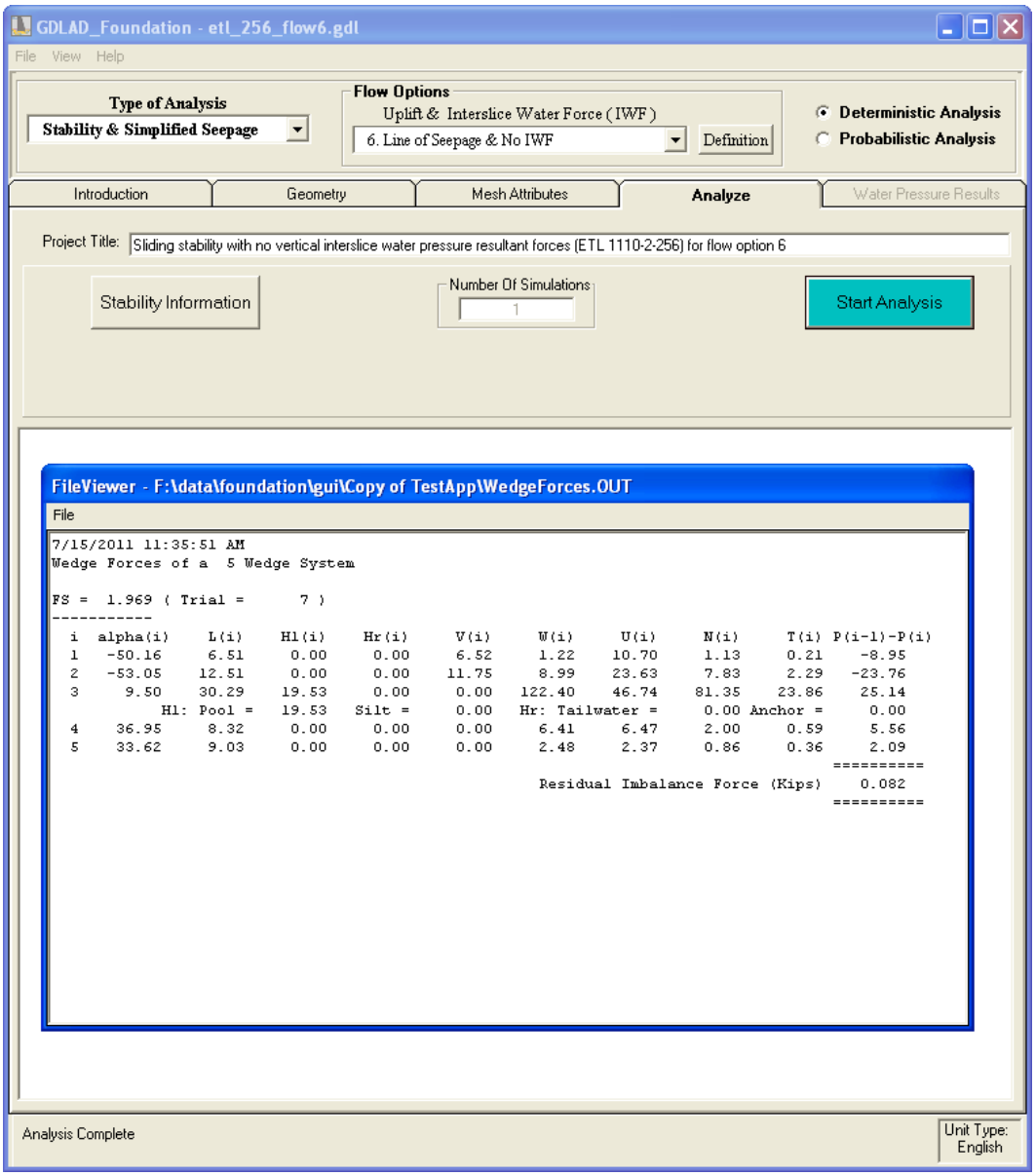

Figure 6.19. Resultant factor of safety with residual imbalance of a five wedge system with Flow Option 6.

vertical distance from the base of the gallery to the point *e*, defined by the intersection of the line of drains (drawn in red) and the user defined potential slip plane is h_d. In this example, the user defined potential slip plane corresponds to the dam-to-rock foundation interface (i.e., the base of the dam). For the closed drainage gallery system of Figure 6.20a, $h_d < [(H_{Tailwater}+h_{e\text{-}d}) - h_{e\text{-}e}]$.

Figure 6.20b displays total head versus distance measured along the user defined slip plane. Figure 6.20b also shows a constant hydrostatic water pressure head at point 1 with a total head of $H_{pool}+h_{e\text{-}a}$; and at point 4 with a

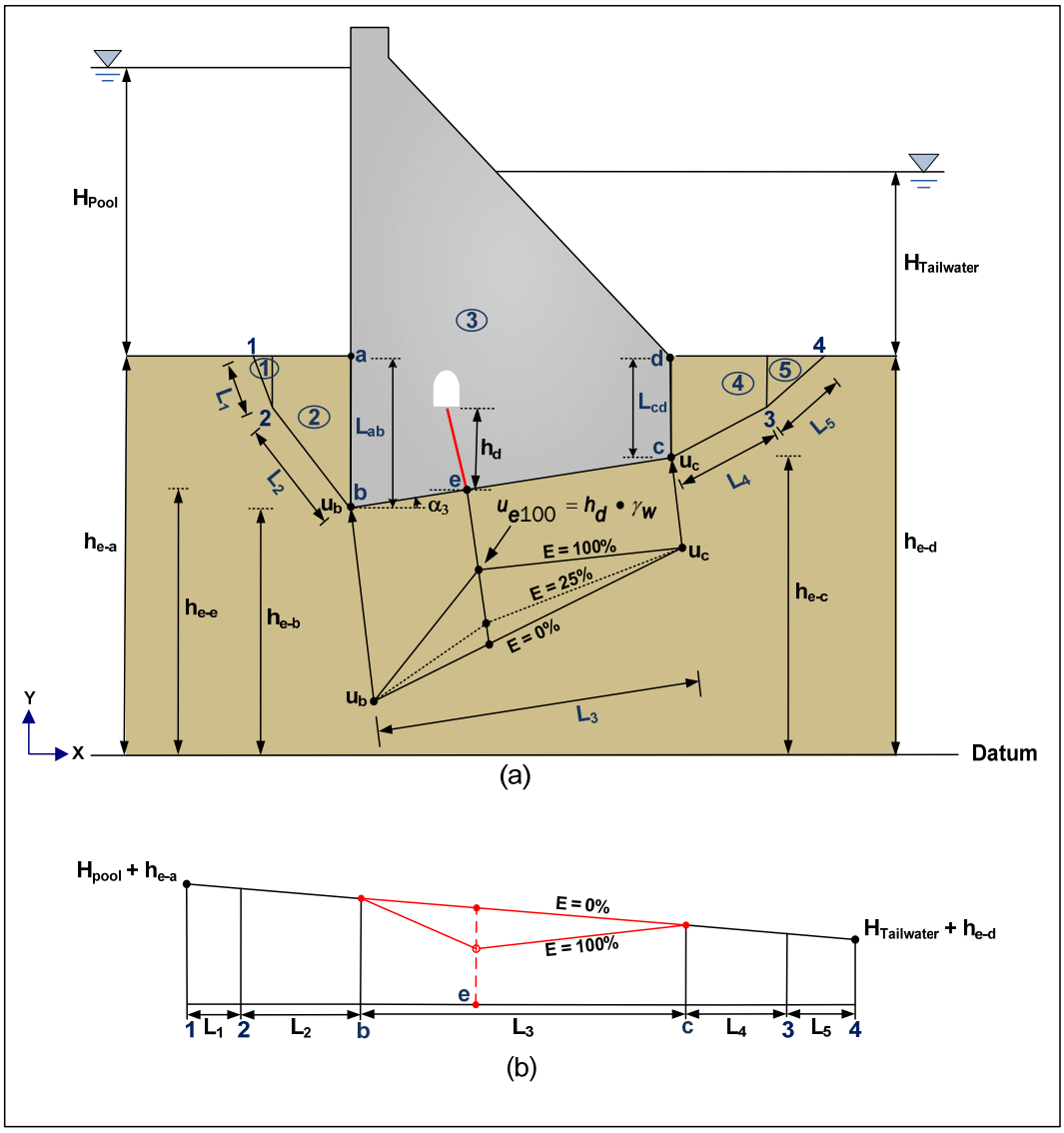

Figure 6.20. Drain efficiency of a closed drainage gallery system with Flow Option 6. (a) Wedge and uplift pressure diagram (water pressures not to scale) (b) Variation on total head along potential slip plane.

total head of $H_{Tailwater} + h_{e\text{-}d}$. There is a linear variation between points 1, 2, *b*, *e*, *c*, 3, and 4 (i.e., along the potential slip plane) when the drain efficiency, E=0 (i.e., the case for no drain or a fully clogged drain). At 100 percent drain efficiency, E=100, the vertical distance from point e up the red dash line to the red circle is comparable to the total head of h_d+$h_{e\text{-}e}$ of Figure 6.20a. From this point, the 100 percent drain efficiency curve can be drawn by connecting a line to the point *b* and drawing a line to point *c*.

6.5.1.2 *Open drainage gallery system*

Figure 6.21a shows an idealized cross-section of the uplift pressure distribution for an open drainage gallery system along a sloping base.[1] The vertical distance from tailwater to the point *e*, defined by the intersection of the line of drains (drawn in red) and user defined potential slip plane is h_d. For the open drainage gallery system of Figure 6.21a, $h_d = H_{Tailwater} + (h_{e\text{-}d} - h_{e\text{-}e})$. In this example, the user defined potential slip plane corresponds to the dam-to-rock foundation interface (i.e., the base of the dam).

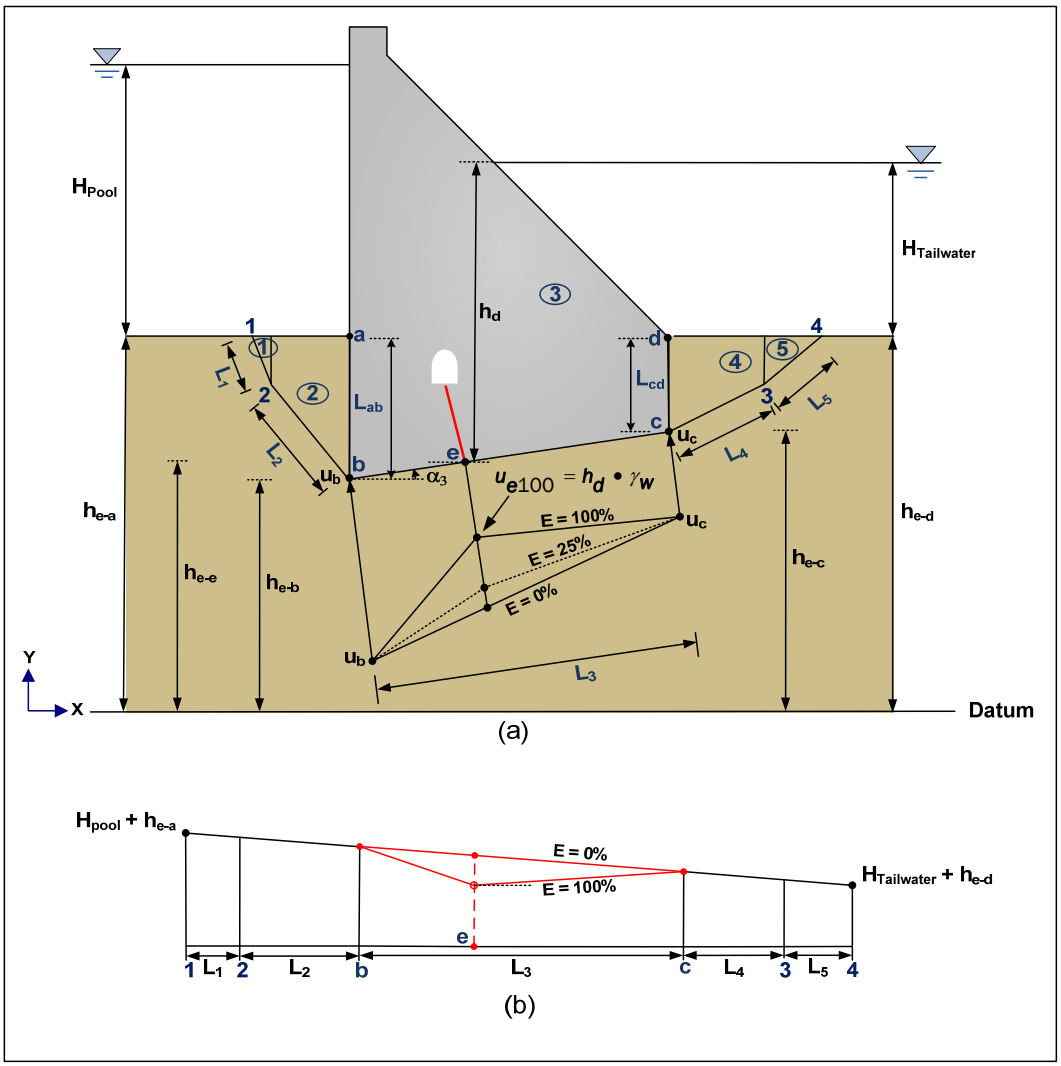

Figure 6.21. Drain efficiency of an open drainage gallery system with Flow Option 6. (a) Wedge and uplift pressure diagram (water pressures not to scale) (b) Variation on total head along potential slip plane.

[1] A constant value for hydraulic conductivity is assumed within the entire rock joint features when applying the Line of Seepage methodology for this figure.

Figure 6.21b displays total head versus distance measured along the user defined slip plane. Figure 6.21b also shows a constant hydrostatic water pressure head at point 1 with a total head of $H_{pool}+h_{e\text{-}a}$; and point 4 with a total head of $H_{Tailwater} + h_{e\text{-}d}$. There is a linear variation between points 1, 2, *b*, *e*, *c*, 3, and 4 (i.e., along the potential slip plane) when the drain efficiency, *E*=0 (i.e., the case for no drain or a fully clogged drain). At 100 percent drain efficiency, *E*=100, the vertical distance from point e up the red dash line to the red circle is comparable to the total head of $h_d+h_{e\text{-}e}$ of Figure 6.21a. From this point, the 100 percent drain efficiency curve can be drawn by connecting a line to the point *b* and to point *c*.

6.5.2 Discussion of drain efficiency *E* value with Flow Option 6

In Flow Option 6 the uplift pressure below the structural wedge is defined by the value the user assigns to the drain efficiency *E*. Recall that Drain efficiency, *E*, is expressed as a percentage ranging from 0 to 100. A value of *E*=100 corresponds to the case of the drains being fully effective and a value of *E*=0 corresponds to the case of the drains being fully clogged and ineffective. Corps of Engineers Engineer Manuals 1110-2-2200, "Gravity Dam Design", and 1110-2-2100, "Stability Analysis of Concrete Structures", restrict the value of *E* to no greater than 50 percent (*E*=50). These manuals state that if foundation testing and flow analysis provide supporting justification, the drain efficiency can be increased beyond 50 percent. The analysis and/or design documentation must contain supporting data to justify the *E* value used. For the user specified value for *E*, the total head is first computed at point e for the Figure 6.20b case of a closed drainage gallery system or at point e for the Figure 6.21b case of a open drainage gallery system by linear interpolation (and measured downward from the *E* = 0 line). Bernoulli's Equation 1.5 (assuming a zero velocity head) in conjunction with Equation 1.8 allows for the calculation of water pressure at point *e*.

6.6 Discussion of results for stability with simplified seepage analysis

Table 6.4 summarizes the uplift resultant water pressure forces acting normal to the base of each of the five wedges/sub-wedges for Flow Options 4, 5 and 6. Recall that wedge number 3 is the structural wedge. The greatest uplift occurs on normal to the base of the structural wedge when using Flow Option 4 and the smallest occurs when Flow Option 5 is specified. Uplift for Flow Option 5 is between these two cases. Flow Option

5 has the largest uplift acting on the structural wedge (i.e., Wedge ID = 3) because all head loss occurs between the starting and ending point along the structural wedge. Flow Option 5 uplift is less than Flow Option 6 uplift because the lead loss computed by the line of seepage occurs along a shorter seepage path.

Table 6.4. Uplift resultant water pressure force *U* for Flow Options 4, 5, and 6.

Wedge ID	Uplift Resultant Water Pressure Force (U_i)		
	Flow Option 4	Flow Option 5	Flow Option 6
1	11.19	11.19	10.70
2	27.37	27.37	23.63
3	47.33	45.19	46.74
4	3.90	3.90	6.47
5	1.41	1.41	2.37

Table 6.5 summarizes the computed Factors of Safety for the Figure 6.1 potential slip plane below the ETL 1110-2-256 hypothetical gravity dam embedded in a rock foundation using Flow Options 4, 5, and 6. Flow Option 6 results in the lowest computed value for Factor of Safety (*FS*) against sliding of 1.969 and Flow Option 5 results in the largest computed value of 2.031, with the result from Flow Option 4 being intermediate with its value of 1.992. In this problem, the authors of this report observe that there is not a large difference among the computed results. The differences among the three results are due to both the uplift pressures applied to the entire potential sliding plane (i.e., not just to the structural wedge) and the interslice water pressure forces assumptions made by each of the three simplified uplift analyses.

Table 6.5. Computed factors of safety for Flow Options 4, 5 and 6.

Factor of Safety	Flow Option 4	Flow Option 5	Flow Option 6
FS	1.992	2.031	1.969

Flow Option 6 represents steady state seepage in conjunction with a line of seepage methodology of a potential slip plane that corresponds to a continuous series of connected rock joints from upstream to downstream of the gravity dam with fluid flow along this singular joint path system and does not apply to fluid flow along a network of interconnected rock joints which has been investigated in detail in Section 4.3 of Chapter 4.

7 Probabilistic Analysis

7.1 Introduction

This chapter focuses on the probabilistic capabilities when assessing the stability of a non-overflow gravity dam cross-section embedded within a rock foundation against sliding as well as the uplift water pressures resulting from flow within rock joints. Most engineering problems involve some form of uncertainty. Whether a particular uncertainty is aleatoric or epistemic, it should be taken into consideration. Certain parameters such as material properties which are variable in nature tend to lean towards these uncertainties. The modeling outcome from these established uncertainties generate a system response curve where stability limits is the engineering performance criteria used in the formulations. This initial version of GDLAD_Foundation addresses the sliding failure mechanism but not bearing failure and not overturning failure (expressed in the Corps EM 1110-2-2100 criteria as base area in compression).

7.1.1 Multivariate probabilistic analysis of uncertain variables

The inherent randomness and uncertainty of some model parameters require numerical methods to obtain solutions to the resulting probabilistic problem. A numerical method such as the Latin Hypercube simulation is a sampling technique used for conducting the analysis. Latin Hypercube sampling (LHS) was selected for its efficiency and its reduction in run time when compared to Monte Carlo simulation. LHS is the preferred method of sampling because it minimizes the number of iterations required to approximate the input distribution. When using LHS in the multivariate case, it is important to maintain statistical independence between variables unless correlation is explicitly specified. This is necessary to preserve randomness between variables. This software is included within GDLAD_Foundation [and GDLAD_Sloping_Base (Ebeling et al. 2008)] analytical programs. This initial version has the ability to account for a limited number of means for specifying correlation(s) among variables.

These random variables can be correlated, independent, or a combination of both. For variables that are correlated, a user specifies the correlation coefficient. To initiate an analysis, each variable is expressed individually

with its statistical parameters, i.e., mean and standard deviation, and its distribution type. If there is knowledge of statistical correlation between variables, these are stated with their respective correlation coefficient. Analytical pre-testing is conducted in order to determine the number of samples or simulations needed to reproduce the original distribution that was sampled. In the multivariate case, the number of samples specified by the user for an entire analysis is deemed to be adequate when increasing the number of samples does not show much improvement to (i.e., change in) the system response curve.

The variables of uncertainty for stability calculations within GDLAD_Foundation are *C*, *Phi*, *E*, K_o, and *Af*, *U*. These variables can also be used in a deterministic analysis or a combination of a probabilistic and deterministic analysis. Examples of model parameters and their default statistical values are given in Table 7.1 for a Stability and Simplified Seepage Analysis with the simplified seepage Flow Options 4, 5, and 6. Table 7.2 gives these parameters for site specific uplift pressures and a corresponding resultant uplift pressure force derived from a more detailed steady-state seepage analysis of flow within a network of rock joints using Joint_FLOW. These parameters will be used for the example problems discussed in the next sections.

Table 7.1. Model parameters with inherent uncertainty and default statistical values for non-site specific uplift pressures.

Parameter Name	Parameter Symbol	Mean	Standard Deviation	Distribution Type
effective cohesion (psf)	C	100.0	25.0	Bounded Normal
effective angle of internal friction (degrees)	Phi	30.0	3.0	Bounded Normal
non-site specific uplift pressure (drain efficiency)	E	0.375	0.1	Bounded Normal
horizontal earth pressure coefficient within the silt	K_0	0.39	0.0975	Bounded Normal
allowable load per Anchor (lbs)	A_f	35000.0	3500.0	Bounded Normal

Table 7.2. Model parameters with inherent uncertainty and default statistical values for site specific uplift pressures.

Parameter Name	Parameter Symbol	Mean	Standard Deviation	Distribution Type
effective cohesion (psf)	C	100.0	25.0	Bounded Normal
effective angle of internal friction (degrees)	Phi	30.0	3.0	Bounded Normal
horizontal earth pressure coefficient within the silt	K_0	0.39	0.0975	Bounded Normal
allowable load per Anchor (lbs)	A_f	35000.0	3500.0	Bounded Normal
site specific resultant uplift pressures force (from Joint_FLOW) (Foundation input in lbs)	U	---	---	---

The variables of uncertainty for seepage calculations within Joint_FLOW are *E_M*, *JRC*, *E_C*, and *K_Direct*. These variables can also be used in a deterministic analysis or a combination of a probabilistic and deterministic analysis. Examples of model parameters and their statistical values are given in Table 7.3 for a Joint_FLOW analysis.

For a Stability and Joint_FLOW Analysis, essential parameters listed within Tables 7.2 and 7.3 will be selected and utilized for the example problems discussed in the next sections.

Table 7.3. Model parameters with inherent uncertainty and statistical values for rock joint attributes.

Parameter Name	Parameter Symbol	Mean	Standard Deviation	Distribution Type
Mechanical Aperture (microns)	E_M	300	13.5	Bounded Normal
Joint Roughness	JRC	8	1	Bounded Normal
Conducting Aperture (microns)	E_C	100	1	Bounded Normal
Hydraulic Conductivity of Clean Joint (m/s)	K_Direct	0.006	0.001	Bounded Normal

7.1.2 System response curves for rock-founded gravity dams with a sloping base

A System Response Curve (SRC) defines the probability of failure or the limit state of a concrete gravity dam. The SRC for sliding is constructed by taking the ratio of the accumulated numbers of simulations with sliding factors of safety that are computed to be less than or equal 1.0, i.e., sliding failure, and the number of simulations for each pool height being analyzed. As an illustrative example, Figure 7.1 below shows the results of a probabilistic analysis in the form of system response curve for the sliding limit state.[1]

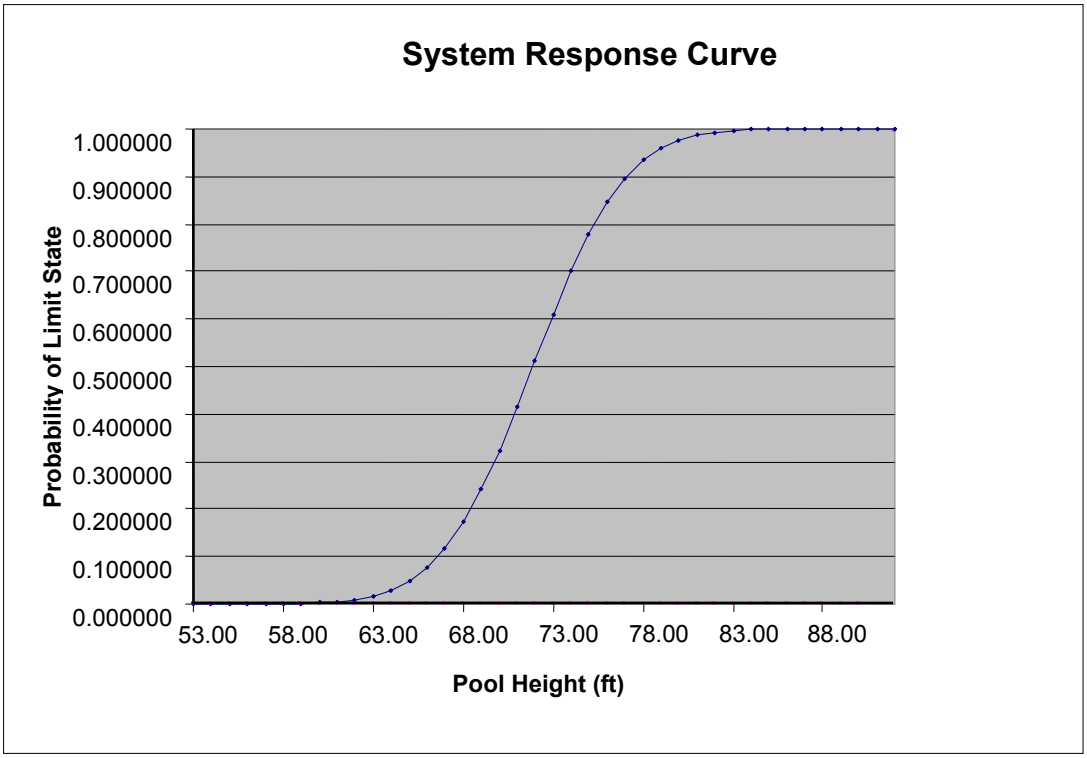

Figure 7.1. System response curve for sliding limit state.

At the incipient of sliding, the shear strength along the base for the dam to foundation interface becomes fully mobilized. The factor of safety (*FS*) against sliding along this interface, *FS*, is defined as defined as the ratio of the Mohr-Coulomb shear strength, τ_F, divided by the shear stress required for equilibrium, τ,

[1] Other limit states (e.g., bearing, overturning, etc.) are not being evaluated in this initial version of GDLAD_Foundation). Consequently, the sliding failure limit state becomes the system response curve for the non-overflow gravity dam cross-section being analyzed.

$$FS = \frac{\tau_F}{\tau} \quad \text{(bis 6.1)}$$

with the Mohr-Coulomb shear strength relationship τ_F defined by Equation 1.2. At the onset of sliding τ is equal to τ_F and FS is equal to 1.0. A factor of safety (FS) is a measure of stability against sliding. For the stability analysis, the factor of safety (FS) against sliding along a potential sliding plane is given in Equation 6.1.

Two analyses will be made of a non-overflow gravity dam cross-section with a shallow, single joint reach system extending from just upstream of the heel to just downstream of the toe. In Section 7.2, a simplified method of establishing uplift water pressures by Flow Option 4 (discussed in Chapter 6) will be used in a deterministic stability analysis in order to validate the engineering equilibrium formulation. The engineering methodology will further be examined in Section 7.3 by the probabilistic analysis of its stability against a sliding failure mechanism.

Section 7.4 summarizes a probabilistic analysis of sliding stability as well as calculated uplift water pressures produced by Joint_FLOW using Flow Option 3. In this option, the stability analysis is made with seepage along the user specified rock joints which define the potential slip plane as well as seepage along the vertical rock joints introduced into the model (via Flow Option 3) at the wedge interslice regions. All water pressures along the network of rock joints are computed at the (joint) nodes by Joint_FLOW. Vertical reaches are created at wedge intersections along the potential slip plane. These reaches will inherit the Mechanical aperture and JRC mean values of the wedge base adjacent rock joints. All elements along the rock joints will very probabilistically.

7.2 Problem 14: Validation of stability analysis

A deterministic analysis of typical static loading conditions for a three wedge system of a Gravity Dam cross-section with foundation drain is presented in Figure 7.2. In this deterministic analysis, Table 7.1 lists the mean values for the Mohr-Coulomb effective shear strength parameters for the three rock foundation wedges. This analysis was conducted to demonstrate the application of the general wedge equation to the sliding analysis of multiple wedge systems. The results of this analysis are also compared to the results from the equations of equilibrium formulated in GDLAD_Sloping_Base (Ebeling et al. 2008).

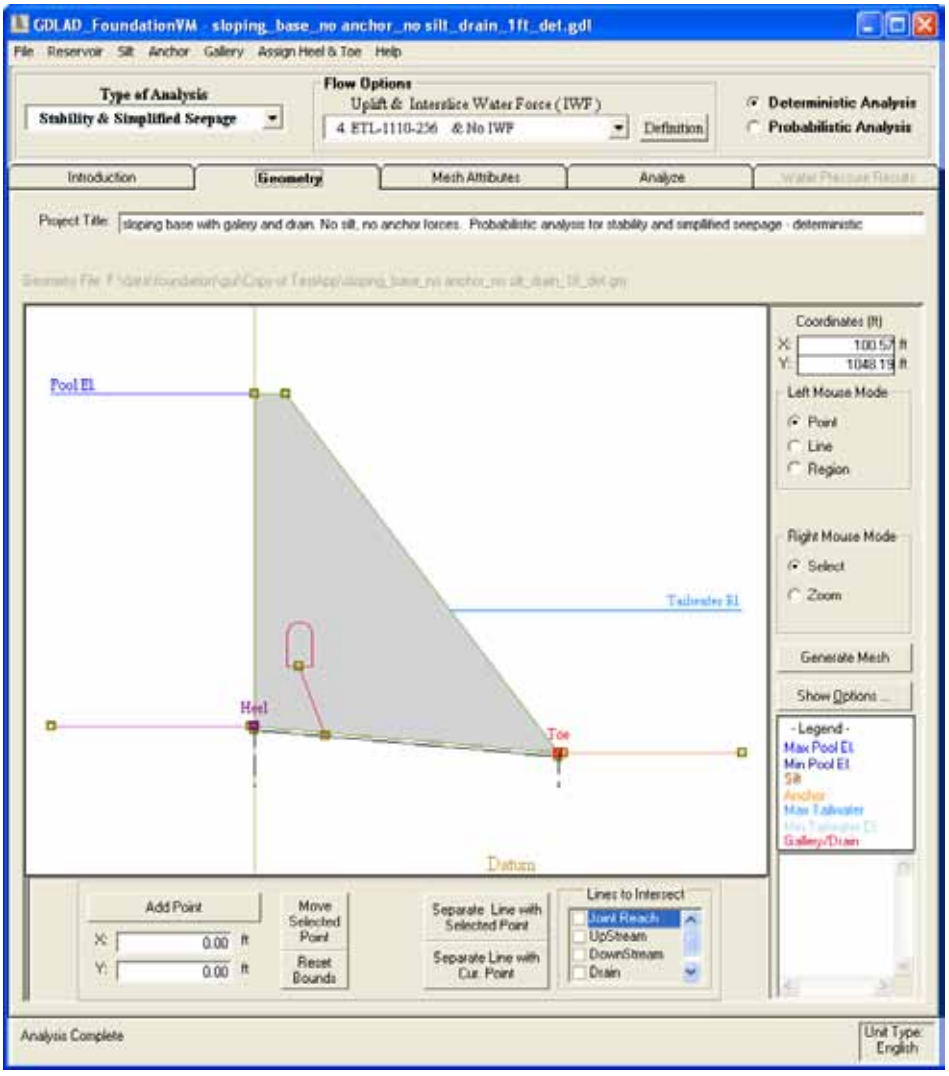

Figure 7.2. Geometry of concrete gravity dam.

The case considered is for a pool at el 1032 ft and tailwater at el 978.7 ft. Top of rock is at el 950 ft at the heel and at el 743.447 at the toe. Table 7.4 gives a listing of the functions and coordinates of all nodes in the geometry. This hypothetical concrete gravity dam is 82 ft high and approximately 74.9 ft wide. The gallery opening is defined by a rectangle that is 6 ft wide and 8 ft high with a half circle added on top.

The three wedge system developed to analyze the stability of this system can be seen in the Figure 7.3 close-up with the brown lines defining all three wedges. The potential slip plane being evaluated is located one foot below the Heel and one foot below the Toe of the rock-founded gravity dam. This potential slip plane is contained within a rock joint that is parallel to the dam-to-rock foundation interface. There is a single driving wedge that

Table 7.4. Description of nodes and locations.

Node Id	Node Description	X-coordinate	Y-coordinate
1	Heel	0	950
2	Toe	74.9	943.45
3	Upstream ground surface extent (Not used in calculations)	-50	950
4	Crest at upstream side	0	1032
5	Crest at downstream side	7.6	1032
6	Downstream ground surface extent (Not used in calculations)	120	943.45
7	Mid-point at base of gallery (i.e., top of drain)	11	964.67
8	Slip plane node Beneath the rock foundation at the toe	74.9	942.45
9	Slip plane node Ground surface at the upstream side	-1	950
10	Slip plane node Beneath the rock foundation at the heel	0	949
11	Slip plane node Ground surface at the downstream side	75.9	943.45
12	Left upper corner of Region	-16.48	954.48
13	Left lower corner of Region	-16.48	939.60
14	Right lower corner of Region	88.91	934.72
15	Left upper corner of Region	88.67	947.65
16	Point where the line of drains Intersect the slip plane at the structural wedge	17.32	947.48

"daylights" one foot upstream of the *x*-position of the heel and a single resisting wedge that "daylights one foot downstream of the *x*-position of the Toe. Observe that both the resisting and driving wedges are quite small compared to the structural wedge.

Figure 7.4 gives the rock strength parameters with the unit weights of concrete and water. In this example, there is only one material defined throughout and shown mapped to region 1.

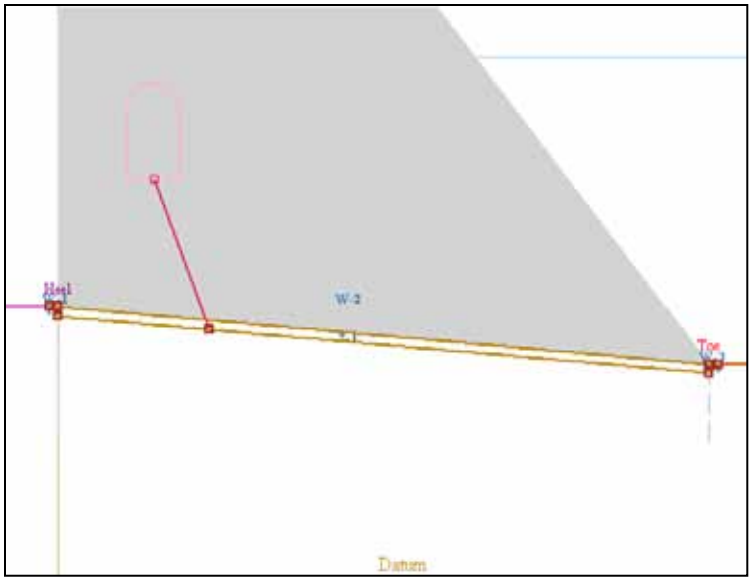

Figure 7.3. Three wedge system at base of dam.

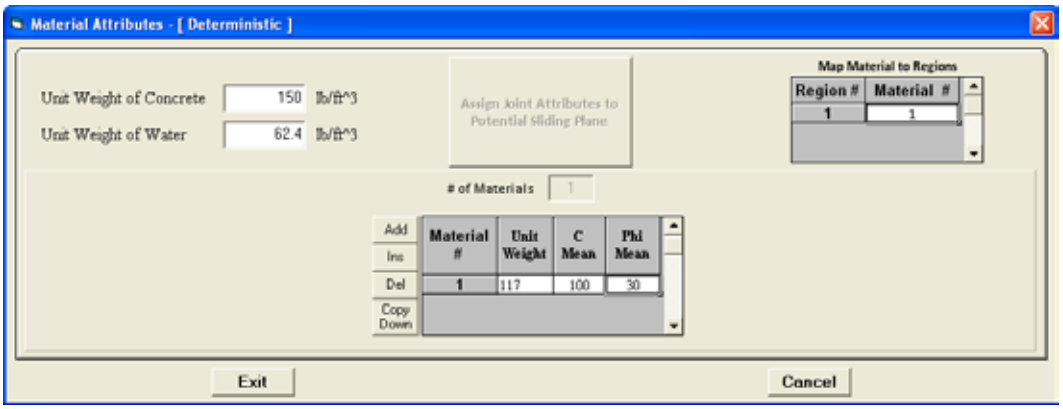

Figure 7.4. Material attributes.

With Flow Option 4 and a user input drain efficiency of 0.375, the uplift force, U_i, normal to each of the three wedges is listed as column 8 in the table of Figure 7.5. The resulting computed factor of safety (*FS*) against sliding for this multiple wedge system was found to be 0.815 with a residual imbalance force of -0.06 kips after 12 iterations and a tolerance for convergence of 100 lbs (see Figure 7.5). The matching of results were good (percent difference of 1.86%) when compared with the results from GDLAD_Sloping_Base reporting a computed value of *FS*=0.8. It is anticipated that the Factor of Safety (*FS*) against sliding is larger by GDLAD_Foundation since it has one foot of embedment as compared to the GDLAD_Sloping_Base model of a sliding surface at the concrete to rock interface (i.e., with no embedment).

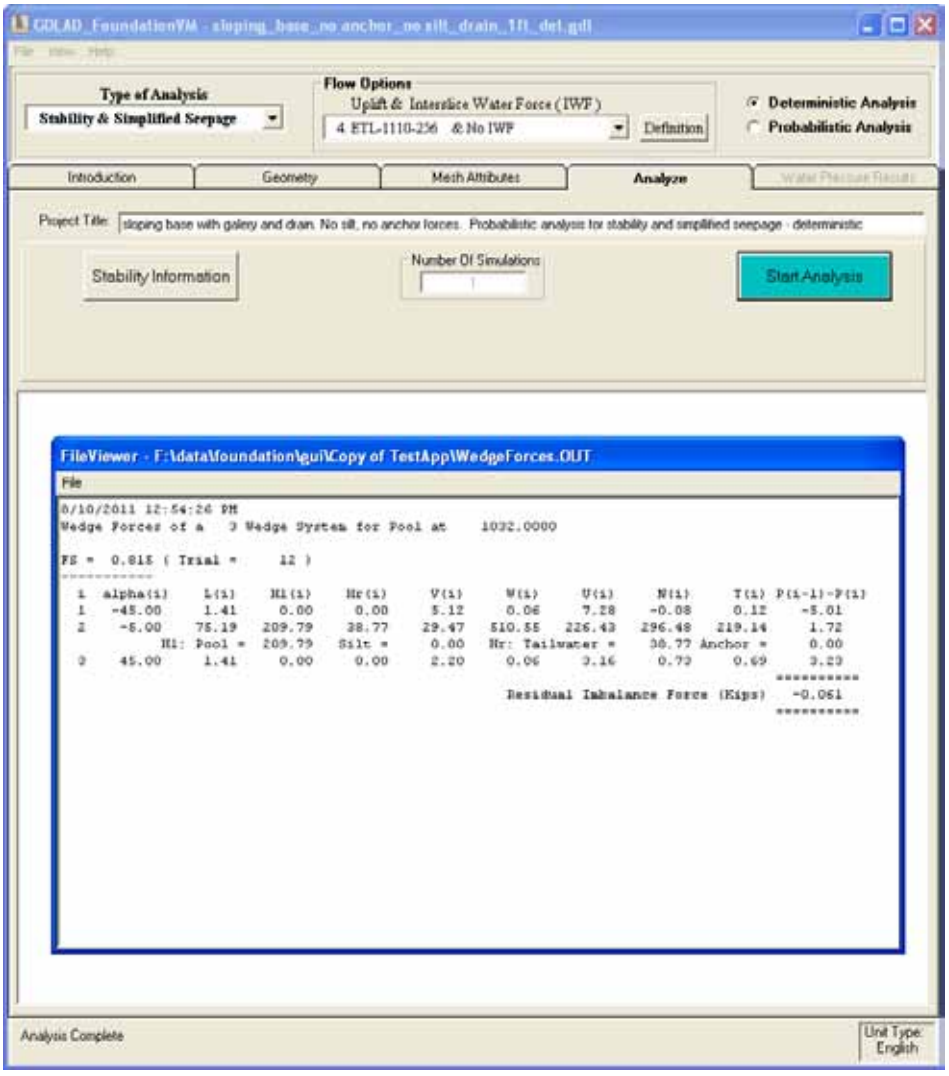

Figure 7.5. Resultant factor of safety with residual imbalance of a three wedge system with Flow Option 4.

7.3 Problem 15: Validation of system response curve

A probabilistic analysis considers the model parameters as random variables. The uncertain variables in our example problem of *C*, *Phi*, and drain efficiency *E* are described in Table 7.1. These uncertain model parameters will be used in the sliding stability calculations previously mentioned.

A probabilistic analysis also requires a large number of samples or simulations. From the example in Section 7.2 of a Gravity Dam cross-section with foundation drain and a three wedge system, Figure 7.6 shows a maximum pool elevation of 1042 ft, a minimum pool elevation of 1012 ft and a constant tailwater of 978.7 ft.

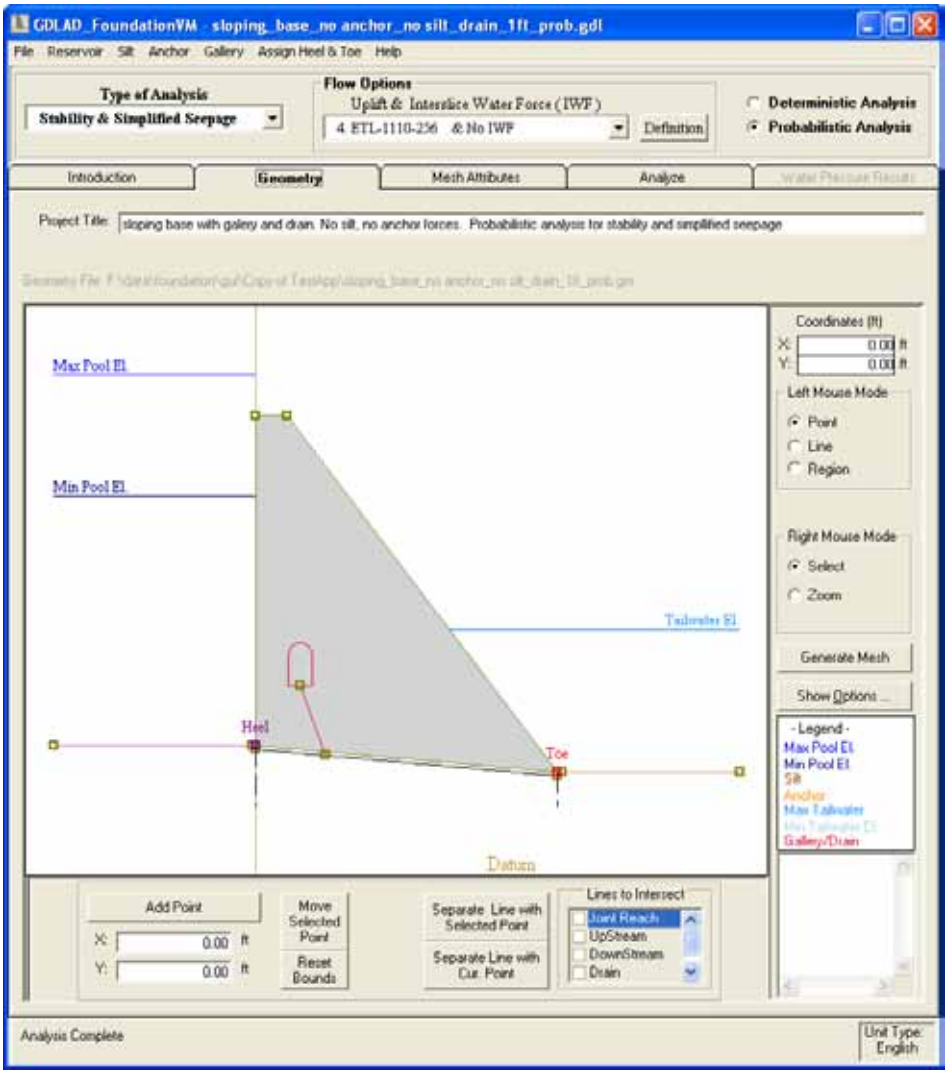

Figure 7.6. Geometry of concrete gravity dam with variable pools.

In this probabilistic analysis, Table 7.1 gives examples of the mean, standard deviation and distribution type values for the Mohr-Coulomb effective shear strength parameters for the three rock foundation wedges.

Figure 7.7 gives the rock strength parameters with the unit weights of rock, concrete and water. In this example, there is only one material defined throughout and shown mapped to region 1.[1] Statistical values of *C* and *Phi* are listed with a correlation coefficient of -0.7.

[1] If more than one material region were specified in this probabilistic analysis, GDLAD_Foundation will allow the user to specify the correlation coefficient between C values and between Phi values for each pair of materials via the "Correlate Material Pairs" input table shown in Figure 7.7.

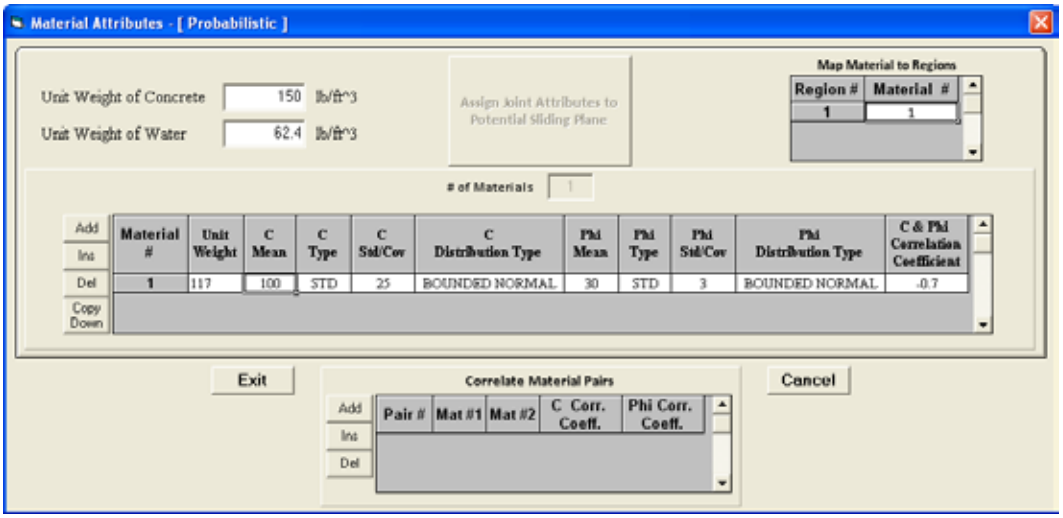

Figure 7.7. Material attributes of probabilistic parameters.

A total of 31 pools were calculated for the given pool elevations at 1 ft increments. Computations for 3,000 simulations for the three random variables (i.e. *C*, *Phi,* and *E*) were evaluated by GDLAD_Foundation to determine the number of times a factor of safety (*FS*) less than or equal to 1.0 is computed for each pool elevation.

The computed system response curve after 3000 simulations per pool for this multiple wedge system is illustrated in Figure 7.8. A second series of computations were made using the same set of pool elevations but using 6,000 simulations. The increase in the number of simulations did not show a significant change in computed results. Figure 7.9 shows the system response curves of both GDLAD_Foundation and GDLAD_Sloping_Base for the same set of parameters and conditions. There is a slight offset of a maximum of 0.04 probability of sliding failure limit state between the two curves. Figure 7.9 shows that GDLAD_Foundation gives a lower probability limit state. The authors of this report conclude that the results from GDLAD_Foundation are consistent with the results from GDLAD_Sloping_Base when shallow embedment is considered.

7.4 Problem 16: Analysis and system response curve

A probabilistic analysis of a Stability and Joint_FLOW Analysis is being considered in this section. The uncertain variables in our example problem are *C*, *Phi*, *U*, *E_M,* and *JRC* and have been categorized in Tables 7.2 and 7.3. These five model parameters introduce uncertainty into the sliding stability calculations previously mentioned.

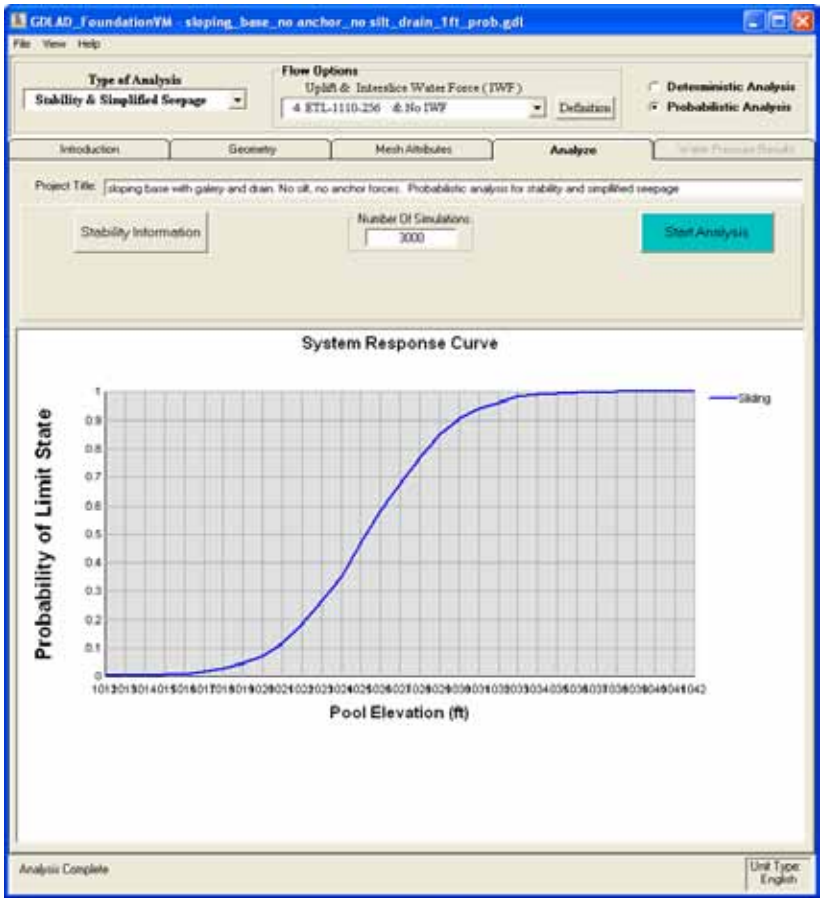

Figure 7.8. System response curve with Flow Option 4 and 3000 simulations.

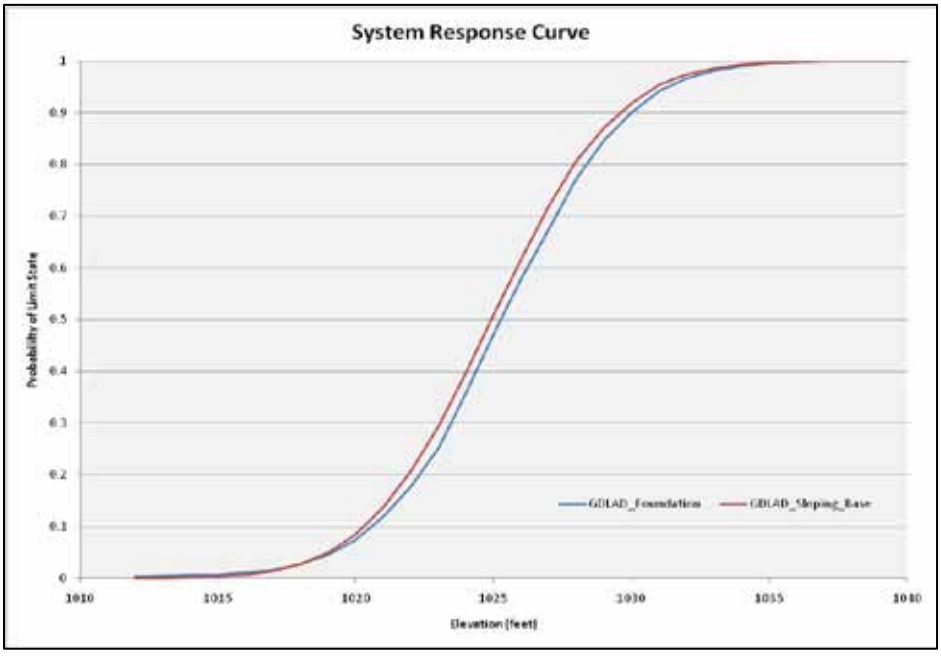

Figure 7.9. System response curves of GDLAD_Foundation and GDLAD_Sloping_Base.

The hypothetical embedded concrete gravity dam cross-section with foundation drainage and a potential sliding plane (highlighted in blue) is shown Figure 7.10. The network of the other rock joints is depicted in black in this figure. This figure also shows a maximum pool elevation of 1042 ft and minimum pool elevation of 1012 ft and a constant tailwater of 978.7 ft which results in 31 variable pools. The dam is 82 feet high above ground surface and approximately 74.9 feet wide. The gallery opening is defined by a rectangle that is 6 feet wide and 8 feet high with a dome or half circle added on top. Table 2.5 gives a listing of the functions and coordinates of all points defining the geometry.

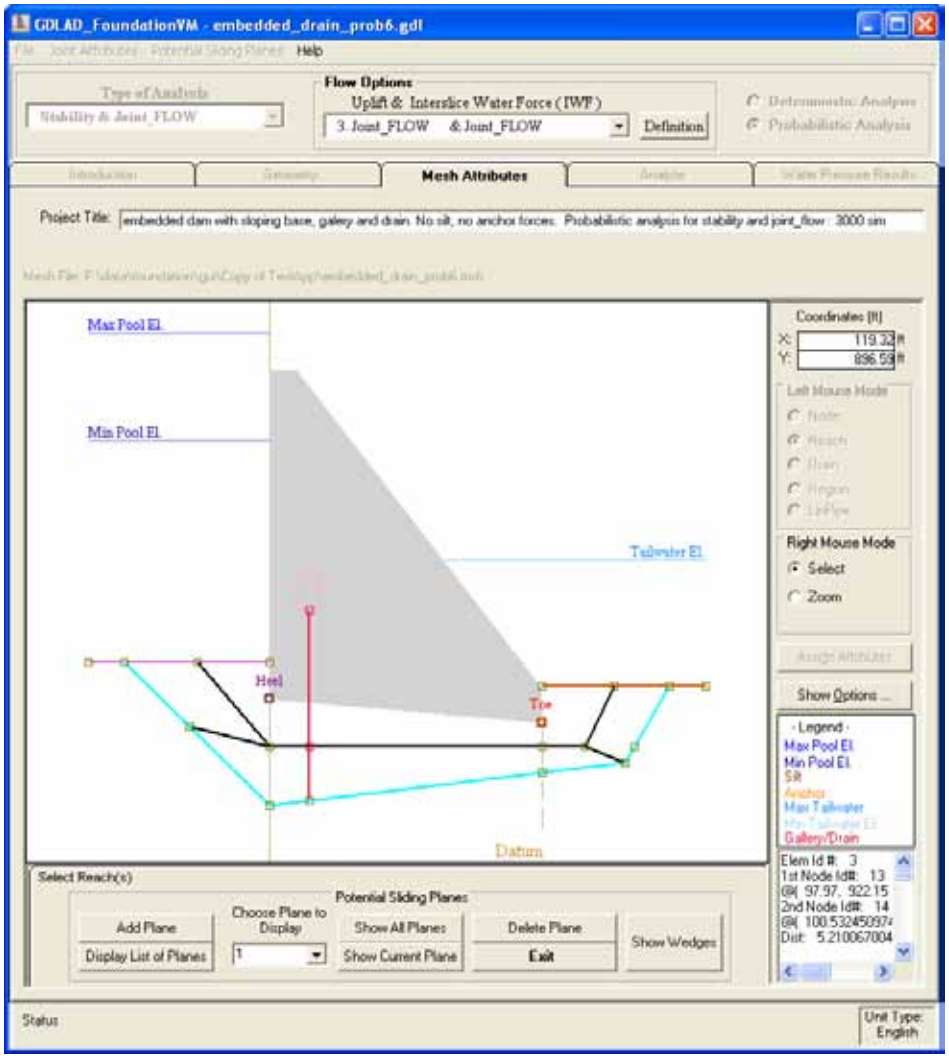

Figure 7.10. Concrete gravity dam embedded in rock with rock foundation drain.

This hypothetical concrete gravity dam also has been defined by two regions and six wedges. The two shaded areas defining the regions are illustrated in Figure 7.11 which shows the lower region as RG-2(M-2) and shaded in

green. The six wedge system (designated W-1 through W-6) has been created from the potential slip plane (highlighted in blue in Figure 7.10) and by the intersection of the regions with the potential slip plane are shown delineated by vertical brown lines.

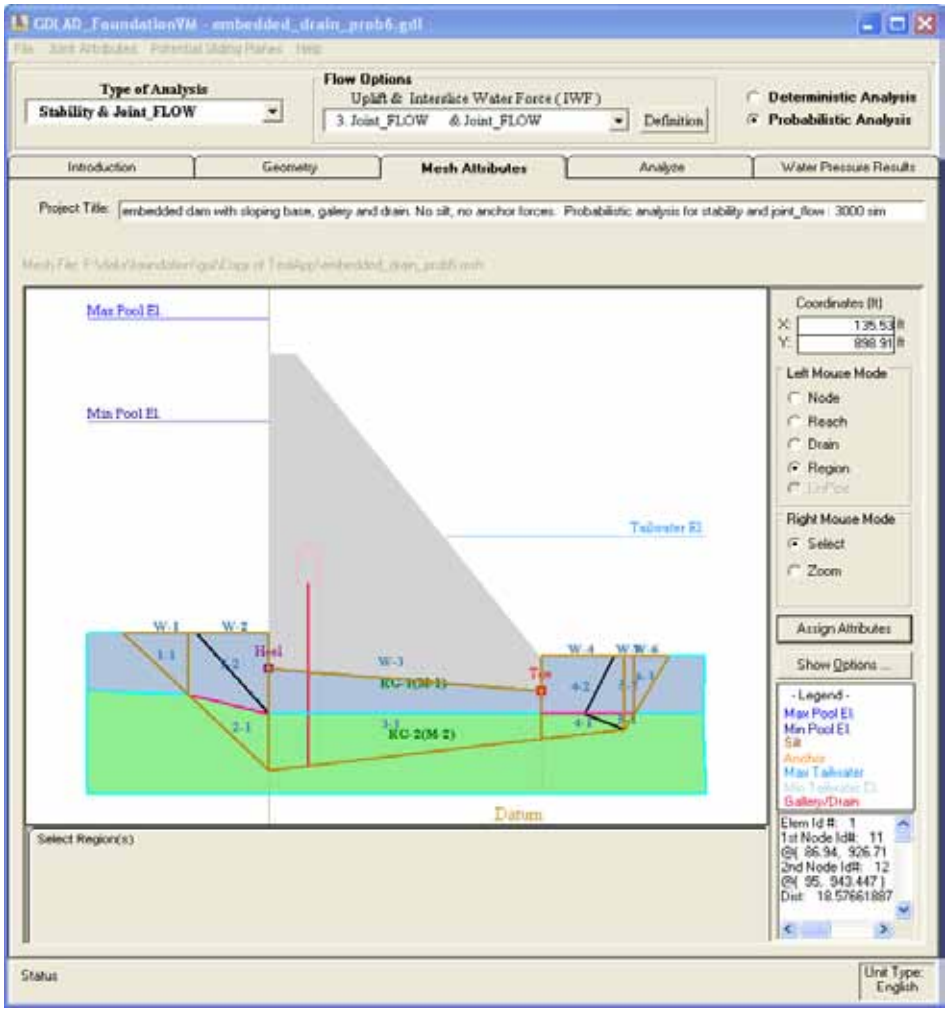

Figure 7.11. Concrete gravity dam with six wedges and two material regions.

Figure 7.12 gives the rock strength parameters with the unit weights of rock, concrete and water. For this example, there are two materials defined and shown mapped to regions 1 and 2 respectively. The selected region is 2 as demonstrated in Figures 7.11 and 7.12. The statistical values of *C* and *Phi* are listed in Figure 7.12 and are inversely correlated with a correlation coefficient of -0.7. The *C* values between regions as well as the *Phi* values between regions are independent and therefore uncorrelated for this example.

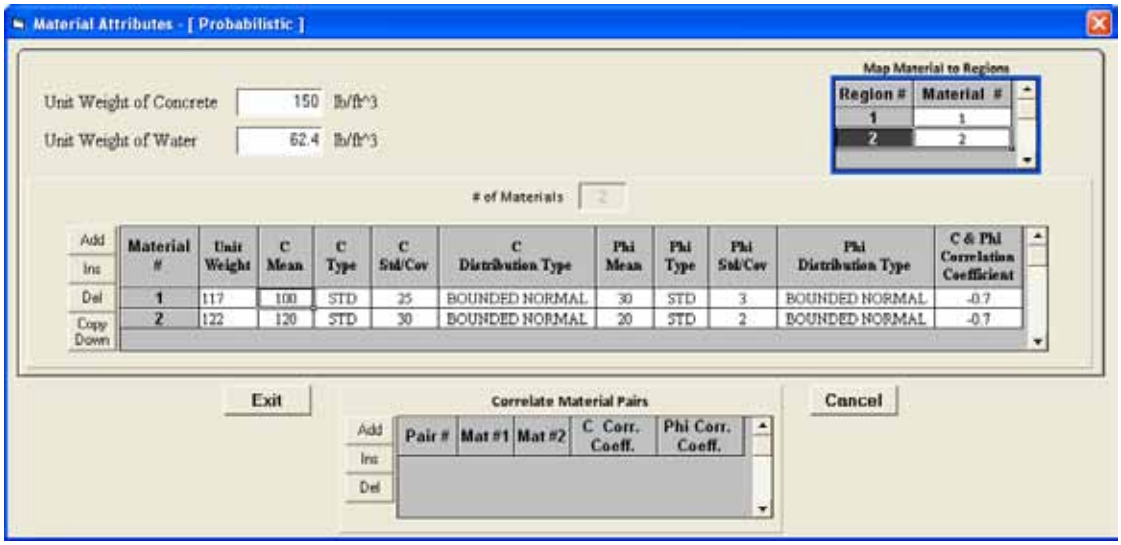

Figure 7.12. Material Attributes of probabilistic parameters.

A drain diameter of 5 in. with an interval of 20 ft between drains (along the gallery) has been assigned to the five elements defining each of the two drain segments. The drain attributes describing the drain model is shown in Figure 7.13.

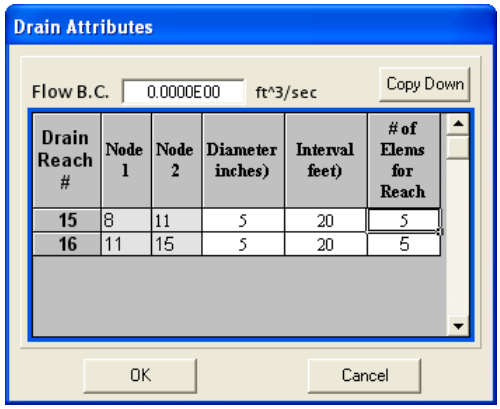

Figure 7.13. Attributes of drain model.

All reaches were given constant mean values with Mechanical Apertures (E_M) ranging from 400 to 900 microns with constant standard deviation values of 135 to 150 microns. The JRC mean values were given a constant value of 8.0 with all standard deviation values set to 1.0. Both E_M and JRC had bounded normal distribution types with each rock joint reach divided into five elements. Values defining the reach attributes are shown in Figure 7.14. Note that the properties of the first five out of a total of fourteen reaches are shown in this figure. Reach numbers possessing a double asterisk in Figure 7.14 are listed for reaches along the potential slip plane.

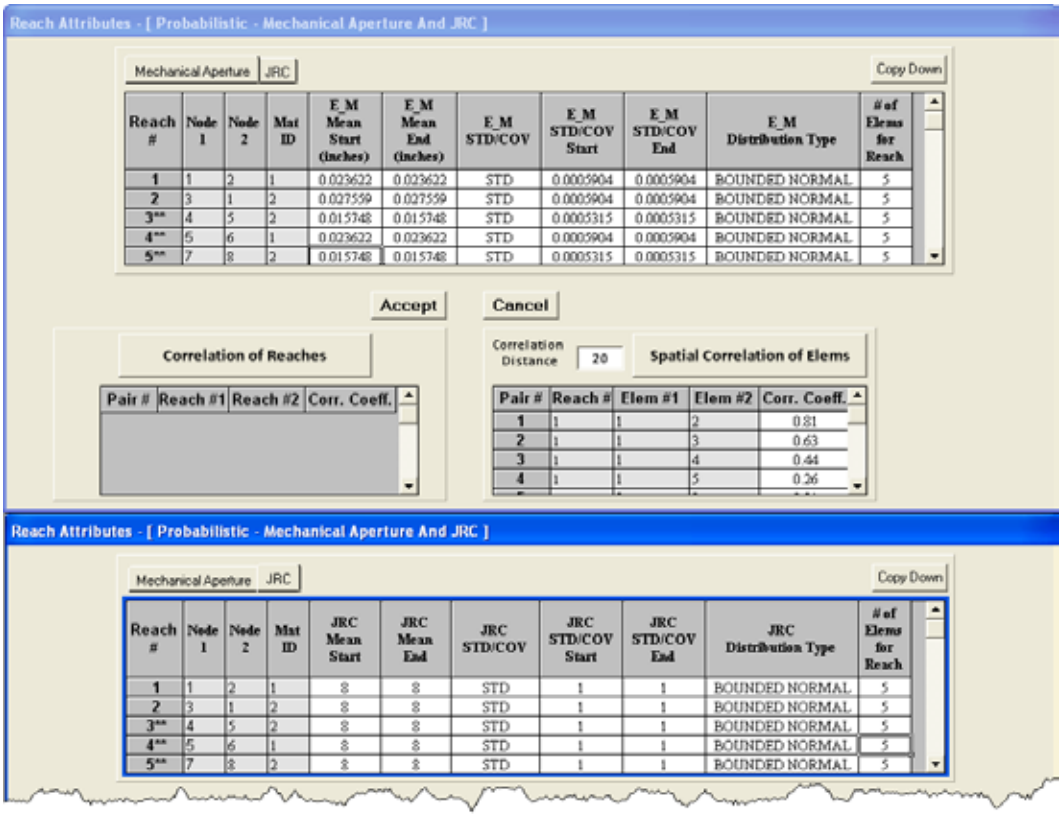

Figure 7.14. Reach attributes defining values for the Mechanical Aperture and JRC.

Also observe in Figure 7.14 that a spatial correlation distance of 20 ft is specified for the hydraulic conductivity of the rock joint elements. Figure 7.15 shows all fourteen reaches for this problem and identified within the Reach Attributes table of Figure 7.14. Figure 7.15 also shows the location of the seven reaches defining the potential slip plane (shown in blue). All rock joint numbers are labeled by a prefix "*R*" and drain elements by a prefix "*D*". The two drain elements in Figure 7.15 are labeled D-16 and D-15 and each is subdivided into five elements.

A probabilistic analysis also requires a large number of samples or simulations. For our example of 31 pools, the computations of 3,000 simulations of five random variables (i.e. *C*, *Phi*, *U*[1], *E_M,* and *JRC*) were evaluated to determine the factor of safety (*FS*) that is less than or equal to 1.0 for each pool height. Thus, there were three thousand probabilistic analyses performed for each pool with each defining a point on the SRC of Figure 7.16.

[1] The uplift resultant force, U, is the outcome of the uncertainties of the rock joint mechanical aperture and roughness. This parameter is therefore a dependent random variable and together with the shear strength parameters are used to compute the sliding limit state in a probabilistic analysis.

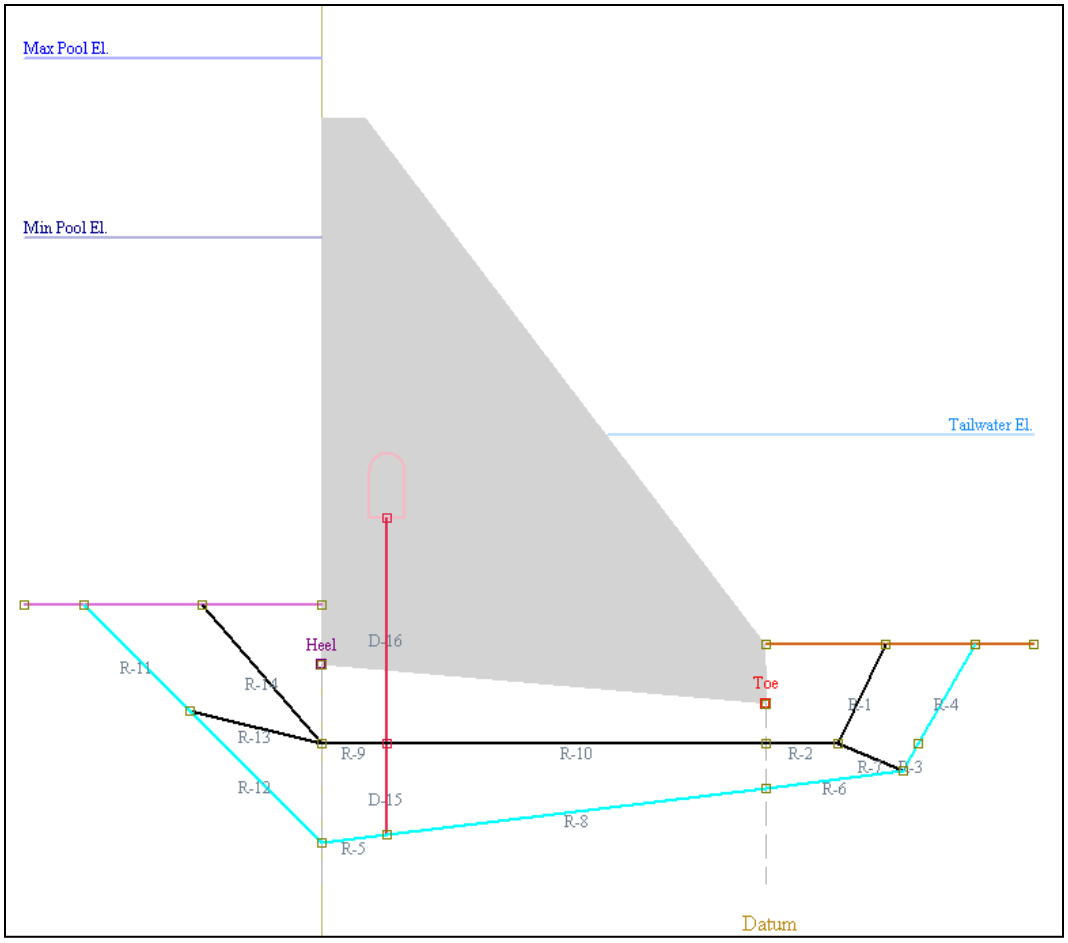

Figure 7.15. Reach numbers defining both rock joint reaches and rock drain reaches.

The computed System Response curve after 3000 simulations for this multiple wedge system is illustrated in Figure 7.16. An increase in the number of simulations (to 6000) did not show a significant change in the results.

Figure 7.17 illustrates both mean and standard deviation water pressure values calculated at the nodes of each rock joint for the pool at top of dam. The mean phreatic surface is drawn for nodes (shown in light blue) along the potential slip plane. This continuous line starts at the Pool (El 1032 ft.), connects at the drain and terminates at the tailwater. The uncertainties of the rock joints and consequent resultant uplift water pressure forces along the potential slip plane is incorporated in the formulation of the sliding limit state and is reflected in the system response curve of Figure 7.16.

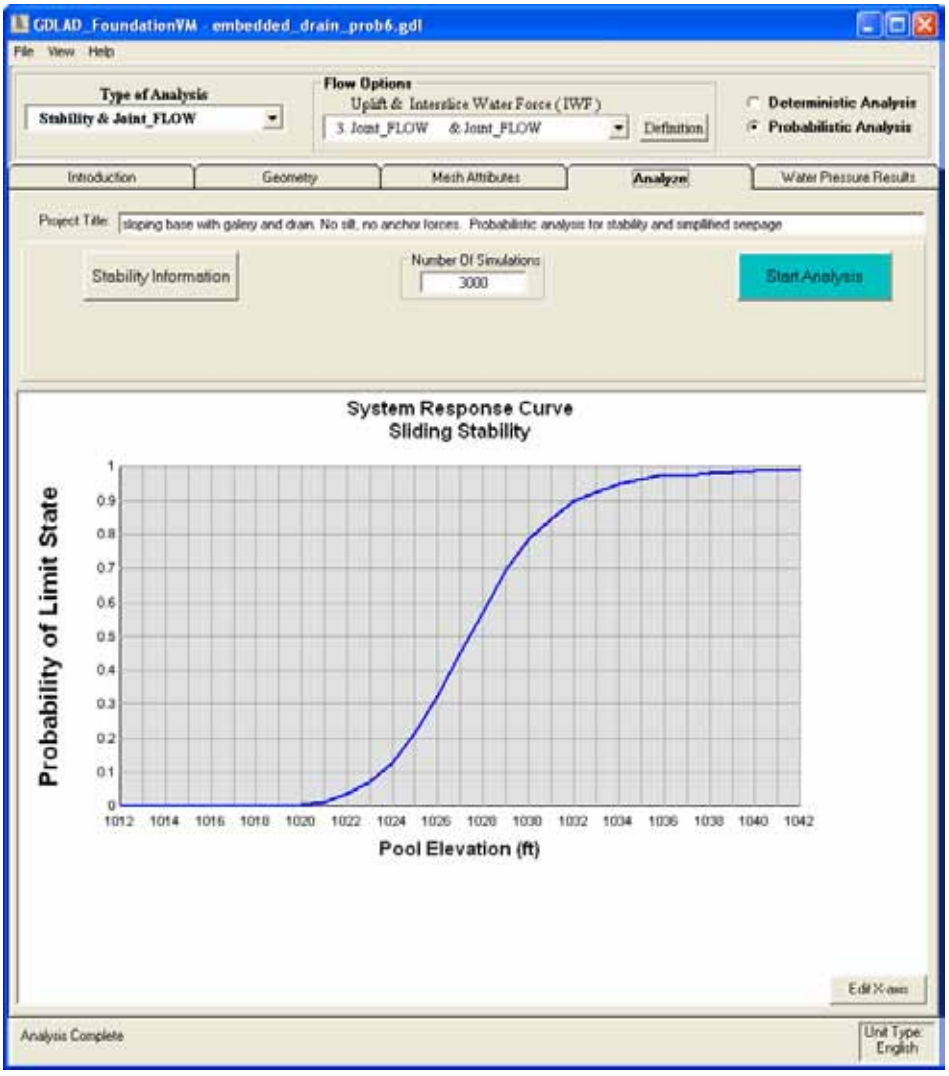

Figure 7.16. System response curve for a Stability and Joint_FLOW analysis.

These mean and standard deviation water pressure values are re-computed at each node for each of the 3,000 simulations. Additionally, this complete set of 3,000 simulations is further computed for each of the 31 pool elevations.

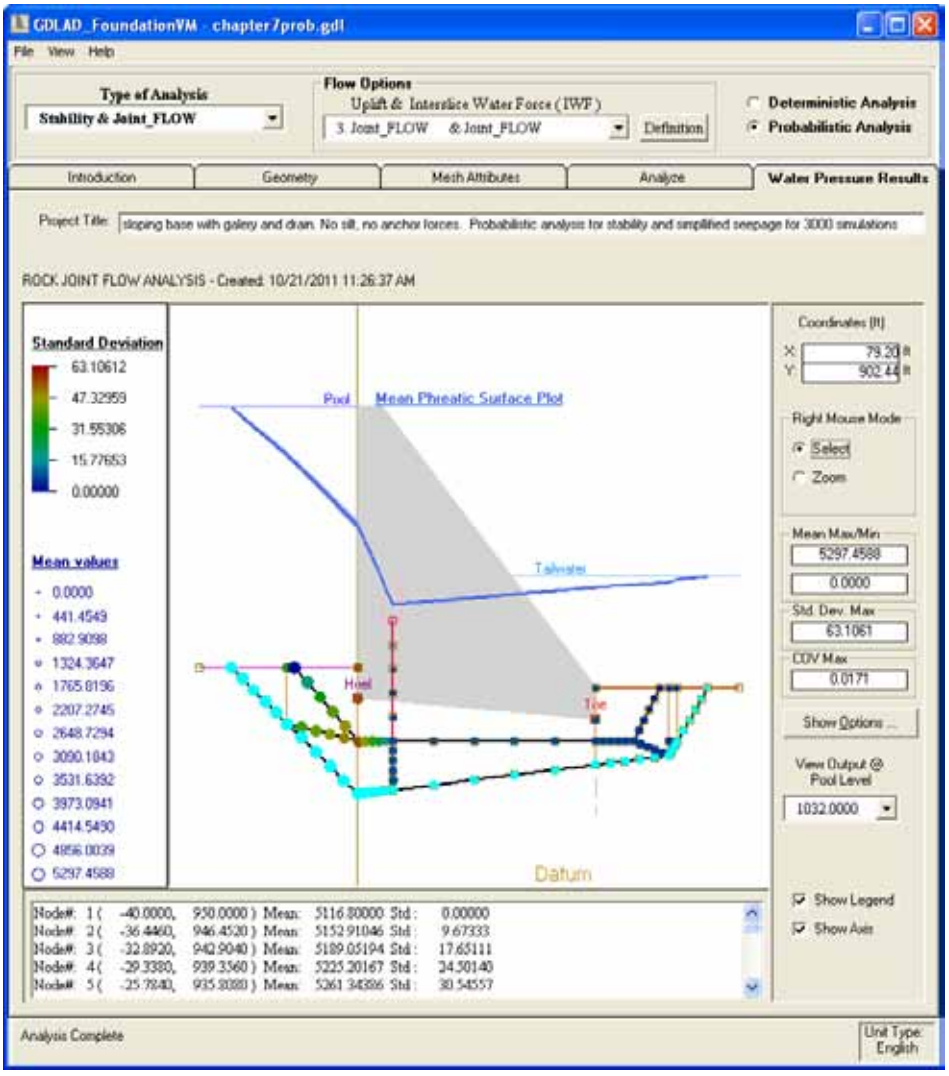

Figure 7.17. Mean phreatic surface at selected nodal points.

8 Summary, Conclusions, and Recommendations

8.1 Summary

Uplift is a major force affecting the stability of concrete gravity dams founded on rock. Uplift forces decrease the resistance of the dam to sliding. A sliding stability assessment of a non-overflow gravity dam embedded in rock requires the assignment of uplift water pressure forces acting on the driving, the structural and the resisting wedges. This report summarizes an engineering methodology and corresponding PC-based software environment, GDLAD_Foundation that is used in the evaluation of the sliding stability analysis of a non-overflow gravity dam (2-D) section embedded in rock for a hydraulic hazard. This software package is referred to as GDLAD_Foundation (Gravity Dam Layout and Design). The PC-based software GDLAD_Foundation offers a comprehensive environment for the following:

1. A Visual Modeler that facilitates problem definition, development of data input, execution of the engineering software and visualization of computed results,
2. FORTRAN engineering software to compute the stability, via the wedge method of analysis, of the embedded gravity non-overflow (2-D) cross-section, and
3. The computation of uplift caused by flow along rock joints contained within the rock foundation. Incorporated within the GDLAD_Foundation software is the FORTRAN program Joint_FLOW that is used to assess fluid flow along rock joints, fissure and/or faults contained within the rock foundation.

From the user specified definition of a network of rock joint reaches within the foundation, the stability of the user selected potential failure plane(s) is made. There are three sets of “wedges” in this methodology, the driving, structural, and resisting wedges. These wedges are evaluated in the equilibrium analysis and include consideration of the distribution of water pressures (derived, e.g., from the flow of water contained within the joints by Joint_FLOW) in the computation of the uplift force acting on the base of each of the wedges.

Deterministic and probabilistic methods of analysis are available by GDLAD_Foundation for the hydraulic hazard. Deterministic analyses currently result in the computation of a factor of safety (*FS*) against sliding. With the specification of a range in pool and tailwater elevations, probabilistic analyses result in the computation of a system response curve for the sliding limit state due to statistically defined uncertainties in rock joint strength parameters and parameters that are used to define rock joint permeability. Statistical uncertainties in silt load and anchor forces, if present, may also be included in the analysis.

There are six flow options available to the user in the two-dimensional sliding stability analysis. The first three options involve the solution of two-dimensional steady state flow within a user defined network of rock joints. An important capability of the first three options is to allow an engineer to investigate the impact of a "network" of rock joints on uplift pressure computations used in a stability analysis. Water pressures are derived within these rock joints from the Joint_FLOW steady state seepage analysis results. The last three "flow options" are, in actuality, simplified procedures evoking different simplified assumptions that are then used to assign uplift water pressures along a single user defined, series of connected rock joints that corresponds to a user defined potential slip plane being investigated. It is stressed that these flow options 4, 5, and 6 do not have the capability to model inter-connected sets of rock joints (i.e., a network of rock joints).

A series of sixteen example problems are used to showcase some of the unique capabilities of the GDLAD_FoundationVM.

8.2 Conclusions

Some of the sixteen examples contained within this report demonstrate some important aspects to the calculation of uplift pressures:

1. The geometric distribution of rock joint aperture and joint roughness along even a single rock joint, impacts the resulting uplift pressure distribution, as well as the magnitude and location of its corresponding resultant force.
2. The size and geometric distribution of a network of inter-connected rock joints can impact the distribution of water flow and water pressures.
3. Rock foundation drains impact the distribution of flow and uplift pressures along a network of rock joints.

4. The data base of sixteen analyses contained within this report do not provide a complete picture of the interplay between (a) the overall scale and geometric distribution of rock joint networks, with (b) geometric distribution of rock joint aperture and joint roughness, and with (c) rock foundation drain characteristics, and their impacts on computed uplift pressure distributions.

8.3 Recommendations

The following three recommendations are made:

1. That this stability formulation with water flow within rock joints (and used to compute uplift water pressures acting on a spillway structural wedge embedded within a jointed rock foundation) formulation and software be extended to the analysis of Spillway Layout and Design (SLAD). Aspects of this extension include accommodating spillway geometry and computation of water pressures acting on the "wetted" surface of the spillway.

   Initial research on a methodology for computing pressures acting on the wetted spillway surface has been initiated. Figure 8.1 and Table 8.1 summarize the wetted spillway surface configuration for this extended formulation. The spillway shown in Figure 8.1 is an ogee shape. The term ogee crest or ogee spillway is used frequently to describe the shape of an overflow spillway. Ogee is often defined as a pointed arch, each of the sides of which has the curve of an ogee, that is, has a reversed curve near the apex. It is also defined as a reverse curve shaped like an elongated letter S. The shape of a spillway crest that represents the lower profile of the undernappe of a jet of water flowing over a sharp-crested weir at a design depth is also referred to as an ogee crest.

   This shape, when designed for a given head, produces pressures that are near atmospheric along the crest. Heads lower than the design head will produce pressures above atmospheric and heads higher than the design head will produce pressures that are below atmospheric. In theory, the length of the spillway that represents the lower profile of the undernappe of a jet of water flowing over a sharp-crested weir will have atmospheric pressures on the surface. Factors such as surface resistance, boundary layer development, and air entrainment will influence the undernappe shape.

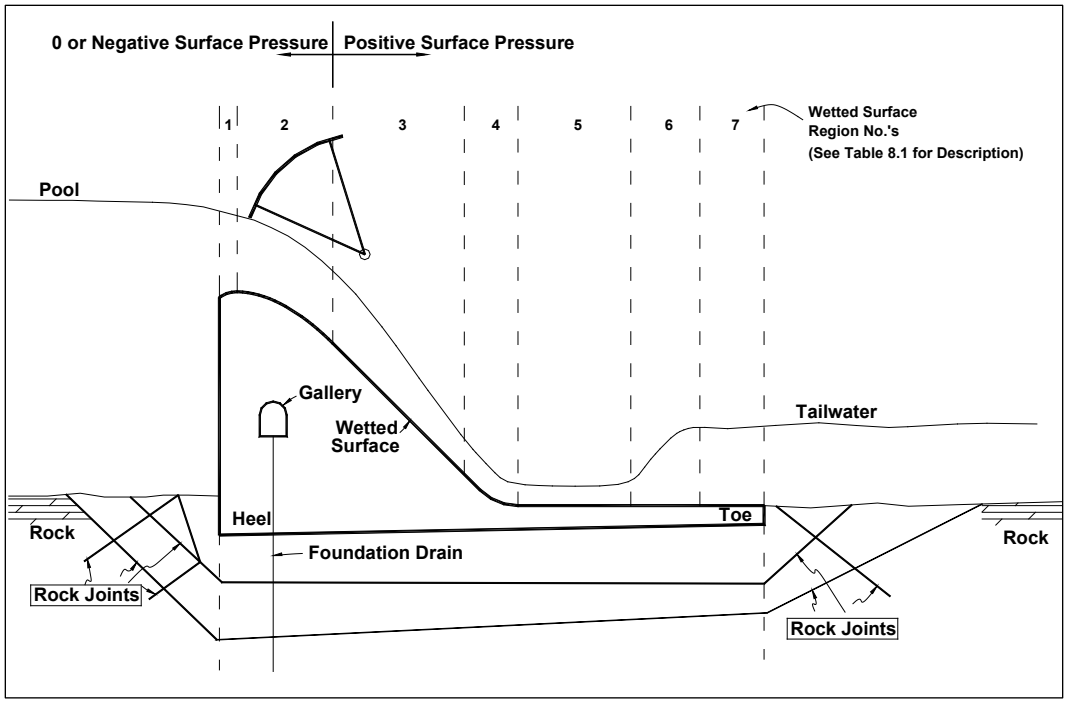

Figure 8.1. Spillway layout and design (SLAD_Foundation).

Table 8.1. Description of wetted surface region no.'s.

Region No.	Description
1	The elliptical shaped section between the upstream face and the crest
2	The elliptical shaped section between the crest and the sloping face of the spillway
3	The slope between the end of the downstream elliptical section to the spillway toe curve. . In this example the slope is 1V on 1H
4	The curve that connects the sloping face to the spillway apron (referred to as toe curve)
5	The section of the spillway apron between the end of the toe curve and the beginning of the hydraulic jump section
6	The section from the beginning to the end of the hydraulic jump. In this example the hydraulic jump is contained on the spillway apron
7	The section from the end of the hydraulic jump to the end of the spillway apron

The term H_e, the actual head on the crest and sometimes referred to as the energy head on the crest, is often used when discussing crest shapes. The term H_d is the head the spillway is designed for. A ratio of H_e/H_d equal to 1 indicates the discharge over the crest is the project design discharge. When H_e/H_d is nearly one, the crest pressures are essentially atmospheric. As this ratio increases, pressures below atmospheric can occur. These negative pressures are the reason for the increase in the discharge coefficient compared to that of a ventilated sharp-crested weir. The intentional use of an H_e/H_d ratio greater than 1 is referred to as underdesigning the spillway with the intent to increase the discharge coefficient. Guidance suggests that this ratio should not exceed 1.33. Crest pressure calculations will provide the design guidance on the limiting pressures that crest underdesigning yields prior to reaching pressures where cavitation damage occurs. The Corps guidance recommends that the crest be designed so that the maximum expected head will result in average pressures on the crest no lower than -15 ft of water at sea level and 40-degree Fahrenheit temperature.

For this discussion, the shape of the undernappe profile will follow that of a jet of water over a sharp-crested weir for the sections near the spillway crest designed based on ellipses. In Figure 8.1, these are sections 1 and 2. The spillway section connected to the lower spillway ellipse, section 3 in Figure 8.1, is a sloped spillway section. In Figure 8.1, section 3 has a slope of 1V on 1H. If this slope is flatter than the trajectory of the undernappe profile, above atmospheric pressures along the spillway surface will occur, and if the slope is steeper than the trajectory of the undernappe profile, sub atmospheric pressures will occur.

The pressures in sections 4-7 are above atmospheric and are dependent on the velocity of the flow entering the spillway apron and the tailwater. Energy and momentum equations are used to compute the hydraulic conditions so the pressures can be determined in these sections.

Determining the spillway surface pressures along the crest, down the slope and along the spillway apron is a challenge due to curving geometry and identifying the hydraulic conditions. A procedure to estimate these pressures is needed for a proper structural stability analysis and will be part of this SLAD development.

2. Results from select example problems have caused the authors of this report to recommend that parametric studies be conducted to sort out the

implications of (a) the overall scale and geometric distribution of rock joint networks, (b) the geometric distribution of rock joint aperture and joint roughness, and (c) rock foundation drain characteristics, on computed uplift pressures and their corresponding resultant forces used in the sliding wedge analysis.

3. Drains intersecting rock joints in a jointed foundation impact the uplift pressures contained within these rock joints and all potential slip plane(s). Because of their importance, an additional investigation of three-dimensional aspects of rock foundation drainage and the use of a simplified two-dimensional the slotted drain model is recommended.

References

Amadei, B., T. Illangesekare, D. Morris, and H. Boggs. 1989a. Estimation of uplift in crack in older concrete gravity dams: Analytical solution and parametric study. *Journal of Energy Engineering* 115(1):19–37.

_____. 1989b. Estimation of uplift in crack in older concrete gravity dams: Effect of head losses in drain pipes on uplift. *Journal of Energy Engineering* 115(1):38–46.

Barton, N. 1973. Review of a new shear strength criterion for rock joints. *Engineering Geology* 7:287–332.

_____. 1982. Modeling rock joint behavior from in situ block tests: Implications for nuclear waste repository design. *Technical Report*. Salt Lake City, UT: TerraTek, Inc., 65–66.

Barton, N., S. Bandis, and K. Bakhtar. 1985. Strength, deformation and conductivity coupling of rock joints. *International Journal of Rock Mechanics, Mining Science, and Geomechanics* Abstracts 22(3):121–140.

Bieniawski, Z. T. 1979. *Tunnel design by rock mass classifications*. Technical Report GL-79-19. Vicksburg, MS: U.S. Army Engineer Waterways Experiment Station.

Cedergren, H. R. 1977 *Seepage, Drainage & Flownets*, second edition. New York, NY: John Wiley & Sons.

Davis, S. N., and R. J. M. DeWiest. 1966. *Hydrogeology*. New York: John Wiley & Sons.

Duncan, J. M. , and S. G. Wright. 2005. *Soil strength and slope stability*. Hoboken, New Jersey: John Wiley and Sons, Inc.

Ebeling, R. M., M. T. Fong, A. Chase, Sr., and E. Arrendondo. 2008. *Fragility analysis of a concrete gravity dam and its system response curve computed by the analytical program GDLAD_Sloping_Base*. ERDC/ITL TR-08-3. Vicksburg, MS: U.S. Army Engineer Research and Development Center.

Ebeling, R. M., L. K. Nuss, F. T. Tracy, and B. Brand. 2000. *Evaluation and comparison of stability analysis and uplift criteria for concrete gravity dams by three Federal agencies*. ERDC/ITL TR-00-1. Vicksburg, MS: U.S. Army Engineer Research and Development Center.

Ebeling, R. M., and M. E. Pace. 1996a. Uplift pressures resulting from flow along tapered rock joints. In *The REMR Bulletin*, February 13(1). Vicksburg, MS: U.S. Army Engineer Waterways Experiment Station.

_____. 1996b. Variation in uplift pressures with changes in loadings along a single rock joint below a gravity dam. In *The REMR Bulletin*, February, 13(1). Vicksburg, MS: U.S. Army Engineer Waterways Experiment Station.

Ebeling, R. M., M. E. Pace, and E. E. Morrison, Jr. 1997. *Evaluating the stability of existing massive concrete gravity structures founded on rock*. Technical Report REMR-CS-54. Vicksburg, MW: U.S. Army Engineer Waterways Experiment Station.

Freeze, A. R., and J. A. Cherry. 1979. *Groundwater*. Englewood Cliffs, NJ: Prentice-Hall, Inc.

Gale, J. E. 1982a. Fundamental hydraulic characteristic of fractures from field and laboratory investigations. In *Papers of AWRC Conference on Groundwater in Fractured Rock*, August 31-September 3, 1982, 79–93.

_____. 1982b. The effects of fracture type (induced versus natural) on the stress-fracture closure-fracture permeability relationships. In *Proceedings of the 23rd U.S. Symposium on Rock Mechanics*, University of California, Berkeley.

Goodman, R. E., B. Amadei, and N. Sitar. 1983. Uplift pressure in crack below dam. *Journal of Energy Engineering* 109(4):207–221.

Grenoble, B. A., C. W. Harris, J. K. Meisenheimer, and D. I. Morris. 1995. Influence of rock joint deformations on uplift pressure in concrete gravity dam foundations: Field measurements and interpretation. In *Fractured and jointed rock masses, Proceedings of the Conference on Fractured and Jointed Rock Masses*, 3-5 June 1992, Lake Tahoe, CA, USA, ed. A. A. Balkema/Rotterdam/Brookfield.

Headquarters, U.S. Army Corps of Engineers (HQUSACE). 1981. *Sliding stability for concrete structures*. ETL 1110-2-256. Washington, DC.

_____. 1994. *Rock foundations*. EM 1110-1-2908. Washington, DC.

_____. 1995. *Gravity dam design*. EM 1110-2-2200. Washington, DC.

_____. 2005. *Stability analysis of concrete structures*. EM 1110-2-2100. Washington, DC.

International Society for Rock Mechanics. 1978. Suggested methods for the quantitative description of discontinuities in rock masses. *International Journal of Rock Mechanics, Mining Science and Geomechanical Abstracts* 15:319–368.

Iwai, K. 1976. Fundamental studies of fluid flow through a single fracture. Ph.D. diss., University of California, Berkeley.

Jeppson, R. W. 1976. *Analysis of flow in pipe networks*. Ann Arbor, MI: Ann Arbor Science Publishers, Inc.

Kranz, R. L., A. D. Frankel, T. Engelder, and C. H. Scholz. 1979. The Permeability of whole and jointed bane granite. *International Journal of Rock Mechanics and Mining Sciences* 16:225–234.

Lee, C.-H., and I. Farmer. 1993. *Fluid flow in discontinuous rocks*. London: Chapman & Hall.

Louis, C. A. 1969. *A study of groundwater flow in jointed rock and its influence on the stability of rock masses*. Rock Mechanics Research Report No. 10. London: Imperial College.

Murphy, W. L., R. M. Ebeling, and J. M. Andersen. 2002. *Assessment of geology as it pertains to modeling uplift in jointed rock: A basis for inclusion of uncertainty in flow models*. ERDC/ITL TR-02-2. Vicksburg, MS: U.S. Army Engineer Research and Development Center.

Nicholson, G. A. 1983. *In-situ and laboratory shear devices for rock: A comparison*. Technical Report GL-83-14. Vicksburg, MS: U.S. Army Engineer Waterways Experiment Station.

Nikuradse, J. 1933. *Stromungsgesetz in rauhren rohren, vdi-forschungsheft* 361. (English translation: *Laws of flow in rough pipes*), 1950. Technical Report, NACA Technical Memo 1292. Washington, DC: National Advisory Commission for Aeronautics.

Pace, M. E., and R. M. Ebeling. 1998. Interaction of a gravity dam, rock foundation, and rock joint with uplift pressures. *Dam Engineering* IX(3):265–305.

Snow, D. T. 1968. Rock fracture spacings, openings, and porosities. *Journal of the Soil Mechanics and Foundations Division*, *Proceedings*, American Society of Civil Engineers, SM1:73-91.

Spangler, M. G., and R. L. Handy. 1973. Soil Engineering, Intext Educational Publishers, New York, NY.

Stone and Webster Engineering Corporation. 1992. *Uplift pressures, shear strengths, and tensile strengths for stability analysis of concrete gravity dams*. TR-100345-V1, Volume 1, Project 2917-05, Final Report, Denver, CO. Prepared for Electric Power Research Institute (EPRI), Palo Alto, CA.

Street, R. L., Watters, G. Z., and J. K. Vennard. 1996. *Elementary fluid mechanics*. 7th ed. New York, NY: John Wiley & Sons.

Tekie, P. B., and B. R. Ellingwood. 2002. *Fragility analysis of concrete gravity dams*. ERDC/ITL TR-02-6. Vicksburg, MS: U.S. Army Engineer Research and Development Center.

Todd, D. K. 1980. *Groundwater hydrology*. 2d ed. New York: John Wiley & Sons.

Tsang, Y. W., and P. A. Witherspoon. 1981. Hydromechanical behavior of a deformable rock fracture subject to normal stress. *Journal of Geophysical Research* 86(10):9287–9298.

Wilson, R. W. 1970. An investigation of laminar flow in fractured porous rocks. Ph.D thesis, University of California, Berkeley.

Witherspoon, P. A., J. S. Y. Wang, K. Iwai, and J. E. Gale. 1980. Validity of cubic law for fluid flow in a deformable rock fracture. *Water Resources Research* 16 (6):1016–1024.

Wood, D. J., and C. O. A. Charles. 1972. Hydraulic network analysis using linear theory. *Journal of Hydraulics Division*, *Proceedings*, American Society of Civil Engineers, 98(HY7).

Wood, D. J. 1966. An explicit friction factor relationship. *Civil Engineering*, American Society of Civil Engineers 36(12):60–61.

Zeigler, T. W. 1976. *Determination of rock mass permeability*. Technical Report S-76-2. Vicksburg, MS: U.S. Army Engineer Waterways Experiment Station.

Appendix A: Stability Analysis of the ETL 1110-2-256 Non-Overflow Dam Embedded in Rock Example

Typical static loading conditions for single- and multiple-wedge systems are presented in this appendix. This example, taken from ETL 1110-2-256 (HQUSACE 1981), is included to validate the formulation programmed in GDLAD_FoundationVM that applies the ETL 1110-2-256 general wedge equation to the sliding analysis of single and multiple wedge systems. Only force equilibrium is satisfied in this analysis; moment equilibrium is not. The shearing force acting parallel to the interface of any two wedges/ sub-wedges is assumed to be negligible. Therefore, the portion of the failure surface at the bottom of each wedge is only loaded vertically by the forces directly above the user specified failure plane because there are no vertical interslice forces acting between the wedges. The free body diagram of Figure A.1 shows the forces acting on the five wedges.

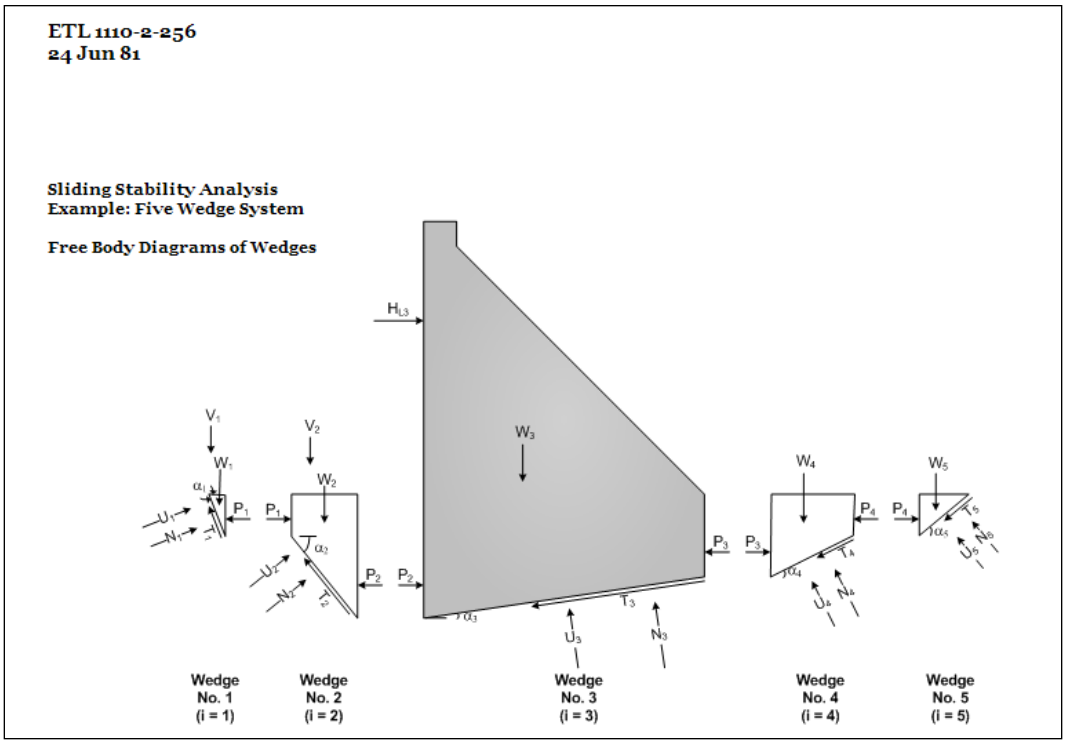

Figure A.1. Free body diagram of forces acting on each wedge.

The governing wedge equation is based on the assumption that shearing forces do not act on the vertical wedge boundaries. The formulation assumes only one structural wedge. Discontinuities in the slip path beneath the structural wedge should be modeled by assuming an average slip plane along the base of the structural wedge. In Figure A.1, the potential slip plane is assumed at the dam to rock foundation interface. According to the ETL 1110-2-256 (HQUSACE 1981) formulation, the governing equation for ($P_{i\text{-}1} - P_i$) applied to each individual wedge is

$$(P_{i-1} - P_i) = \frac{\left[(W_i + V_i)\cos\alpha_i - U_i + (HL_i - HR_i)\sin\alpha_i\right] \frac{\tan\varphi_i}{FS_i} - (HL_i - HR_i)\cos\alpha_i + (W_i + V_i)\sin\alpha_i + \frac{c_i}{FS_i} L_i}{\left(\cos\alpha_i - \sin\alpha_i \frac{\tan\varphi_i}{FS_i}\right)} \quad \text{(bis 6.6)}$$

The interface between the group of driving sub-wedges and the structural wedge is assumed to be a vertical plane located at the heel of the structural wedge and extending to the base of the structural wedge. The magnitudes of the driving sub-wedge forces depend on the value of the Factor of Safety (*FS*) and the inclination angles of the slip path. The general equation only applies directly to active wedges with assumed horizontal active forces.

The interface between the group of resisting sub-wedges and the structural wedge is assumed to be a vertical plane located at the heel of the structural wedge and extending to the base of the structural wedge. The magnitudes of the resisting sub-wedges forces depend on the value of the Factor of Safety (*FS*) and the inclination angles of the slip path. The general equation only applies directly to resisting sub-wedges with assumed horizontal interslice forces. Rock that may be subjected to high velocity water scouring should not be used unless amply protected. Also the compressive strength of the rock layers must be sufficient to develop the wedge resistance. In some cases wedge resistance should not be assumed without resorting to special treatment such as installing rock anchors.

The results from the ETL 1110-2-256 (HQUSACE 1981) calculation of the Factor of Safety (*FS*) against sliding for the five wedge/sub-wedge system (Figure 6.1, Table 6.1, and Table 6.2) are shown in Figure A.2. An iterative procedure is made to converge to the value for the Factor of Safety (*FS*) of approximately 2.0. The convergence is achieved when the sum of all interslice forces is minimized to a small tolerance. This iterative solution is

used to determine the factor of safety for sliding equilibrium. Complete details regarding this procedure of wedge solution analysis using hand-calculations is given in ETL 11102-256 (HQUSACE 1981).

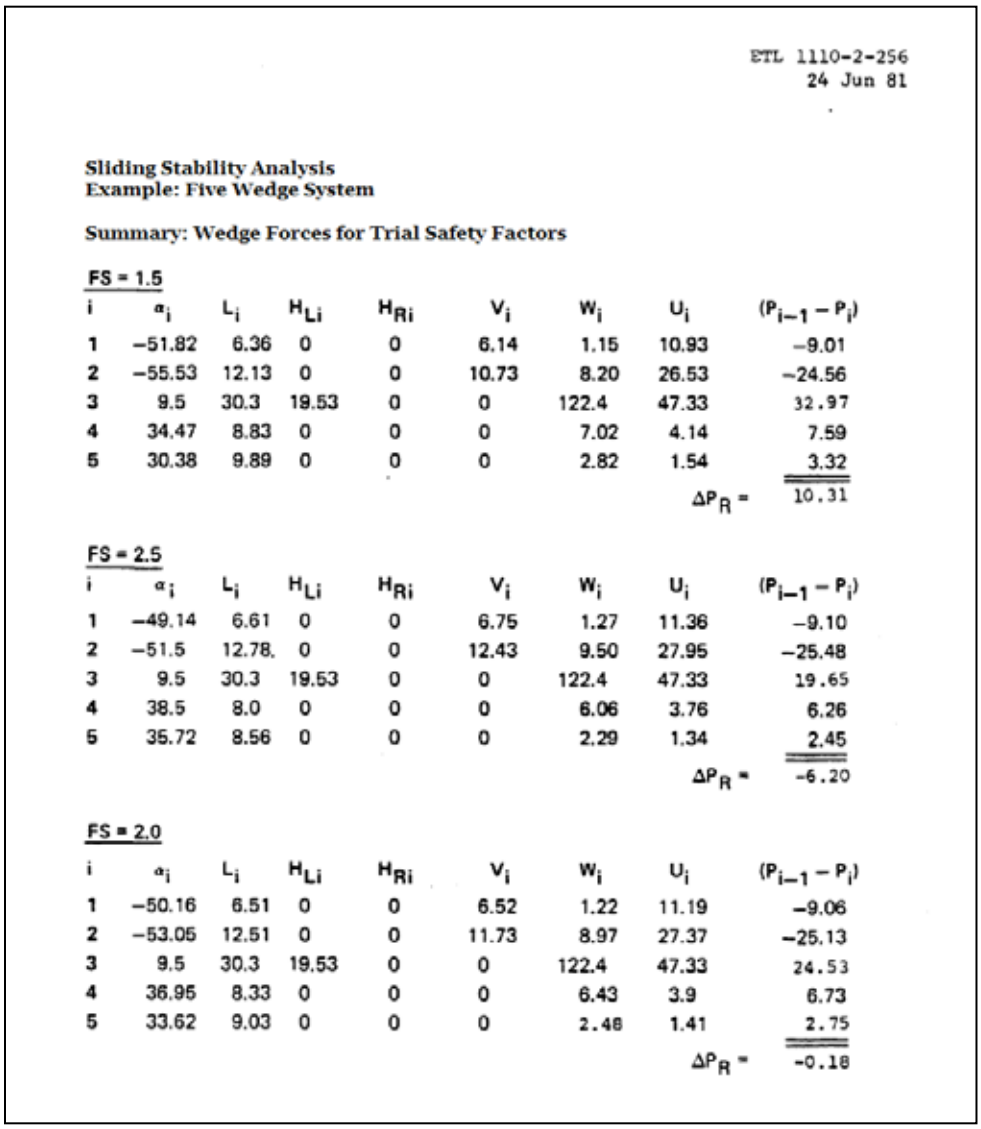

ETL 1110-2-256
24 Jun 81

Sliding Stability Analysis
Example: Five Wedge System

Summary: Wedge Forces for Trial Safety Factors

FS = 1.5

i	α_i	L_i	H_{Li}	H_{Ri}	V_i	W_i	U_i	$(P_{i-1} - P_i)$
1	−51.82	6.36	0	0	6.14	1.15	10.93	−9.01
2	−55.53	12.13	0	0	10.73	8.20	26.53	−24.56
3	9.5	30.3	19.53	0	0	122.4	47.33	32.97
4	34.47	8.83	0	0	0	7.02	4.14	7.59
5	30.38	9.89	0	0	0	2.82	1.54	3.32
							ΔP_R =	10.31

FS = 2.5

i	α_i	L_i	H_{Li}	H_{Ri}	V_i	W_i	U_i	$(P_{i-1} - P_i)$
1	−49.14	6.61	0	0	6.75	1.27	11.36	−9.10
2	−51.5	12.78.	0	0	12.43	9.50	27.95	−25.48
3	9.5	30.3	19.53	0	0	122.4	47.33	19.65
4	38.5	8.0	0	0	0	6.06	3.76	6.26
5	35.72	8.56	0	0	0	2.29	1.34	2.45
							ΔP_R =	-6.20

FS = 2.0

i	α_i	L_i	H_{Li}	H_{Ri}	V_i	W_i	U_i	$(P_{i-1} - P_i)$
1	−50.16	6.51	0	0	6.52	1.22	11.19	−9.06
2	−53.05	12.51	0	0	11.73	8.97	27.37	−25.13
3	9.5	30.3	19.53	0	0	122.4	47.33	24.53
4	36.95	8.33	0	0	0	6.43	3.9	6.73
5	33.62	9.03	0	0	0	2.48	1.41	2.75
							ΔP_R =	-0.18

Figure A.2. Table of wedge forces for trial safety factors.

Appendix B: Mathematical Equations Representing Steady State Flow along Rock Joints (Joint_FLOW)

The flow of groundwater through rock joints can be mathematically modeled as flow through smooth parallel plates with a conducting aperture, e. The hydraulic conductivity (K_{RJ}) of rock joints for two-dimensional (2-D) steady-state flow is a function of the conducting aperture and presented as

$$K_{RJ} = \left(\frac{\gamma_w}{12 \cdot \mu_w} \right) \cdot e^2 \qquad \text{(bis 1.17)}$$

where:

γ_w = unit weight of water
μ_w = dynamic viscosity
e = conducting aperture.

Joint aperture is further discussed in Chapter 4 of this report.

In finite element analysis, a region or specifically rock joints have to be distributed into elements. Figure B.1 gives a representation of multiple rock joints. Each rock joint or element is identified by its number or element id (value highlighted in blue). Each node is also identified by a node id (value with no text highlight). In Figure B.1 there are 5 elements, 6 nodes and 2 junctions (more than 1 element connected to a node). Nodes 2 and 4 are junction nodes.

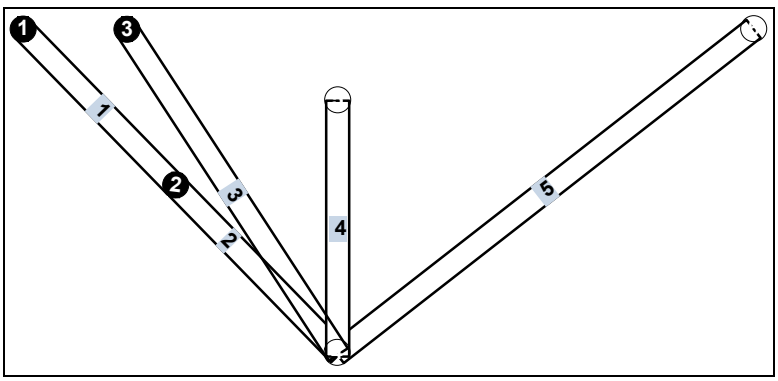

Figure B.1. Five rock joints.

To calculate flow entering or leaving each element, from Darcy's Law, the flow equation in matrix form is defined as the product of the Transmissibility Matrix, S_{ij}, and the total head vector at each node, H_j and is equal to the flow into or out of the node, Q_i. Note that a non-zero value for Q_i is a sink (if negative) or source (if positive) of flow out of or into the node, respectfully, by an external source (e.g., by a pump).

$$(S_{ij}) \cdot (H_j) = (Q_i) \tag{B.1}$$

Each row of the Transmissibility Matrix defines an equation for each element with the coefficients of the Transmissibility Matrix derived as

$$\begin{bmatrix} s_1 & -s_1 & 0 & 0 & 0 & 0 \\ -s_1 & (s_1+s_2) & 0 & -s_2 & 0 & 0 \\ 0 & 0 & s_3 & -s_2 & 0 & 0 \\ 0 & -s_2 & -s_3 & (s_2+s_3+s_4+s_5) & -s_4 & -s_5 \\ 0 & 0 & 0 & -s_4 & s_4 & 0 \\ 0 & 0 & 0 & -s_5 & 0 & s_5 \end{bmatrix} \tag{B.2}$$

Observe the symmetry in the Transmissibility Matrix. Each coefficient is subscripted by its element number and is defined as

$$s_i = \frac{\gamma_w}{12\mu} \cdot (e_i)^3 \cdot \left(\frac{1}{L_i}\right) \tag{B.3}$$

where L_i is the length of the i-th element or rock joint within which steady state seepage occurs.

Flow Equation B.1 is further expanded for the six nodes of Figure B.1. Each equation derived from the Transmissibility Matrix of Equations B.2 and B.3 will result in a series of six simultaneous equations relating heads to flow quantities with the Transmissibility Matrix coefficients represented with their indices in matrix form.

$$\begin{bmatrix} S_{11} & S_{12} & 0 & 0 & 0 & 0 \\ S_{21} & S_{22} & 0 & S_{24} & 0 & 0 \\ 0 & 0 & S_{33} & S_{34} & 0 & 0 \\ 0 & S_{42} & S_{43} & S_{44} & S_{45} & S_{46} \\ 0 & 0 & 0 & S_{54} & S_{55} & 0 \\ 0 & 0 & 0 & S_{64} & 0 & S_{66} \end{bmatrix} \cdot \begin{bmatrix} H_1 \\ H_2 \\ H_3 \\ H_4 \\ H_5 \\ H_6 \end{bmatrix} = \begin{bmatrix} Q_1 \\ Q_2 \\ Q_3 \\ Q_4 \\ Q_5 \\ Q_6 \end{bmatrix} \tag{B.4}$$

The total head boundary conditions (B.C.) at nodes 1, 3 and 6 of Figure B.2 are specified as (H_{Pool} + $h_{e\text{-}1}$), (H_{Pool} + $h_{e\text{-}3}$) and ($H_{Tailwater}$ + $h_{e\text{-}6}$) levels respectively. Observe the pressure head B.C.'s at these three nodes are H_{Pool} , H_{Pool} and $H_{Tailwater}$, respectively. With node 1 and node 3 at the same the elevation, the elevation head $h_{e\text{-}1}$ will be the used to denote the elevation head for both nodes. This is also true for node 6. Flow B.C.'s at the drain at node 5 of Figure B.2 is set equal to Q_{Drain} and are zero elsewhere.

$$H_1 = H_{Pool} + h_{e-1} \tag{B.5}$$

$$H_3 = H_{Pool} + h_{e-1} \tag{B.6}$$

$$H_6 = H_{Tailwater} + h_{e-1} \tag{B.7}$$

$$Q_1 = Q_2 = Q_3 = Q_4 = Q_6 = 0 \tag{B.8}$$

$$Q_5 = -Q_{Drain} \tag{B.9}$$

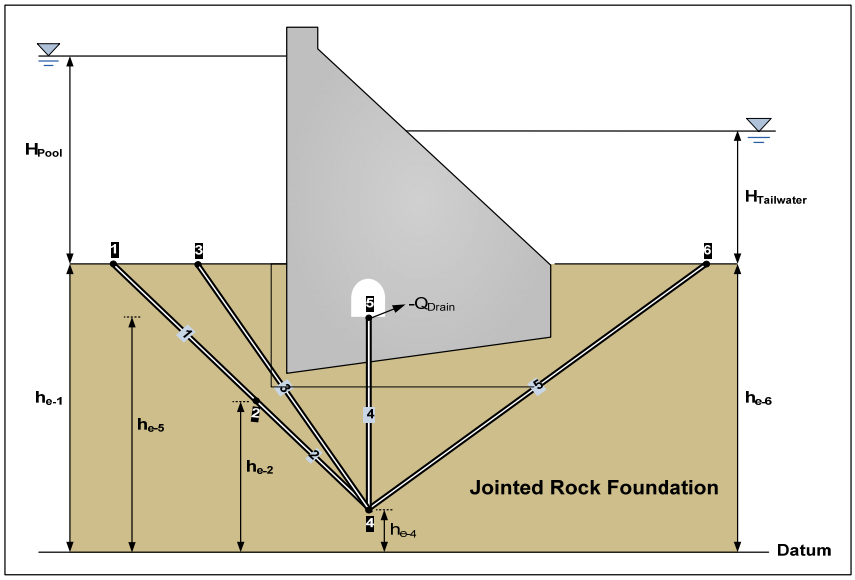

Figure B.2. Head boundary conditions.

Recall that if negative flow is specified for Q_{Drain} (at node 5), an external sink is identified. The user is therefore indicating that water is being pumped out of the node by a pump as idealized by the direction of the Q_{Drain} vector. If positive flow is specified for Q_{Drain} (at node 5), a source is indicated and water is being pumped into the node. These external boundary conditions (a source and a sink, respectively) are depicted by the representation of conditions at each of the two nodes that define element 2 in Figure B.3(a) by the vectors in black. Figure B.3(a) also shows a cross-sectional area of element 2 with the direction of flow (red vector) entering at node 2 from the adjacent element (not shown) and flow (red vector) leaving at node 4 into the adjacent element(s) (not shown). Positive flow represents flow entering an element. This is also true for external sources, as discussed previously. Figure B.3(b) shows the total head values for the same element 2. Note that the direction of flow is from node 2 towards node 4 since node 4 has a lower total head value.

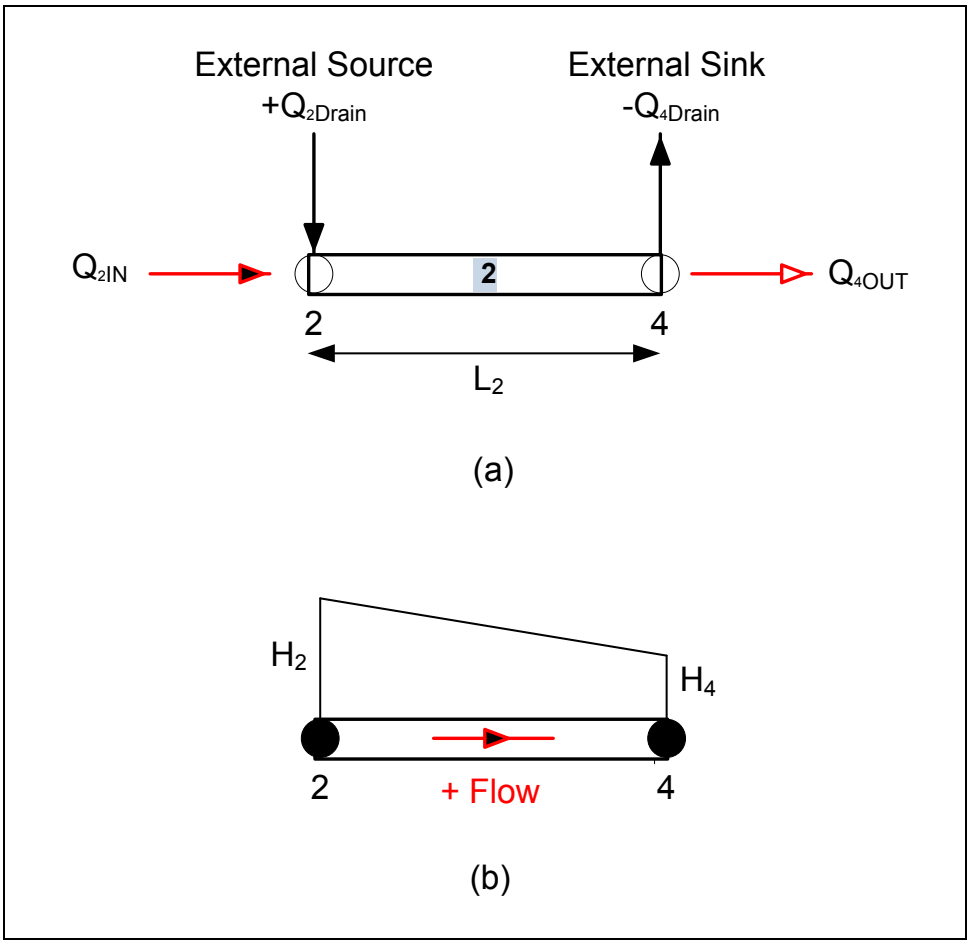

Figure B.3. Generated rock joint element: (a) external sources, and (b) total head boundary conditions.

Introducing the boundary conditions given by Equations B.5 through B.9, Equation B.4 becomes

$$\begin{bmatrix} S_{11} & S_{12} & 0 & 0 & 0 & 0 \\ S_{21} & S_{22} & 0 & S_{24} & 0 & 0 \\ 0 & 0 & S_{33} & S_{34} & 0 & 0 \\ 0 & S_{42} & S_{43} & S_{44} & S_{45} & S_{46} \\ 0 & 0 & 0 & S_{54} & S_{55} & 0 \\ 0 & 0 & 0 & S_{64} & 0 & S_{66} \end{bmatrix} \cdot \begin{bmatrix} H_1 \\ H_2 \\ H_3 \\ H_4 \\ H_5 \\ H_6 \end{bmatrix} = \begin{bmatrix} Q_1 \\ Q_2 \\ Q_3 \\ Q_4 \\ Q_5 \\ Q_6 \end{bmatrix} \tag{B.10}$$

The boundary conditions of Equation B.10 are reported with the total head B.C.'s listed in blue within the total head vector and the sink with a negative value specified for Q_5 (or for a source with a positive value specified for Q_5) external flow B.C. (Q_5 in red) reported in the flow vector (i.e., on the right-hand side of the Equation B.10 equal sign).

An equation solver is then used to solve for the unknown total head values. B.C.'s are introduced into the set of equations and the matrices are manipulated as follows: First, the external B.C. for flow is introduced into the right-hand side flow vector Q_i (i.e., Equations B.8 and B.9). For each node possessing a known total head B.C., the Equation B.10 Transmissibility Matrix will possess a one on the diagonal with all other entries in the row set equal to zero. In the other rows of the Transmissibility Matrix that do not possess a total head B.C., but has entries that are associated with a total head B.C., the product of the Transmissibility Matrix, S_{ij}, entry and the total head B.C. value, H_j, is transferred to the right-hand side vector, as depicted in the Equation B.11 matrices and vectors. Then by Gaussian elimination the Equation B.11 matrices and vectors can be used to solve for the unknown head values (i.e., H_2, H_4 and H_5).

$$\begin{bmatrix} 1 & 0 & 0 & 0 & 0 & 0 \\ 0 & S_{22} & 0 & S_{24} & 0 & 0 \\ 0 & 0 & 1 & 0 & 0 & 0 \\ 0 & S_{42} & 0 & S_{44} & S_{45} & 0 \\ 0 & 0 & 0 & S_{54} & S_{55} & 0 \\ 0 & 0 & 0 & 0 & 0 & 1 \end{bmatrix} \cdot \begin{bmatrix} H_1 \\ H_2 \\ H_3 \\ H_4 \\ H_5 \\ H_6 \end{bmatrix} = \begin{bmatrix} H_{Pool} + h_{e-1} \\ -S_{21}H_1 \\ H_{Pool} + h_{e-1} \\ -S_{43}H_3 - S_{46}H_6 \\ -Q_{Drain} \\ H_{Tailwater} + h_{e-6} \end{bmatrix} \tag{B.11}$$

The equation solver used in *Joint_FLOW* was verified by setting up this example and comparing the output results from the *Joint_FLOW* software with results obtained from using the MATLAB software.

Appendix C: Head Loss in Rock Joint Flow Using Linear Method (LinPipe)

C.1 Introduction

The behavior of flow through natural rock joint network is very similar to the behavior of flow through a pipe network. The technology that has developed for pipe network analysis can be very useful for analyzing flow through rock joint. Goodman et al. (1983) and Amadei et al. (1989a, 1989b) make use of the Darcy-Weisbach equation in calculating the flow head loss in an angle rock joint connection and in the entrance and exit of a rock joint slot into a drain hole. This appendix discusses the analysis of rock joint flow by adopting several technologies that have been developed for pipe networking.

In pipe networking technology, the flow distribution is analyzed by obtaining the continuity equation at each junction and the conservation of energy equation around any closed loop. The continuity equation is generally a linear algebraic equation while the conservation of energy equation around a closed loop generally is a non-linear algebraic equation. There is currently no known method for a direct simultaneous solution of these equations is known.

Most solutions begin by assuming values for the flows, which satisfy the continuity conditions. Corrections to these assumptions are made by utilizing the energy equations with some predetermined methods until a solution with a tolerable difference is reached, in which, both continuity and conservation of energy condition are satisfied.

This technique is used by the following methods:

1. The first, and probably the most widely used, is the Hardy-Cross method. The method makes correction to the initial assumed value by using a first order expansion of the energy equation in terms of a correction factor for the flow rate in each loop. This repetitive process depends on the accuracy of the initial guess. In certain cases, the technique may converge very slowly.

2. The second method, which has been successfully used for the hydraulic network, is Newton-Raphson. This method formulates a set of simultaneous linear equations that can be solved for the flow correction of each loop in the network. Because the method adjusts the flow rates in all loops simultaneously, it converges much faster than Hardy-Cross method.

Both Hardy-Cross and Newton-Raphson methods require an initial guess for flow distribution. A bad estimation may consequently lead to a slow convergence or no convergence at all. The linear method tries to overcome these disadvantages. In pipe networking analysis there are several types of head losses, these are friction head loss, entrance and exit loss, and angle connection loss. The next subsection discusses some basic equations related to the head loss.

C.2 Friction head loss

In moving fluid, energy is dissipated due to friction. Major head losses or friction head losses are associated with energy losses per length of pipe due to friction. Several equations are used to evaluate friction head loss and are discussed in the following sections.

C.2.1 Darcy-Weisbach equation

The most fundamental method used to calculate friction head loss is the Darcy-Weisbach equation

$$h_f = \frac{\Delta P}{\gamma} = f \frac{L}{D} \frac{V^2}{2g} \tag{C.1}$$

where:

h_f = head loss
ΔP = pressure loss
γ = unit weight of water
f = dimensionless friction factor
L = length of pipe
D = pipe diameter
V = average velocity
g = gravity.

For non-circular pressure conduits, D is replaced by four times the hydraulic radius,

$$D = 4R \tag{C.2}$$

and the hydraulic radius is defined as the cross-sectional area divided by perimeter,

$$R = \frac{A}{P} \tag{C.3}$$

where:

A = cross-sectional area
P = wetted perimeter.

C.2.1.1 Friction factor

A systematic test performed by Nikuradse in 1933 (after Jeppson 1976) showed that the friction factor, f, depends on two parameters: the Reynolds number (R_e) and the relative roughness of a pipe wall (e/D),

$$R_e = \frac{V D}{\upsilon} \tag{C.4}$$

where:

υ = kinematic viscosity
e = equivalent roughness.

Nikuradse concluded that

1. When the Reynolds number, R_e <2100, all data regardless of the magnitude of (e/D), will have a friction factor, *f, that* will be a linear function of R_e, i.e., $f = 64/R_e$, and is called laminar flow.
2. For R_e >2100, the flow is turbulent. For a very smooth wetted pipe, the data will fall on the same line. The flow is defined as turbulent smooth or hydraulically smooth.
3. For large Reynolds number and/or large value of (e/D), the friction factor f becomes independent of R_e, and only a function of e/D. The flow is referred as rough

Equations identifying the friction factors for various types of flows are listed in Table C.1 below.

Table C.1. Summary of friction factor equations for Darcy-Weisbach equation (after Jeppson 1976).

Type of Flow	Friction Factor (f)	Range of Application
Laminar	$f = 64/R_e$	$R_e < 2100$
Hydraulically smooth or turbulent smooth	$f = 0.316/R_e^{0.25}$ $\frac{1}{\sqrt{f}} = 2\log_{10}\left(R_e \sqrt{f}\right) - 0.8$	$4000 < R_e < 10^5$ $R_e > 4000$
Transition between hydraulically smooth and wholly rough	$\frac{1}{\sqrt{f}} = -2\log_{10}\left(\frac{e/D}{3.7} + \frac{2.52}{R_e\sqrt{f}}\right)$ $= 1.14 - 2\log_{10}\left(e/D + \frac{9.35}{R_e\sqrt{f}}\right)$	$R_e > 4000$
Hydraulically rough or turbulent rough	$\frac{1}{\sqrt{f}} = 1.14 - 2\log_{10}\left(e/D\right)$ $= 1.14 - 2\log_{10}\left(D/e\right)$	$R_e > 4000$

C.2.1.1.1 Friction factor for laminar flows

For laminar flow, the Reynolds number R_e:

$$R_e = \frac{v\,D}{v} < 2100 \tag{C.5}$$

and friction factor f

$$f = \frac{64}{R_e} \tag{C.6}$$

Using the shear stress equation

$$\tau = -\mu \frac{dv}{dr} \tag{C.7}$$

The head loss equation of (Equation C.1) can be expressed as

$$h_f = \frac{\Delta P}{\gamma} = \frac{\mu}{\gamma} \frac{8\,L}{R^2} V \tag{C.8}$$

Equation C.8 shows that for laminar flow, friction head loss is proportional to the average velocity since the other parameters are constants.

C.2.1.1.2 Friction factor for turbulent flows

The equations relating f to R_e and e/D for turbulent flow cannot be obtained from elementary analysis, but summarized in Table C.1.

For rough flows

$$\frac{1}{\sqrt{f}} = 1.14 - 2\log_{10}\left(\frac{e}{D}\right) \tag{C.9}$$

For hydraulically smooth pipe flows

$$\frac{1}{\sqrt{f}} = 2\log_{10}\left(R_e\sqrt{f}\right) - 0.8 \tag{C.10}$$

Since the friction factor f, appears on both sides of Equation C.10, it must be solved using an iterative scheme. For R_e <100,000, Blasius (see Street et al. 1996) proposes

$$f = \frac{0.316}{R_e^{0.25}} \tag{C.11}$$

For the transition zone between smooth and rough, Colebrook and White (see Street et al. 1996) give the following equation which may also be used for all turbulent flows.

$$\frac{1}{\sqrt{f}} = 1.14 - 2\log_{10}\left(\frac{e}{D} + \frac{9.35}{R_e\sqrt{f}}\right) \tag{C.12}$$

C.2.1.2 Solving Darcy–Weisbach equation using Newton-Raphson iteration

The equation for smooth flow and transitional flow is implicit. This can be solved using a trial and error method. The following states a very effective method for determining f with a computer program.

1. Obtain an estimate of f using the equation for rough flow

$$\frac{1}{\sqrt{f}} = 1.14 - 2\log_{10}\left(\frac{e}{D}\right) \tag{C.14}$$

2. Iteratively correcting this value of f using the following equation

$$\frac{1}{\sqrt{f}} = 1.14 - 2\log_{10}\left(\frac{e}{D} + \frac{9.35}{R_e\sqrt{f}}\right) \tag{C.15}$$

A more general method is the Newton-Raphson method. This process can be done using the Newton-Raphson iteration method with the following equations,

$$slope = f'_{x_i} = \frac{f_{x_i} - 0}{x_i - x_{i+1}} \tag{C.16}$$

$$x_{i+1} = x_i - \frac{f_{x_i}}{f'_{x_i}} \tag{C.17}$$

$$F_f = \frac{1}{\sqrt{f}} - 1.14 + 2\log_{10}\left(\frac{e}{D} + \frac{9.35}{R_e\sqrt{f}}\right) \tag{C.18}$$

$$\frac{dF}{df} = -\frac{1}{2f\sqrt{f}} - \frac{9.35\log_{10}\varepsilon}{f\sqrt{f}\left(\frac{e}{D} + \frac{9.35}{R_e\sqrt{f}}\right)} \tag{C.19}$$

The Newton-Raphson method requires an initial guess that can be given using the equation for turbulent rough flow. It is desirable to be able to distinguish rough flow from transitional flow without looking at the Moody (see Street et al. 1996) diagram. A close approximation of the curve that separates the two conditions is

$$\frac{V\sqrt{\frac{f}{8}}}{\upsilon} e = 100 \tag{C.20}$$

The five steps listed below give the logic for a computer program for solving f, in the Darcy-Weisbach equation using Newton-Raphson method

1. Reading input D, e, υ, v, and L
2. If Re is not given, compute R_e and test whether $R_e < 2100$. If so, $f = 64/R_e$. Otherwise it is turbulent flow.
3. Compute an initial value for f from rough equation.
4. Compute a checking parameter $\frac{eV\sqrt{\frac{f}{8}}}{\upsilon}$ and if this checking parameter >100 then step 3 is correct.
5. Otherwise solve Equation C.16 using Newton-Raphson Method.

C.2.1.3 Explicit friction factor by Wood (1966)

Approximation of f for turbulent equation

$$f = a + \frac{b}{Re^c} \tag{C.21}$$

where:

$$a = 0.094\left(\frac{e}{D}\right)^{0.225} + 0.53\left(\frac{e}{D}\right) \tag{C.22}$$

$$b = 88\left(\frac{e}{D}\right)^{0.44} \tag{C.23}$$

$$c = 1.62\left(\frac{e}{D}\right)^{0.134} \tag{C.24}$$

C.2.1.4 Empirical equations

Instead of Darcy-Weisbach equation, empirical equations are sometimes used to determine a head loss or a pressure drop. Two such equations are

listed in Table C.1. The most widely used one is the Hazen-Williams equation:

English: $$Q = 1.318\, C_{HW}\, A\, R^{0.63}\, S^{0.54} \quad \text{(C.25)}$$

SI: $$Q = 0.849\, C_{HW}\, A\, R^{0.63}\, S^{0.54} \quad \text{(C.26)}$$

where:

C_{HW} = Hazen-Williams roughness coefficient
R = the hydraulic radius
S = the slope of energy line = h_f/L.

The Manning Equation is another equation used to determine head loss or a pressure drop

English: $$Q = \frac{1.49}{n} A\, R^{2/3}\, S^{1/2} \quad \text{(C.27)}$$

SI: $$Q = \frac{1}{n} A\, R^{2/3}\, S^{1/2} \quad \text{(C.28)}$$

English: $$h_f = \frac{4.637\, n^2\, L}{D^{5.333}} Q^2 \qquad (D \text{ and } L \text{ in } ft) \quad \text{(C.29)}$$

$$h_f = \frac{2.64\, x10^6\, n^2\, L}{D^{5.333}} Q^2 \qquad (D \text{ in inches and } L \text{ in } ft) \quad \text{(C.30)}$$

SI: $$h_f = \frac{10.29\, n^2\, L}{D^{5.333}} Q^2 \quad \text{(C.31)}$$

Table C.2 lists values for C_{HW} and n.

C.3 Minor head loss

The head loss relating to exits, entrances, and elbow connection is considered to be minor head loss. In general, the minor head loss can be approximated with an equation that is proportional to the flow velocity squared.

Table C.2. Values of the Hazen-Williams Coefficient, C_{HW}, and the Manning's n, for common pipe materials (after Jeppson 1976).

Type of Pipe	C_{HW}	n
PVC Pipe	150	0.008
Very Smooth Pipe	140	0.011
New Cast Iron or Welded Steel	130	0.014
Wood, Concrete	120	0.016
Clay, New Riveted Steel	110	0.017
Old Cast Iron, Brick	100	0.020
Badly Corroded Cast Iron or Steel	80	0.035

$$h_L = K_L \frac{V^2}{2g} \tag{C.32a}$$

or

$$h_L = C_L Q^2 \tag{C.32b}$$

in which

$$C_L = \frac{K_L}{2gA^2} \tag{C.33}$$

For elbow connection, the value of K_L can be expressed in a linear relationship proportional to the angle of the elbow.

$$K_L\alpha = 0.00286 \qquad \alpha < 25° \tag{C.34a}$$

or

$$K_L\alpha = 0.00077 \quad + 0.03077 \qquad 25° < \alpha < 90° \tag{C.34b}$$

For exit and entrance head loss

$$h_L = K_L \frac{(V_1 - V_2)^2}{2g} \tag{C.35}$$

The incorporation of the minor head loss in rock joint network can be done by adding an equivalent length of the related rock joint

$$\Delta L = \frac{K_L D}{f} \tag{C.36}$$

C.4 Network analysis using linear method

In a rock joint network of n joints, j junctions and l loops, Wood and Charles (1972) showed that the following identity holds:

$$n = j + l - 1 \tag{bis 5.1}$$

Figure C.1 shows a schematic diagram describing the relationship expressed in Equation 5.1. There are six joints (n = 6), five junctions (j = 5), and two loops (l = 2).

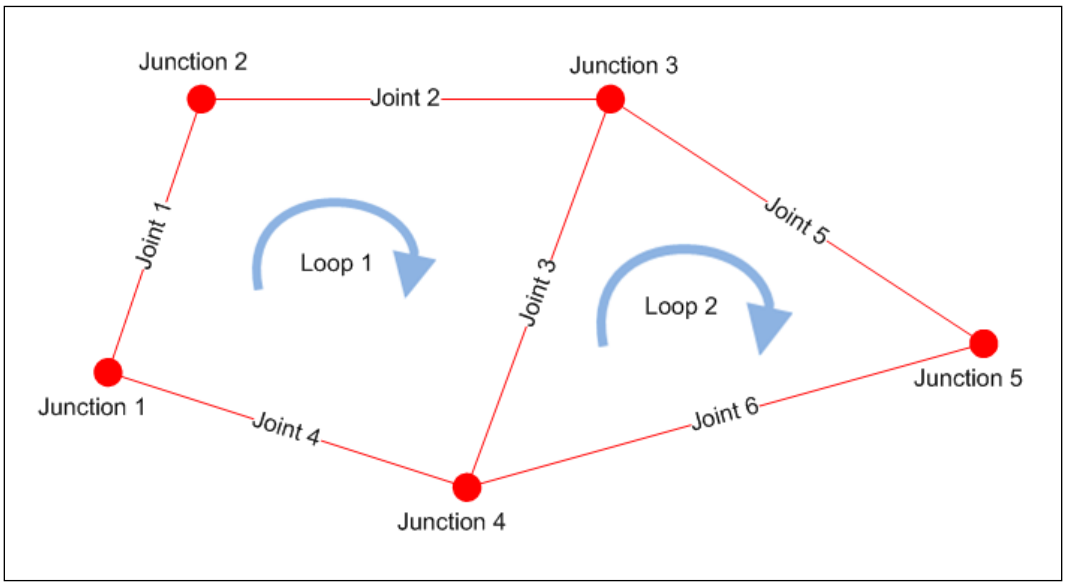

Figure C.1. Schematic diagram describing relationship expressed in bis 5.1.

It is possible to write j-1 linear continuity equations for all but one junction in the rock joint networks. The discharge into the junctions is equal to the discharge out of the junctions:

$$Q_{in} = Q_{out} \tag{C.37}$$

There are l nonlinear energy equation on each loop, such that

$$\sum h_L = 0 \tag{C.38}$$

where h_L represent the head loss in a rock joint in that loop and is a function of the discharge Q. Theoretically, these equations can be solved for the discharge, however the head loss in pipe i is best represented by the following relationship

$$h_{Li} = K_i \, Q_i^a \tag{C.39}$$

in which K_i is a pipeline constant, which normally is a function of line length diameter and type of pipe material; a is an empirical head loss exponent, usually ranging between 1.8 and 2.0. This relationship makes each loop equation nonlinear and there is no method known for the direct solution of this simultaneous equation. Wood and Charles (1972) proposed a transformation of the nonlinear equation into a linear equation by approximating the head loss

$$h_{Li} = K_i \, Q_i^a = K_i \, Q_{i0}^{a-1} \, Q_i = K_i' \, Q_i \tag{C.40}$$

where Q_{i0} is the approximate discharge in line i. When Q_{i0} approaches the actual discharge, the above expression becomes the exact head loss. Using an approximate discharge to compute K_i', the loop equation can be expressed as linear equations and combined with the continuity equations will result in n linear simultaneous network equations, which can be readily solved for the discharge in each line.

The original method proposed setting the initial flow rates to unity, (Q = 1), which would give

$$K_i' = K_i \tag{C.41}$$

However, in Linear Method (LinPipe), the output value of Q from Joint_FLOW is used as an initial value of flow rates.

In Joint_FLOW, for convergence of the solution, the average values of the two prior sets of calculations for flow rates used to compute the best value of the discharge.

$$Q_{i0} = \frac{Q_{i-1} + Q_{i-2}}{2} \tag{C.42}$$

where Q_{i-1} is the flow rates obtained from the previous trial for line i and Q_{i-2} is the flow rates obtained for the trial previous to that.

Example of stiffness matrix development

As an example, consider 2-D pipe or rock joint system illustrated in following Figure C.2: five junctions, six pipes or joints and two loops. Q_A is a known real number, an input flow (or sink) at junction 1, Q_B and Q_C are also known real numbers, out flows (or source) at junctions 4 and 5 respectively. From five (j) junctions, four (j-1) continuity equations can be developed and from the two loops two energy equations can be written. The directions of flows are assumed following the arrow shown in the figure with the flows toward the junction are considered positive.

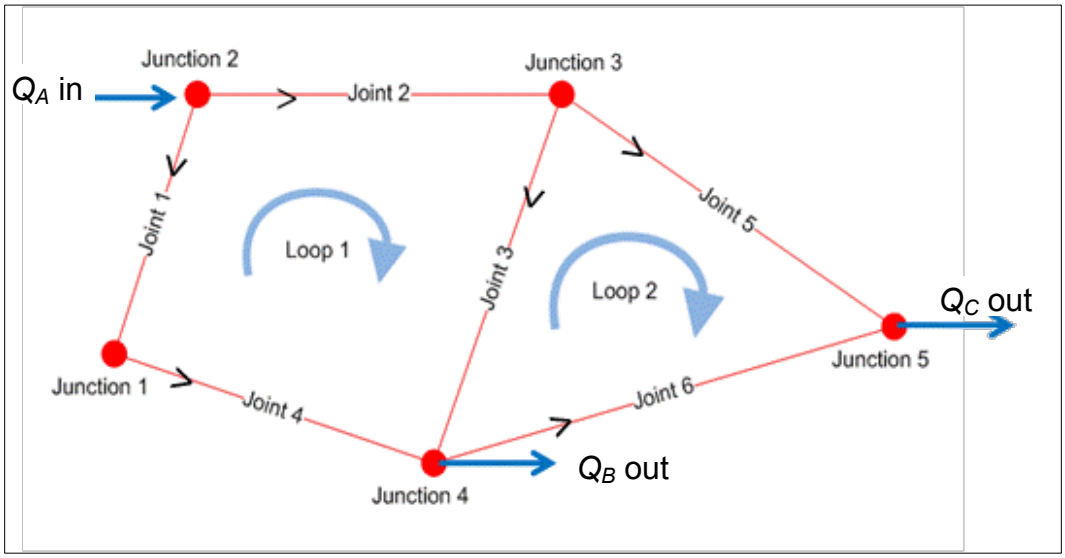

Figure C.2. Schematic diagram example to illustrate the development of stiffness matrices.

The output values of the discharge will be negative if the assumed directions are wrong. The clockwise loop direction is considered positive. In the development of energy equations, the sign is positive when the flows have the same direction with the loop positive direction.

The four continuity equations are:

$$\text{Junction 2:}\quad -Q_1 - Q_2 + Q_A = 0 \tag{C.43}$$

$$\text{Junction 3:}\quad Q_2 - Q_3 - Q_5 = 0 \tag{C.44}$$

$$\text{Junction 4: } Q_3 + Q_4 - Q_6 - Q_B = 0 \tag{C.45}$$

$$\text{Junction 5: } Q_5 + Q_6 - Q_C = 0 \tag{C.46}$$

And the two energy equations are:

$$\text{Loop 1: } -K_1'Q_1 + K_2'Q_2 + K_3'Q_3 - K_4'Q_4 = 0 \tag{C.47}$$

$$\text{Loop 2: } -K_3'Q_3 + K_5'Q_5 - K_6'Q_6 = 0 \tag{C.48}$$

The initial value of K_i' is calculated using the following expressions:

$$K_i' = K_i Q_{Joint\_FLOW} \tag{C.49}$$

Using Hazen-Williams equation, the value of

(English unit)
$$K_i = \frac{4.77L}{C^{1.852} D^{4.87}} \tag{C.50}$$

or

(SI unit)
$$K_i = \frac{10.78L}{C^{1.852} D^{4.87}} \tag{C.51}$$

where:

L = pipe or joint length (ft or m)
C = pipe or joint surface coefficient (from Table C.2)
D = pipe diameter or joint diameter equivalent (ft or m) (from Equation C.2).

Combining the four continuity equations and two energy equations, the simultaneous equations are expressed in the following matrix:

$$\begin{bmatrix} -1 & -1 & 0 & 0 & 0 & 0 \\ 0 & 1 & -1 & 0 & -1 & 0 \\ 0 & 0 & 1 & 1 & 0 & -1 \\ 0 & 0 & 0 & 0 & 1 & 1 \\ -K_1' & K_2' & K_3' & -K_4' & 0 & 0 \\ 0 & 0 & -K_3' & 0 & K_5' & -K_6' \end{bmatrix} \cdot \begin{bmatrix} Q_1 \\ Q_2 \\ Q_3 \\ Q_4 \\ Q_5 \\ Q_6 \end{bmatrix} = \begin{bmatrix} -Q_A \\ 0 \\ Q_B \\ Q_C \\ 0 \\ 0 \end{bmatrix} \tag{C.52}$$

Appendix D: Description of the GDLAD_ Foundation ASCII Input Data File (GDLAD_Foundation.in)

D.1 Introduction

This appendix lists and describes the contents of the ASCII input data file to the FORTRAN engineering computer program of the stability analysis portion of GDLAD_Foundation. This input data file, always designated as GDLAD_Foundation.in, is created by the graphical user interface (GUI), the visual modeler portion of GDLAD_Foundation.

The ASCII input data to GDLAD_Foundation is provided in the following 10 groups of data.

D.2 Group #1 – Project identification

DT Stamp

Header

with

DT Stamp = Information pertaining to file creation date and time.

Header = Comment line regarding project information.

D.3 Group #2 – Geometry, parameters and properties of a concrete gravity dam

Num_Dam_Points, Num_Materials, K_type

X_Dam (i), Y_Dam (i) [i = 1 to Num_Dam_Points; i = 1 corresponds to the Heel and i = Num_Dam_Points corresponds to the Toe**]**

Drain_System, L_Drain

GAMA_concrete, GAMA_water

Unit_index, Gconstant

Tolerance

with

Num_Dam_Points	=	Number of points identifying the structure of the concrete gravity dam. These points are specified in a clockwise orientation, from the Heel to the Toe.
Num_Materials	=	Number of materials specifying various rock strength properties.
K_type	=	1, Mechanical Aperture with JRC
	=	2, Conducting Aperture
	=	3, Permeability of joint with filling (Not available)
	=	4, Hydraulic Conductivity of Clean joint
X_Dam	=	global x-coordinate of the points defining the dam geometry region
Y_Dam	=	global y-coordinate of the points defining the dam geometry region
Drain System	=	0, No Galley or line of drains
	=	1, Closed Drainage Gallery system
	=	2, Open Drainage Gallery system (only available for Key_Flow options of 4, 5, and 6 from group 6, section 7)

L_Drain = Distance along the base of the gravity dam as measured from the Heel to the intersection of the line of drains (refer to Figure 1.1)

GAMA_concrete = Unit weight of concrete

GAMA_water = Unit weight of water

Unit_Index = 1, English Unit

= 2, Metric Unit

Gconstant = The gravitational constant. The value for Gconstant identifies the units of length, density, force and pressure being used according to the Table D.1 below.

Tolerance = Value which determines the residual interslice imbalance force has reached equilibrium.

Table D.1. Table of units.

Value for Gconstant	Units of Length	Units of Silt and Concrete Densities	Units of Force	Units of Pressure
32.174	feet	lb/ft^3	lbs	lb/ft^2
386.086	inches	lb/in^3	lbs	lb/in^2
9.80665	meters	kN/m^3	kN	kN/m^2 (=kPa)
980.665	centimeters	kN/cm^3	kN	kN/cm^2
9806.65	millimeters	kN/mm^3	kN	kN/mm^2

D.4 Group #3 - Characteristics of the Gallery

Key_Gallery

H_Gallery, B_Gallery, R_Gallery

X_W_Gallery, Y_B_Gallery, Y_Gallery

X_T_Drain, Y_T_Drain, X_B_Drain, Y_B_Drain

with

Key_Gallery = 0, silt is not considered in this analysis

= 1, generate at rest lateral pressure coefficient uncertainties

= 2, deterministic analysis

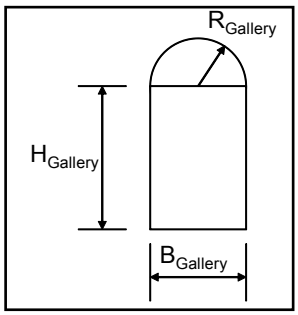

H_Gallery = Height of rectangular portion of the gallery

B_Gallery = Width of gallery

R_Gallery = Radius of gallery ceiling

X_W_Gallery = Horizontal distance from center of gallery to toe.

Y_B_Gallery = Vertical distance from the center of gallery to toe.

Y_Gallery = Vertical distance from the base of the gallery to the point where the line of drains intersect the base of structure.

X_T_Drain = X-coordinate of the center base of gallery

Y_T_Drain = Y-coordinate of the center base of gallery

X_B_ Drain = X-coordinate of the point where the line of drains intersect the base of the gravity dam.

Y_B_ Drain = Y-coordinate of the point where the line of drains intersect the base of the gravity dam.

D.5 Group #4 - Characteristics of the anchor forces and moment

Key_FA

MeanFA

X_top_Anchors, Y_top_Anchors, X_base_Anchors, Y_base_Anchors

with

Key_FA	=	0, anchor forces are not considered in this analysis
	=	1, generate resultant anchor force uncertainties
	=	2, deterministic analysis
MeanFA	=	Resultant anchor force
X_top_Anchors	=	x-coord of anchor point at top of dam
Y_top_Anchors	=	y-coord of anchor point at top of dam
X_base_Anchors	=	x-coord of anchor point at base of dam
Y_base_Anchors	=	y-coord of anchor point at base of dam

D.6 Group #5 - Characteristics of silt parameters

Key_Ko

Mean_Ko

H_Silt, Gamma_Moist, Gamma_Saturated

with

Key_Ko	=	0, silt is not considered in this analysis
	=	1, generate at rest lateral pressure coefficient uncertainties
	=	2, deterministic analysis

MeanKo = Mean value of pressure coefficient (for Key_Ko > 0)

H_Silt = the depth of silt as measured from the Heel

Gamma_Moist = moist unit weight of silt (above the water)

Gamma_Saturated = saturated unit weight of silt (below the water)

D.7 Group #6 – Simulations with probabilistic and/or deterministic parameters

Key_Analysis, Key_Flow

NumberOfSimulations

Key_C_PHI(i) [i = 1 to Num_Materials]

with

Key_Analysis = 1, probabilistic analysis

= 2, deterministic analysis

Key_Flow = 1, Flow along slip plane (Joint_FLOW results) and no flow between vertical wedge interfaces.

= 2, Flow along slip plane (Joint_FLOW results) and simplified calculations for flow between vertical wedge interfaces.

= 3, Flow along slip plane and flow between vertical wedge interfaces (Joint_FLOW results)

= 4, Calculate uplift from hydrostatic pressures and incorporate an implied crack at the dam.

= 5, Compute the uplift from the Line of Seepage Method along the structure wedge

= 6, Compute the uplift from the Line of Seepage Method along a potential sliding plane

NumberOfSimulations = Number of simulations (or samples) per pool elevation

= 1, deterministic analysis

Key_C_PHI = 1, generate C and PHI probabilistic values,

= 2, generate only C probabilistic values,

= 3, generate only PHI probabilistic values,

= 4, deterministic analysis;

D.8 Group #7 – Classification of pool elevations

Num_Pools

PoolArray (i), TailArray (i) [i = 1 to Num_Pools]

with

Num_Pools = Number of pool elevations

PoolArray = Array of pool elevation values

TailArray = Array of tail water elevation values

D.9 Group #8 –Configuration of the wedge system

Num_Wedges, Structural_Wedge

Wedge_Id, Num_Sub_Wedges (i) [i = 1 to Num_Wedges]

Sub_Wedge_Id, Num_Nodes (k, i) [k = 1 to Num_Sub_Wedges)

X_W (j, k, i), Y_W (j, k, i) [j = 1 to Num_Nodes (k, i)]

matid(i,k), C(i,k), Phi(i,k), G(i,k)

Surface_Nodes

X_S(j), Y_S(j) [j = 1 to Surface_Nodes]

with

Num_Wedges	=	the total number of wedges
Structural_Wedge	=	the wedge id of the structural wedge
Wedge_Id	=	wedge number
Num_Sub_Wedges	=	number of sub-wedges within each wedge
Sub_Wedge_Id	=	sub-wedge number
Num_Nodes	=	number of nodes within each sub-wedge
X_W	=	x-coordinate of node
Y_W	=	y-coordinate of node
Matid	=	material number for each sub-wedge within a wedge
C	=	cohesion value for each sub-wedge within a wedge

Phi = internal friction angle for each sub-wedge within a wedge

G = Unit weight for each sub-wedge within a wedge

Surface_Nodes = number of ground surface nodes topping each wedge

X_S = x-coordinate of ground surface node

Y_S = y-coordinate of ground surface node

D.10 Group #9 – Calculations of uplift pressures

Key_JointFLOW*

Key_E, MeanE****

Path*, Wedge***, MeanHP***, MeanHF***, MeanLHF***, MeanU(i)***, MeanLU(i)***[i = 1 to Num of Simulations]**

with

Key_JointFLOW* = 0, Non-site specific uplift pressures

= 1, Site specific uplift pressures and locations using Joint_FLOW results

= 2, generate **only** uplift pressures using Joint_FLOW results

= 3, generate **only** location of uplift pressures using Joint_FLOW results

= 4, deterministic analysis of uplift pressures and locations using Joint_FLOW results (Key_E = 0)

Key_E**	=	0, Drain efficiency not considered to compute uplift pressure, (when Key_JointFLOW=1)
	=	1, generate non-site specific uplift pressure, E values for structural wedge
	=	2, deterministic analysis
MeanE**	=	Mean value of the drain efficiency (for Key_E > 0)
Path**	=	the potential sliding plane id
Wedge***	=	the wedge number for this Path**
MeanHP***	=	mean water_pressure for this Wedge**
MeanHF***	=	resultant horizontal force for this Wedge**
MeanLHF***	=	location of the resultant horizontal force at this Wedge**
MeanU***	=	Mean value of uplift force normal to the base of this Wedge**
MeanLU***	=	Mean value of uplift force's resultant location as measured along the base of this Wedge**

*Note: Values for this parameter are specified when the site specific (i.e., Key_JointFLOW > 0) uplift pressure distribution as described in Appendix E is to be used in the analysis. Otherwise, non-site specific data is specified.

*Note: For site-specific uplift pressures (i.e. Key_JointFLOW > 0), the analysis type of probabilistic or deterministic is considered for the entire analysis and not on a per pool/tailwater basis.

**Note: Values for these parameters are necessary when the non site-specific drain efficiency (i.e. Key_JointFLOW = 0) is to be calculated in this analysis.

***Note: Values for these parameters are specified when the site specific pressure distribution (Key_JointFLOW = 1) is to be used in the analysis, otherwise, the values for these parameters are set to zero. These parameters are computed for each pool and tailwater elevation pair and are specified within the ASCII file (Uplift.dat) which is produced from the program *Joint_FLOW*, executed externally from GDLAD_Foundation.

D.11 Group #10 – Output forces for all wedges

Num_Trials

ItrPool

Trials (i), [i = 1 to Num_ Iterations]

with

Num_Trials	=	Specifies number of trials to output (includes the converged data at the end)
	=	0, no output documented.
	=	-1, writes out only the converged data for specified Pool
	=	-2, writes out all data for specified Pool
ItrPool	=	Pool at which to write out data
Trials	=	identify the trial numbers to record forces.

Appendix E: Description of the Joint_FLOW with optional LinPipe ASCII Input Data File (Jointflow.in)

E.1 Introduction

This appendix lists and describes the contents of the ASCII input data file to the FORTRAN engineering computer program, *Joint_FLOW*, which conducts the seepage analysis portion of GDLAD_Foundation. This input data file, always designated as Jointflow.in, is created by the graphical user interface, GDLAD_FoundationVM, the visual modeler portion of GDLAD_Foundation.

Guidance to the ASCII input data is provided in the following 10 groups of data.

E.2 Group #1 – Project identification

DT Stamp

Header

with

DT Stamp = Information pertaining to file creation date and time.

Header = Comment line regarding project information.

E.3 Group #2 – Specifications of types of analysis

Method, K_type, Unit_type, Drain_model, linpipe, analysis

with

Method = 1, Deterministic analysis

= 2, Probabilistic analysis

K_type	= 1, Mechanical Aperture with JRC
	= 2, Conducting Aperture
	= 3, Permeability of joint with filling (Not available)
	= 4, Hydraulic Conductivity of Clean joint
Unit_type	= The units of length, head, flow, hydraulic conductivity, aperture, viscosity and roughness are listed in Table E.1 below
	= 1, English Units
	= 2, Metric Units
Drain_model	= 0, No drains
	= 1, Drain model is a simple model
	= 2, Drain model is a linear model (Not available)
linpipe	= 0, Linear pipe model not used
	= 1, Linear pipe model used for pipe networking
analysis	= 1, Stability and Joint_FLOW analysis
	= 2, Stability and Simplified Seepage analysis
	= 3, Joint_FLOW analysis only (includes calculated Uplift)

Table E.1 Table of units.

Units	X, Y* Coordinates	Head**	Q	Hydraulic Conductivity	Mechanical Aperture E***	Conducting Aperture e***	Joint_FLOW	Linear Pipe	
							Dynamic Viscosity	Kinematic Viscosity	Pipe Roughness
English	feet	ft	ft^3/sec	ft/sec	inches	inches	lb-sec/ft^2	ft^2/sec	ft
Metric	meters	m	m^3/sec	m/sec	microns***	microns***	N-sec/m^2	m^2/sec	m

* Joint coordinates are specified with respect to a specified datum for each problem analyzed.

** Heads are specified without regard to datum.

*** 100 μm = 1 x 10-6 m.

E.4 Group #3 – Quantification of parameters

N_EL, N_ND, N_HEAD_BC, N_FLOW_BC, N_DRAIN, IDRSEG, NUM_MAT, NPATHS, N_RESLVL, N_POOL, N_TAILWATER, N_sim

with

N_EL = Number of elements

N_ND = Number of nodes

NUMHEAD_BC = Number of head boundary conditions

NUMFLOW_BC = Number of flow boundary conditions

N_DRAIN = Drain Element

IDRSEG = Number of drain segments

NUM_MAT = Number of materials

NPATHS = Number of flow paths (only 1 available)

N_RESLVL = Number of reservoir levels for simulations

N_POOL = Number of upstream surface nodes

N_TAILWATER = Number of downstream surface nodes

N_sim = Number of simulations

= 1, Deterministic Analysis

> 1, Probabilistic Analysis

Appendix F: Line of Seepage Formulation

This appendix discusses the Line of Seepage associated with Flow Option 6, a simplified procedure for seepage analysis. The transformation procedure for the Line of Seepage Method is for one-dimensional flow along a singular path consisting of a series of rock joints. For the generalized formulation, these rock joints may contain different values for the hydraulic conductivity of the rock joints.

The simplified formulation referred to as the Line of Seepage Formulation for one-dimensional flow within rock joint reaches in a single series configuration is based on the fact that the specific discharge v must be the same entering each reach as it is leaving; in fact, it must be constant from rock reach *j* to the next rock joint reach *j+1*. A constant value for hydraulic conductivity in each rock joint reach *j*, k_j, is assumed in this formulation. Freeze and Cherry (1979) discuss these issues using their analogous Figure 2.9 problem for one-dimensional (vertical) seepage from one stratified soil layer through to another layer. The basic principle of the Line of Seepage Formulation will be shown using the Figure F.1 of two horizontal rock joint reaches in a single series. The total head loss along the two rock joint reaches is designated ΔH with the head loss along rock joint reach 1 and rock joint reach 2 designated as ΔH_1 and ΔH_2, respectively,

$$\Delta H = \Delta H_1 + \Delta H_2 \tag{F.1}$$

From Darcy's law

$$v = k_1 \frac{\Delta H_1}{L_1} = k_2 \frac{\Delta H_2}{L_2} \tag{F.2}$$

Observe that the second term on the right hand side in Equation F.2 is the hydraulic gradient i_j for each rock joint reach j, equal to the change (i.e., drop) in total head per distance L_j along the flow path in rock joint reach *j* in which this drop occurs

$$i_j = \frac{\Delta H_j}{L_j} \tag{F.3}$$

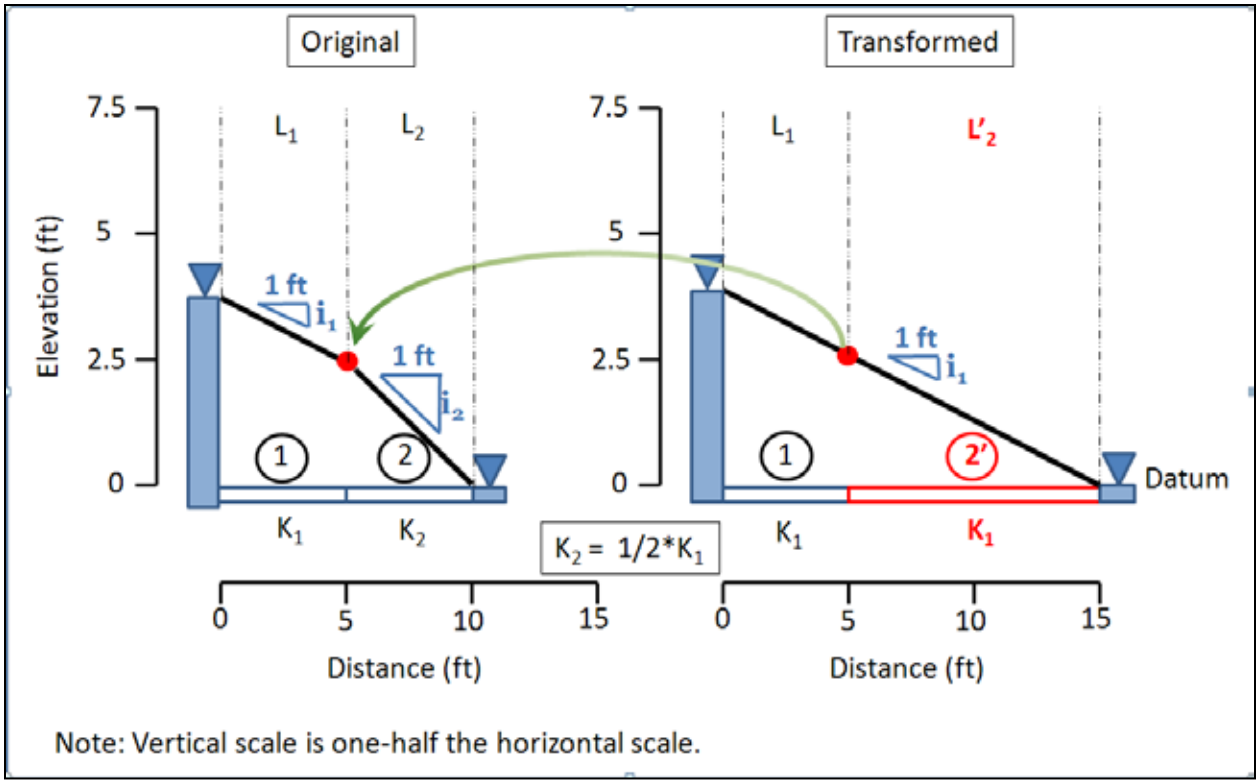

Figure F.1 Original and Transformed sections for one-dimensional flow within two rock joint reaches in a single series.

Introducing Equation F.3, Equation F.2 becomes

$$k_1 i_1 = k_2 i_2 \tag{F.4}$$

The objective is to construct a transformed section for rock joint reaches which will all posses a constant value of hydraulic conductivity, set equal to that of the first rock joint reach, k_1 , in this formulation. The Spangler and Handy (1973) Figure 12-1 demonstrates using a simple flow net for steady state, one-dimensional seepage through a horizontal layer of length "*d*" filled with a homogenous sand of constant hydraulic conductivity *k* and subjected to a head differential ΔH from one end to the other end, this signifies that a constant value for the hydraulic gradient is developed along the entire length. With known head boundary conditions at the start and end points of the soil layer of length "*d*" and with a constant hydraulic gradient, the distribution of head at all points along the soil layer may be established from these three problem features. This is the essential feature of the solution process being used in the Line of Seepage Formulation for one-dimensional flow within rock joint reaches in a single series configuration. The hydraulic conductivity and length of rock joint of reach 1 in the

Original and Transformed sections remains the same. The transformation used in this formulation will be applied to all other rock joint regions. In our case of the Figure F.1 problem, this will require the calculation of a transformed length for rock joint reach 2, L'_2, such that the hydraulic gradient for this transformed rock joint reach 2, i'_2, be equal to i_1. Thus, the gradient is constant along all rock joint reaches (of the transformed section) mirroring the result from the Spangler and Handy (1973) Figure 12-1 example for one dimensional flow in a porous material (of length "*d*") possessing a constant value for hydraulic conductivity. The requirement for the transformed section for rock joint reach 2 is expressed as

$$i'_2 = i_1 \tag{F.5}$$

With the head drop for rock joint reach 2, ΔH_2, being the same for the original and the transformed section, the hydraulic gradient i'_2 is

$$i'_2 = \frac{\Delta H_2}{L'_2} \tag{F.6}$$

Introducing Equation F.6 into Equation F.5,

$$\frac{\Delta H_2}{L'_2} = i_1 \tag{F.7}$$

Rearranging Equation F.7 and solving for L'_2, allows for the observation that the transformed section length is required to be

$$L'_2 = \frac{\Delta H_2}{i_1} \tag{F.8}$$

The authors of this report observe that a more convenient transformed length equation may be developed that is a function of known geometry and material property terms. This more convenient transformation relationship is derived from the introduction of Equations F.7 and F.3 (for rock joint reach $j = 2$) into Equation F.4,

$$k_1 \frac{\Delta H_2}{L'_2} = k_2 \frac{\Delta H_2}{L_2} \tag{F.9}$$

Solving for the transformed length of rock reach 2, Equation F.9 becomes

$$L_2' = \frac{k_1}{k_2} L_2 \tag{F.10}$$

Equation F.10 expresses the transformation that is the core of the simplified Line of Seepage procedure of analysis. The transformed length for rock joint reach 2 is dependent on the known values for hydraulic conductivity, k_1 and k_2, and the original length of rock joint reach 2, L_2. The values for these three terms are known. Observe in the Figure F.1 Transformed section, that the transformed length of the entire series of rock joint reaches posses the same slope in head loss with distance along the length of each of rock joint reaches, i.e., a constant value for the hydraulic gradient. This constant hydraulic gradient is equal to that for rock joint reach 1 in the Original section, i_1. Using the Transformed section feature of a single (i.e., constant) hydraulic gradient along with the head boundary conditions at the starting and ending point of the single reach series of rock joints, the distribution of total head may be established along the entire length of Transformed space. These head values can then be transformed back to the Original section for use in the stability calculation using the inverse of Equation F.10 for rock joint region 2 as a measurement from the starting point of rock joint reach 2. The coordinate of the point in the transformed section rock joint region 2 back into the Original system is established by using the relationship

$$x = L_1 + \frac{k_2}{k_1} \Delta x_2' \tag{F.11}$$

with $\Delta x'_2$ being the distance to the point of interest as measured from the start of rock joint region 2 in the transformed section. The total head is the same value in both the Original and Transformed plots at this point (i.e., only the position of the point will change when reverting back to the Original plot). As an example, consider the point defined at the end of rock joint reach 2. The distance from the start of transformed rock joint reach 2 to the end point in rock joint region 2, $\Delta x'_2$, in the transformed section is 10 ft. The ratio of k_2 divided by k_1 is equal to 0.5. The length of rock joint reach 1, L_1, is 5 ft. Substitution of these values into Equation F.11 results in an x-coordinate of 10 ft, at which point the total head is equal to zero feet. Recall that its total distance as measured along the transformed x-axis is 15 ft.

The transformation of Figure F.1 distribution of head conditions along all of the Transformed rock joint reaches back to the Original section shows that the gradient for rock joint reach 1 is the same as in the Transformed

section (a requirement set at the beginning of this formulation). But the actual gradient in the Original rock joint reach section 2, i_2, differs from the gradient value in the transformed section, i'_2.

The development of a Transformed section in Figure F.1 (via Equation F.10,) allows for the introduction of total head boundary conditions on either end of the rock joint reaches in a single series, at the reach in contact with the upstream pool and at the end reach in contact with the downstream tailwater. These end total head boundary conditions along with the fact that a constant gradient exists along the entire length of the transformed sections allow for the establishment of the distribution of total heads at all points along the transformed rock joint reaches by using these three problem features. The total heads at all points may then be "mapped back" to the Original section using Equation F.11 for rock joint reach 2. Additionally, in Section 6.5 of Chapter 6 of this report for Flow Option 6, it has been shown that a user defined value for drain efficiency, *E*, for closed or open drainage gallery systems may be introduced into the transformed section to help establish the interior head boundary condition at the intersection of the line of drains and the rock joint reaches and along this single series of reaches. These head values can then be transformed back to the Original section for use in the stability calculation as well.

Consider the case of the two horizontal rock joint reaches, labeled Original, in Figure F.1. Flow is one-dimensional within the two rock joint reaches in a single series. Each of the two reaches is 5 feet in length. The left-hand side of reach 1 is subjected to a total head of 3.75 ft and the right-hand side of reach 2 is subjected to a total head of 0 ft. The datum is as noted in this figure. The hydraulic conductivity of rock joint reach 2 is one-half that of rock joint reach 1 (Table F.1). By application of Equation F.10, the transformed length of rock joint reach 2 becomes 10 ft. The total differential head ΔH for the Figure F.1 Transformed section is equal to 3.75 ft and is applied to the total length of Transformed section, equal to 15 ft. The hydraulic gradient for the Transformed section is

$$i = \frac{\Delta H}{L_1 + L'_2} = \frac{3.75\ ft}{15\ ft} = 0.25 \tag{F.12}$$

Recall that since the Transformed section was constructed assuming a hydraulic conductivity equal to k_1, the value for rock joint region 1, the value

Table F.1. Summary of Original and Transformed section rock joint reach lengths and hydraulic gradients.

Reach No. j	Hydraulic Conductivity		Reach Length's		Hydraulic Gradient's	
	Hydraulic Conductivity Designation k_j (ft/sec)	Value for Hydraulic Conductivity per Reach (ft/sec)	Original Length of Reach, L_j (ft)	Transformed Length of Reach, L'_j (ft)	Hydraulic Gradient per Original Reach	Hydraulic Gradient for the Transformed Reaches
1	k_1	k_1	5	5	0.25	0.25
2	k_2	(1/2)* k_1	5	10	0.50	

for hydraulic gradient calculated using Equation F.12 corresponds to the value for i_1, as noted in this Transformed figure. Additionally, by imposing the total head boundary conditions of (1) the left-hand side and (2) the right-hand side, along with (3) a hydraulic gradient of 0.25, the distribution of total head is established at all points along the Transformed rock joint feature. For example, at the intersection of rock joint reaches 1 and 2, a distance of 5 ft along the *x*-axis, the total head is established on the Transformed figure to be equal to 2.5 ft. For rock joint region 1, the *x*-coordinates in the Original and Transformed systems are the same for all points (i.e., L_1 is equal to L'_1). For all points in rock joint reach 2 (i.e., beyond the end of rock joint reach 1), the Original system *x*-axis points are determined using the transformation Equation F.11. Observe in Figure F.1 that at each point, the total head value obtained in the Transformed system transfers directly horizontally to the Original system at this same point (when the two plots are made side by side).

Once the distribution of total head is determined in the Transformed section and transferred back to the Original system, the gradient in rock joint region 2 may be determined by using Equation F.3. Observe the L_2 is distance taken from the Original section. For this example, ΔH_2 is equal to 2.5 ft (=2.5 ft minus 0 ft) and L_2 is 5 ft, resulting in i_2 equal to 0.5 (Table F.1). By Equation F.6, the Transformed section i'_2 is equal to 0.25 with ΔH_2 equal to 2.5 ft and L'_2 equal to 10 ft.

This formulation may be applied to more than two reaches, as will be shown later in this section. Cedergren (1977), in his Figure 3.12 using a simple flow net to analyze the steady state, one-dimensional seepage through a horizontal "tube" filled with three zones of sand possessing two different hydraulic conductivity values (the first and third sand region possessing the same value for hydraulic conductivity). The "tube" is subjected to a head

differential ΔH from one end to the other end of the sand filled tube. The seepage analysis showed that the same hydraulic gradient was obtained in the two outer sand zones, which possessed the same length and the same value of hydraulic conductivity. The center zone of sand, possessing a one-fifth length of either of the outer sand regions and a much lower value for hydraulic conductivity (one-twentieth of the two outer sand layers), resulted in a much steeper gradient. This three sand region problem subjected to one-dimensional flow could also be analyzed using the Line of Seepage Formulation described in this appendix.

Figure F.2 is for an idealized non-overflow gravity dam embedded within a rock foundation that contains three unique rock regions. No rock foundation drain is included for the sake of clarity of concept explanation. Each rock joint contained within each rock region has a unique value for its hydraulic conductivity, K. The hydraulic conductivity of the rock joints contained within rock regions 2 and 3 are greater than the hydraulic conductivity of the rock joints contained within rock region 1.

The transformed horizontal axis is first constructed (Figure F.2(b)) using the two transformed lengths L_2' and L_3' by means of the equations given in the figure. Note that starting with the second rock joint reach (of transformed length L_2'), there is a transformed position denoting the end of rock joint 2, designated as point 3′. Similarly for rock joint 3 of transformed length L_3', it's starting and ending transformed points are 3′ and 4′ respectively. There exists a linear variation in total head from point 1 to point 4′ as denoted in Figure F.2(b). Also at points 2 and 3′ of Figure F.2(b) the value for total head is obtained and is designated as h_2' and h_3', respectively. A key feature of the transformed Figure F.2(b) is that the hydraulic gradient is constant. The total head values h_2' and h_3' are easily obtained from a linear relationship in total head with distance between Figure F.2(b) points 1 and 4′. The hydraulic conductivity for all three Figure F.2(b) transformed rock joints is equal to K_1.

Figure F.2(c) shows the original axis for the problem using the actual dimensions (labeled L_1, L_2 and L_3) for the length of the potential slip plane contained within the three rock regions. The values for total head are mapped from points 1, 2, 3′ and 4′ from Figure F.2(b), to points 1, 2, 3, and 4 in Figure F.2(c). Observe that the transformed Figure F.2(b) is required to compute the head values h_2' and h_3' at the transformed

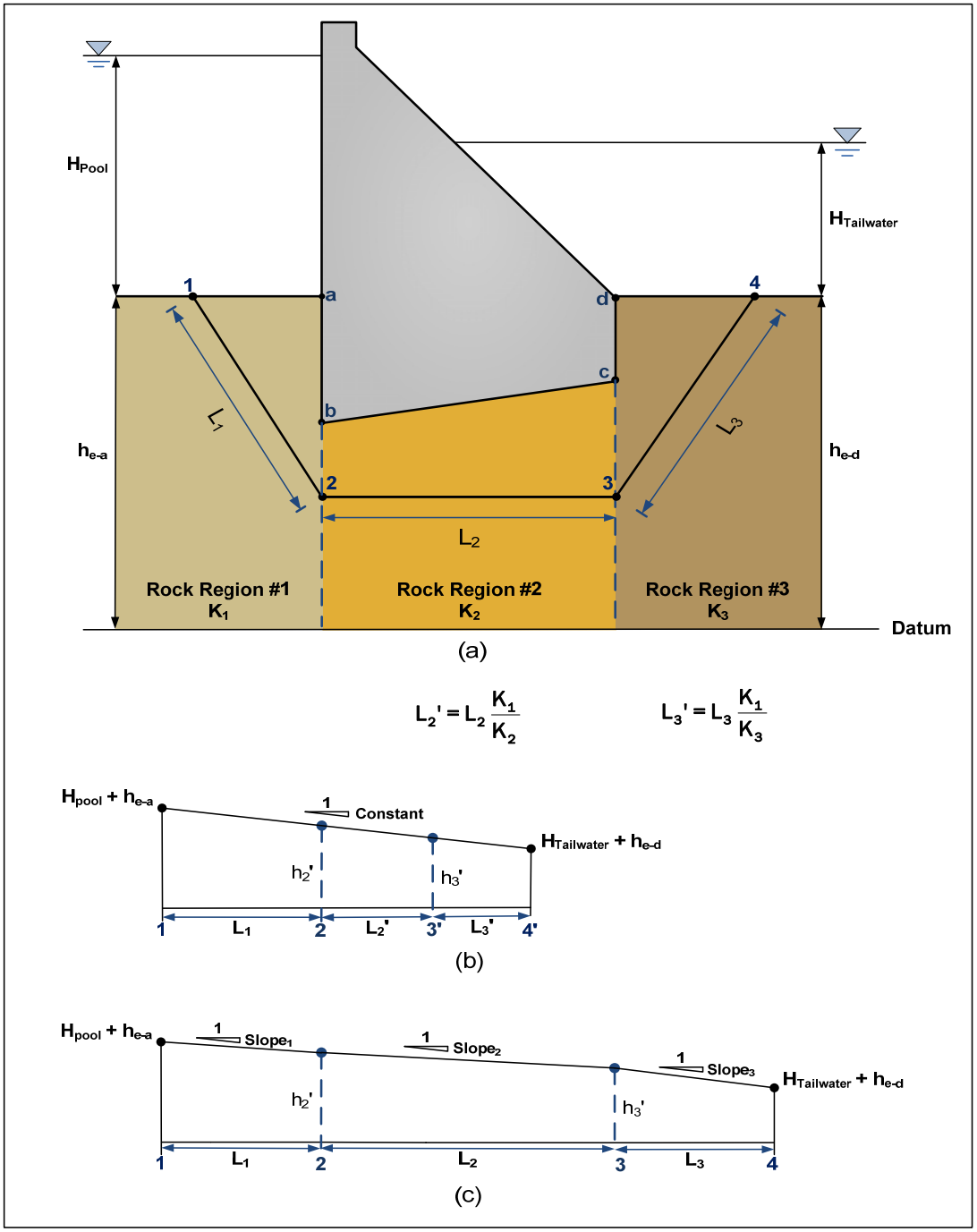

Figure F.2. Non-overflow gravity dam embedded within a rock foundation: (a) Potential slip plane within rock regions with different hydraulic conductivities (K) (rock joint lengths not to scale), (b) Constant slope in total head with distance along the transformed length of the potential slip plane, and (c) Variation of slope in total head with distance along the three rock regions of the potential slip plane.

position points of 2′ and 3′, respectively. Figure F.2(c) shows these computed heads of h_2' and h_3' at the actual position points 2 and 3, respectively.

Further observe in Figure F.2(c) that the slope of total head with distance along each of the three rock joints is no longer constant as is the case for the transformed horizontal axis plot of Figure F.2(b). The hydraulic gradient is constant along the segment of slip plane contained within each of the three rock regions. Recall that each rock joint possesses a different value for hydraulic conductivity, resulting in a different hydraulic gradient for each rock joint.

Bernoulli's Equation 1.5 (assuming a zero velocity head) in conjunction with Equation 1.8 allows for the calculation of water pressure from Figure F.2(c) at any point as measured along the potential slip plane.

REPORT DOCUMENTATION PAGE

Form Approved
OMB No. 0704-0188

1. REPORT DATE *(DD-MM-YYYY)*	2. REPORT TYPE	3. DATES COVERED *(From - To)*
June 2012	Final report	

4. TITLE AND SUBTITLE

Fragility Analysis of a Concrete Gravity Dam Embedded in Rock and its System Response Curve Computed by the Analytical Program GDLAD_Foundation

5a. CONTRACT NUMBER

5b. GRANT NUMBER

5c. PROGRAM ELEMENT NUMBER

6. AUTHOR(S)

Robert M. Ebeling, Moira T. Fong, Johannes L. Wibowo, and Amos Chase, Sr.

5d. PROJECT NUMBER

5e. TASK NUMBER

5f. WORK UNIT NUMBER

7. PERFORMING ORGANIZATION NAME(S) AND ADDRESS(ES)

U.S. Army Engineer Research and Development Center
Information Technology Laboratory
Geotechnical and Structures Laboratory
3909 Halls Ferry Road
Vicksburg, MS 39180-6199

8. PERFORMING ORGANIZATION REPORT NUMBER

ERDC TR-12-4

9. SPONSORING / MONITORING AGENCY NAME(S) AND ADDRESS(ES)

Headquarters, U.S. Army Corps of Engineers
441 G. Street, NW
Washington, DC 20314-1000

10. SPONSOR/MONITOR'S ACRONYM(S)

11. SPONSOR/MONITOR'S REPORT NUMBER(S)

12. DISTRIBUTION / AVAILABILITY STATEMENT

Approved for public release; distribution is unlimited.

13. SUPPLEMENTARY NOTES

14. ABSTRACT

This research report describes the engineering formulation and corresponding software developed for expressing the computed stability results for an idealized two-dimensional cross-section of a non-overflow concrete gravity dam embedded in rock in terms of a fragility curve for a potential sliding mode of failure. Within the Corps, the term system response curve is being used to describe what is commonly referred to in the technical literature as the fragility curve; used for the hydrologic fragility assessment of concrete gravity dams embedded in rock. This report uses this Corps terminology. Uncertainty in strength, rock joint parameters that impact the flow of water within the rock joints, silt induced earth pressure and (post-tensioned) anchor force(s) are accounted for in a multivariate probabilistic stability analysis resulting in the computation of a system response curve. The PC software package GDLAD_Foundation (Gravity Dam Layout And Design) is used in this R&D effort to perform the computations and construct the system response curve.

A sliding stability assessment of a non-overflow gravity dam embedded in rock requires the assignment of uplift water pressure forces acting on the driving, structural and resisting wedges. Incorporated within the GDLAD_Foundation software package is the program Joint_FLOW that is used to assess laminar fluid flow within rock joints, fissure and/or faults contained within the rock foundation. Results from the analysis of steady state laminar seepage within the joints provides for the calculation of uplift water pressures along the joints. Resultant uplift forces are then computed from the distribution of water pressures along these rock joints.

(Continued)

15. SUBJECT TERMS

16. SECURITY CLASSIFICATION OF:			17. LIMITATION OF ABSTRACT	18. NUMBER OF PAGES	19a. NAME OF RESPONSIBLE PERSON
a. REPORT	b. ABSTRACT	c. THIS PAGE			19b. TELEPHONE NUMBER *(include area code)*
UNCLASSIFIED	UNCLASSIFIED	UNCLASSIFIED		297	

14. ABSTRACT (Concluded).

The resulting engineering methodology and corresponding software is applicable to a two dimensional model of a non-overflow (concrete) gravity dam founded within rock. GDLAD_Foundation is also capable of performing a deterministic steady state seepage analysis of laminar flow within rock joints or a seepage analysis followed by a sliding stability evaluation.

15. SUBJECT TERMS (Concluded).

Concrete dam embedded in rock
Flow in rock joints
Flow within rock joints
Fragility analysis
Fragility curve
Multivariate probabilistic analysis
Non-overflow gravity dam
Rock joint flow
Seepage in rock joints
System response curve
Uplift pressure force